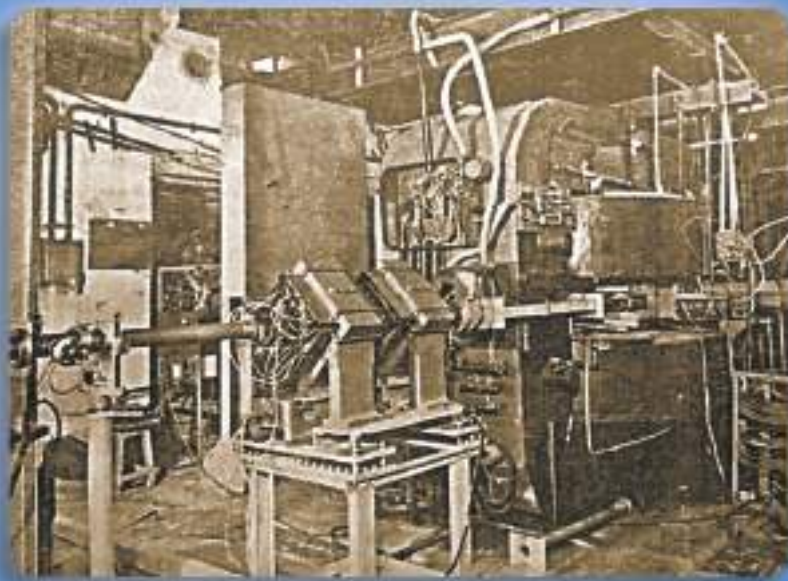


Application of Radiotracers and Energetic Beams in Sciences

Volume 5



Editor
Susanta Lahiri



SAHA INSTITUTE OF NUCLEAR PHYSICS

Kolkata, India

Application of Radiotracers and Energetic Beams in Sciences

Volume 5

**Extended abstracts of the invited lectures and contributed papers
of**

The Fourth International Conference

on

**Application of RadiotraCers and Energetic Beams in Sciences
(ARCEBS-2018)**

November 11-17, 2018

EDITOR

Susanta Lahiri

Organized by

The Saha Institute of Nuclear Physics

1/AF Bidhannagar, Kolkata, India

in cooperation with

The International Atomic Energy Agency

Published

November 11, 2018

Printed at

Sailee Press Pvt. Ltd.
4A Manicktala Main Road
Kolkata 700054, India
Ph: 0091-33-23522263

The editor cannot accept any responsibility or liability for the accuracy of any statement or information given in the papers.

Neither this book nor any part of it may be reproduced or transmitted in any form or by any means, electronic or mechanical, including photocopying, microfilming, and recording, or by any information storage and retrieval system, without permission in writing from the editor.

ARCEBS-2018

International Advisory Committee

Navin Alahari, France
Ramiz Aliev, Russia
Nevenka Antovic, Montenegro
A. Chatt, Canada
Swapan Chattopadhyay, USA
J.G. Correia, Portugal
Christoph E. Dullmann, Germany
Flavia Groppi, Italy
Hiromitsu Haba, Japan
Xiaolin Hou, Denmark
Karl Johnston, CERN
Dinakar Kanjilal, India
Kattesh V. Katti, USA
Gunther Korschinek, Germany

Mats Lindroos, Sweden
Ajit Kumar Mohanty, India
Yuichiro Nagame, Japan
Pradeep K Pujari, India
Syed M. Qaim , Germany
Zsolt Revay, Germany
Amitava Roy, India
Chhanda Samanta, USA
Thierry Stora , CERN
Zoltan Szucs , Hungary
B.S. Tomar , India
Meera Venkatesh, IAEA
Bert Wolterbeek, The Netherlands

National Organizing Committee

Raghunath Acharya, Mumbai
Arup Bandyopadhyay, Kolkata
Sundeep Chopra, New Delhi
N.R. Das, Kolkata
Tapas Das, Mumbai
Susanta Lahiri, Kolkata – Chairperson
Moumita Maiti, Roorkee

P. K. Mohapatra, Mumbai
Vaishali Naik, Kolkata
Yerol Narayana, Mangalore
Abhijit Saha, Kolkata
Suparna Sodaye, Mumbai
Alok Srivastava, Chandigarh
Diwakar Tiwari, Aizawl

Local Organizing Committee

Kakoli Banerjee, Prabhu Jagatbandhu College
Tapas Bandyopadhyay, BARC
Debashis Banerjee, BARC
Samita Basu, SINP
Punarbasu Chaudhuri, University of Calcutta
Pabitra Chattopadhyay, University of Burdwan
Dibyasree Choudhury, SINP, Joint Secretary
N. R. Das, Ex-SINP
S. K. Das, Ex-BARC

Supriyo Ganguly, SINP
Susanta Lahiri, SINP, Chairperson
Padmaja P. Mishra, SINP
Debashis Mukhopadhyay, SINP
Nabanita Naskar, University of Calcutta & SINP, Joint Secretary
S.K Wasim Raja, BARC
Pradip Roy, SINP
Subinit Roy, SINP
Kamalika Sen, University of Calcutta

GOLDEN Sponsor of ARCEBS-2018:



NOKI TECHNOLOGIES PRIVATE LIMITED

SILVER Sponsors of ARCEBS-2018:



ADVANCETECH Controls Pvt. Ltd.

thermoscientific

ThermoFisher SCIENTIFIC

ARCEBS – An Onward Journey

The journey under the flagship name of “ARCEBS” started with a two days national level discussion meeting at the Saha Institute of Nuclear Physics (SINP), Kolkata on 15-16 April, 2004, which motivated towards organizing full fledged international conference every four years. The first two international conferences of the ARCEBS series were held at SINP during 23-27 January, 2006 and 7-13 November, 2010 with the name as “Application of Radiotracers in Chemical, Environmental and Biological Sciences.” Because of its increasing multi-faceted and inter-disciplinary approach, the definition of ARCEBS was modified to “Application of Radiotracers and Energetic Beams in Sciences” from last edition of ARCEBS-14 that was held at Ffort Raichak, Kolkata from 12-14 January, 2014. However, the elegant symbol of “ARCEBS” remained unchanged which contains all the colors of the “chart of the nuclides”.

The organization of such an event requires cooperation from many – individuals and organizations. We are grateful to all of them. We are thankful to Professor A. K. Mohanty, Director, SINP for his encouragement and extending all administrative support. We are grateful to the International Atomic Energy Agency (IAEA) for extending cooperation and also for financial support. Special thanks to Dr. Meera Venkatesh, Director, Division of Physical and Chemical Sciences, Department of Nuclear Science and Applications, IAEA. The Department of Atomic Energy (DAE), Govt of India, extended their full administrative support for organization of ARCEBS-2018. We sincerely acknowledge help and co-operation received from DAE. I take this opportunity to note our sincere thanks to Sri Amitava Roy, Director, Variable Energy Cyclotron Centre (VECC), Kolkata for his cooperation in organizing the event. We are thankful to all the members of International Advisory Committee, National Organizing Committee and Local Organizing Committee for their valuable suggestions to make the conference success.

The success of the conference depends on its quality. The ARCEBS series of conference is recognized as a bench mark conference in the peer community, which has been reflected by the rigorous review process of the extended abstracts of ARCEBS-2018. We extend our heartiest thanks to all the reviewers. The eminent scientists all over the globe agreed to deliver invited talks in the conference in addition to 120 contributed papers. We are thankful to all of them. Four mini-

symposiums are organized in ARCEBS-2018. We acknowledge the valuable contributions of the chairpersons of these mini-symposiums.

The selected papers of ARCEBS-2018 will be published in Journal of Radioanalytical and Nuclear Chemistry (JRNC). In this respect, we express our sincere gratitude to Dr. Zsolt Révay, Editor-in-chief, JRNC and Professor Amares Chatt, Editor, JRNC

The ARCEBS 2018 has brought out a beautiful souvenir covering the life and works of Professor Meghnad Saha and Professor S. N. Bose as well as two important articles in the field of nuclear science. My colleague, Dr. Kamalika Sen, Assistant Professor, University of Calcutta is responsible for this souvenir. I am thankful to her. I am also thankful to Professor Debashis Mukhopadhyay, SINP, for coordinating all the audiovisual related activities including cultural program.

A uniform formatting has been maintained throughout the volume. Ms. Kousiki Ghosh Jana, Scientific Officer, BARC (VECC) and Ms. Sayantani Mitra checked all the editing styles of all the articles. I note my sincere thanks to both of them.

Finally I would like to mention the immense contribution of my younger colleagues, Ms. Nabanita Naskar and Ms. Dibyasree Choudhury. They handled more than thousand e-mails, all the abstracts, arranging accommodation and local hospitalities for all the participants, managing finance and all other co-ordinations required for smooth arrangement of the conference. All these they did by sacrificing their own research time in their early career. No word is sufficient to acknowledge their contributions. I just want to say – “Thank you Nabanita and Dibyasree for all”.

I wish all of you scientifically fruitful days and a pleasant stay during ARCEBS-2018 and hope to meet you again in ARCEBS-2022.

Susanta Lahiri

Contents

ARCEBS – An Onward Journey	v
-----------------------------------	----------

Plenary and Invited Lectures

Separations Science for Radioactive Materials: Some Perspectives	3
<i>P.R. Vasudeva Rao</i>	
Beaming Ubiquitous Neutrinos and The “Dark” Universe	5
<i>Swapan Chattopadhyay</i>	
Recent Highlights and Trends Applying Radioactive Ion Beams to Solid State Physics: ISOLDE and Beyond	9
<i>Karl Johnston</i>	
Local Probing Complex Oxides Using Perturbed Angular Correlations	11
<i>J. P. Araújo, G. N. P. Oliveira, R. C. Teixeira, P. Rocha-Rodrigues, T. Leal, R. Moreira, J. G. Correia, A. M. L. Lopes</i>	
Forty Years of VECC	13
<i>Amitava Roy</i>	
FRENA- A Low Energy, High Current Accelerator Facility in Nuclear Astrophysics	15
<i>Subinit Roy</i>	
Overview of the Pelletron Linac Facility, Mumbai	17
<i>Vandana Nanal</i>	
Radioactive Tumor Specific Gold-198 Nanoparticles in Nuclear Medicine: Green Nanotechnology and Radiochemical Approaches in Nano Radiopharmaceuticals	19
<i>Kattesh V. Katti, Kavita K Katti and Ademar B Lugao</i>	
Production and Application of The Non-Standard-PET Radionuclides ⁵²Mn and ⁷³Se	23
<i>B. Neumaier, U. Königs, S.M. Qaim, K. Giesen, I. Spahn</i>	
Converging Technologies for Improving Human Health - Contribution of Ionizing Radiation and Nanotechnology	25
<i>Kattesh V. Katti, Ademar B. Lugão</i>	
Medical Cyclotron Program and PET-CT Imaging: Status and Trends in India	27
<i>M.R.A.Pillai</i>	

Proton Boron Therapy: Sense or Nonsense?	29
<i>Bert Wolterbeek, Tuur Vermunt, Zoltan Perko, Jeremy Brown</i>	
News from Research on Superheavy Elements	31
<i>Christoph E. Düllmann</i>	
In the Fission Valley of HE and SHE	33
<i>Tilak Kumar Ghosh</i>	
Atomic/Chemical Properties of the Heaviest Actinide Element Lawrencium	35
<i>Tetsuya K. Sato</i>	
Speeding Up Gas-phase Chemistry to Access Elements Beyond Fl, Element 114	37
<i>S. Götz, M. Block, Ch. E. Düllmann, F. Giacoppo, M. Götz, S. Raeder, P. Chhetri, E. Jäger, O. Kaleja, B. Kindler, J. Krier, B. Lommel, A.K. Mistry, A. Yakushev, V. Yakusheva</i>	
Liquid-Phase Chemistry of Superheavy Elements	39
<i>Yuichiro Nagame</i>	
Superheavy Nuclei to Hypernuclei	41
<i>Chhanda Samanta</i>	
On Laser Spectroscopy of Nobelium and Lawrencium	43
<i>Mustapha Laatiaoui</i>	
CERN-MEDICIS: Non-Conventional Radioisotopes for Medical Applications	45
<i>A.P. Bernardes, L. Buehler, R. Catherall, T. Cocolios, K. Kershaw, S. Marzari, J. Prior, T. Stora and the MEDICIS Collaboration</i>	
Accelerators and Research with Non-conventional Medical Isotopes	47
<i>F. Haddad</i>	
From Isotope Separation Online at CERN ISOLDE to Radioisotopes for Medical Research at CERN MEDICIS	49
<i>Thomas Elias Cocolios, Kristof Dockx, Yisel Martinez-Palenzuela, Joao Pedro Ramos, Simon T. Stegemann, Thierry Stora</i>	
Production of Radioisotopes for Application Studies at RIKEN RI Beam Factory	51
<i>Hiromitsu Haba for RIKEN Nuclear Chemistry Collaboration</i>	
The ISOLPHARM Project: Production Method of High Specific Activity Beta-emitting Radionuclides as Radiopharmaceutical Precursors	53
<i>A. Andrichetto, F. Borgna, M. Ballan, S. Corradetti, E. Vettorato, G. Marzaro, F. Mastrotto, N. Realdon, V. Di Marco</i>	
Radionuclides Production For Theranostic Applications	55
<i>Flavia Groppi, Simone Manenti</i>	

Photonuclear Production and Radiochemical Separation of Medically Relevant Radionuclides	57
<i>Ramiz Aliev, Andrey Kazakov, Ekaterina Furkina, Sergei Belyshev</i>	
Determination of Low-level Radionuclides: Radiometric vs. Mass Spectrometric Methods	59
<i>Xiaolin Hou</i>	
Status of XCAMS Facility at IUAC	61
<i>Sundeep Chopra</i>	
AMS of ⁹³Zr and ⁹⁹Tc: Developments and First Results	63
<i>G. Korschinek, T. Faestermann, B. Deneva, C. Busser, K. Hain, D. Koll, F. Kortmann, P. Ludwig, F. Quinto</i>	
Limits in AMS for Nuclear Physics and Nuclear Astrophysics Applications	65
<i>Anton Wallner</i>	
In-Beam Neutron Activation Analysis at Garching	67
<i>Zsolt Révay, Christian Stieghorst</i>	
AMS Determination of Radiocarbon in Dilute Biofuels: Method Uncertainties and Detection Limit	69
<i>Randy Culp, Ravi G. V. Prasad and Hai Pan</i>	
Recent Developments and Applications of <i>In Situ</i> Current Normalized PIGE Method Using Proton Beams for Quantification of Low Z Elements in Energy Materials	71
<i>R. Acharya</i>	
A Multitechnique Approach to Study Bioelements	73
<i>A. Chatt, N. Bahroun, A. Lefsay, C.K. Jayackwreme, D.M. Chevrier, P. Zhang</i>	
Separation of Radio-cesium and Radio-strontium from Acidic Radioactive Wastes	75
<i>Prasanta K. Mohapatra</i>	
Chemical Properties of Flerovium (element 114)	77
<i>L. Lens</i>	
Revisiting The Protocols for Low Level NORM Measurement in Environmental Samples	79
<i>Nabanita Naskar</i>	
Research using LBE target at SINP	81
<i>Dibyasree Choudhury, Susanta Lahiri</i>	

Contributed Papers

Hyperfine Interaction of Electron and Nuclear Spins in InSb Two-Dimensional Electron Gas Towards Quantum Information Processing	85
<i>M. M. Uddin, H. W. Liu, K. F. Yang, T. D. Mishima, M. B. Santos, K. Nagase, Y. Hirayama</i>	
Radiotracer Application for Rapid Measurement of Contribution of Stem Assimilates Towards Grain Filling in Wheat	87
<i>Bhupinder Singh, Sumedha Ahuja and Poonam Yadav</i>	
^{99}Mo / $^{99\text{m}}\text{Tc}$ Generator Based on Alumina ^{99}Mo-Molybdate (VI) Gel of High Radionuclidic Purity	89
<i>M.A. El-Absy, T.W.Fasih, M.A. El-Garhy, M.A. El-Amir, H.E.Ramadan, M.F. El-Shahat</i>	
Elemental Analysis of <i>Pterocarpus Santalinus</i> by PIXE and ICP-MS: Chemometric Approach	91
<i>J. C. Rao, B. Gowri Naidu, S. Srikanth, P. Sarita and G. J. Naga Raju</i>	
Environmental Radioactivity Around the European Spallation Source facility	93
<i>D. Ene, R. Avila, T. Hjerpe, B. Jaeschke and K. Stenberg</i>	
Microarray Immunoassay for Thyrotropin on Track-Etched Membranes Using Radiotracers	95
<i>Bharti Jain, Savita Kulkarni, S.Banerjee, M.G.R.Rajan</i>	
Assessment of Heavy Metals in Poultry Chicken Giblets Using ICP-MS	97
<i>Mayeen Uddin Khandaker and Nwokoma Oliver Chijioko</i>	
Evaluation of Radon Concentration in Irrigation and Drinking Waters from Eastern Part of Oman Using Nuclear Track Detectors and Estimation of Corresponding Doses to Human Health	99
<i>Saleh Mansoor Nasser and Mayeen Uddin Khandaker</i>	
Comparative Study of $^{110\text{m}}\text{Ag}(\text{I})$ Removal from Aqueous Media by Humic Substances	101
<i>Sabrina A. Shaikh, Hemlata K. Bagla</i>	
Removal of $^{60}\text{Co}(\text{II})$ from Simulated Low Level Waste by an Eco-Friendly Biosorbent	103
<i>Sajida Sayed, Hemlata K. Bagla</i>	
Application of Tracer Technique in Remediation of $\text{Sr}(\text{II})$ Polluted Waters	105
<i>Asma Khan, Hemlata K. Bagla</i>	
Measurement of ^{40}K in Surface Soil Samples Collected from Sundarbans Biosphere Reserve, India	107
<i>Nabanita Naskar, Susanta Lahiri, Punarbasu Chaudhuri</i>	
Uranium Intake by Population Around Upcoming BARC Facilities at Visakhapatnam, Andhra Pradesh – a Baseline Data	109
<i>P. Padma Savitri, T. Sambamurty, J. Sudhakar, N.S. Krishna, A. Vinod Kumar</i>	

Dual Displacer-Gamma Ray System for Level Measurement of Fluids-Interface in Oil Separator	111
<i>Nader M. A. Mohamed</i>	
Cross Section Calculations of (n, p) and (n, 2n) Nuclear Reactions on Zn, Mo and Pb Isotopes with ~14 MeV Neutrons	113
<i>A. Gandhi, Y. Sawant, B. J. Roy, B. K. Nayak, A. Saxena, S. Ganesan, S. Kailas, Yu. N. Kopatch, I. N. Ruskov, D. N. Grozdanov, N. A. Fedorov, A. Kumar</i>	
New Dates from the Site of Erenda, East Medinipur District, West Bengal: Implications for Indian Protohistory	115
<i>Nabanita Naskar, Kaushik Gangopadhyay, Susanta Lahiri, Ahana Ghosh, Punarbasu Choudhuri, Rajveer Sharma, Pankaj Kumar, S. Ojha and S. Chopra</i>	
Production of ¹⁹⁰⁻¹⁹³Au Radionuclides through ¹¹B Induced Reactions on Natural Tungsten Target	117
<i>Dibyasree Choudhury, Susanta Lahiri</i>	
Investigation of Radon Concentration in Drinking Water to Assess The Whole Body Dose and Excess Lifetime Cancer Risk along Coastal Kerala, India	119
<i>Prakash V, Divya P V</i>	
Distribution of Natural Radionuclides and Assessment of Excess Lifetime Cancer Risk Along Coastal Areas of Varkala in Kerala	121
<i>Divya P V, Prakash V</i>	
Production and Separation of No-Carrier Added ^{43,44,44m}Sc from ¹²C Irradiated BaCl₂ Target	123
<i>Kousiki Ghosh, Dibyasree Choudhury, Susanta Lahiri</i>	
Alpha Track Detection Employing Tetraethyl Ammonium Bromide (TEAB) as New Chemical Etchant of CR-39	125
<i>Sushma S. Chavan, Amol M. Mhatre, Ashok K. Pandey, Hemlata K. Bagla</i>	
Preparation and Evaluation of Freeze-dried Kits of BPAMD Suitable for Labelling with ⁶⁸Ga Eluted from Different Commercial Generators	127
<i>Mohini Guleria, Tapas Das, Jeyachitra Amirdhanayagam, Haladhar D. Sarma, Ajit S. Shinto, K.K. Kamaleshwaran, Arun Pandian, Ashutosh Dash</i>	
Synthesis and Evaluation of a Novel ^{99m}Tc Labelled Folic Acid Derivative for Targeting Folate Receptor Positive Cancers	129
<i>Soumen Das, Navin Sakhare, Anupam Mathur, Shubhangi Mirapurkar, Sheela M., S.S. Sachdev</i>	
Studies on Indoor and Outdoor Radon/Thoron Concentration and Estimation of Radiological Parameters from Gamma Dose Rates along the Coastal Regions of Trivandrum and Kollam Districts, Kerala, India	131
<i>K. Nadira Mahamood, V. Prakash</i>	

Design, Characterization and Evaluation of ^{99m}Tc Labeled Functionalized Gold Nanoparticles for Imaging FR Positive Cancers	133
<i>Dheeraj Kumar, Navin Sakhare, Pooja Kale, Soumen Das, Anupam Mathur, Shubhangi Mirapurkar, Sheela M., S.S. Sachdev</i>	
Effect of γ-Irradiation on Ruthenium-Morin Nanocomposite for Trace Detection of Ce(IV), Ce(III) and Dy(III)	135
<i>Pritam Singh and Kamalika Sen</i>	
²¹⁰Po and Uranium Sequential Analysis By Extractive Liquid Scintillation Spectrometry	137
<i>Vandana Pulhani, Priyanka J. Reddy, Moushumi Chaudhury and R M Tripathi</i>	
Physico-Chemical Investigation of Gamma Irradiated Guanidine Nickel(II) Sulphate	139
<i>T A Jayashri, G Krishnan, K Viji</i>	
Graphene Quantum Dots Prepared From Glucose as a Fluorescent Sensor of Uranium In Environmental Samples	141
<i>Pradeep Kumar Dewangan, Fahmida Khan, Kamlesh Shrivastava, Vinayak</i>	
Tritium Analysis in Radioactive Waste Solution using Liquid Scintillation Counter	143
<i>B. Arun, Y. Ramani, I. Vijayalakshmi, S. Viswanathan</i>	
Highly Selective Removal of Perchnetate by Donnan Dialysis through Supported Liquid Membrane	145
<i>Sanhita Chaudhury, V. G. Mishra, D. J. Shah</i>	
Size Dependent Ion Exchange Property of Nanosilica As Green Inorganic Exchanger In Radiochemical Separations	147
<i>Rajesh Chakraborty, Pabitra Chattopadhyay</i>	
Fission Analysis of Z=114 Superheavy Isotopes Formed Via Heavy-ion Induced Reactions	149
<i>Gurjit Kaur, Kirandeep Sandhu, and Manoj K. Sharma</i>	
Role of Biomolecules in Extraction of U(VI) using an Aqueous Biphasic System	151
<i>Rajib Karmakar and Kamalika Sen</i>	
An Analysis of The Production of Neutron Deficient Platinum Radionuclides	153
<i>Rinku Prajapat, Moumita Maiti</i>	
Experimental Investigation of Soil to Grass Transfer Factor for ¹³⁷Cs and ⁶⁰Co using Lysimetry Facility	155
<i>S.S.Wagh, A. K. Patra, Jaison T. John, J. S. Mistry, P.M.Ravi, R.M. Tripathi</i>	
Uptake and Distribution of Ceria Nanoparticles in Plants Using Radiotracer Techniques	157
<i>Zhiyong Zhang, Xiao He, Yuhui Ma</i>	
Sources and Tracer Significance of Radionuclide ²¹⁰Po in the Atmosphere of Beijing, China	159
<i>Jie Ouyang, Li-Juan Song, Ling-Ling Ma, Min Luo, Xiong-Xin Dai, Dian-Dou Xu</i>	

Generation of Site Specific Washout Parameters Using ^7Be as a Tracer at Kakrapar Gujarat Site	161
<i>T.J. Jaison , A. K. Patra , D. P.Nankar, A. Jain , P.M. Ravi P, R.M. Tripathi</i>	
Production of Polonium Isotopes in p-induced Reaction on the LBE Target up to 150 MeV	163
<i>Moumita Maiti, Deepak Kumar, Rinku Kumar Prajapat</i>	
Determination of Boron in In-house Graphite Reference Material by Instrumental Charged Particle Activation Analysis	165
<i>S. Dasgupta, J. Datta and. K. K. Swain</i>	
Production Estimates of $^{101,100}\text{Pd}$ Radionuclides in Lower Energy Region: An Indirect Route of $^{101\text{m}}\text{Rh}$ Isomer	167
<i>Amit Chauhan, Moumita Maiti</i>	
The Alpha+LBE Reaction up to 37.5 MeV/A	169
<i>Gayatri Sarkar, Deepak Kumar, Moumita Maiti</i>	
Pertraction of Americium(III) Through Supported Liquid Membranes Containing Benzene Centered Tripodal Diglycolamides	171
<i>Bholanath Mahanty, Prasanta K. Mohapatra, and Willem Verboom</i>	
Estimation of Uranium in Water and Urine by Liquid Scintillation Spectrometry	173
<i>Priyanka J. Reddy, Sonal M. Wankhede and Pramilla D. Sawant</i>	
Radiochemical Studies and Pre-clinical Evaluation of ^{111}In-Pentetreotide using Indigenously Produced $^{111}\text{InCl}_3$ Via $^{109}\text{Ag} (\alpha, 2n)$ Nuclear Reaction	175
<i>A. Chakraborty, A. Mitra, S. Lad, T. Upadhye, M. Tawate, S. Satamkar, R. Bhoite, S. S. Das, L. Barua, S. Chattopadhyay, S. Banerjee</i>	
Study of Pre and Post Edge Structure Effect on Mass Attenuation Coefficients	177
<i>Anand B C, Sharanabasappa, B. R. Kerur</i>	
A New Sephadex Based Separation of ^{43}Sc from Alpha Irradiated $^{\text{nat}}\text{CaCO}_3$ Target	179
<i>S. S. Das, S. Chattopadhyay, L. Barua, Md. N. Alam, Madhusmita, A. K. Pal, U. Kumar, A. K. Hudait, S. Banerjee</i>	
Simulation Study on Purification of Spent ^{100}Mo and $^{99\text{m}}\text{Tc}$ from Nb, Zr, Y and Ru Traces	181
<i>S. Chattopadhyay, S.S.Das, Madhusmita, Md. N. Alam, S. Banerjee</i>	
Estimation of ^{14}C in Irradiated Graphite using CO_2 Gasification Method	183
<i>Susheela Sivakumar, Sanjay Singh, K. S Babu, D. Banerjee, R. K. Gopalkrishnan</i>	
Study on Thermoluminescence Properties of Commercial Glasses Used in Bangladeshi Dwellings for Accidental Dosimetry	185
<i>Sabina Yasmin, Bijoy Sonker Barua, Mayeen Uddin Khandakr, Z.Siti Rozaila, Md. Abdur Rashid, Faruque-Uz-Zaman Chowdhury</i>	
Evaluation of Excitation Function for the Productions of Polonium-207 and Polonium-208 Isotopes from Bismuth-208 Nucleus	187
<i>Idris Ahmad, Yahaya Ibrahim Yola</i>	

Sequential Separation of Pu, Am and U in Urine Using Solid Extraction Chromatography Technique	189
<i>Rupali Dubla, Ranjeet Kumar, J.R.Yadav P.D.Sawant</i>	
He⁺ Ions Induced Effects in Nd-doped Zirconolite	191
<i>Merry Gupta, S. S. Ghumman, R. Kumar, P. K. Kulriya</i>	
Assessment of Radiological Hazards in Indian Sundarbans	193
<i>Nabanita Naskar , Susanta Lahiri, Punarbasu Chaudhuri</i>	
Importance of Voxel Size in Localizing Defect Using Gamma Ray Scattering	195
<i>Akash Tondon, Mohinder Singh, B. S. Sandhu ,Bhajan Singh</i>	
Study on Groundwater Quality in Parts of Rajasthan with Special Reference to Uranium Contamination	197
<i>Diksha Pant, Tirumalesh keesari, A.Roy, U.K.Sinha, Manveer Singh, S.K.Jain, R.M.Tripathi</i>	
Determination of ⁹⁰Sr in Environmental Samples Using Solid Extraction Chromatography	199
<i>Amar D. Pant, R. Ruhela, B. S. Tomar and Anilkumar S.</i>	
Certification of Iodine Filters NPP Using ¹³¹I and ¹²⁷I	201
<i>Volodymyr Levenets, Oleksiy Lonin, Oleksandr Omelnik, Volodymyr Sokolenko, Andrey Shchur</i>	
Natural Radioactivity in Alluvial soil of Indo-Gangetic Plain	203
<i>Rupali Karpe, Ajay Kumar, Y.P. Gautam, M.K.Mishra, V.M.Joshi, Vandana Pulhani, R.M.Tripathi</i>	
Effect of Electron Irradiation on Optical, Thermal and Electrical Properties of Polymer Electrolyte	205
<i>B. K. Mahantesha, V. Ravindrachary, R. Padmakumari, R. Sahanakumari, Pratheeka Tegganamata, Ganesh Sanjeev, V. C. Petwal, V. P. Verma</i>	
Accumulation of ²¹⁰Po in Medicinal Plants in the Environment of Mangalore, Southwest Coast of India	207
<i>V. Prakash, K. M. Rajashekara, Y. Narayana</i>	
Distribution and Enrichment of ²¹⁰Po and ²¹⁰Pb in the Environment of Mangalore, Southwest Coast of India	209
<i>V. Prakash, V. Vineethkumar, K. M. Rajashekara, Y. Narayana</i>	
The Behavior of Neptunium In Natural Objects	211
<i>A.M. Emelianov, E.A. Lavrinovich, T.A. Goryachenkova, A.P. Novikov</i>	
Development of Radiolabeled Chemotherapeutics for Tumor Theranosis: A Preliminary Study with ⁶⁸Ga- and ¹⁷⁷Lu-labeled Gemcitabine	213
<i>Subhajit Ghosh, Tapas Das, Haladhar D. Sarma, Ashutosh Dash</i>	
Regulating Energetic Beams for Medical Isotope Production in Canada	215
<i>Abdul Alwani</i>	

Monte Carlo Simulation Approach to Evaluate Radon Suppression in Low Background Gamma-ray Spectroscopy	217
<i>Sy Minh Tuan Hoang, Gwang Min Sun, Hoai-Nam Tran, Ngoc-Thiem Le, Manh-Dung Ho, Tuan-Anh Tran</i>	
The Innovative PIXE/PIGE Facility at the 2-MV KIST Tandem Ion Accelerator: Design and Calculation	219
<i>Sy Minh Tuan Hoang, Gwang Min Sun, Hoai-Nam Tran, Ngoc-Thiem Le, Manh-Dung Ho, Tuan-Anh Tran</i>	
Solid State Synthesis and Phase Confirmation of Ce-Doped Zirconolite	221
<i>Rajveer Kaur, M. Gupta, P. K. Kulriya, S. S. Ghumman</i>	
Surface Properties of Neutron-rich Thermally Fissile Nuclei at Finite temperature	223
<i>Abdul Quddus, M Bhuyan, Shakeb Ahmad, S.k. Patra</i>	
The Study of Natural Radioactivity Levels in Beach Sand Samples of Kollam, Kerala, India	225
<i>Ramsiya M, Antony Joseph, Vishnu Prasad AK, Eappen KP, Vishnu CV</i>	
Gamma ray Irradiated Ni-Hesperidin Nanocomposite for Selective Trace Level Sensing of Sulfide Ions	227
<i>Zarina Ansari, Kamalika Sen</i>	
Radiation Dosimetry of ^{99m}Tc-DTPA-bis-choline based on Mice Data	229
<i>Aruna Kaushik, Puja Panwar Hazari, Ambika Parmar Jaiswal, Anil K. Mishra</i>	
The Radiation Dose and Distribution Coefficient of ²¹⁰Po and ²¹⁰Pb Concentrations in Aquatic Environs of Major Rivers of Coastal Karnataka	231
<i>Rajashekara K M, Prakash V and Narayana Y</i>	
Rapid, Simultaneous Analysis of Anthropogenic and Naturally Occurring Radionuclides in Seawater	233
<i>Sugandhi Suresh, Sonali P.D. Bhade, Vandana A. Pulhani and R M Tripathi</i>	
Low Specific Activity ⁶⁴Cu ions – Bio-marker for Melanoma	235
<i>A. Gopalakrishna, S. Chakraborty, A.Chakraborty, Y. Pawar , B.Mohanty, M.Tawate, K. V. Vimalnath, R. Chakravarty, S.Banerjee, B.K.Nayak, S.V.Suryanarayan, H.Naik, P.C.Chaudhari, A. Kumar, P.Maletha, Kamaldeep, A.Dash</i>	
Comparative Uptake Study of Cesium on Encapsulated Nano Magnetites	237
<i>Joyeeta Mukherjee & Pranesh Sengupta</i>	
Study of the Dependence of Evaporation Residue Cross Section on Incident Channel Parameters	239
<i>K Hajara, M M Musthafa</i>	
ED-XRF Analysis of Some Herbs Used to Cure Respiratory Diseases in Ayurvedic Treatment	241
<i>S. Ibrahim, M. M. Musthafa, K. P. Binsiya</i>	

Environmental impact of natural radioactivity in soil and groundwater of a uranium mineralized zone of Indian Himalaya	243
<i>Mukesh Prasad, G. Anil Kumar, R. C. Ramola</i>	
Identification of Radionuclides Found in Deflector Cleaning Waste of K-130 Cyclotron	245
<i>K.Srihari, Kousiki Ghosh Jana, Mausumi Sengupta Mitra, R.Ravishankar, Tapas Bandyopadhyay</i>	
High Dose Gamma Irradiation Effect on The Properties of Copper Nanowires	247
<i>R P Chauhan, Pallavi Rana, Suresh Panchal, Chetna Narula</i>	
Efficient Adsorption of Uranium from Aqueous Solutions and Simulated Seawater by Zeolite Imidazolate Framework	249
<i>Jagannath Panda, Abinash Sahu, Rojalin Sahu</i>	
Radiochemical Purification of ³²P from Sulphur Target Irradiated in KAMINI Reactor	251
<i>J. S. Brahmaji Rao, G. V. S. Ashok Kumar, R. Senthilvadivu, R. Kumar</i>	
Application of ²¹⁰Pb Chronology Assessing for Marine Contamination in Mumbai Harbour Bay	253
<i>Moushumi D. Chaudhury, Vandana Pulhani, Vikram Joshi, Sujata Gothankar, S.K.Jha, R. M. Tripathi</i>	
Validation of Irradiation Parameters f and α for k_0 Based IM-NAA Method in KAMINI Reactor	255
<i>Manish Chand, J.S. Brahmaji Rao and R.Kumar</i>	
Analysis of Muscle Tissue Substitute with Respect to Photon Interaction, Build-up Factor and Relative Kerma	257
<i>Inderjeet Singh, Rohit, Bhajan Singh, B.S. Sandhu and Arvind D. Sabharwal</i>	
A New Approach to Measure Milk Fat Content by Using Multiple Back-scattering of Gamma Photons	259
<i>Rohit, Inderjeet Singh, Bhajan Singh, B.S. Sandhu and Arvind D. Sabharwal</i>	
Distribution of Radionuclides in Beach Sand Samples Along the Coastal Line of Kerala, India	261
<i>Ramsiya M, Vishnu CV, Antony Joeph, Eappen KP</i>	
Technetium-99: New Resins Developments For Separation And Isolation From Various Matrices	263
<i>N Maudoux, L. Phelippeau, M. Bas , N. Vajda, A. Bombard, S. Happel, C. Dirks</i>	
New TK200 Resin: Uses for Actinides Preconcentration and Separation	265
<i>A Bombard, S Happel, M Bas, N Vajda, C Dirks</i>	
Use of Electron Beam Irradiation for Improving Reactivity of Dissolving Pulp for Viscose Process	267
<i>Sachin Gondhalekar, Pravin Pawar, Sunil Dhumal</i>	

Measurement of Natural Radioactivity and Gamma Self Absorption Correction in Construction Materials	269
<i>Salma Boukhalfa, Rachid Khelifi</i>	
Studies on ²⁰⁸Po-Hesperidin Association	271
<i>Susanta Lahiri, Dibyasree Choudhury, Nabanita Naskar, Kalpita Ghosh</i>	
Hot Fusion of Fission Fragments for The Synthesis Of Doubly Magic Nucleus ³¹⁰₁₂₆X₁₈₄	273
<i>Dalip Singh Verma and Kushmakshi</i>	
Calculation Method for Detection Efficiency of Voluminous Samples	275
<i>Salma Boukhalfa, Kahina Belkessa and Rachid Khelifi</i>	
Studies on Extraction of Zirconium by Potato Peel - a Potential Bio-sorbent	277
<i>Nabanita Naskar, Dibyasree Choudhury, Shalmali Basu, Kakoli Banerjee</i>	
Evaluation Of The β-delayed Neutron Emission Probability Data And A Study of Their Systematics[#]	279
<i>G. Mukherjee and K. Bannerjee</i>	
Shell Effect on the Dynamics of the Fusion Fission Process	281
<i>A. Sen, T.K. Ghosh, S. Bhattacharya, K. Bannerjee, C. Bhattacharya, Samir Kundu, G. Mukherjee, A. Asgar, A. Dey, A. Dhal, Moin Shaikh, J.K. Meena, S. Manna, Pratap Roy, R. Pandey, T.K. Rana, T. Roy, V. Shrivatava</i>	
Electron Beam Irradiation Effect on Structure, Morphology and, Optical Properties of PVDF HFP/PEO Blend Polymer Electrolyte Film	283
<i>Yesappa L, Ashokkumar SP, Vijeth H, Vandana M, Basappa M, Niranjana M, Ganesh S, Devendrappa H</i>	
Assessment of Natural Radionuclide Enrichment and Radiation Hazard from Building Materials in Kannur District, Kerala	285
<i>K. Nadira Mahamood, C.S. Kaliprasad, Y. Narayana, V. Prakash</i>	
Local Structural investigation of NBS glass for Beta irradiation damage using EXAFS & TDPAC	287
<i>Ashwani Kumar, Nidhi Sharma, S.A. Khader, R.K. Mishra, D. Bhattacharya, Neetika Rawat</i>	
Probing electronic environment in Simulated Waste glass for β-irradiation damage using TDPAC	289
<i>Ashwani Kumar, S.A. Khader, R.K. Mishra, Neetika Rawat</i>	
Radiological Status in Marine Materials Collected from the St. Martin Island of Bangladesh	291
<i>Al Amin, M.H.Miah, Shahadat Hossain, Mayeen Uddin Khandaker, M. N. Mustafa</i>	
Indoor Radon Measurements in Newly Houses of Tashkent City by CR-39 Detectors	293
<i>Abdisamat Vasidov, Sevara Vasidova</i>	

Applications of dosimetric measurements to Quality studies and optimization of operating conditions at a linear accelerator	295
<i>Abdelmajid Choukri, Ahmed El Mouna Ould Mohammed Yeslem, Oum Keltoum Hakam, Slimane Semghouli</i>	
Measurements of U Isotopes Activities in Drinking Water Samples by Alpha Spectrometry and Ra Isotopes by Gamma Spectrometry	297
<i>Abdelmajid Choukri, Oum Keltoum Hakam</i>	
Production of ^{186}gRe Using 12MeV Protons on Natural WO_3 Target	299
<i>S.V.Thakare, K.C.Jagadeesan, Rubel Chabraborty, S.V. Suryanarayana, K.P.Muthe, Ajay Singh, B.K.Nayak, A.Dash and A. Saxena</i>	
Photons from Low Power X-Ray Tube for Chemical Shift Studies	301
<i>Preeti Rao and Raj Mittal</i>	
Projected Application of a Mixer-settler in Transactinide Elements (TAN) Separation Science	303
<i>Rupesh H. Gaikwad</i>	
Determination of Radiation Shielding Parameters for Organic Compounds at Different Gamma Photon Energies Using Compton Scattering Geometry	305
<i>Mohinder Singh, Akash Tondon, Bhajan Singh, B. S. Sandhu</i>	
Effect of Aluminium Ion Implantation on Structural, Morphological, Electrical and Mechanical Properties of a Template Electrosynthesized Cu Nanowires	307
<i>Rashi Gupta and Rajesh Kumar</i>	
A Comparison of Expanded Uncertainties by Pseudo-Cyclic Epithermal INAA in Conjunction with Anticoincidence Counting using Comparator and k_0 Procedures for measuring Iodine Levels in Ghanaian Foods	309
<i>B.J.B. Nyarko, E.H.K. Akaho, J.J. Fletcher, A. Chatt</i>	
Fusion - fission Dynamics for The Pre-actinides and Actinides Near The Coulomb Barrier Energies	311
<i>Abhirup Chaudhuri</i>	
Measurement of Natural Radionuclides For Samples Very Rich In Thorium By Gamma Spectrometry - Mandena Deposit, South Madagascar	313
<i>Duong Van Hao</i>	
Measurement of Excitation Functions of The $^{206/207/208}\text{Pb}(^{11}\text{B},x)^{212}\text{Fr}$ Reactions and Complex Formation Studies of Fr With Crown Ethers	315
<i>Y. Komori, H. Haba, T. Yokokita, S. Yano, N. Sato, K. Ghosh, Y. Sakemi, H. Kawamura</i>	
Quantification of Short-Lived Radioisotopes from 1.4 GeV Proton Irradiated LBE Target	317
<i>Dibyasree Choudhury, Susanta Lahiri, Nabanita Naskar, Melanie Delonca, Thierry Stora, Joao Pedro Ramos, Elodie Aubert, Alexandre Dorsival, Joachim Voltaire, Ricardo Augusto, Alfredo Ferrari</i>	

Measurement of Gross α, β in Water Samples Collected from Indian Sundarbans	319
<i>Nabanita Naskar, Sayantani Mitra, Susanta Lahiri, Punarbasu Chaudhuri</i>	
Study of Natural Radioactivity and Radon Exhalation Rate in Rocks and Water samples in Garhwal Himalaya Region	321
<i>Manjulata Yadav, Mukesh Prasad, R.C Ramola</i>	
Determination of ^{129}I in Aerosols Using Pyrolysis and AgI-AgCl Coprecipitation Separation and Accelerator Mass Spectrometry Measurement	323
<i>Luyuan Zhang, Xiaolin Hou , Yunchong Fu , Miao Fang , Ning Chen</i>	
Clinical Dose Formulation and Evaluation of ^{177}Lu-DOTA-bisphosphonate: A Next Generation Radiopharmaceutical for Palliative Care of Painful Bone Metastases	325
<i>Sudipta Chakraborty, K. V. Vimalnath, Rubel Chakravarty, H. D. Sarma, K. Kamaleswaran, Ajit Shinto, Ashutosh Dash</i>	
Potential Use of Iron-oxide Immobilized Natural Sand in The Removal of Cs(I) and Sr(II) From Aqueous Solutions	327
<i>Diwakar Tiwari, Lalhmunsiam</i>	
Heavy Ion Activation: Treasure of Non-Conventional Neutron Deficient Radionuclides	329
<i>Susanta Lahiri</i>	
Author Index	331

Plenary and Invited Lectures

Separations Science for Radioactive Materials: Some Perspectives

*P.R. Vasudeva Rao**

Homi Bhabha National Institute, Mumbai

*E-mail: vasudeva@hbni.ac.in

Separation of actinides, fission products and other radioisotopes at various concentration levels continues to demand the development of innovative procedures. This includes development of new separation systems, based on solvent extraction, ion exchange, membrane separation, etc. The issues to be addressed by development are based on the targeted application. The challenges for macro level extraction include the phenomenon of third phase formation, in many extraction systems. Choice of the extractant should also be based on overall evaluation taking into account related aspects such as wastes generated by the process, impact of the extractant and diluent used on environment, ease of synthesis, radiation and chemical stability, recyclability, etc. For applications related to analysis and for other separations at small scale, including tracer scale separations, many such restrictions may not apply, and a host of new procedures including ion imprinted polymers, chelating ion exchangers etc. can be envisaged. In more recent times, the emphasis on “green chemistry” has made it attractive to develop environment friendly extraction systems. The impetus on room temperature ionic liquids has further diversified the design of extraction systems.

This presentation deals with the challenges related to the design of the separations systems and particularly the solvent extraction systems.

Beaming Ubiquitous Neutrinos and The “Dark” Universe

*Swapan Chattopadhyay**

Fermilab and Northern Illinois University, USA

*E-mail: swapan@fnal.gov

Introduction

The paradigm of present-day accelerator-driven nuclear and particle physics research started in the early 1930s. At earlier times (and overlapping somewhat in 1930s, 1940s and 1950s with accelerator-driven research), exploration of energetic ‘cosmic rays’ via scientifically-equipped balloon launches in the atmosphere and photographic plates carried to high altitudes in mountaineering expeditions continued. However with the advent of inventions and innovative laboratory techniques from 1930s onwards (Lawrence’s invention of the cyclotron, subsequent invention of synchrotrons by McMillan and Veksler, linear charged particle accelerators by Wideroe and Varian and particle colliders in the 1960s onwards), it proved much easier to create the required high energies and energy densities in a charged particle accelerator facility in a ground-based laboratory rather than the arduous, difficult and inefficient balloon launches and high altitude expeditions.

From 1920s until today, spanning almost a century of these explorations, these atmospheric expeditions and later terrestrial accelerator-driven laboratory investigations have offered us a reasonably satisfactory description of the material world in the form of the Standard Model of Particle Physics down to a certain space-time scale (0.1 femtometer i.e. 10^{-16} meter and zepto-seconds i.e. 10^{-21} seconds) and up to a certain mass-energy scale of elementary particles (approximately 10 TeV). But this theory is highly incomplete and fundamental questions remain. Two such very basic questions at the frontier of our present-day knowledge of the material world are: (a) the question of the ubiquitous ‘Neutrinos’ as totally mysterious particles to be ‘understood’ in terms of their properties and alleged role in the big picture of the universe and cosmos; and (b) the question of the ‘dark universe’, which appears to constitute about 95% of the entire energy-matter content of the universe and yet so far have

eluded any direct detection while teasing scientists with latent evidences in multiple experiments. We describe below two avenues to chase these two questions via beams.

Chasing Neutrinos with High Intensity Proton Beams

The first of these two fundamental questions, that of the nature and role of neutrinos, is being addressed today via terrestrial laboratory experiments utilizing energetic and intense beams of neutrinos traveling long distances of thousands of kilometers and detected at multiple locations along its linear traverse on earth in large specially designed detectors. Half of this lecture will provide an overview of the currently envisaged landscape of charge particle accelerators at the energy and intensity frontiers to explore particle physics beyond the Standard Model via multi-Megawatt proton accelerators for short- and long-baseline neutrino experiments. The particle beam physics, associated technological challenges and progress to date for the frontier accelerator facility – the high intensity proton accelerator complex PIP-II at Fermilab in support of the international experiment DUNE (Deep Underground Neutrino Experiment) and its planned future upgrade -- will be outlined [1]. Advanced “nonlinear dynamic techniques” --- to be developed and tested at Fermilab Accelerator Science Test (FAST) facility and its Integrable Optics Test Accelerator (IOTA) --- will be touched upon. These facilities are envisaged to advance accelerator science of Coulomb-dominated high intensity hadron beams and the underlying nonlinear dynamics as well as offer innovative precision experiments to test novel techniques of beam phase-space manipulation and control. These experiments will advance the future potential of the high power long baseline neutrino experiments using high intensity proton beams going beyond the currently envisioned PIP-II capabilities.



Figure 1. Long baseline Neutrino Experiment DUNE

Atomic Beams as Quantum Sensors of the “Dark” Universe

The second of these two fundamental questions --- that of the nature and role of the “dark universe” – is a very broad and deep subject with multiple facets. At a very coarse level, the so-called “visible” and “dark” universe appears to be composed of “ordinary matter”, “dark matter” and “dark energy”

components, in an approximate ratio of 5 : 20 : 70 or 1 : 4 : 14. Tremendous advances have been made in the last two decades in precision ‘Quantum’ technologies and techniques in multiple disciplines e.g. cavity electrodynamics, atomic beam interferometry, SQUIDS, quantum optical “squeezed state” techniques for noise-free single photon detection, qubit-based quantum entanglement techniques, high-Q superconducting cavities, precision NMR detection via designer materials, etc. These advances offer us an alternative research paradigm – rather than producing the necessary energies and energy densities via brute force application of particle beams in an expensive and large laboratory-based accelerator complex, these techniques promise to enable transformational research using ultra-sensitive compact probes as passive ‘sensors’ in a compact laboratory scale to explore very “weak effects” and “ultra-weak signals”, left over from the early history of the universe. This is sort of an ‘archaeological’ approach of searching for the left-over fossils. These weak effects are manifest everywhere in nature in material and living systems from the laboratory to outer space. Potential “mezzo-scale” experiments and facilities can be envisaged using “quantum sensors” to search for ultra-weak physical, chemical or biological signals of fundamental significance to the material and living world around us as well as explore the “inner” and “outer” dimension of “vacuum” believed to be manifest in the so-called “dark” universe. I will illustrate this potential via an elegant but exciting example of a planned atomic beam interferometer experiment known as “MAGIS-100” [2], as a sensor of the “dark universe” and ‘primordial’ gravitational waves -- the tremor in space-time left over as the aftershock of the cataclysmic event that took place approximately 13.8 billion years ago in the so-called “Big Bang” beginning of our current universe that we find ourselves in.

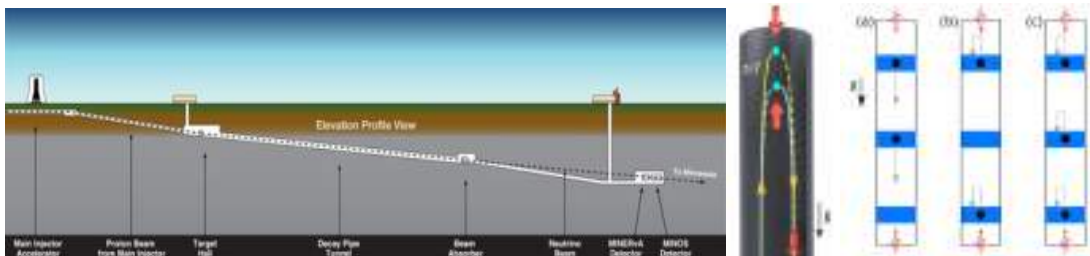


Figure 2. Proposed MAGIS - 100 Experiment at Fermilab

References

- /1/ M. Syphers and S. Chattopadhyay, “ Landscape of Future Accelerators at the Energy and Intensity Frontiers”, PROCEEDINGS of SCIENCE (<https://pos.sissa.it/>), 38th International Conference on High Energy Physics, ICHEPP 2016, 3-10 August, 2016, Chicago, USA.
- /2/ J. Coleman et al., “MAGIS100@FERMILAB”, 39th International Conference on High Energy Physics, ICHEPP 2018, 4-11 June, 2018, COEX, SEOUL, South Korea

Recent Highlights and Trends Applying Radioactive Ion Beams to Solid State Physics: ISOLDE and Beyond

*Karl Johnston**

ISOLDE/CERN, EP Dept, Geneva 23 CH-1211, Switzerland

*E-mail: karl.johnston@cern.ch

1. The Materials science programme at ISOLDE

Solid state Physics research at ISOLDE (CERN) has been running since the mid-1970s and accounts for about 10-15% of the overall physics programme. ISOLDE is the world flagship for the on-line production of exotic radioactive isotopes, with high yields, high elemental selectivity and isotopic purity. Consequently, it hosts a wide variety of state-of-the-art nuclear techniques which apply nuclear methods to research on life sciences, material science and bio-chemical physics. The ease of detecting radioactivity – < 1 ppm concentrations – is one of the features which distinguishes the use of radioisotopes for materials science research. The manner in which nuclear momenta of excited nuclear states interact with their local electronic and magnetic environment, or how charged emitted particles interact with the crystalline lattices allow the determination of the location, its action and the role of the selected impurity element at the nanoscopic state. ISOLDE offers an unrivalled range of available radioactive elements and this is attracting an increasing user community in the field of nuclear solid state physics research and brings together a community of materials scientists and specialists in nuclear solid state techniques [1].

1.1 Recent trends in materials science and radioactive ion beams: This talk will detail the use of specific isotopes which are available either only at ISOLDE or at other select facilities worldwide – but which will be readily available at the next generation of radioactive ion beam facilities worldwide – and their uses in materials science and medicine. In addition to a presentation of the current state of the art – including the application of radioactive ions to novel materials such as two-dimensional materials such as graphene, topological insulators and multi-layered solar cells. Some of the challenges will be

presented along with perspectives for the forthcoming facilities currently under construction worldwide, see figure 1.

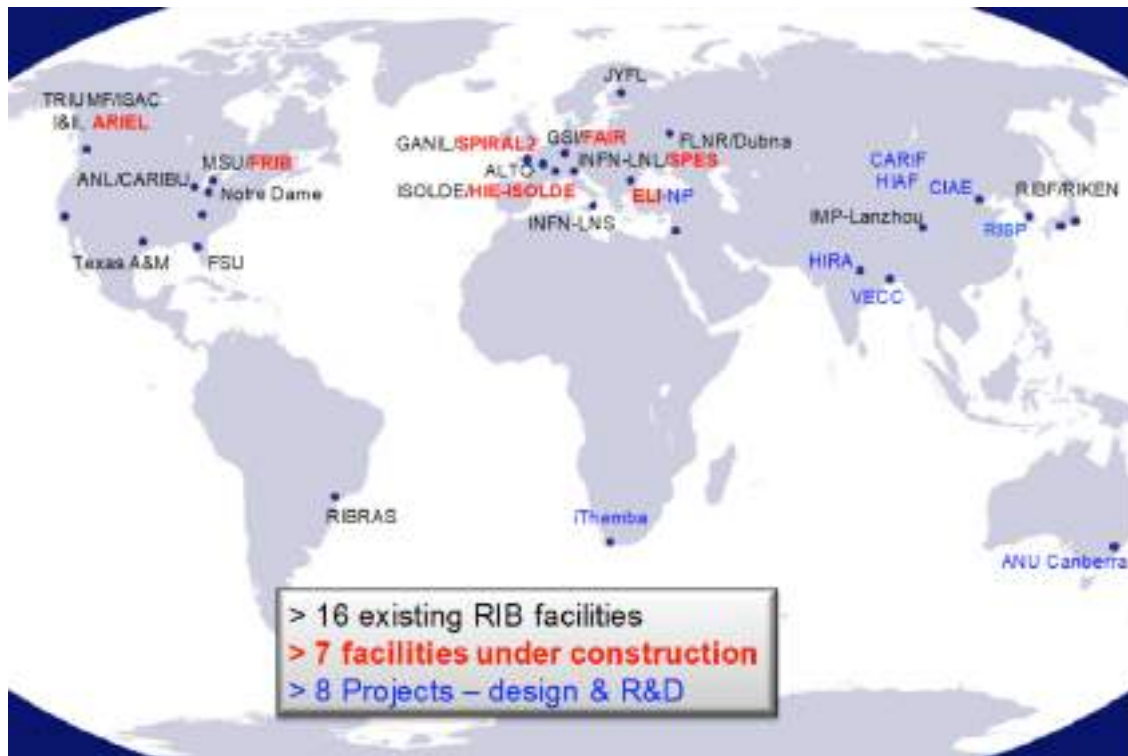


Figure 1. An overview of RIB facilities worldwide either operating or currently under construction.

References

- /1/ K. Johnston, J. Schell, J. G. Correia, M. Deicher, H. P. Gunnlaugsson, A. S. Fenta, E. David-Bosne, A. R. G. Costa and Doru C Lupascu, J. Phys. G: Nucl. Particle Phys. 44 (2017) 104001

Local Probing Complex Oxides Using Perturbed Angular Correlations

J. P. Araújo^{1}, G. N. P. Oliveira¹, R. C. Teixeira¹, P. Rocha-Rodrigues¹, T. Leal¹,
R. Moreira¹, J. G. Correia², A. M. L. Lopes¹*

¹IFIMUP and IN—Institute of Nanoscience and Nanotechnology, Departamento de Física e Astronomia da Faculdade de Ciências da Universidade do Porto, Rua do Campo Alegre, 687, Porto 4769-007, Portugal.

²Centro de Ciências e Tecnologias Nucleares, Instituto Superior Técnico, Universidade de Lisboa, 2686-953 Sacavém, Portugal

*E-mail: jearaujo@fc.up.pt

1. Introduction

Systems with entangled degrees of freedom and cross-coupling effects, especially complex magnetic oxides, multiferroic and magnetoelectric materials, are fascinating field of material science. The high sensitivity of these complex systems to lattice-distortions leads to outstanding physical properties, where the manipulation of these distortions offers prospects for new functionalities. In fact, this by far unexploited capability promises new paradigm-shift technologies.

In such compounds, lattice local distortions have a fundamental influence in the macroscopic proprieties and these features are not well described by methods based on long-range average structural models. Local probe studies are thus of the most importance to understand the microscopic mechanisms inherent to the macroscopic proprieties. In the last years we used the perturbed angular correlations (PAC) technique to locally monitor different magnetic oxides systems allowing the determination of Electrical-Field Gradients (EFG) and Hyperfine Magnetic Fields.

2. Case studies

This technique complemented with other local or macroscopic techniques allowed to report several studies focus on polaron dynamics, charge order, magnetostructural and multiferroic phase transitions.

2.1 *SmCrO3 Orthochromites and related systems:* In the rare earth (R) orthochromite SmCrO₃ the EFG temperature dependence at the R site was followed via perturbed angular correlation measurements.

The data shows that a distortion of the high temperature Pbnm environment start to develop locally below room temperature within the paramagnetic phase. Although the data might be compatible with the most recent reports, where polar octahedral rotations and/or cation displacements are at the origin of a polar order in the paramagnetic state [1], the results point to a subtler scenario, where locally an inhomogeneous state emerges.

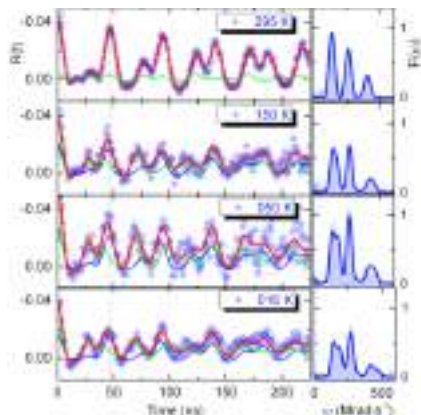


Figure 1. Representative $R(t)$ functions, corresponding fits and respective Fourier transform at different temperatures for SmCrO_3

2.2 Manganite perovskites and Ruddlesden Popper systems: Recent theoretical calculations suggest that $\text{Ca}_3\text{Mn}_2\text{O}_7$, a member of the Ruddlesden Popper family, may undergo a structural transition to a ferroelectric state above this temperature [1]. Here, a spontaneous ferroelectric polarization is expected, resultant of a tri-linear coupling of two non-polar lattice distortion modes (octahedral rotation/tilting modes) with a polar displacement mode. Within the reported related perovskite materials, the $\text{Ca}_3\text{Mn}_2\text{O}_7$ also exhibits a peculiar large uniaxial negative thermal expansion, reaching a maximum between. However, the microscopic mechanism governing these phenomena is not yet fully understood. Here, the unique behavior of $\text{Ca}_3\text{Mn}_2\text{O}_7$, the several structural, charge and magnetic phase transitions, is studied by combining theoretical and experimental PAC method, in a window range of 11 K to 1153 K, in order to unravel the local electronic and magnetic properties. The theoretical approach is performed using ab-initio electronic structure calculations, in the framework of the Density Functional Theory (DFT). Through this comparison, a local scenario of the complex behavior in this class of systems is derived.

References

- /1/ N. A. Benedek, J. M. Rondinelli, H. Djani, P. Ghosez, and P. Lightfoote, Dalton Trans., 44 (2015) 10543-10558.

Forty Years of VECC

*Amitava Roy**

Variable Energy Cyclotron Centre, 1/AF Bidhannagar, Kolkata 700064, India

*E-mail: amitav@vecc.gov.in

The research on nuclear science in India was initiated in an organized form by Dr. Homi J. Bhabha in 1945 when he setup TIFR at Mumbai. The importance of Cyclotron for research in nuclear physics was conceived by Dr. Bhabha in 1965 and the K130 machine similar to LBL K130 machine was decided upon. The activity at Kolkata (the then Calcutta) started in 1969 by BARC. The machine was commissioned in 1977 and first beam came out on 16th June, 1977. The mandate of the Centre was to carry out research in experimental nuclear physics, radiation damage studies and isotope production for research and nuclear medicine. The centre became a national facility with full-fledged design and development facilities for mechanical engineering, power electronics, RF engineering and computation. To support the experimental nuclear physicist a strong theory group also emerged. The centre became an independent unit of DAE in May, 1990. Over the years the expertise grew in other fields of science like accelerator design and related technology development, cryogenics, VECC also emerged as a hub for international collaboration in High Energy Physics and accelerator technology. VECC has active collaborations with CERN, BNL, FAIR, TRIUMF, RIKEN, GANIL, DUBNA.

The present cyclotron started operating with proton and alpha beam with PIG ion source and delivered light ion beams upto 20 MeV/n. The machine was upgraded to accelerate light heavy ion with ECR ion source and accelerated heavy ion beams up to 8-10 MeV/n ¹⁶O, ²⁰Ne ⁴⁰Ar. In 2009 the machine was put back to light ion again to facilitate testing of thick target for RI production due to availability of high current from light ion. At present the machine is running with both PIG ion source and an indigenously built ECR to cater to wide range of gaseous ion beams from Proton to Argon.

To enhance the experimental capability Superconducting cyclotron with bending limit of the magnet of K=520 and RF range of 9 MHz to 27 MHz was built. The machine is expected to deliver beams of 80 MeV/n for light ion and 20 MeV/n for ⁸⁶Kr and around an 8 to 10 MeV/n for Uranium.

Apart from the cyclotron, to widen the scope of experiments in the field of exotic nuclei, the RIB facility was conceived to produce Radioactive Ion Beam with energy 1.3 MeV/n with cyclotron as

the primary beam to produce radioactive beam which would further be ionized with ECR ion source followed by pre-acceleration and focusing by RFQ followed by acceleration through series of Linacs. As a natural following step in the research on exotic nuclei VECC has also undertaken a flagship program of ANURIB (Advanced National facility for Unstable & Rare-Isotope Beams). The proposed project is conceived to be completed in two phases. In the first phase RIB produced with photo-fission with high energy photon emitted, by stopping electron beam of 50 MeV and 2 mA (100 KW beam power) produced in superconducting electron Linac, will be accelerated by heavy-ion Linac upto 1 MeV/n and with Linac booster upto 7 MeV/n. The S-e-Linac is being jointly designed by TRIUMF at Canada and VECC. The fabrication and testing has been carried out at TRIUMF.

VECC being a knowledge base of Cyclotrons, DAE ventured to commission a Medical Cyclotron at Kolkata with VECC taking the lead role. This is a fixed energy cyclotron of 30 MeV proton up to a current of 500 micro-amp. This would not only be used for production of radioisotopes for nuclear medicine as a DAE's contribution to societal cause but also can be used to study on radiation damage of nuclear reactor material, as well as it can be used to study space material with accelerated aging through radiation damage.

The experimental research area on nuclear physics at VECC are broadly in the field of i) Nuclear Structure Studies in both continuum and discrete gamma ray spectroscopy, ii) Nuclear Reaction studies including Hoyle state of ^{12}C , binary complex fragment decay of the nucleus, transfer reactions etc, iii) Nuclear Fission studies such as fusion fission dynamics, fission time scales etc iv) Neutron Spectroscopy. In the area of material science and radiation damage studies using charged particle on different nuclear core structural materials are being done with respect to structural changes, microstructural changes, changes in mechanical properties like U.T.S, Y.S., percentage elongation or ductility, microhardness etc. in order to simulate the reactor damage. Modification of surface topography and nano-patterning in solids by low energy ion beams from ECR is also an area of research. Study of defects induced ferromagnetic ordering using low energy ion beam on semiconductor materials are also investigated.

The board research areas of research on theoretical nuclear physics are the quark-hadron phase transition at high temperature and density, the space-time evolution and signals of quark gluon plasma, Spectral function of hadrons at finite temperature and density, Hadrons in high magnetic field, Relativistic viscous hydrodynamics, Liquid-gas phase transition in nuclear system, Microscopic studies of fission dynamics, Dynamical study of nuclear collisions using Boltzmann transport equation, Nuclear reactions and nuclear astrophysics, Many body physics and quantum chaos.

Apart from the above, research on chemical separation of radio isotopes, separation of isotopes for use in radio pharmaceuticals and trace element studies are also carried out.

FRENA – A Low Energy, High Current Accelerator Facility For Research in Nuclear Astrophysics

*Subinit Roy**

Nuclear Physics Division, Saha Institute of Nuclear Physics, 1/AF Bidhannagar, Kolkata 700064, India.

**E-mail: subinit.roy@saha.ac.in*

Following the seminal work of Burbidge, Burbidge, Fowler and Hoyle in 1957 [1], Nuclear Astrophysics has evolved as a vibrant field studying the fundamental questions related to the synthesis of elements through various nuclear processes [2]. The study of nuclear astrophysics involves precise measurement of reaction rates with very low cross sections at astrophysical energies. The effort requires intense, stable beams of different species from the accelerators with energies ranging from several keV to tens of MeV in order to cover the various astrophysical conditions. Each reaction of relevance represents a case of its own and requires specialized experimental tools.

With the aim of developing a facility for research in experimental nuclear astrophysics, Saha Institute of Nuclear Physics, Kolkata proposed FRENA, Facility for Research in Experimental Nuclear Astrophysics. The proposed facility is presently under the process of installation.. This accelerator has primarily been procured from High Voltage Engineering, The Netherlands. The machine is capable of delivering high beam currents required for experiments studying the reactions of astrophysical interest.

The accelerator uses a Cockroft-Walton type voltage generator that can provide terminal voltages in the range of 0.2-3.0 MV [3]. The machine uses three different ion-sources to provide light-ion beams like ^1H , ^3He and ^4He as well as all heavy-ions up to ^{197}Au . The light ion source consists of a dual source injector with a multi-cusp ionsource for ^1H and another multi-cusp source for ^3He and ^4He . A facility for chopper-buncher arrangement is also included with the light ion channel to obtain pulsed ^1H , ^3He and ^4He beams. The heavy ions are provided by a SNICS type sputter ion source. The negative sputter multi-target (50 target carousel) heavy ion source has been specially configured in view of the long-duration measurements, essential in the study of reactions with low cross-sections that necessitate repeated change of ion-source targets. One of the strong features of Tandatron-based accelerators is the stable operation at low energies.

A sketch of the accelerator along with its components is shown in Fig.1. The system is provided with two beam lines at present, one for the nuclear astrophysics applications after the second high energy switching magnet and the other is a beam line for pulsed beam applications.



Figure 1. Schematic diagram of the accelerator of FRENA. The red box highlights the ion-source station of the machine.

The energy domain of FRENA will be most suitable to study the heavy ion fusion reactions in nuclear astrophysics [3]. Hence, the $^{12}\text{C} + ^{12}\text{C}$ reaction, the rate of the reaction is one of the key quantities needed to understand the evolution of massive stars (> 8 Solar Mass) may be the first one which will be attempted. The proton capture reaction $^{14}\text{N}(p,\gamma)^{15}\text{O}$, the slowest reaction of the CNO cycle, regulates the power generated by the cycle and thus influences the structure and evolution of every star. Studying this reaction at FRENA is a part of the immediate physics goal. Studying the sub-coulomb transfer reactions as an indirect technique to extract the astrophysically relevant quantities, especially for reactions like alpha capture reaction $^{12}\text{C}(\alpha,\gamma)$, will also be pursued.

References

- /1/ E. M .Burbidge, G. R. Burbidge, W. A. Fowler, F. Hoyle, Rev. Mod. Phys. 29 (1957) 547.
- /2/ Almudena Arcones, et al., Prog. In Particle and Nucl. Phys. 94 (2017) 1.
- /3/ G.W.W. Quax, A. Gott dang, D.J.W. Mous, Rev. Scientific Instrum. 81 (2010) 02A701.
- /4/ B.B.Back, et al., Rev. Mod. Phys. 86 (2014) 317.

Overview of The Pelletron Linac Facility, Mumbai

*Vandana Nanal**

Department of Nuclear and Atomic Physics, Tata Institute of Fundamental Research, Mumbai, India 400005

*E-mail: nanal@tifr.res.in

The Pelletron LINAC Facility at Mumbai, comprising the 14 MV Pelletron and indigenously developed superconducting LINAC booster, set up as a collaborative project between the Bhabha Atomic Research Centre and the Tata Institute of Fundamental Research, has been serving as a major facility for heavy ion accelerator based research in India for about three decades. The Pelletron was commissioned in 1988 [1] and the superconducting LINAC booster has been operational since 2007 [2,3]. The Pelletron serves both as a standalone accelerator and as an injector to the superconducting LINAC booster. Several advanced experimental facilities have been established at this centre to pursue research in nuclear, atomic, condensed matter physics and interdisciplinary areas. A number of application based research programmes have also been taken up using this accelerator. The research work in nuclear physics, which forms the main thrust of activities at this facility, covers areas of nuclear structure studies at high angular momentum and excitation energies and the heavy ion reaction dynamics. A successful campaign with the INGA (Indian National Gamma array) setup, designed for 24 HPGe Clover detectors, was recently completed. A high current ($\sim\mu\text{A}$) proton irradiation facility has been setup above the analysing magnet. This is also extensively used for neutron irradiation/reaction studies using Li/Be targets. While the majority of the researchers at this facility are from BARC and TIFR, the experimental community encompasses scientists and students from other research centres and universities within and outside the country. These three decades of operations have been scientifically stimulating and very productive. More than 120 Ph.D. theses and over 700 publications in refereed international journals have resulted from the research activities in this laboratory. The talk will present an overview of the facility including experimental programs and a brief description of future plans.

References

- /1/ S.S. Kapoor, V.A. Hattangadi and M.S. Bhatia, Indian J. Pure and Appl. Phys. 27 (1989) 623
- /2/ R.G. Pillay, Proceedings of DAE symposium on Nuclear Physics, 52 (2007) 182
- /3/ V. Nanal *et al.* <http://accelconf.web.cern.ch/AccelConf/HIAT2009/papers/th-07.pdf>, HIAT09 proceedings, 2009

Radioactive Tumor Specific Gold-198 Nanoparticles in Nuclear Medicine: Green Nanotechnology and Radiochemical Approaches in Nano-Radiopharmaceuticals

Kattesh V. Katti^{1}, Kavita K Katti¹, Ademar B Lugao²*

¹Curators' Professor of Radiology and Physics, Director, Institute of Green Nanotechnology, University of Missouri Hospitals and Clinics, One Hospital Drive; University of Missouri; Columbia, Missouri 65212, USA.
² Nanotechnology Program Coordinator, Instituto de Pesquisas Energeticas e Nucleares- IPEN-CNEN, Sao Paulo, Brazil.

*E-mail: KattiK@health.missouri.edu

Although the various isotopes of Gold, including Gold-198 and Gold-199, were discovered in the early 1930s (1), the wide spread utility of these dual beta and gamma emitting isotopes has lagged mostly due to ineffective delivery vehicles that afford tumor selectivity and retention of optimum therapeutic payloads within tumors. The most common radioisotope of gold (Gold-198) is made by a neutron capture reaction in a nuclear reactor. This radiochemical transformation is particularly attractive for two reasons: (i) The target material is metallic gold which is available in a high state of purity readily and the metal is both chemically and physically stable; and (ii) the high cross-section of the neutron capture reaction 98.8 barns in a nuclear reactor of a moderate size—enables the production of optimum specific activity for clinical applications. Au-198 and its nanoparticles comprise of over 85 % of the nonradioactive gold. The radiative emissions (Beta and gamma) irradiation provide effective photoelectric interactions and a pronounced generation of Auger and/or Coster-Kronig electrons. These electron cascades present realistic prospects in cancer therapy. The ejection of electrons leaves the decaying atoms transiently in a state of high positive charge as the burst of low energy electrons results in highly localized energy deposition (106–109 cGy) in an extremely small volume of several cubic nanometers around the decay site, and these electrons will irradiate molecules in the immediate vicinity of the decaying atoms. Immense clinical advantages can be derived through the dissipation of the potential energy associated with the high positive charge and its neutralization occurring concomitantly leading to localized tumor therapeutic effects. Our series of recent studies have already

generated extensive therapeutic efficacy data from the treatment of tumors in mice and tumor bearing dogs (where the disease mimics human cancers)

Typically, with a neutron flux of $2 \times 10^{13} \text{ n/cm}^2/\text{s}$, 1 curie per gram of specific activity is feasible in 6.5 hours or 77 curies per gram in 65 hours. A vast majority of nuclear medicine applications of ^{198}Au , to date, have been in the form of implants known as "gold grains or brachy gold seeds" in the treatment of malignancies in the brain and prostate. If effective delivery vehicles and tumor retention technologies are developed, the radioactive properties of ^{198}Au ($\beta_{\text{max}} = 0.96 \text{ MeV}$; $t_{1/2} = 2.7 \text{ d}$) and ^{199}Au ($\beta_{\text{max}} = 0.46 \text{ MeV}$; $t_{1/2} = 3.14 \text{ d}$) make them ideal candidates for use in extensive radiotherapeutic applications. Imageable gamma emissions for both ^{198}Au and ^{199}Au provide unprecedented theranostic features for dosimetry and pharmacokinetic studies. Despite these favorable properties, Gold-198/199 radiopharmaceuticals have not been pursued due to significant challenges in stabilizing them *in vivo*. Nanoparticles of gold, when conjugated with tumor receptor specific biomolecules, present attractive characteristics to achieve tumor selectivity and tumor retention. This hypothesis was for the first time experimentally validated by Katti. et al(2). The pioneering work utilized an innovative approach wherein trimeric glycine or alanine conjugates (P(A)_3 ; A = Glycine or Alanine), recently referred to as 'Katti Peptides', were used to transform ^{198}Au precursor ($^{198}\text{AuCl}_4$) to the corresponding ^{198}Au nanoparticles with well-defined particulate size (15-20 nm)(2). Traditional methods, which use NaBH_4 (and other reducing agents) for the production of gold nanoparticles (AuNPs) at macroscopic levels, fail when used at ^{198}Au tracer levels to produce ^{198}Au nanoparticulate radioactive gold. Therefore, the radioactive gold nanotechnology pioneered by Katti et al, is efficient for the production of nanoparticulate ^{198}Au gold agent even at concentrations of 10^{-10} - 10^{-12}M with no toxic chemical byproducts.

One particularly attractive feature of radioactive gold nanoparticles is that it does not have to be incorporated into every tumor cell to have a therapeutic effect. The path length of the emitted radiation is sufficient to allow effective therapy following uptake into a subpopulation of tumor cells. This feature has attracted recent attention to apply nanotechnology for the effective delivery of therapeutic doses of beta emitting gold-198 nanoparticles selectively to tumor tissue and tumor cells. Subsequently, we have carried out extensive *in vitro* and *in vivo* investigations to validate the hypothesis that glyco protein (Gum Arabic (GA)) functionalized radioactive ^{198}Au nanoparticles are stable and biocompatible under *in vivo* conditions. Our research efforts have demonstrated that the complex polysaccharides and protein structures within the GA backbone can effectively lock gold nanoparticles on the protein matrix to produce non-toxic gold nanoparticulate constructs (GA-AuNP) which are stable under *in vivo* conditions for potential applications in tumor therapy (2). Our detailed

in vivo studies, through intratumoral administration of GA-¹⁹⁸AuNP (1.5μCi/tumor), in SCID mice bearing human prostate cancer xenografts, have demonstrated retention of over 154.05 ±40.7 %ID/gm within the tumor at 30 min that declined to 87.0±16.9 %ID/gm by 24 h. The overall reduction in tumor volume was 80% three weeks after a single dose intratumoral administration of GA-¹⁹⁸AuNP (408μCi). The therapeutic efficacy data for GA-¹⁹⁸AuNP corroborate their ability to induce tumor staticity because tumors harvested from the treatment group consisted largely of necrotic tissue, indicating extensive tumor cell kill. In our continued efforts to develop tumor specific radioactive gold nanoparticles, we have pioneered the application of Green Nanotechnology for the development of therapeutic radioactive gold nanoparticles. Recently we have discovered that the high antioxidant capacity of Epigallocatechin gallate (EGCG), which is the most abundant catechin polyphenol in tea, and Mangiferin (MGF)—a glucose bearing phytochemical from mango, can be used to convert radioactive Gold-198 precursor to the corresponding biocompatible tumor specific radioactive gold nanoparticles functionalized with Laminin receptor specific EGCG or MGF. Laminin receptors are overexpressed in a large number of human tumors and the high *in vivo* affinity of EGCG and MGF toward Laminin receptors has allowed the development of Laminin receptor specific radioactive gold nanoparticles to achieve tumor specificity (2, 3). This lecture will present: (a) scope and prospects of beta emitting Au-198/Au-199 radioisotopes in the development of nano radiopharmaceuticals; (b) details on the intervention of nuclear activation analysis and various radioanalytical approaches for the production of tumor specific radioactive gold-198 nanoparticles; and (c) full *in vivo* investigations on therapeutic properties of EGCG/MGF-198-AuNP tumor specific radiotherapeutic agents in treating prostate tumors and (d) the overall implications of Green Nanotechnology of therapeutic beta emitting nanoparticles in oncology.

References

- /1/ E. McMillan, M. Kamen, and S. Ruben Phys. Rev. 52 (1937) 375; A.J. Demster, Nature 136 (1935) 65; M.L. Pool, J.M. Cork, and R.L. Thornton, Phys. Rev. 52 (1937) 239; E. Fermi, E. Amaldi, O. D'Agostino, F. Rasetti, and E. Segre, Proc. Roy. Soc. 146A (1934) 483; E. Amaldi, O. D'Agostino, F. Rasetti, and E. Segre, Proc. Roy. Soc. A149 (1935) 522.
- /2/ K. V. Katti et al; J. Radioanal. Nucl. Chem. 309 (2016) 5–14; K. V. Katti, et.al: Wiley Interdisciplinary Reviews: Nanomedicine and Nanobiotechnology; 4 (2012) 42–51; K. V. Katti, et.al; Proceedings of the National Academy of Sciences-PNAS; 109 (2012) 12426-12431
- /3/ K. V. Katti, A. Lugao, et al; Dalton Trans., 46 (2017) 14561-14571.

Production and Application of The Non-Standard-PET Radionuclides ^{52}Mn and ^{73}Se

B. Neumaier^{1,2}, U. Königs, S.M. Qaim, K. Giesen, I. Spahn*

¹Forschungszentrum Jülich GmbH, Institute of Neuroscience and Medicine, INM-5: Nuclear Chemistry, 52425 Jülich, Germany

²Institute of Radiochemistry and Experimental Molecular Imaging, University Hospital Cologne, 50937 Cologne, Germany.

*E-mail: b.neumaier@fz-juelich.de

1. Introduction

Besides the short-lived “organic” PET radionuclides (^{18}F , ^{15}O , ^{13}N and ^{11}C), non-standard positron emitters exhibiting longer half-lives gain more and more clinical relevance. The two main reasons are: A) examination of slow metabolic processes requires extended scan intervals B) opportunity to quantify the radionuclide distribution for targeted therapy [1]. The positron emitter $^{52\text{g}}\text{Mn}$ ($t_{1/2} = 5.59$ d, $\beta^+ = 29.6\%$, $E_{\beta^+} = 0.58$ MeV) has suitable imaging properties. Moreover, the element Mn is employed in MRI contrast agents and thus is also suitable to be used in bimodal PET/MR imaging approaches [2]. ^{73}Se as a sulphur homologue is very interesting for PET imaging ($t_{1/2} = 7.15$ h, $\beta^+ = 64.7\%$, $E_{\beta^+} = 1.3$ MeV). Se can serve as a surrogate in sulphur containing compounds since S itself has no suitable PET imaging isotope. However, there are difficulties in its accessibility and production [3].

2. $^{52\text{g}}\text{Mn}$ for bimodal PET/MR probes

Our aim was to design a PSMA-selective bimodal PET/MR imaging agent. The prostate specific membrane antigen (PSMA) is overexpressed in prostate cancer (PCa) and represents an attractive target for the detection of PCa recurrence. Glu-urea-Lys was identified as a motif with high binding affinity for PSMA. Therefore, this pharmacophoric group should be equipped with a chelator for Mn forming finally a bimodal PET/MR probe.

2.1 Production and Synthesis: $^{52\text{g}}\text{Mn}$ was produced at the BC 1710 cyclotron *via* the $^{nat}\text{Cr}(p,x)^{52\text{g}}\text{Mn}$ reaction over the energy range of $E_p = 16 \rightarrow 10$ MeV in quantities of about 250 MBq.

It was isolated using anion exchange chromatography. The isolation yield of n.c.a. [^{52g}Mn]MnCl₂ amounted to 95.5%. 1,2-Cyclohexandiaminetetraacetic acid (CDTA) was applied as a chelator. For the preparation of the PET/MR probe, CDTA was modified with a linking unit containing an alkyne moiety for Cu-catalyzed azide-alkyne cycloaddition (CuAAC) and was coupled to the azide functionalized Glu-urea-Lys by CuAAC. The labeling yield of this PSMA-selective conjugate with ^{52g}Mn amounted to > 99 %.

2.2 In vivo experiment: After HPLC purification, the ^{52}Mn -labelled probe was administered in rats bearing a U87 human brain tumour. Due to neovascularization PSMA overexpression accumulation of this probe was expected to occur in tumour tissue. A significant enrichment of the tracer in the peripheral zone of the tumour was observed. However, to exclude tracer accumulation owing to blood brain barrier disturbance further control measurements have to be carried out.

3. ^{73}Se for radiopharmaceutical labelling

3.1 Production and Synthesis: ^{73}Se was produced at the JULIC cyclotron *via* the $^{75}\text{As}(p,3n)^{73}\text{Se}$ reaction over the energy range $E_p = 40 \rightarrow 30$ MeV. The irradiated As₂O₃ target was dissolved in sodium hydroxide solution and Se was converted to a piaszelenol complex by addition of 2,3-diaminonaphthalene. Lipophilic [^{73}Se]piaszelenol was separated from the polar arsenic using a RP-18 SPE cartridge. [^{73}Se]piaszelenol was decomposed by heating in hydrogen peroxide solution. After fixation of residual organic compounds on a RP-18 SPE cartridge, the solution was evaporated and selenium was isolated. Finally, elemental ^{73}Se was obtained by reduction with hydrazine.

3.2 Discussion: The yield of this separation process, which took about 3 hours, was 48% in average and the batch yield obtained was about 220 MBq. The suitability of separated ^{73}Se for further labeling reactions was demonstrated by the radiosynthesis of [^{73}Se]Selenomethionine in RCYs of 30 to 50%.

4. References

- /1/ Workshop on Innovative Positron Emitting Radionuclides. Special issue of Radiochim Acta 89 (2011) 607.
- /2/ C. Vanasschen, E. Molnár, G. Tircsó, F.K. Kálmán, É. Tóth, M. Brandt, H.H. Coenen, B. Neumaier, Inorg. Chem. 56 (2017) 7746-7760.
- /3/ U. Königs, S. Humpert, I. Spahn, S.M. Qaim, B. Neumaier, Radiochim. Acta 106 (2018) 497-505.

Converging Technologies for Improving Human Health - Contribution of Ionizing Radiation and Nanotechnology

Kattesh V. Katti², Ademar B. Lugão^{1}*

¹*Nuclear and Energy Research Institute, IPEN-CNEN/SP, Sao Paulo, Brazil*

²*University of Missouri, Department of Radiology, One Hospital Drive, Columbia, MO, 65212, USA*

*E-mail: ablugao@gmail.com

Converging technologies comprises of combinations of nanotechnology, biotechnology, information technology, and cognitive science to serve the ever-changing societal needs for improving health standards. In IPEN-Brazil and, in cooperation with the Missouri University Medical School, and IAEA programs, we have focused on the use of ionizing radiation to develop new advanced hydrogels with high content of green nanoparticles (silver and gold) for wound dressing applications and also for pro-aging cosmetic masks (new concept encompassing anti-aging effect with the natural touch of time). Hydrogels with nanoparticles have been prepared by an innovative one-pot synthetic technology based on Rosiak's process for hydrogel dressing with the addition of simultaneous synthesis of silver and/or gold nanoparticles. Radiation-induced synthesis of metal nanoparticles depend on the reduction power of e_{aq}^- , formed during water radiolysis.

1. Green synthesis of Albumin and Albumin/Au-198 nanoparticles

The delivery of therapeutic and diagnostic radiopharmaceuticals using nanotechnology is the central goal of many researches works as nanoparticles can be made very specific and can deliver much higher energy payload to the tumor. However, there is a great concern in decreasing the production cost and avoid any extra toxicity by using cleaner and natural routes. The green synthesis of nanoparticles can be entirely based on radiation induced reactions or based on the use of powerful phytochemicals with reducing and stabilizing features. Protein nanoparticles are already in the market, but they can also be synthesized and from water radiolysis in a entirely green process [1]. Albumin particles from macro to nanosized are well established platforms. For instance, Tc labelled Nanoalbumin is a SPECT agent for localization of sentinel node in breast cancer. There are new propositions on the use of albumin

nanoparticles as radiopharmaceuticals carrier as it features set of characteristics that assures applications as natural drug carriers with attractive properties in oncology. Albumin may be easily crosslinked and engineered towards loading of hydrophobic molecules as well as hydrophilic ones [2,3]. Radiation-induced crosslinking of Albumin was developed with the support of Mariano Grasselli (Quilmes University) and now further developments were done for the radiation induced crosslinking of papain and crosslinking of Albumin on Gold and Gold -198 nanoparticle surface to improve its circulating time in the blood. Gold-Albumin nanoparticles produced by this chemical free route has been tested as a carrier for radiopharmaceuticals and chemotherapeutics [4,5] (Figure 1).

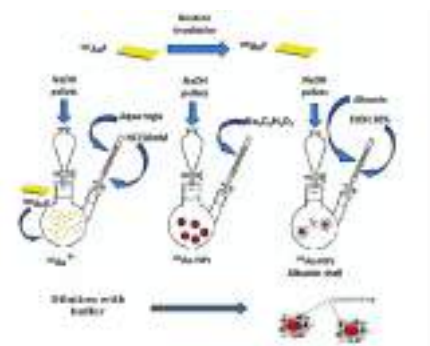


Figure 1. Gold 198 nanoparticle preparation stabilized by BSA



Figure 2. Green synthesis of Gold nanoparticles using tea leaves extract

Green nanotechnology synthesis of silver and gold nanoparticles have been performed by using natural antioxidants for reduction and stabilization, a protocol pioneered by Katti et al, and using ionizing radiation for the reduction step followed by natural polymers stabilization (Figure 2).

Acknowledgments:- We would like to thanks the funding from CNPq Science Without Borders Program # 401438/2014-7 and IAEA coordinated research project CRP# 15459.

References

- /1/ E. Miele, G. P. Spinelli, E. Miele, F. Tomao, S. Tomao, *Int. J. Nanomedicine*, 4 (2009) 99–105.
- /2/ G. H.C. Varca, R. G. Queiroz, A. B. Lugão, *Radiat. Phys. Chem.*, (2016). <http://dx.doi.org/10.1016/j.radphyschem.2016.01.021>.
- /3/ N. Chanda, V. Kattumuri, R. Shukla, A. Zambre, K. Katti, A. Upendran, R. R. Kulkarni, P. Kan, G. M. Fent, S. W. Casteel, C. Jeffrey Smith, E. Boote, J. D. Robertson, C. Cutler, J. R. Lever, K. V. Katti, and R. Kannan, *PNAS* 107 (2010) 8760-8765.
- /4/ R.G. Queiroz, G. H.C. Varca, S. Kadlubowski, P. Ulanski, A. B. Lugão, *Int. J. of Biol. Macromolecules*, 85 (2016) 82– 91.
- /5/ G.H.C. Varca, G.G. Perossi, M. Grasselli, A.B. Lugão, *Radiat. Phys. Chem.*, 105 (2014) 48– 52.

Medical Cyclotron Program and PET-CT Imaging: Status and Trends in India

*M.R.A.Pillai**

Molecular Group of Companies, Puthuvype, Ernakulam, Kerala 682508
*E-mail: Pillai.m.r.a@gmail.com

1. Introduction

PET-CT scan is an indispensable part of cancer management at all stages. Since the first PET machine installation at the Radiation Medicine Centre in October 2002, the growth of this modality in India is in tune with the rest of the World. As of now there are 206 PET-CT machines licensed and another 20 are at various stages of installation. This number is likely to grow much faster as every major hospital in the country having an oncology wing is likely to invest in a PET-CT machine. Despite the high cost of PET-MRI, there are a few machines already installed and several more must be in the planning stage. At present Kerala has have 14 PET-CT machines and one PET-MRI in operation.

As of today there are 21 medical cyclotrons with beam energy upto 18 MeV in different parts of India. The major share is the 16.5 MeV GE PETtrace (11 numbers), followed by the 11 MeV Siemens RDS/HP (7 machines), 18 MeV IBA (2 machines) and one 18 MeV Sumitomo machine. This is excluding the 30 MeV IBA machine under installation at the VECC satellite campus in Kolkata. Nine cyclotrons are in Government Institutions and the radiopharmaceuticals are used in single institution. An exception is the cyclotron at RMC which had a successful commercial operation for the last fifteen years. The entry of private players in PET radiopharmaceuticals had a very favourable outcome. In order to recover the cost of installation, most of them developed transportation logistics by which FDG is now distributed to not only to nearby cities but also to distant places by air.

2. Setting up a medical Cyclotron

The Atomic Energy Regulatory Board (AERB) has brought out clear directives for setting up medical cyclotrons in India. The approvals are needed at three stages [1], site assessment approval, design and construction approval and finally approval for commissioning. Once the site approval process is

completed it is important to submit a preliminary safety analysis report (PSAR). AERB approval is also needed to start trial operation. Once trial operation is completed, a final safety analysis report (FSAR) needs to be prepared and submitted to AERB for obtaining license. The license once given is valid for three years. Every quarter of the year, the facility must submit a report to AERB.

The IAEA has brought out several technical reports giving guidelines for setting up cyclotrons and the author was the responsible officer to bring out these documents [2-5].

3. Molecular Cyclotrons at Cochin

The state of Kerala has excellent quality private medical Institutions most of whom have invested or have the potential to procure PET-CT. The first and only available medical Cyclotron was set up in Kerala by the Molecular group at Cochin. The cyclotron is Siemens HP having a beam energy of 11 MeV. It has dual beams with beam current of 60 μ A each. There are a total of three hotcells in which four synthesis modules can be placed and another hot cell for dispensing of the finished products. The radiochemistry laboratory is in Class C environment and the dispensing hot cell maintains Class A cleanliness. There are three synthesis modules, an Explora FDG4 and two Neptis modules. Explora FDG4 is used for the production of upto four batches of FDG without intervention. The Neptis module is cassette based and can be used for the production of fluorine-18 radiopharmaceuticals including FDG. The entire chemistry is done through software intervention. At present ^{18}F -DOPA, ^{18}F -Choline and ^{18}F -PSMA-1007 are prepared; however, has capability to produce ^{18}F -FLT, ^{18}F -FET, ^{18}F -FES etc.

The quality control laboratory is equipped with all the necessary equipments needed for FDG quality control including a gas chromatography, radio TLC scanner and a multi channel analyzer. For endotoxin testing a Charles River Endosafe machine is used. For sterility testing two types of media are used, fluid thioglycolate and tryptone soyabroth are used. Molecular Cyclotron caters to most of the Pet-CT centres in Kerala. FDG is also exported to Sri Lanka on regular basis.

References

- 1/ Guidelines to start medical cyclotron facility <http://www.aerb.gov.in/AERBPortal/pages/English/t/publications/CODESGUIDES/mcf%20guidelines.pdf>
- 2/ Technical Report Series 465: Cyclotron Produced Radionuclides: Principles and Practice (IAEA 2008). <http://www-pub.iaea.org/MTCD/publications/PubDetails.asp?pubId=7849>
- 3/ Cyclotron Produced Radionuclides: Guidance on Facility Design and Production of [^{18}F] Fluorodeoxyglucose. (IAEA 2012), http://www-pub.iaea.org/MTCD/Publications/PDF/Pub1515_web.pdf
- 4/ Technical Report Series 471: Cyclotron Produced Radionuclides: Guidelines for Setting up a Facility (IAEA 2009). <http://www-pub.iaea.org/MTCD/publications/PubDetails.asp?pubId=8046>.
- 5/ Cyclotron Produced Radionuclides: Guidance on Facility Design and Production of [^{18}F] Fluorodeoxyglucose. (IAEA 2012). http://www-pub.iaea.org/MTCD/Publications/PDF/Pub1515_web.pdf

Proton Boron Therapy: Sense or Nonsense?

Bert Wolterbeek, Tuur Vermunt, Zoltan Perko, Jeremy Brown*

Delft University of Technology, Reactor Institute Delft (RID), Dept. Radiation Science and Technology (RST)
*E-mail: h.t.wolterbeek@tudelft.nl

1. Introduction

The history of proton therapy began in 1946 with the Robert Wilson paper in which accelerator-produced proton beams were suggested to treat tumors in humans [1]. Since then, insight in the physics of proton therapy has advanced considerably, as shown in a topical review by Newhauser and Zhang [2]. During the same time span, several nuclear reactions have been considered as potential reactions for controlled thermonuclear fusion for energy production [3,4]. Aneutronic fusion, as a form of fusion power in which neutrons carry no more than 1 % of the total released energy, could reduce problems with neutron radiation such as ionizing damage, neutron activation, and biological shielding, and one of the promising fusion reactions discussed in that context is the proton-boron fusion reaction [3,4]: the fusion of a boron nucleus with a proton produces slow-moving alpha particles but hardly any neutrons.

Very recently, Yoon et al. [5] proposed the proton boron fusion reaction as an application to proton radiation therapy: they argued that the release of alpha particles in the fusion reaction could enhance proton therapy efficiency [5]. In a follow-up paper, Jung et al. [6] indeed modelled a up to 96 % higher integrated dose in the Bragg peak volume at high boron presence. Cirrone et al. [7] decided to start up experimental work to test the theoretical ideas [5,6] in cell irradiation trials with clinical proton beams in the presence of a BSH boron compound [7]. They observed a significant increase in cytogenetic effects, both in terms of cell death and in induced DNA damage in boron treated cells. Mazzone et al. [8], addressing the Cirrone paper, doubted that the effect could be due to the alpha effect from the fusion reaction, and suggested that the observed decrease in cell survival should be explained by other mechanisms. In turn, in a reaction to the Mazzone report, Cirrone et al. [9] replied that the data do suggest that the $p + {}^{11}\text{B} \rightarrow 3\alpha$ reaction is responsible for the observed phenomena, but that there is no current simple analytical computation possible to explain the results.

Within The Netherlands, three proton therapy centers are currently opening up. The reports, argumentation, confusion and discussion as outlined above, prompted us to step into investigating the possibility that boron may enhance proton therapy efficiency.

We decided to first try and reproduce the Jung et al. [6] results: we used MCNP6.2 for modelling, after we extended its cross-section library by adding the TENDL-2017 proton cross-section files, needed because the default cross-section database did not contain the proton-boron reaction. The presentation will go into details of all foregoing data, discussions and points of view, and will give the latest results of our current modelling efforts.

References

- /1/ R.R. Wilson, Radiology 47 (1946) 487.
- /2/ W.D. Newhauser, R. Zhang, Phys. Med. Biol. 60 (2015) R155
- /3/ D.C. Moreau, Nucl. Fusion 17 (1977) 17
- /4/ H. Hora, S. Eliezer, N. Nissim, P. Lalouis, Matter and Radiation at Extremes 2 (2017) 177
- /5/ D. Yoon, J. Jung, T.S. Suh. Appl. Phys. Lett. 105 (2014) 223507
- /6/ J. Jung, D. Yoon, H.C. Lee, Lu, B., T.S. Suh, AIP Advances 6 (2016) 095119
- /7/ G.A.P. Cirrone, L. Manti, D. Margarone, G. Petringa, L. Giuffrida A. Minopoli, A. Piccioto, G. Russo, F. Cammarata, P. Pisciotto, F.M. Perozziello, F. Romano, V. Marchese, G. Milluzzo, V. Scuderi, G. Cuttone, G. Korn,. Nature Scientific Reports 8 (2018) 1141.
- /8/ A. Mazzone, P. Finocchiaro, S. Lo Meo, N . Colonna, arXiv:1802.09482v2 [physics.med-ph] 3 March 2018
- /9/ G.A.P. Cirrone, L. Manti, D. Margarone, G. Petringa, L. Giuffrida, A. Minopoli, A. Piccioto, G. Russo, F. Cammarata, P. Pisciotto, F.M. Perozziello, F. Romano, V. Marchese, G. Milluzzo, V. Scuderi, G. Cuttone, G. Korn, www.researchgate.net/publication/323723174

News from Research on Superheavy Elements

Christoph E. Duëllmann^{1,2,3}*

¹Institut of Nuclear Chemistry, Johannes Gutenberg University Mainz, 55122 Mainz, Germany

²GSI Helmholtzzentrum für Schwerionenforschung GmbH, 64291 Darmstadt, Germany

³Helmholtz Institute Mainz, 55099 Mainz, Germany

*E-mail: duellmann@uni-mainz.de

1. Introduction

Superheavy element (SHE) research has always been a pillar of the research program at GSI Darmstadt. A broad experimental program addresses all relevant aspects of accelerator-based superheavy element research, including i) nuclear reaction studies on the synthesis of superheavy elements; ii) nuclear structure investigations via decay spectroscopy and, most recently, via hyperfine structure studies; iii) atomic mass measurements using Penning trap mass spectrometry; as well as iv) chemical studies addressing atomic and molecular systems. Since my last report at ARCEBS 2010 [1], exciting new results were obtained in all of the above mentioned areas and many will be discussed in detail in the Superheavy Element Mini-Symposium.

I will introduce the current status of SHE research and discuss the main motivation for physics and chemistry programmes in the field. The relevant region of the chart of nuclei is shown in figure 1.

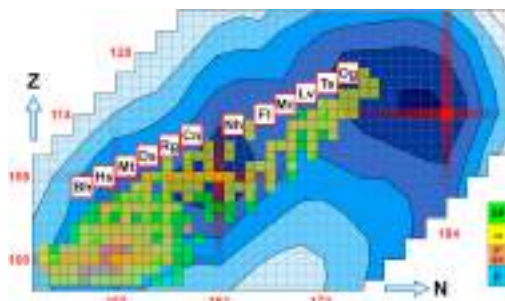


Figure 1. The heaviest elements in the chart of nuclei. Blue contours show calculated shell correction energies, and red line magic numbers in a mic-mac model. Known nuclei are shown color-coded according to their decay mode.

A recent summary of the status of SHE research can be found in a Special Issue of Nucl. Phys. A [2]. Relevant aspects include the status of accelerator facilities providing intense heavy-ion beams – close to the main aspect of the ARCEBS conference – , but also the production of targets withstanding these beams over extended periods – a topic in which new techniques are still being developed [3]. SHE synthesis programs focus on the search for nuclides with ever higher Z [4] – new elements – as well as higher N , reaching deeper into the realm of the “island of stability”, located near $Z=114 / N=184$ in Fig. 1. Nuclear structure studies are typically performed using decay-spectroscopy [5,6]; recently, first hyperfine structure studies using single-atom quantities have been successful [7,8], opening a complementary avenue. Chemical studies currently focus on single-atom interaction with reactive surfaces and have reached element 114, flerovium [9,10], with work towards heavier elements currently being under way [11]. Elements accessible at higher rates are also studied in molecular systems. Here, volatile carbonyl compounds are currently in the focus [12].

I will close with showing perspectives arising with the installation of a continuous wave heavy ion accelerator, for which R&D work is currently ongoing [13].

References

- /1/ Ch. E. Düllmann, *Radiochim. Acta* 100 (2012) 67.
- /2/ Ch. E. Düllmann, R. D. Herzberg, W. Nazarewicz, Y. Oganessian, (Eds.) *Nucl. Phys. A* 944 (2015).
- /3/ K. Eberhardt, *AIP Conf. Proc.* 1962 (2018) 030019; Haas R. *Nucl. Instrum. Meth. A* 874 (2017) 43.
- /4/ Ch. E. Düllmann, *EPJ Web. Conf.* 163 (2017) 00015.
- /5/ D. Rudolph et al., *Phys. Rev. Lett.* 111 (2013) 112502.
- /6/ M. Asai, F.P. Hessberger, D. Ackermann, *Nucl. Phys. A* 944 (2015) 308.
- /7/ M. Laatiaoui, et al., *Nature* 538 (2016) 495, and contribution to the SHE mini-symposium.
- /8/ S. Raeder, et al., submitted for publication (2018).
- /9/ A. Yakushev, *Inorg. Chem.* 53 (2014) 1624; *EPJ Web. Conf.* 131 (2016) 07003;
- /10/ L. Lens , contribution to the SHE mini-symposium.
- /11/ S. Götz contribution to the SHE mini-symposium.
- /12/ J. Even et al. *Science* 345 (2014) 1491; Eichler, R. *EPJ Web. Conf.* 131 (2016) 07005.
- /13/ W. Barth et al. *Phys. Rev. Accel. Beams* 21 (2018) 020102.

In The Fission Valley of HE and SHE

*Tilak Kumar Ghosh**

Variable Energy Cyclotron Centre, 1/AF, Bidhan Nagar, Kolkata 700064, India
Homi Bhabha National Institute, Training School Complex, Anushakti Nagar, Mumbai - 400094, India
*E-mail: tilak@vecc.gov.in

1. Introduction

Synthesis of heavy elements (HE) and superheavy elements (SHE) in the laboratory requires fusion of two heavy nuclei. The fusing nuclei must have enough kinetic energy to overcome the repulsive Coulomb barrier in order to come within the range of the attractive nuclear forces and fuse to form compound nucleus (CN). However, the evolution of the fusion path is actually governed by the complicated multidimensional potential energy landscape, which depends critically upon the entrance channel. The reactants may reach a fusion meadow in the potential energy landscape, equilibrate to form compound nucleus and it may then either cool down through particle evaporation to form evaporation residue (ER). The other path is that it undergoes shape oscillations over unconditional saddle point to reach the fission valley. Alternatively, the system may bypass the fusion meadow to reach the fission valley; this is known as quasi-fission.

The topography of the potential energy surface is far too complicated to predict theoretically the path taken by the system in its evolution. This is even more so, because of possible microscopic effects such as nuclear shell effects. So, it is of paramount importance to use different experimental probes together with a phenomenological understanding or microscopic calculation to explore various facets of the formation mechanism of heavy and superheavy elements. This study helps us not only to understand the basic nuclear fission mechanism but to pick up the right kind of target and projectile combination to produce super heavy elements beyond Oganesson ($Z=118$).

2. Experiment

At Variable Energy Cyclotron Centre, Kolkata, we are engaged in the study of the interplay of dynamics (fusion-fission vs quasi-fission [1- 3]) and microscopic effects (nuclear shell effects [4 -7])

in fission. While quasi-fission is believed to be the main culprit for the formation of SHE, it is because of the shell effects SHE exists. We use fission fragment mass distribution as the probe to understand these two counter effective processes. In the experiments, we measure the time of flights of the fission fragments with large area position sensitive Multi Wire Proportional Counters (MWPC) developed at VECC, or CORSET in Dubna. We use light heavy ions (^4He , ^{11}B , ^{12}C , ^{16}O , ^{19}F) from the Indian accelerator facilities (Kolkata cyclotron, Mumbai and Delhi pelletron) and heavy beams ^{52}Cr , $^{84,86}\text{Kr}$ from the FLNR JINR, Dubna U-400 Cyclotron.

3. Results and Discussion

We have systematically studied the fission dynamics of actinides and pre-actinides nuclei at beam energies close to the Coulomb barrier. We have presented a direct experimental evidence that the nuclear shell effect washes out at excitation energy ~ 40 MeV for actinide nucleus ^{236}U [5]. The recent fission fragment mass distribution study for $N=126$ closed shell nuclei ^{210}Po , has helped to settle the long debated issue of the nature of shell correction at saddle point [6]. Our recent study of fission dynamics in ^{243}Am and ^{254}Fm [2] clearly indicated the gaps in present understanding of the non-equilibrium fission phenomenon. Our experiments, carried out at Dubna cyclotron facility, to study of fusion-fission dynamics of Flerovium ($Z=114$) and Moscovium ($Z=115$) allow us to have a more systematic understanding of the formation mechanism of the HE and SHE [3].

Acknowledgement: The author would like to thank accelerator staffs and all his collaborators. Funding support from DAE, DST, and RFBR are thankfully acknowledged.

References

- /1/ A. Chaudhuri, A. Sen, T. K. Ghosh, et al. .Phys. Rev. C 94 (2016) 024617.
- /2/ K. Banerjee, T. K. Ghosh, P. Roy, et al., Phys. Rev. C 93 (2016) 064602.
- /3/ E. M. Kozulin, G. N. Knyazheva, K. V. Novikov, et al., Phys. Rev. C 94 (2016) 054613.
- /4/ A. Sen, T. K. Ghosh, S. Bhattacharya, et al., Phys. Rev. C 96 (2017) 064609.
- /5/ A. Chaudhuri, T.K. Ghosh et al. Phys. Rev. C 92 (2015) 041601 (R) .
- /6/ A. Chaudhuri, T. K. Ghosh, K. Banerjee, et al., Phys. Rev. C 91 (2015) 044620.
- /7/ T K Ghosh, A Chaudhuri, K Banerjee , et al., Pramana J. Phys. 85 (2015) 291.

Atomic/Chemical Properties of The Heaviest Actinide Element Lawrencium

Tetsuya K. Sato^{1}*

¹Advanced Science Research Center, Japan Atomic Energy Agency, Tokai, Ibaraki 319-1195, Japan

*E-mail: sato.tetsuya@jaea.go.jp

The chemical and atomic properties of heavy elements with atomic numbers greater than 100 are attracting an interest; their properties are affected by strong relativistic effects, and advanced techniques are required to conduct experiments at an-atom-at-a-time scale.

The first ionization potential (IP_1), a measure of the energy required to remove one valence electron from a neutral atom, yields information on the valence electronic structure. Recently, we successfully determined the IP_1 value of the heaviest actinide element, lawrencium (Lr, $Z = 103$) on scales of one atom at a time by using a surface ion-source installed in the Isotope Separator On-Line (ISOL) at the JAEA tandem accelerator [1]. The experimental value clearly showed that the IP_1 of Lr is distinctly low among actinide elements, which was in good agreement with that predicted by state-of-

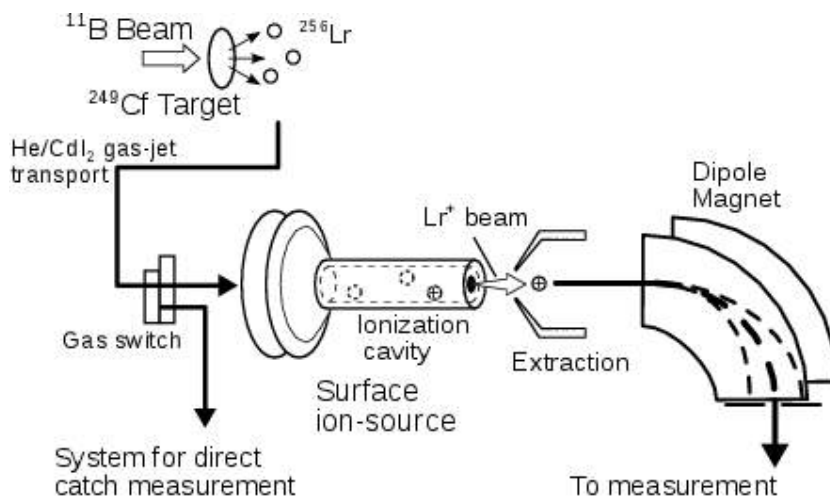


Figure 1. Experimental setup

the-art relativistic calculations. This suggests that the outermost electron of the Lr atom is bound in a $7p_{1/2}$ orbital, although a 6d orbital is anticipated to be occupied simply from the analogy to its lighter homologue lutetium (Lu) where a 5d orbital is occupied. Namely, our experimental result strongly suggested that the Lr atom would have the electronic configuration $[\text{Rn}]7s_25f^{14}7p_{1/2}$ for the ground state.

This result motivates us to explore the volatility of elemental Lr because the volatility or an adsorption on a material surface of a metal is expected to depend on a type of its valence electronic configurations. Thus, the adsorption behavior of Lr is studied by a newly developed method combining vacuum chromatography with surface ionization in a metallic column/ionizer of the ISOL.

In vacuum chromatography, adsorption-desorption processes of single atoms on a surface depend on the temperature of the chromatographic column and on the adsorption enthalpy of the species under investigation. On a metallic surface at high temperature, atoms are ionized during the desorption process from the surface; ionization efficiencies are described by the Saha-Langmuir (S-L) equation. If the loss of atoms due to adsorption on the surface of the column/ionizer is negligible, the ionization efficiency fully follows the equation. In case a fraction of all atoms keeps remains adsorbed until their decay occurs during adsorption, the ionization efficiency becomes lower than that expected.

An experimental setup is shown in Figure 1. ^{256}Lr with a half-life of 27 s was produced in the $^{249}\text{Cf}(^{11}\text{B}, 4n)$ reaction at the JAEA tandem accelerator facility. Reaction products recoiling from the target were transported to the ionization site (ionizer) by an aerosol gas-jet transport system. ^{256}Lr atoms were surface-ionized at different temperatures. Formed ions were mass-separated and then implanted into a Mylar foil of a rotating-wheel type α -particle measurement system (MANON) [2]. Ionization efficiencies of Lr were measured as a function of the ionizer temperature. At lower temperatures, the ionization efficiencies of Lr become lower than those expected by the S-L equation. This indicates that a significant fraction of the Lr atoms was adsorbed on the surface and decayed there.

Details of the experiments of the IP_1 measurement and study on adsorption-desorption behavior of Lr will be presented. Additionally, current status of the chemical/atomic studies of Lr at JAEA will be briefly discussed.

References

- /1/ T. K. Sato *et al.*, Nature 520 (2015) 209-211.
- /2/ T. K. Sato *et al.*, Rev. Sci. Instrum. 84 (2013) 023304.

Speeding Up Gas-phase Chemistry to Access Elements Beyond Fl, Element 114

S. Götz^{1,2,3}, M. Block^{1,2,3}, Ch. E. Düllmann^{1,2,3}, F. Giacoppo^{1,2}, M. Götz^{1,2,3}, S. Raeder^{1,2}, P. Chhetri^{2,5}, E. Jäger², O. Kaleja^{2,3,4}, B. Kindler², J. Krier², B. Lommel², A.K. Mistry^{1,2}, A. Yakushev^{1,2}, V. Yakusheva²*

¹Helmholtz-Institut Mainz, 55099 Mainz, Germany

²GSI Helmholtzzentrum für Schwerionenforschung GmbH, 64291 Darmstadt, Germany

³Institut für Kernchemie, Johannes Gutenberg University, 55122 Mainz, Germany

⁴Max-Planck-Institut für Kernphysik, 69117 Heidelberg, Germany

⁵Technische Universität Darmstadt, 64289 Darmstadt, Germany

*E-mail: s.goetz@gsi.de

In recent years, the chemical properties of the SuperHeavy Elements (SHE) copernicium (Cn, $Z = 112$) and flerovium (Fl, $Z = 114$) have been extensively studied [1]. The main motivation of such experiments is elucidate the influence of relativistic effects on chemical properties [2]. Due to low production rates and short half-lives, $T_{1/2}$, only single atoms are available in chemical experiments. The combination of gas-phase chromatography setups with an electromagnetic preseparator like TASCA proved to be the best experimental approach for reaching the required sensitivity for atom-at-time chemical studies [3]. After production via fusion-evaporation reactions and separation in, e.g., TASCA, these atoms are thermalized in gas-filled volumes and flushed to the chromatography setup with a rapidly flowing gas. This approach is currently applicable to isotopes with half-lives longer than about 0.5 seconds [4], and is limited by the extraction time of recoils under such conditions, which is of the order on hundreds of milliseconds. For elements beyond Fl, half-lives of suitable isotopes drop significantly below that level. An isotope of moscovium (Mc, $Z = 115$), ^{288}Mc , which is accessible directly via the $^{48}\text{Ca} + ^{243}\text{Am}$ reaction with a comparatively high cross section of about 10 pb, the half-life is only $164 \left(\begin{smallmatrix} +30 \\ -21 \end{smallmatrix} \right)$ ms [5]. To overcome this limitation, exploratory experiments were carried out on the coupling of the gas phase chromatography setup COMPACT [3,4] to an existing buffer gas stopping cell operated with electric fields [6], see Fig. 1. In off-line experiments an 8 kBq ^{223}Ra source was used to study the extraction efficiency of the $^{219}\text{Rn}^+$ daughter recoil ions. The source was placed in the centre of the gas cell, which was filled with ultrapure He at a pressure of 50 – 100 mbar. The ion

extraction, shown in figure 1, is achieved by a combination of a DC gradient field (DC cage and funnel) and an RF field (only funnel), whereby the ion extraction times can be significantly reduced compared to extractions with gas flow only [5]. After exiting the buffer gas stopping cell, the ions were transported by the He gas flow through a short capillary made from Teflon to the COMPACT detector array. The steel part of the connection line served to neutralize the extracted ions, as the element of interest should be present in elemental form in COMPACT.

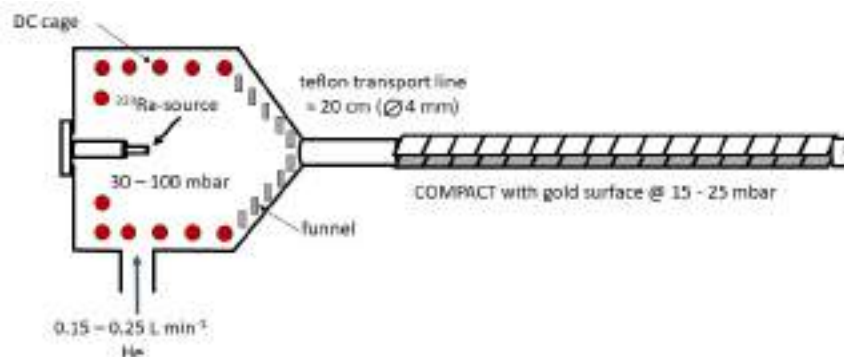


Figure 1. Schematic structure of the gas-stop-cell with attached COMPACT detector

A first on-line experiment was performed at Texas A&M University using short-lived alpha-decaying Hg isotopes preprepared in the MARS separator [6]. In this contribution, the development of the gas stopping cell and of a new COMPACT-design will be discussed. An overview of the offline (GSI) and online (Texas A&M University) results will be given and the perspectives for future chemical studies of SHE beyond Fl will be discussed.

References

- /1/ Türler, R. Eichler, A. Yakushev., Nucl. Phys. A 944 (2015) 640.
- /2/ K. Pitzer, J. Chem. Phys. 63 (1975) 1032.
- /3/ A. Yakushev *et al.*, Inorg. Chem. 53 (2014) 1624.
- /4/ L. Lens, contribution to this mini-symposium
- /5/ Y. Oganessian, V.K. Utyonkov, Nucl. Phys. A 944 (2015) 62.
- /6/ J. Neumayr et al. Nucl. Instr. and Meth. B 244 (2006) 489.
- /7/ C.M. Folden III , M.C. Alfonso, D.A. Mayorov, K.R. Lawrence, A.A. Alharbi, E. Berdugo, P.J. Cammarata, A.C. Raphelt, B.T. Roeder, T.A. Werke. Nucl. Instrum. Meth. A 678 (2012) 1.

Liquid-Phase Chemistry of Superheavy Elements

Yuichiro Nagame^{1,2*}

¹Advanced Science Research Center, Japan Atomic Energy Agency, Tokai, Ibaraki 319-1195, Japan

²Graduate School of Science and Engineering, Ibaraki University, Mito, Ibaraki 310-8512, Japan

*E-mail: nagame.yuichiro@jaea.go.jp

Chemical studies of superheavy elements provide not only crucial and challenging opportunities to advance our understanding of properties of matter at the limits of existence but they also elucidate the influence of relativistic effects on atomic electrons and the architecture of the Periodic Table of the Elements at the farthest reach [1, 2]. These elements are all man-made ones synthesized at accelerators using nuclear reactions of heavy-ion beams with heavy element target materials and they can only be identified by measuring their characteristic nuclear decay, or that of their known daughter nuclei, with sensitive detection techniques. As both half-lives and cross sections of these nuclides are rapidly decreasing with increasing atomic number, they are usually available in quantities of only a few atoms or often one atom-at-a-time.

The chemical characterization of superheavy elements in liquid-phase experiments has been accomplished by partition methods with single atoms, e.g., liquid-liquid extraction, ion-exchange chromatography, and reversed-phase extraction chromatography [3-5]. The ultimate goal of the partition experiments is to determine the so-called distribution coefficient (K_d) as a function of ligand concentration. The K_d value is given in its simplest definition as the ratio of the number of atoms - determined by its radioactivity - either in the organic phase (in liquid-liquid extractions) or in the stationary phase (in column chromatography) to that in the aqueous phase. To get statistically significant results, it is indispensable to repeat the same experimental procedure several hundred or even several thousand times with cycle times of about the lifetime of the nuclide under investigation. In these processes, the behaviour of the heaviest elements is compared with that of its lighter homologues under identical conditions.

The liquid-phase experiments with superheavy elements have been carried out on the basis of the following steps: (i) synthesis of a specific isotope of the heaviest nuclides, (ii) rapid transport of this nuclide to chemical separation devices by an aerosol loaded gas-jet transport technique, (iii) fast

chemical characterization that includes dissolution in an aqueous solution containing inorganic or organic ligands for complex formation, (iv) preparation of a sample suitable for nuclear spectroscopy (α -spectroscopy), which usually requires the evaporation of an aqueous solution to dryness, and (v) detection of nuclides through their characteristic nuclear decay properties for an unambiguous identification.

Recent partition experiments have been conducted using the automated rapid ion-exchange separation apparatus ARCA II (Automated Rapid Chemistry Apparatus) with a miniaturized computer-controlled liquid chromatography system [6] and AIDA (Automated Ion-exchange separation apparatus coupled with the Detection system for Alpha spectroscopy) [7]; AIDA consists of ARCA II and an automated on-line α -particle detection system. AIDA enables cyclic discontinuous column chromatographic separations of short-lived nuclides in aqueous phases and automated detection of α -particles within a typical cycle time of 60 s. Very recently, AMBER (AutoMated Batch-type solid-liquid Extraction apparatus for Repetitive experiments of transactinides) has been developed for the study of liquid-phase chemistry of superheavy elements [8].

In the presentation, we summarize recent studies of the chemical separation and characterization of rutherfordium (Rf) and dubnium (Db), the only ones which so far have been investigated in detail in liquid phases. Perspectives for liquid-phase chemistry experiments are also briefly discussed.

References

- /1/ Türler, V. Pershina, Chem Rev. 113 (2013) 1237.
- /2/ M. Schädel, D. Shaughnessy (eds.), The Chemistry of Superheavy Elements, 2nd ed., Springer, Berlin (2014).
- /3/ J. V. Kratz, Radiochim. Acta 99 (2011) 477.
- /4/ J. V. Kratz, Y. Nagame, Liquid-phase chemistry of superheavy elements, In: M. Schädel, D. Shaughnessy (eds.), The Chemistry of Superheavy Elements, 2nd ed., Springer, Berlin (2014) 309.
- /5/ Y. Nagame, J. V. Kratz, M. Schädel, Nucl. Phys. A 944 (2015) 614.
- /6/ M. Schädel et al., Radiochim. Acta 48 (1989) 171.
- /7/ Y. Nagame et al., Radiochim. Acta 93 (2005) 519.
- /8/ Y. Kasamatsu et al., Radiochim. Acta 103 (2015) 513.

Superheavy Nuclei to Hypernuclei

*Chhanda Samanta**

Department of Physics & Astronomy, Virginia Military Institute, Lexington, VA 24450, USA

*E mail: samantac@vmi.edu

1. Introduction

In nuclear physics, superheavy and hypernuclei are two of the most important fields of research. In the fifties, a new kind of nucleus, called hypernucleus, was discovered. Recent discovery of a strange nucleus, called anti-hypertrion, has enabled extension of the nuclear chart into three dimensions.

1.1 Superheavy Nuclei: In the late sixties, the possibility of an "island of stability" was first proposed by G. T. Seaborg, whose involvement in the synthesis, discovery and investigation of ten trans-uranium elements earned him a share of the 1951 Nobel Prize in Chemistry. S. G. Nilsson et al. [1], Mosel and Greiner [2] predicted that for some superheavy nuclei (SHN) the shell effect will counteract the disruptive Coulomb forces. Hence these nuclei can be formed in the midst of the sea of fission. Strong influence of nuclear shells was predicted to produce some SHN with a life-time comparable to the age of the earth. These predictions drew considerable attention of experimentalists to investigate the existence of SHN beyond the valley of stability. To investigate whether the so-called "stability island" could really exist, the alpha-decay half-lives, spontaneous fission and beta-decay half-lives of nuclei with $100 \leq Z \leq 130$ were studied in a quantum tunnelling model [3-7]. Amongst several results, the alpha-decay half-life of ^{294}Og ($Z=118$) was predicted to be $0.66^{+0.23}_{-0.18}$ ms [3].

Experimental investigations in finding the SHN around $Z=107-118$ were pursued mainly at three different places: GSI (Germany), JINR (Russia), and RIKEN (Japan). The heaviest element discovered so far has 118 protons. It is named 'Oganesson (Og)'. The half-life derived from observed lifetimes is $0.89^{+1.07}_{-0.31}$ ms [8], in close agreement of the prediction of ref. [3]. With the success of discovery of the element with $Z=118$, new searches have started for SHN with $Z=120$. In 2008, at the 235th national meeting of the American Chemical Society, Yuri Oganessian presented the idea of a second island of stability centered on element 164.

Extremely small production cross-section is a great hindrance that calls for a huge improvement of the current technology.

1.2 Hypernuclei: Hypernucleus is a strange nucleus first observed in a stack of photographic emulsions exposed to cosmic rays at about 26 km above the ground [9]. A hyperon has strange quarks (s) in addition to up (u) and down (d) quarks. The normal matter has proton ($p= uud$) and neutron ($n= udd$), and the strange matter has hyperons like Lambda ($\Lambda= uds$), Sigma ($\Sigma= uus$), Cascade ($\Xi= dss$) etc. A hypernucleus contains hyperon(s) in addition to proton and neutrons. So far, the existence of about thirty-five Λ -hypernuclei, six Λ - Λ -hypernuclei and five Ξ -hypernuclei have been reported, but very little is known about the hyperon-hyperon interactions and its variations with the neutron number (N), proton number (Z) and hyperon number (Y). We prescribed a generalized mass formula, applicable to both normal and hyper-nuclei, in which a hypernucleus is considered as a core of a normal nucleus plus hyperon(s) [10, 11]. This mass formula is in good agreement with the experimental data (Figure 1). It also provides a glimpse of the Λ - Λ bonding inside a hypernucleus, and its variation with N and Z.

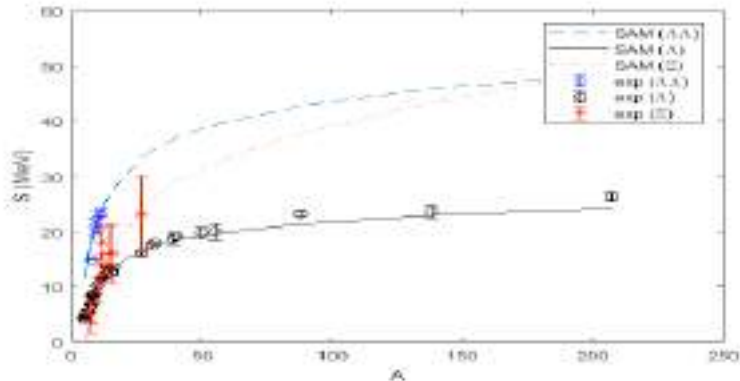


Figure 1. Plot of experimental data on Lambda (Λ)-, double-Lambda ($\Lambda\Lambda$)- and Cascade (Ξ)-hypernuclei separation energies vs. total particle number ($A = N + Z + Y$), and results of our mass formula (SAM).

References

- /1/ S. G. Nilsson et al., Nucl. Phys. A115 (1968) 545.
- /2/ U. Mosel and W. Greiner, Z. Phys. 217 (1968) 256; 222 (1969) 261.
- /3/ P. Roy Chowdhury, C. Samanta, D.N. Basu, Phys. Rev. C. 73 (2006) 014612
- /4/ C. Samanta, P. Roy Chowdhury and D.N. Basu, Nucl. Phys.A789 (2007) 142.
- /5/ P. Roy Chowdhury, D.N. Basu and C. Samanta, Phys. Rev. C75 (2007) 047306.
- /6/ C. Samanta, D.N. Basu and P. Roy Chowdhury, J. Phys. Soc. Jpn.76 (2007) 124201.
- /7/ P. Roy Chowdhury, C. Samanta and D.N. Basu, Atomic Data and Nuclear Data Tables 94 (2008) 781.
- /8/ Yu. Ts. Oganessian et al., Phys. Rev C74 (2006) 044602.
- /9/ M. Danysz and J. Pniewski, Philos. Mag. 44 (1953) 348.
- /10/ C. Samanta, P. Roy Chowdhury, D.N. Basu, J. Phys.G32 (2006) 363.
- /11/ C. Samanta, P. Roy Chowdhury, D.N. Basu, J. Phys.G35 (2008) 065101.

On Laser Spectroscopy of Nobelium and Lawrencium

Mustapha Laatiaoui^{1,2*}

¹Helmholtz Institute Mainz, 55099, Germany,

²Johannes Gutenberg University, 55099 Mainz, Germany,

*E-mail: mlaatiaoui@uni-mainz.de

Optical spectral lines constitute key fingerprint messengers for astronomy for exploring the abundance and unveiling the astrophysical sites of the chemical elements. The spectral lines are vastly studied in lab-based experiments, and some of them have already been identified in star light. With the recent identification of kilonova transients [1], new facets of spectral diagnostics start to emerge in the search for superheavy elements in the universe [2,3]. However, spectroscopic data for elements beyond fermium ($Z > 100$) are completely missing and the experimental access generally lags decades behind an element's discovery. Lacking primordial isotopes of these elements combined with the inability of breeding macroscopic amounts in high-flux nuclear reactors render the traditional way of studying the atomic emission spectra such as with light from primed arc-discharge tubes impossible. Alternatively, common laser spectroscopy techniques lack existing tabulated spectral lines and excitation schemes.

Only recently, Radiation Detected Resonance Ionization Spectroscopy (RADRIS) was proven the method of choice for atomic structure studies on the transfermium elements [4]. Applied on nobelium ($Z=102$), the method enabled the identification of atomic spectral lines of this element for the first time [5]. In these experiments, nobelium isotopes $^{252-254}\text{No}$ were produced in the $2n$ -exit channel of the nuclear fusion reactions $^{206-208}\text{Pb}(^{48}\text{Ca}, 2n)$ at cross sections ranging between 0.5 and 2 μb , respectively. The velocity filter SHIP at GSI in Darmstadt was used to isolate and deliver the recoil ions to a stopping cell placed in the SHIP's focal plane, see Fig. 1. During an accumulation phase, the stopped ions were neutralized on a catcher filament. Then, the recoil beam was turned off and the accumulated fusion products were released from the pulse-heated filament as neutral atoms. They were ionized with suitable laser radiations in a resonant two-step photoionization process and subsequently guided and implanted into a silicon (PIPS) detector for radioactive decay detection.

Detailed investigations on ^{254}No enabled a precise measurement of the first ionization potential of the element [6], supporting former findings [5] and providing powerful benchmarks for atomic

modeling. The investigation of the isotope shift of the element's dominant spectral line enabled (in conjunction with modern atomic calculations) the extraction of changes in the nuclear mean square charge radii along the isotope chain [7]. In addition, from the hyperfine splitting of this line in ^{253}No the nuclear magnetic moment and the spectroscopic quadrupole moment were obtained independent of nuclear models. The nucleus exhibits a prolate shape, confirming theoretical predictions and corroborating findings from in-beam spectroscopy on ^{254}No .

In this talk, results from laser spectroscopy of nobelium will be summarized and first RADRIS experiments on the next heavier element lawrencium ($Z=103$) will be presented.

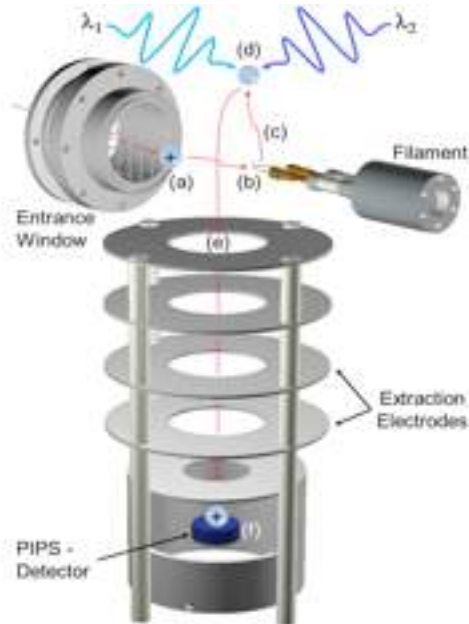


Fig 1: Laser spectroscopy on radionuclides after their production and transmission through the velocity filter SHIP using the RADRIS technique. (a) Thermalization of the fusion products in the buffer gas; (b) accumulation on the catcher filament; (c) re-evaporation from the filament; (d) two-step photoionization of neutral atoms; (e) accumulation of re-ionized fusion products on the PIPS detector; (f) decay detection

References

- /1/ I. Arcavi, et al., Nature 551 (2017) 6466.
- /2/ E. Pian, et al., Nature 551 (2017) 6770
- /3/ I. Petermann, et al., Eur. Phys. J. A 48 (2012) 122.
- /4/ H. Backe, et al., Nucl. Phys. A, 944 (2015) 492.
- /5/ M. Laatiaoui, et al., Nature 538 (2016) 495.
- /6/ P. Chhetri, et al., Phys. Rev. Lett. 120 (2018) 263003.
- /7/ S. Raeder, et al., Phys. Rev. Lett. 120 (2018) 232503.

CERN-MEDICIS: Non-Conventional Radioisotopes for Medical Applications

A.P. Bernardes¹, L. Buehler², R. Catherall¹, T. Cocolios³, K. Kershaw¹, S. Marzari¹, J. Prior⁴, T. Stora^{1} and The MEDICIS Collaboration*

¹CERN, Geneva, Switzerland

²HUG, Geneva, Switzerland

³KULeuven, Leuven, Belgium

⁴CHUV, Lausanne, Switzerland

*E-mail: thierry.stora@cern.ch

The Isotope mass Separation OnLine has been developed for over fifty years to address fundamental questions in nuclear structure and astrophysics. In parallel, applications for solid state physics have benefited from the diversity and purity of the radioactive ion beams available in these facilities, as seen with the large variety of beams and with the research program of ISOLDE at CERN. In the past fifteen years, medical applications have also been developed, culminating with the recent construction of a dedicated extension, CERN-MEDICIS, which has started to produce its first isotope batches this year, figure 1 [1].



Figure 1. The new MEDICIS facility at CERN

Dedicated targets are irradiated in the beam dump position of the Isolde HRS target station, and radioisotopes fractions are extracted thanks to a dedicated isotope mass separator. Details on the first isotope collections will be reported, figure 2.

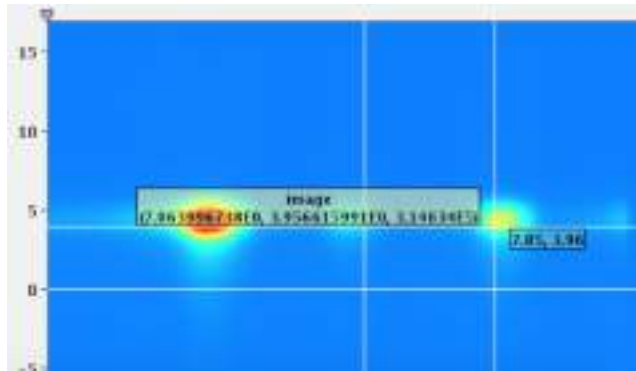


Figure 2. Mass separated beams during the collection of ^{169}Er from an ^{168}ErO target irradiated at ILL for the MEDICIS project MED-011 [2].

With an access to dedicated isotope batches for the medical research, projects will be developed in the fields of targeted radiotherapy, surgery, and PET-aided hadron therapy within a network of medical and fundamental research institutions. This program is further stimulated by a European Marie Curie training network, MEDICIS-Promed, across fifteen institutes in the H2020 framework program of the European Commission [3]. Some highlights will be provided, for instance the synthesis of graphene related to isotope production targets by the group of prof. Novozelov, and possibility of using radioactive ion beams for treatment of cancer with improved imaging capabilities.

References

- /1/ R. M. dos Santos Augusto, et al. "CERN-MEDICIS (medical isotopes collected from ISOLDE): a new facility." Appl. Sci. 4 (2014) 265-281.
- /2/ R. Formento Cavaier "Very high specific activity Er-169 production at MEDICIS from external ILL target", MEDICIS Project MED-011, <http://cds.cern.ch/record/2632033>.
- /3/ This project has received funding from the European Union's Horizon 2020 research and innovation programme under grant agreement No. 642889. www.cern.ch/medicis-promed.

Accelerators and Research with Non-conventional Medical Isotopes

*F. Haddad**

GIP Arronax and Subatech laboratory, Nantes, France

*E-mail: haddad@subatech.in2p3.fr

Radionuclides are used in different fields of medicine like oncology, neurology and cardiology, either for diagnostic or therapy. In most cases, radionuclides must be coupled to a carrier molecule to target the cells of interest. Many radionuclides may be of medical interest due to their emitted radiations (beta / alpha emitters, Auger emitters) and/or their half-lives that can be adapted to the carrier molecule transit time and to the pathology.

Recently, the theranostic approach [1] has emerged. It combines imaging information and therapeutic use of radionuclides. This approach shows great promises especially because it may allow personalizing the treatment to each patient. The diagnosis test done prior to the treatment allows to determine patient response and to determine the needed injected dose for the therapeutic agent. After treatment, the imaging agent can be used to follow the patient response to the injected radiopharmaceutical. Finally, this approach allows a better control of the targeting and increases the benefit/toxicity ratio as useless treatments on patients with no response to the diagnosis test are avoided. All these points lead to a renewal interest on radionuclide production and in particular on metals for which chelation can be used to bind radionuclides to the vector molecules.

This renewal leads, on the one-hand, to studies on accelerators to be able to produce radionuclides of interest with the best quality at an affordable price. This has led to the development of new generation of accelerators, more powerful and, in some case, with higher energy and possibility to accelerate not only protons but also different types of particles (alpha particles and electrons). On the other-hand, many different radionuclides have been identified and studied (like ^{68}Ga used as the imaging agent for ^{177}Lu) with an emphasize on matched pairs ($^{44}\text{Sc}/^{47}\text{Sc}$, $^{64}\text{Cu}/^{67}\text{Cu}$, $^{124}\text{I}/^{131}\text{I}$, ...) which allows, just by changing the radionuclide, to have a radiopharmaceutical for imaging and an other one for therapy. Finally, the complementarity of alpha emitter to the beta emitters used in therapy have been recently demonstrated using ^{225}Ac and ^{177}Lu .

Production of non-conventional radionuclides is the main objective of the Arronax cyclotron [2], acronym for "Accelerator for Research in Radiochemistry and Oncology at Nantes Atlantique", has been built to support research in nuclear medicine. ARRONAX, is a high energy (70 MeV) and high intensity (2*375 μ A) multi-particles cyclotron located in Nantes (France). It is operating since 2011. On the technical aspects, two proton beams can be extracted at the same time (dual beam mode) and experimental vaults are equipped with irradiation stations connected to hot cells via a pneumatic transport system. In 2017, a radio-pharmacy able to produce sterile radiopharmaceutical according to the Good manufacturing Practices (GMP) for human use has opened in our site.

The accelerator use is now stabilized around 4000 hours of RF time per year with beam intensities up to 350 μ Ae for protons, 90 μ Ae for deuterons and 20 μ Ae for alpha particles. Regular high activity production runs are made for Strontium-82 [3], Copper-64 [4], Astatine-211 and Scandium-44. Dedicated targetry systems as well as original radiochemistry processes have been developed in-house. In all case, a particular attention is paid on the final product specifications.

- The produced ^{82}Sr is fully in accordance to the FDA specifications.
- ^{64}Cu is used routinely for preclinical studies and clinical trials are foreseen in collaboration with the Nantes hospit In addition, it is possible with metals to use chelation. This offers versatility and enlarge our capabilities to bind radionuclides to the vector molecules.al.
- ^{211}At is used both for fundamental science [4] and for preclinical trials in the Multiple Myeloma.
- ^{44}Sc in-vivo generator principle have been demonstrated [5] and a first preclinical study is foreseen in the near future

New developments are conducted on germanium-68, Scandium-47 and Cu-67.

Acknowledgements:- This work has been, in part, supported by a grant from the French National Agency for Research called "Investissements d'Avenir", Equipex Arronax-Plus noANR-11-EQPX-0004 and Labex IRON noANR-11-LABX-18-01

References

- /1/ S C. Srivastava, J. Personalized Med. 47 (2013) 31-46
- /2/ F. Haddad et al.. Eur. J. Nucl. Med. Mol. Imaging, 35 (2008) 1377–1387.
- /3/ C. Alliot et al, Appl. Radiat. Isotopes 74 (2013) 56-60.
- /4/ D-C. Sergentu et al., Chem. Eur. J., 22 (2016) 2964-2971.
- /5/ S. Huclier-Markai et al, Nucl. Med. Biol. 41 (2014) e36-e43.

From Isotope Separation Online at CERN ISOLDE to Radioisotopes for Medical Research at CERN MEDICIS

Thomas Elias Cocolios^{1}, Kristof Dockx¹, Yisel Martinez-Palenzuela¹,
Joao Pedro Ramos², Simon T. Stegemann¹, Thierry Stora²*

¹KU Leuven, Institute for Nuclear and Radiation Physics, 3010 Heverlee, Belgium,

²EN Department, CERN, 1211 Geneva 23, Switzerland,

*E-mail: thomas.cocolios@kuleuven.be

1. Isotope separation online – ISOL

With more than 50 years since its first operation, the isotope separation online device (ISOLDE) at CERN has produced over 1,700 radioisotopes of more than 70 elements [1]. It relies on a powerful primary beam, provided by the CERN Proton Synchrotron Booster as a 1.4 GeV, 2 μ A proton beam, onto a thick target where numerous nuclear reactions occur (fragmentation, spallation, fissions, etc). The target material is held at high temperature ca. 2000°C to enhance the diffusion of the nuclear reaction recoils from the target matrix until those finally effuse towards an ion source where mostly singly-charged ions are extracted at an energy ranging from 30 to 60 keV. The mono-energetic beam is analyzed through the magnetic field of a dipole magnet providing an A/q selection.

2. The CERN ISOLDE medical radioisotopes program

2.1. A long history: The interest in ISOL-produced radioisotopes has long been recognized, e.g. the research program on a ⁸¹Rb-^{81m}Kr generator [2]. Although these activities form only a short portion of the ISOLDE activities, the impact of the ISOL technique on medical research has been recognized [3].

2.2. Radiolanthanides: The availability of radiolanthanides at ISOLDE has resulted in a strong and lasting research program around the terbium isotopes, where a quadruplet of isotopes for theranostics applications has been identified [4]. One to two weeks of collections have been possible in the last years to support the research carried, e.g., at the Paul Scherrer Institute in Villigen (Switzerland).

2.3. Actinides: The ISOLDE facilities covers the nuclear landscape up to uranium, giving access to heavy, α -emitting radioisotopes, such as the heavy elements and some minor actinides. In particular, the resonance laser ionization ion source (RILIS) has enabled the production of astatine and the accurate determination of its ionization potential [5]. Current research programs include the study of the electron affinity of astatine, or the study of the production of ^{225}Ac and $^{225}\text{Ac}/^{213}\text{Bi}$ generators.

3. CERN MEDICIS

The progress of these research topics has been hampered by the limited access to the facility. In order to provide more regular access to radioisotopes, a new facility has been built at CERN, called MEDical Isotopes Collected from ISOLDE (MEDICIS). It consists in an irradiation point behind the ISOLDE target, a robotic suite to extract and manipulate the irradiated target, and an offline front end to extract, ionize, and separate radioisotopes.

CERN MEDICIS has now entered full operation using both ISOLDE-irradiated and externally-produced radioactivity. Isotopes are delivered to regional medical partners in Geneva and Lausanne as well as international partners (e.g. Portugal or UK). Medical radioisotopes are substantially different from the most exotic isotopes typically studied at ISOLDE. As such, the research for the production of radioisotopes at CERN MEDICIS has taken a new route for target and ion source geometry and design.

4. Conclusion

The ISOL technique is a promising approach for the production of novel radioisotopes for medical applications, which is used regularly at CERN ISOLDE and CERN MEDICIS. New research is being performed to improve the performance specifically for the isotopes of interest to the medical community.

Acknowledgement: - This project has received funding from the European Union's Horizon 2020 research and innovation programme under grant agreement No. 642889 MEDICIS-PROMED, from the Flemish FWO, and from KU Leuven.

References

- /1/ M.J.G. Borge, B. Jonson. J. Phys. G. 44 (2017) 044011.
- /2/ G.J. Beyer, H.L. Ravn, Y. Huang. Int. J. Appl. Radiat. Isotopes. 35 (1984) 1075.
- /3/ G.J. Beyer, T.J. Ruth. Nucl. Instrum. Methods Phys. Res. B. 204 (2003) 694.
- /4/ C. Müller, K. Zhernosekov, U. Köster, et al., J. Nucl. Med. 53 (2012) 1951.
- /5/ R.M. dos Santos Augusto, L. Buehler, Z. Lawson, et al., Appl. Sci. 4 (2014) 265.

Production of Radioisotopes for Application Studies at RIKEN RI Beam Factory

*Hiromitsu Haba**
for RIKEN Nuclear Chemistry Collaboration

Nishina Center for Accelerator-Based Science, RIKEN, Wako, Saitama 351-0198, Japan

*E-mail: haba@riken.jp

At RIKEN RI Beam Factory (RIBF), Wako, Japan, we have been developing production technologies of radioisotopes (RIs) and conducting RI application studies in the fields of physics, chemistry, biology, engineering, medicine, pharmaceutical and environmental sciences [1–3]. With light- to heavy-ion beams from the AVF cyclotron (AVF), we produce more than 100 RIs from ${}^7\text{Be}$ (atomic number $Z = 4$) to ${}^{262}\text{Db}$ ($Z = 105$). Recently, we developed production technologies of ${}^{67}\text{Cu}$ [4] and ${}^{211}\text{At}$ [5] in the ${}^{70}\text{Zn}(d,an){}^{67}\text{Cu}$ and ${}^{209}\text{Bi}(\alpha,2n){}^{211}\text{At}$ reactions, respectively, for nuclear medicine. ${}^{65}\text{Zn}$, ${}^{85}\text{Sr}$, ${}^{88}\text{Y}$, and ${}^{109}\text{Cd}$ are delivered to Japan Radioisotope Association for fee-based distribution to the general public in Japan.

RIs of a large number of elements (multitracer) are simultaneously produced from metallic targets such as ${}^{\text{nat}}\text{Ti}$, ${}^{\text{nat}}\text{Ag}$, ${}^{\text{nat}}\text{Hf}$, and ${}^{197}\text{Au}$ irradiated with a $135\text{-MeV nucl.}^{-1} {}^{14}\text{N}$ beam from RIKEN Ring Cyclotron [1,6]. The multitracer is useful to trace the behavior of many elements simultaneously under an identical experimental condition.

An isotope of element 113 was synthesized in the cold fusion reaction of ${}^{209}\text{Bi}({}^{70}\text{Zn},n){}^{278}113$ using the GAs-filled Recoil Ion Separator (GARIS) at the RIKEN Linear ACcelerator (RILAC) facility [7]. The name nihonium and symbol Nh were approved for the new element by the International Union of Pure and Applied Chemistry [8].

Chemical characterization of newly-discovered superheavy elements (SHEs, $Z \geq 104$) is an interesting and challenging subject in modern nuclear and radiochemistry. We have installed a gas-jet transport system to GARIS as a novel technique for SHE chemistry [9]. SHE RIs of ${}^{261}\text{Rf}$ ($Z = 104$), ${}^{262}\text{Db}$, ${}^{265}\text{Sg}$ ($Z = 106$), and ${}^{266}\text{Bh}$ ($Z = 107$) are produced in the heavy-ion induced reactions on a ${}^{248}\text{Cm}$ target [10–12]. The chemical synthesis and gas-chromatographic analysis of the first organometallic compound of SHEs, $\text{Sg}(\text{CO})_6$ were successfully conducted [13]. A rapid solvent extraction apparatus

coupled to the GARIS gas-jet system is under development for the first aqueous chemistry of Sg and Bh [14]. On the other hand, a conventional target/gas-jet system for the production of SHEs was installed on the beam line of AVF [15]. The distribution coefficients of Rf were determined in hydrochloric acids by observing extraction equilibrium [16] with the automated batch-type solid-liquid extraction apparatus for repetitive experiments of transactinides (AMBER). Reversed-phase extraction behavior of Db with tributyl phosphate in hydrofluoric acids was also investigated using the JAEA Automated Rapid Chemistry Apparatus (ARCA) [17].

Using Superconducting Ring Cyclotron and the fragment separator BigRIPS, RIBF can generate more than 3,000 RI beams with the world's highest intensity [18]. We propose to use these RI beams for application studies by implanting them into various materials such as water, acids, physiological saline, and pharmaceuticals [1]. One can select an RI with suitable decay properties for its application. Since the RI beams are mass-separated from other fragments, they are very pure, and no or easy chemical separation is required for preparations of tracer solutions.

References

- /1/ H. Haba et al., in Handbook of Nuclear Chemistry (2nd ed.), edited by A. Vértes, S. Nagy, Z. Klencsár, R. G. Lovas, and F. Roesch, Vol. 3, Springer, (2010) 1761–1792.
- /2/ H. Haba, J. Part. Accel. Soc. Jpn. 12 (2015) 206 (in Japanese).
- /3/ RIKEN Accel. Prog. Rep., Sect. Radiochemistry and Nuclear Chemistry in each volume, (http://www.nishina.riken.jp/researcher/APR/index_e.html).
- /4/ K. Fujiki et al., Sci. Rep. 7 (2017) 1912.
- /5/ N. Sato et al., RIKEN Accel. Prog. Rep. 50 (2017) 262.
- /6/ H. Haba et al., Radiochim. Acta 93 (2005) 539.
- /7/ K. Morita et al., J. Phys. Soc. Jpn. 81 (2012) 103201.
- /8/ L. Öhrström and J. Reedijk, Pure Appl. Chem. 88 (2016) 1225.
- /9/ H. Haba et al., Chem. Lett. 38 (2009) 426.
- /10/ H. Haba et al., Phys. Rev. C 83 (2011) 034602.
- /11/ H. Haba et al., Phys. Rev. C 85 (2012) 024611.
- /12/ H. Haba et al., Phys. Rev. C 89 (2014) 024618.
- /13/ J. Even et al., Science 345 (2014) 1491.
- /14/ H. Haba, EPJ Web of Conferences 131 (2016) 07006.
- /15/ H. Haba et al., Eur. Phys. J. D 45 (2007) 81.
- /16/ T. Yokokita et al., Dalton Trans. 45 (2016) 18827.
- /17/ M. Murakami et al., RIKEN Accel. Prog. Rep. 48 (2015) 279.
- /18/ Y. Yano, Nucl. Instrum. Methods Phys. Res. B 261 (2007) 1009.

The ISOLPHARM Project: Production Method of High Specific Activity Beta-emitting Radionuclides as Radiopharmaceutical Precursors

A. Andrichetto^{a}, F. Borgna^a, M. Ballan^a, S. Corradetti^a, E. Vettorato^b, G. Marzaro^b, F. Mastrotto^b, N. Realdon^b, V. Di Marco^c.*

^a INFN, Laboratori Nazionali di Legnaro, Viale dell'Università, 2, 35020 Legnaro (PD), Italy.

^b Department of Pharmaceutical Sciences, University of Padua, Via Marzolo, 5 35100 – Padova, Italy.

^c Department of Chemical Sciences, University of Padua, Via Marzolo, 1 35100 – Padova, Italy.

* E-mail: Alberto.Andrichetto@lnl.infn.it

At INFN-LNL (Istituto Nazionale di Fisica Nucleare – Laboratori Nazionali di Legnaro) a new facility for the production of radioactive ion beams is implemented, SPES (Selective Production of Exotic Species). This new facility, besides being operated for nuclear physics studies, may play a pivotal role in the production of medically relevant radionuclides by means of the ISOL (Isotope Separation On-Line) technique.

In the case of SPES at INFN-LNL radioactive ion beams of neutron-rich nuclei with high purity, in the range of mass between 80 and 160 amu, will be produced.

The production of the radioactive isotopes will be obtained by nuclear reactions induced by 40 MeV protons, accelerated by a cyclotron, that will collide on a target composed of 7 discs of carbon dispersed uranium carbide (UCx), properly spaced in order to dissipate the heat (8 kW) generated by the reaction. The uranium contained in the target material will be ²³⁸U, so that the produced radioactive isotopes will belong to elements having an atomic number between 28 and 57 (elements placed between nickel and lanthanum). In particular, most of the produced nuclides will be neutron-rich, so with an excess of neutrons with respect to the element stable nuclear configuration.

The reaction products will be extracted from the target by evaporation at high temperature (about 2000 °C), then forced to pass through a transfer tube towards an ionization cavity, where they will be ionized to the 1+ state. The ionization source used will vary depending on the ionization potential of the elements of interest. Once ionized, the isotopes will be accelerated through an electrode at high potential (up to 40 kV). The formed beam will be subsequently directed and focalized

using different electromagnetic systems, and purified in order to have a pure isotope beam without contaminants.

The core of the method is the possibility to obtain pure isobaric beams following mass separation; in this way no isotopic contaminations will be present in the beam and afterwards in the trapping substrate. Only potential isobaric contaminations can affect radiochemical and radionuclide purity, but proper methods can be developed to separate chemically different elements

The goal of the ISOLPHARM project is to provide a feasibility study for an innovative technology for the production of extremely very high specific activity beta emitting radionuclides as radiopharmaceutical precursors. This revolutionary technique will allow to obtain radiopharmaceuticals, impossible in most cases to obtain in the standard production facilities (neutron reactors or cyclotrons), with lower costs with respect to traditional techniques and reduced environmental impact.

The ground-breaking idea of the ISOLPHARM method **was granted an International patent (INFN).**

The steps to be addressed for the preparation of the radiopharmaceutical are: 1) Trapping of the radionuclide of interest present in the beam by means of the construction and placement of a suitable substrate; 2) Preparation of a medicinal product compatible with the method of administration; 3) Agreement with the requirements of quality guaranteed by compliance with the principles of Good Manufacturing Practice (GMP) in the field of radiopharmaceuticals

Radionuclides Production For Theranostic Applications

Flavia Groppi^{1}, Simone Manenti¹*

¹L.A.S.A., Radiochemistry Laboratory, Università degli Studi di Milano, UNIMI and Istituto Nazionale di Fisica Nucleare, INFN, Via F.lli Cervi 201, I-20090 Segrate, MI, Italy

*E-mail: flavia.groppi@mi.infn.it

1. Introduction

The use of High Specific Activity Radionuclides HSARNs, obtained by either proton, deuteron or alpha cyclotron irradiation, followed by selective radiochemical separation from the irradiated target in *No Carrier Added (NCA)* form, is a powerful analytical tool for plenty applications in pure and applied sciences and technologies. The main applications of these RNs are in medical radiodiagnostics and metabolic radiotherapy in addition to toxicological, environmental and industrial studies. Nowadays the new challenge in Nuclear Medicine is the so called theranostic medicine, a relatively novel paradigm that involves specific individual ‘dual-purpose’ radionuclides or radionuclide pairs with emissions that are suitable for both imaging, therapy and monitor the response to therapy. The theranostic radionuclides would potentially bring us closer to the age-long dream of personalized medicine [1]. A subchapter is the multifunctional nanoplatform that is an emerging highlight in nanomedicine, in which a suitable radionuclide is encapsulated in nanocarriers. Many of the “neutron-rich” radionuclides suitable for metabolic radiotherapy are produced by nuclear reactor with a very low specific activity (AS). In selected cases, they can be produced by bombardment of targets by charged particle beams in NCA with very high AS. If the irradiations are made with deuteron beams some more advantages are obtained as reported, as an example, in ref [2] for ^{186g}Re production.

2. Experiment

At the Radiochemistry Laboratory of LASA, wide range of high specific activity accelerator- produced radionuclides have been produced since the 70-ties in *NCA* form. Presently, nuclear activations are carried out at the cyclotron IBA K=70 of ARRONAX Center in Nantes France, that can deliver proton

and alpha beams, with variable energy up to 70 MeV and deuteron beams up to 35 MeV. The gamma and X-ray spectra are measured at Physics Measurements Laboratory in LASA with several 15 % efficient, 2.3 keV resolution at 1332 keV, coaxial 50 cm³ active volume HPGe detectors connected to Ortec 918 and 919A MCAs. Detectors are calibrated with reference sources and standard geometries with overall uncertainties no more than 3 % at 1 σ . All samples are measured in the same geometrical assembly as the calibration sources. The quality control tests are carried out for both chemical and radiochemical purities, using electrothermal atomic absorption spectrometry, instrumental neutron activation analysis in conjunction with liquid scintillation counter and HPGe spectrometry.

We present as an example the optimization of the production of ¹⁰³Pd radionuclide ($T_{1/2} = 17$ d, mean photon energy emitted: 27 keV) a suitable alternative and more performing than compared to ¹²⁵I ($T_{1/2} = 59.4$ d, mean photon energy emitted: 21 keV) and ¹³¹Cs ($T_{1/2} = 9.7$ d, mean photon energy emitted: 29 keV), for the brachytherapy of the prostate cancer. With the rapid development of nanoscience and nanotechnology, it starts to become feasible the possibility to substitute the implantation of the seeds of millimetric dimension with the injection in the affected tissue of radioactive NPs, the synthesis of which requires that high AS has to be achieved.

3. Results and Discussion

The optimization of the production of ¹⁰³Pd by deuteron beams irradiation has been investigated [3]. The experimental cross-sections for the ¹⁰³Rh(d,2n)¹⁰³Pd reaction were determined with the well-known stacked foil technique and compared with the data present in literature and the curves of theoretical calculations with EMPIRE-II, EMPIRE-3.2.2 and TENDL-2015 codes, showing a very good agreement in 5 – 33 MeV energy interval. Also the Thick Target Yields, obtained as integration of the thin target yields, present a good agreement with the only four data present in literature and demonstrate that the production by deuteron is about 3 times greater in respect to protons at 22.5 MeV.

Acknowledgement: - Thanks to INFN financial support (Gr V—Interdisciplinary Commission—TECHN_OSP experiment) and to the whole staff of the ARRONAX Cyclotron.

References

- /1/ S. C. Srivastava, Semin. in Nucl. Med. 42(3) (2012) 151.
- /2/ F. Groppi, S. Manenti, L. Gini, M. L. Bonardi, J. Rad. Nucl. Chem. 305 (2015) 179.
- /3/ S. Manenti, M.C. Ali Santoro, G. Cotogno, C. Duchemin, F. Haddad, U. Holzwarth, F. Groppi, Nucl. Med. Biol. 49 (2017) 30.

Photonuclear Production and Radiochemical Separation of Medically Relevant Radionuclides

Ramiz Aliev^{1,2}, Andrey Kazakov^{1,2}, Ekaterina Furkina², Sergei Belyshev³*

¹National Research Center “Kurchatov Institute”, Akademika Kurchatova pl., 1, Moscow, Russia 123182

²Chemistry Department of Lomonosov Moscow State University, Leninskie Gory, 1, Moscow, Russia 119991

³Physics Department, Lomonosov Moscow State University, Leninskie Gory, 1, Moscow, Russia 119991

*E-mail: ramiz.aliev@gmail.com

1. Introduction

At present, the application of radionuclides in nuclear medicine is largely limited by their availability. Many radionuclides, for example ⁴⁷Sc, ⁶⁷Cu and others, have optimal nuclear characteristics for endoradiotherapy, but they are practically not used, because of lack of optimal ways of their production. In the present work we have been looking for photonuclear methods of production of medical radionuclides. The most common reactions (γ, n) can not be used for nca radionuclides production, so we investigated such pathways as (γ, p), (γ, np), (γ, n) β^- , ($\gamma, 2n$) β^- .

2. Experiment

HfO₂, ZnO and Ti targets of natural isotopic composition were irradiated on a multipurpose pulse race-track microtron with electron beam energy of 55 MeV. The bremsstrahlung target was a 0.2 mm thick tungsten plate (0.2-2.1 mm). The photon beam was monitored by two targets of copper foil installed before and after the container. To evaluate the yields after irradiation, a series of gamma-ray measurements was carried out. Cu radioisotopes were separated from Zn using Cu resin in HCl media. Lu radioisotopes were separated from Hf on Lu resin in HF+HNO₃. Sc radioisotopes were separated from Ti on DGA resin in HCl media. All sorbent obtained from TrisKem.

3. Results and Discussion

To calculate the cross section of photoproton reactions, a combined model of photonuclear reactions was used.

This was done taking into account the effect of isospin effects on the evolution of the excited state of the nucleus that arose after the absorption of the photon (Figure 1). The measured yields are given in Table 1. It should be noted that the yield of photonuclear reactions strongly depends on the parameters of the target and the converter.

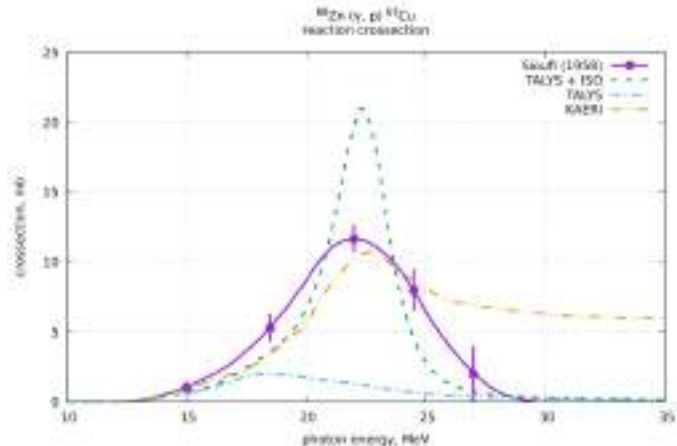


Figure 1. Cross-section of $^{68}\text{Zn}(\gamma,p)^{67}\text{Cu}$ reactions measured by Siuofi /1/ and calculated using different models.

Table 1. Yield of radionuclides

Radionuclide	Reaction	Target	Yield EOB, Bq/($\mu\text{A}\cdot\text{h}\cdot\text{g}/\text{cm}^2$)
^{67}Cu	$^{68}\text{Zn}(\gamma,p)$	W 2.1 mm / ZnO 0.19 g/cm ²	$(2.34 \pm 0.07) \cdot 10^5$
^{47}Sc	$^{48}\text{Ti}(\gamma,p)$	W 2.1 mm / Ti 0.74 g/cm ²	$(1.50 \pm 0.04) \cdot 10^6$
^{44}Ti	$^{46}\text{Ti}(\gamma,2n)$	W 2.1 mm / Ti 0.74 g/cm ²	$(1.50 \pm 0.16) \cdot 10^0$
^{177}Lu	$^{178}\text{Hf}(\gamma,p)$	W 0.2 mm / HfO ₂ 0.99 g/cm ²	$(4.1 \pm 0.2) \cdot 10^3$
	$^{179}\text{Hf}(\gamma,np)$		
	$^{180}\text{Hf}(\gamma,2np)$		

4. Conclusion

It is shown that photonuclear reactions can be successfully used for the production of ^{67}Cu , ^{47}Sc , ^{177}Lu . For all reactions, production yields are determined, radiochemical techniques for isolating radionuclides using extraction chromatography are proposed.

References

/1/ S. Von, A. El., P. Erdös, P. Stoll, (γ, np)-Prozesse am ^{92}Mo und ^{66}Zn . Helv. Phys. Acta 30 (1958) 264–265.

Determination of Low-level Radionuclides: Radiometric vs. Mass Spectrometric Methods

Xiaolin Hou^{1,2*}

¹ Center for Nuclear Technologies, Technical University of Denmark, Risø Campus, Roskilde 4000, Denmark

² Xi'an AMS Center, Institute of Earth Environment, CAS, Xi'an 710061, China

* E-mail: xih@dtu.dk

1. Application of radionuclides and requirement for their measurement at low-level

In the studies of radioecology and environmental processes using radionuclide tracer, as well as characterisation of nuclear waste for decommissioning of nuclear facilities and depository of radioactive waste, nuclear forensics and geological dating using radioisotopes, the key issue is to accurate determination of concentrations of various radionuclides in different materials. Radioanalysis therefore plays a central and critical role in these works. Besides sophisticate chemical separation and purification of radionuclides from sample matrix and interfering radionuclides, sensitive detection of ultra-trace amount of radionuclides is the key point for these application. Radiometric methods by measuring the radioactive decay are the conventional and widely utilized method for their measurement. While, mass spectrometric techniques by counting the numbers of atoms of the target radionuclides can be also used for their measurement. In the recent years, with the rapid development and installation in many laboratories, ICP-MS and accelerator mass spectrometry (AMS) have become important techniques in the determination of radionuclides, especially the long-lived radionuclides.

2. Measurement of radionuclides using radiometric methods

Depending on the decay models, radionuclides can be measured using different radiometric techniques, including γ - and α - spectrometry, liquid scintillation counting (LSC), proportional counter and G-M counter. For the gamma emitter with short half-life (<100 a), e.g. ⁷Be, ¹³⁷Cs, ¹³⁴Cs, ¹³¹I, ⁶⁰Co, ⁵⁴Mn, ¹⁵²Eu, etc., γ -spectrometry is still the dominant technique for their sensitive measurement. For the short-lived alpha emitters, e.g. ²¹⁰Po, ²³⁸Pu, ²⁴²Cm, ²⁴³Cm, α - spectrometry is still the best method.

While for the pure beta emitters, especially the short lived ones such as ^3H , ^{55}Fe , ^{63}Ni , ^{93}Mo , LSC is still the most suitable method for their measurement. The features of these techniques, especially the major advantage and limitation highlighted are presented and discussed. The major effort will be focus on the newly improvement in LSC technique and its application in the determination of pure beta emitting radionuclides, as well as some alpha emitters (e.g. ^{222}Rn), especially the rapid developed and applied LSC measurement using TDCR technique and plastic scintillation.

3. Measurement of radionuclides using mass spectrometric methods

The ICP-MS and AMS techniques has been rapidly developed in the recent years, the sensitivity and techniques for elimination of interferences have been significantly improved, and the number of AMS instrument installed are rapidly increased, which has become an often applied techniques for determination of long-lived radionuclides. The present status and most outstanding features of ICP-MS in the determination of radionuclides will be highlighted and discussed, and some applications of ICP-MS in the determination of long-lived radionuclides, such as isotopes of plutonium (^{239}Pu , ^{240}Pu , ^{241}Pu) and uranium (^{234}U , ^{235}U , ^{236}U , ^{238}U), ^{99}Tc and ^{237}Np are presented.

4. Comparison of radiometric and mass spectrometric methods on the measurement of low-level radionuclides

Although mass spectrometric methods are developed very fast in the past 10 years, and become one often used method for the determination of long-lived radionuclides. Since the principles of two types of measurement techniques are different, the long-lived radionuclides have low specific radioactivity (low Bq/g), therefore mass spectrometric methods are more sensitive and suitable. However, the radiometric method still have a strong advantage in the measurement of short-lived radionuclides and without the isobaric interference of stable isotopes, therefore is still the dominant techniques using in the Radioanalytical laboratories. The two techniques are compensation in the determination of radionuclides. The features of these two types of techniques are compared, aims to discuss the principle criteria in the selection of the measurement techniques. Some examples are given to compare two techniques, and illustrate their key features in the measurement of some radionuclides.

References

/1/ X.L. Hou and P. Roos. *Anal. Chim. Acta* 606 (2008) 105-139.

Status of XCAMS Facility at IUAC

*Sundeep Chopra**

Inter University Accelerator Centre, New Delhi-110067

*E-mail: choprasundeep@gmail.com

1. Introduction

A dedicated AMS facility mainly for the Earth Scientists is being set up at IUAC. New lines of research in the areas of multi-element isotope geochemistry and geochronology will be supported in this proposed facility. The equipment like FE-SEM, XRD, XRF, LA-HR-ICPMS and Q-ICPMS have been installed. A new HR-SIMS and a suitable Ion accelerator for performing heavy mass AMS measurements are being planned. The new AMS system at IUAC as XCAMS – the Compact ^{14}C Accelerator Mass Spectrometer eXtended for ^{10}Be and ^{26}Al is continuously operating for measurements and is extensively used by various research groups across India [1].

2. Facility description and Radiocarbon Measurements

The main components of XCAMS system are two MC-SNICS (Multi-Cathode Source of Negative Ion by Cesium Sputtering) ion sources (40 cathodes with option of adding gas cathodes and 134 cathodes), a 45° rotatable electrostatic, a 90° double focusing injector magnet, 500kV Pelletron accelerator with re-circulating argon gas stripper, a 90° double focusing analyzer magnet, a chamber with off-axis three Faraday cups for stable isotopes measurements, a retractable silicon nitride foil for ^{10}Be - ^{10}B separation, a double focusing 90° electrostatic analyzer at the high energy side (HE-ESA), a 45° bending magnet and a two anode gas ionization detector. The required places have beam focusing instruments like quadrupole lenses and steerers and AccelNET user interface application program running on a computer under scientific Linux remotely controls the XCAMS system. A clean chemistry laboratory for ^{10}Be and ^{26}Al and a sample preparation laboratory having automatic graphitization equipment (AGE) with carbonate handling system (CHS) have also been set up. Organic samples (charcoal, wood, sediments etc.) are graphitized using automatic graphitization equipment and carbonate samples (shell, foram etc.) are graphitized using carbonate handling system.

3. Measurements and Results

Total 2000 measurements have been performed using this facility. Figure 1 show the error distribution of the radiocarbon samples measured in last three years.

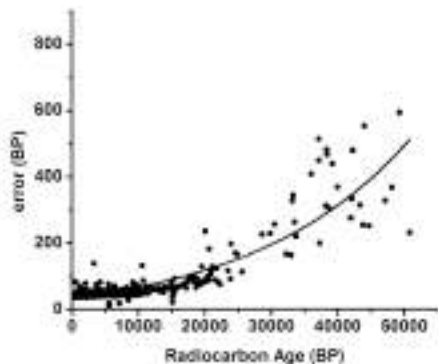


Figure 1. Error distribution of the radiocarbon samples measured in last three years

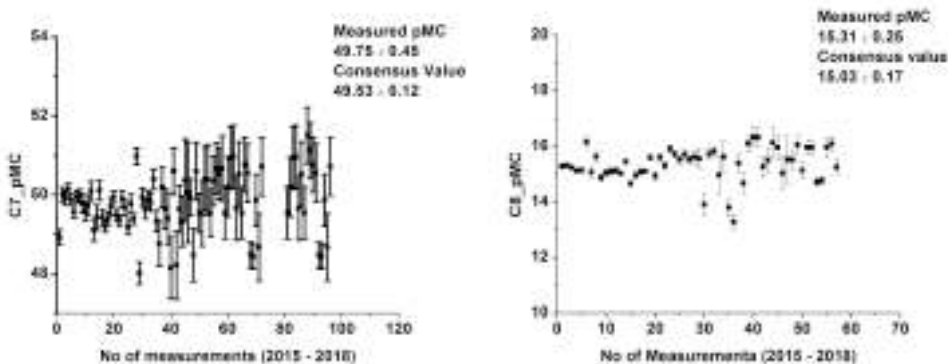


Figure 2. Measurement of IAEA C7 and C8 in last three years

IAEA radiocarbon standards are routinely measured for quality control. Figure 2 (a) and (b) shows that average measured pMC values of IAEA C7 and C8 in last three years are matching with their consensus values with in error. It can also be observed from these figures that errors are decreasing from 2015 to 2018 because of improvement in ion source performance.

Precision of better than 1% in the ratio of $^{14}\text{C}/^{12}\text{C}$ for the modern carbon sample has been achieved and the background level from dead carbon sample was 1×10^{-15} . Total 2000 measurements have been performed using this facility.

References

/1/ P. Kumar, J. K. Pattanaik, S. Ojha, S. Gargari, R. Joshi, S. Chopra, and D. Kanjilal, A new AMS facility at Inter-University Accelerator Centre, New Delhi, Nucl. Instrum. Methods Phys. Res. B 361 (2015) 115-119

AMS of ^{93}Zr and ^{99}Tc : Developments and First Results

G. Korschinek^{1}, T. Faestermann¹, B. Deneva^{1a}, C. Busser¹, K. Hain^{1b}, D. Koll¹,
F. Kortmann², P. Ludwig^{1c}, F. Quinto³*

¹Physics Department, Technical University of Munich, 85748 Garching, Germany,

²Radiochemie München RCM, Technical University of Munich, 85748 Garching, Germany

³Institute for Nuclear Waste Disposal, Karlsruhe Institute of Technology, 76131 Karlsruhe, Germany

^aNow Helmholtz Zentrum Dresden Rossendorf, Bautzener Landstrasse 400, 01328 Dresden, Germany

^bNow Faculty of Physics, University of Vienna, Währinger Strasse 17, 1090 Vienna, Austria

^cNow TÜV SÜD IS GmbH, Munich, Germany

*E mail: korschin@tum.de

1. Introduction

The long-lived radionuclides ^{93}Zr and ^{99}Tc are of great interest in different scientific areas. However their detection and measurements, especially at low concentrations, are strongly hampered because of their long half-lives. E.g. ^{93}Zr ($T_{1/2}=1.64\pm 0.06\text{Ma}$) [1] is a relevant radionuclide in nuclear waste management as it is produced with a high yield in nuclear fission and as well as by neutron capture on ^{92}Zr since most power reactor design use Zircaloy as fuel rod cladding. Hence studies of its migration behavior in the environment in case of accidental release either by a reactor or from a final repository are needed. It is also of interest to improve the knowledge of the cross section the $^{92}\text{Zr}(n,\gamma)^{93}\text{Zr}$ at different neutron energies, either for dosimetry for advanced nuclear reactor designs, but also for s-process nucleosynthesis in asymptotic giant branch stars.

Most of the ^{99}Tc ($T_{1/2}=211.100\text{a}$) is formed as fission product in nuclear reactors and it is of major concern for spent nuclear fuel because of its radiotoxicity and the high mobility of TcO_4^- in the environment. It is formed in much smaller amounts at nuclear bomb tests and even at less amounts via the metastable nuclear isomer of technetium-99 that is used in medical diagnostic procedures.

2. Method and measurements

All these applications need highly sensitive detection methods to determine minute amounts of ^{93}Zr and ^{99}Tc . In Munich we have an AMS (accelerator mass spectrometry) arrangement, which allows, because of the high energy of the tandem and the dedicated gas-filled-magnet (GAMS) [2] to tackle these heavy radioisotopes.

In case of ^{93}Zr is the interfering nuclide ^{93}Nb . Normalizing to a sample of known concentration of $^{93}\text{Zr}/\text{Zr}$ and depending on the Nb content in the sample, detection limits in the range of 10^{-10} to 10^{-11} for $^{93}\text{Zr}/\text{Zr}$ have been achieved.

It is different for ^{99}Tc , there doesn't exist a stable Tc isotope and none of the other long-lived Tc radionuclides are commercial available as reference material. Therefore we produced ^{99}Tc ($T_{1/2}=4.21\text{Ma}$), firstly via $^{96}\text{Ru}(n,\gamma)^{97}\text{Ru}$ which decays by $\beta^+ \rightarrow ^{97}\text{Tc}$ and secondly via $^{93}\text{Nb}(^7\text{Li},2n)^{97}\text{Ru}$ and by $\beta^+ \rightarrow ^{97}\text{Tc}$. After a chemical separation [3], ^{97}Tc has been cross calibrated by AMS to a known ^{99}Tc standard; thus we got ^{99}Tc reference material. In another approach we used a Mn or a Nb matrix in the ion source as reference. Figure 1 shows a dilution series and ^{99}Tc measurements relative to Mn and Nb.

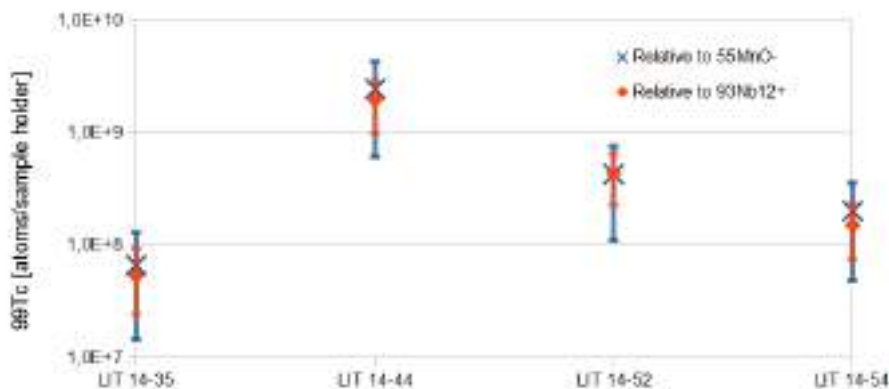


Figure 1. Dilution series of ^{99}Tc relative to Mn and Nb ions..

Our high sensitivity could be demonstrated by a first measurement of a natural water sample (Black forest, Germany) of only 100ml where we determined a value of $\sim 8 \times 10^7$ ^{99}Tc , originating from the nuclear bomb tests in the 50th and 60th as global fallout.

References

- /1/ P. Cassette et al. Appl. Radiat. Isot. 68 (2010) 122-130.
- /2/ Knie K., Faestermann T, Korschinek G., Nucl. Instrum. Meth. B 123 (1997) 128-131.
- /3/ M. Maiti and S. Lahiri, Radiochim. Acta 99 (2011) 359–364 .

Limits in AMS for Nuclear Physics and Nuclear Astrophysics Applications

*Anton Wallner**

Department of Nuclear Physics, The Australian National University, ACT 2601, Australia

*E-mail: anton.wallner@anu.edu.au

1. Introduction

Accelerator Mass Spectrometry (AMS) is an ultra-sensitive atom-counting technique commonly applied for measurements of long-lived radionuclides at natural concentrations. A drawback of its high sensitivity is a complex measurement-setup.

Recently, more AMS facilities extended their measurement capabilities beyond the ‘routine’ isotopes ^{14}C , ^{10}Be and ^{26}Al . New isotopes, e.g. actinides (U, Pu, Th) are now used in many environmental applications utilizing the signals released into the environment by atmospheric nuclear tests, reprocessing plants or nuclear accidents. AMS measurements of actinides are performed in various applications, such as human health and nuclear safeguard issues, environmental sciences and nuclear non-proliferation but also in nuclear astrophysics.

Other examples are medium mass radionuclides such as ^{53}Mn , ^{60}Fe or ^{59}Ni with half-lives between 0.1 and 3.5 Ma which suffer from strong isobaric interference. These isotopes are of importance to nuclear astrophysics but also for nuclear data and nuclear waste considerations.

2. Examples

Some applications related to nuclear physics and nuclear astrophysics, their limits with respect to measurement background and also their overall detection efficiency are discussed below:

(i) The search for live supernova (SN)-produced radionuclides in terrestrial archives [1]: such studies probe directly specific nucleosynthesis sites and will help understanding heavy element nucleosynthesis in massive stars. We demonstrated recently that indeed multiple supernova explosions happened in our galactic neighbourhood within the last 10 million years and left their fingerprint on

Earth [2]. Our work was complemented by additional AMS measurements at Munich and independent observations [3-6].

(ii) Still unknown is the astrophysical site where the heaviest elements are made in nature. Low concentrations measured for interstellar ^{244}Pu ($t_{1/2}=81$ Myr) signals a rarity of heavy element nucleosynthesis, incompatible with standard supernovae as the predominant actinide-producing sites [7-9]. These data provide new insights into recent nearby supernova explosions but also into heavy element nucleosynthesis and r -process sites. This work is based on a major improvement in Pu detection efficiency that was crucial in indicating for the first time a real detection of interstellar ^{244}Pu – a work performed in collaboration with the Australian Nuclear Science and Technology Organisation (ANSTO).

(iii) The complex isotopic signature of our solar system and that observed in stars can be understood as interplay between fundamental nuclear physics properties and the specific conditions of the stellar environment. Nuclear reactions shape the stellar evolution of stars and determine the different astronomical abundances. Key ingredients to our understanding of nucleosynthesis and the isotopic pattern of our environment are accurate cross-section data. The simulation of stellar nucleosynthesis processes in the laboratory via the study of dedicated nuclear reactions helps to elucidate current open questions in astrophysics. AMS represents a sensitive technique for studying nuclear reactions through ultra-low isotope ratio measurements while simulating stellar nucleosynthesis processes in the lab.

(iv) Moreover, the combination of sample activation and subsequent AMS measurement can be applied in general where off-line decay counting is difficult or impossible. I will present work related to nuclear data of relevance to nuclear fusion and advanced reactor concepts. For example, a novel approach [10] for neutron-capture studies of U and Th provided highly accurate nuclear data that are urgently required for the design of advanced reactor concepts..

References

- /1/ K. Knie et al., Phys. Rev. Lett. 83, 18 (1999) & Phys. Rev. Lett. 93 (2004) 171103.
- /2/ A. Wallner et al., Nature 532 (2016) 69.
- /3/ L. Fimiani et al., Phys. Rev. Lett. 116 (2016) 151104.
- /4/ P. Ludwig et al., PNAS 113 (2016) 9232.
- /5/ M. Kachelrieß et al. Phys. Rev. Lett. 115 (2015) 181103.
- /6/ W.R. Binns et al. Science 352 (2016) 677.
- /7/ A. Wallner et al., Nature Comm .6 (2015) 5956.
- /8/ M. Paul et al. Astrophysical J. Lett. 558 (2001) L133.
- /9/ C. Wallner et al. New Astr. Rev. 48 (2004) 145150.
- /10/ A. Wallner et al., Phys. Rev. Lett. 112 (2014) 19250.

In-Beam Neutron Activation Analysis at Garching

Zsolt Révay^{1}, Christian Stieghorst¹*

¹Technical University Munich, Heinz Maier-Leibnitz Center (MLZ), 85747 Garching, Germany
*E-mail: zsolt.revay@frm2.tum.de

1. Introduction

Neutron Activation Analysis (NAA) has become a well-established analytical technique when research reactors became widespread all over the world. This type of neutron source is well understood, with performing a set of calibration measurements, one can monitor the parameters needed for the precise chemical analysis. Detectors and the gamma spectrometers have gone through an enormous development, too, all this led NAA to become an indispensable tool in trace-element analysis. Prompt Gamma Activation Analysis has started its development somewhat later, because the prompt gamma spectra are much more complicated, and the computational technology needed to reach the level of the other equipment, which happened at the very end of the last century.

Neutron generators and isotopic neutron sources play an important role in industrial and in-field applications, while reactor-based facilities are used in scientific research. A new type of neutron source appeared in the past decades: high-flux guided cold neutron beams which are mainly used for scattering experiments in material science. The latest neutron beams are already strong enough for performing NAA, too, and this enabled the development of a new approach with combining PGAA and NAA. Cold neutron beams offer several important advantages when compared to any previously used facilities: 1) with no fast or epithermal neutrons, the activation can be calculated in a much more straightforward way; 2) the beam irradiation simplifies the geometry and thus controlling the neutron self-shielding and gamma-ray self-absorption; 3) at cold-neutron energies, all nuclides behave strictly regularly, thus the spectroscopy data are transferable to other facilities.

2. Experimental

At the Heinz Maier-Leibnitz Centre (MLZ) of the Technical University Munich in Garching, an in-beam neutron activation analysis facility has been established, and successfully used in a great variety

of applications. The maximum thermal-equivalent flux of the cold-neutron beam is $6 \times 10^{10} \text{ cm}^{-2} \text{ s}^{-1}$, and it can be attenuated with three orders of magnitude. The typical sample masses are 10–100 mg, but it can be as high as several grams, and the sample volumes up to 10 cm^3 . The operation is continuous, so the fluence compares with those of the NAA facilities at smaller reactors. The facility is equipped with an automatic sample changer, and with two HPGe detectors: one with a high relative efficiency (60%), ideal for the detection of high-energy gamma radiation, the other is a planar detector with improved resolution at low energies. Both detectors are equipped with Compton suppressors. There is a third Compton-suppressed HPGe detector in a low-background chamber, using which the activated samples can be counted in close geometry. A small pneumatic transfer system is planned between the beam and this counting position to increase the throughput of the NAA measurements. [1] The samples do not need any preparation before placing them in the beam, so the investigation is non-destructive.

3. Applications

The facility is mainly used for PGAA whose major field of application is the determination of low-Z elements, typically the bulk analyses of the matrices. It offers a unique opportunity for the determination of hydrogen (down to ppm level) or boron (down to ppb level). For several other elements (Cd, a series of rare-earths), PGAA enables trace-element analysis (ppb level), too, however, when combined with NAA, i.e. when detecting the delayed gamma radiation after irradiation, the circle of elements can be significantly broadened, and another large set of elements can be added to the trace-element list, like Na, Sc, Mn, Br, In, Re, Ir, Au, and most rare-earths etc.

The recent applications of the in-beam activation analysis cover the determination of hydrogen in meteorites, heavy metals in exhaust filters, chlorine in archaeological iron, boron in Co-Re superalloys, elements from pollution in environmental lichens, the composition of cell phones as electronic waste. The large number of elements determined can be used for detailed statistical investigation, like principal components analysis, ultimately for provenance studies in case of archaeological objects.

References

/1/ Zs. Révay, P. Kudejova, K. Kleszcz, S. Söllradl, Ch. Genreith, Nucl Instrum Meth, A799 (2015) 114.

AMS Determination of Radiocarbon in Dilute Biofuels: Method Uncertainties and Detection Limit

Randy Culp, Ravi G. V. Prasad, Hai Pan*

Center for Applied Isotope Studies, University of Georgia, Athens, Georgia, USA

* E-mail: rculp@uga.edu

1. Introduction

Agricultural fuels are an important component of the energy economy of developing nations. Countries with well-developed agricultural practices, or those beginning to, have the potential to reduce reliance on fossil fuel imports, improve their economy through self-reliance and make a worthwhile impact on the environment. Innovative technologies for the production of biofuels from renewable resources have matured and are now mainstay in the developing world energy sector. Unlike fossil fuels, Bio-fuels are

1. renewable and easily produced from raw agricultural materials ensuring their continued availability.
2. Produced at less cost as Biofuel production develops, unlike fossil fuel production, which will increase as demand increases and availability decreases.
3. Promote and develop energy independence as biofuels are relatively easy to produce relative to the exploitation of fossil fuels, allowing small and large manufacturers to benefit the local and regional economy. Many countries incentivize producers to use renewable resources for Biofuel production through reduced taxation and preferred procurement status. To guarantee the truth and integrity of producer's source materials, radiocarbon measurement stands as the only unambiguous determinant of fossil derived carbon. This allows for the accurate assessment of the biobase content in fuels and other bio-produced materials. This study reviewed the radiocarbon method as described in ASTM D6866-18, and applied it to various Bio-diesel samples of less than 10% bio sourced materials. Larger Biofuel concentrations are simple to quantify by the radiocarbon method as biobase materials have much higher concentrations of ^{14}C than fossil fuel derived materials. However, as the concentration of biobase material decreases through dilution with fossil derived material, the quantification becomes more difficult due to the detection limit of modern accelerator mass spectrometers. Therefore, the aim of this study was to quantify the detection limit of biofuel mixtures below 10%. Today, fuel producers are profiting from a small addition of biobase fuels

in petroleum (fossil) fuels. It is therefore critical to accurately define the capability of the radiocarbon method, its uncertainties and limits of detection.

2. Experiment

A series of biofuels, specifically biodiesel, were analyzed for their ^{14}C content. These samples ranged from 0 to approximately 10% biodiesel with the balance from standard diesel fuel produced from fossil carbon. Duplicate analyses were made from all samples under various processes. These included two different preparation lines, one made from stainless steel and the other from pyrex glass. Vacuum conditions were tested which included comparison of turbo-molecularly pumped systems and roughing pumped systems to ascertain parameters of concern in the processing of samples in general. As a check of the system parameters, stable isotope ratios of carbon were also determined for each sample tested, to determine any fractionation that might occur during processing.

3. Conclusion

The detection of fossil fuel, through its absence of ^{14}C , or at least extremely low level and below detection by modern accelerator mass spectrometers, is relatively easy to determine, though difficult to precisely quantify. Therefore, slight additions of biobase carbon, that produced from modern agricultural products with measureable ^{14}C content, are difficult to quantify if the baseline or background levels are not well known and quantified. To quantify an addition of biofuel, in a predominance of fossil fuel, can be difficult and uncertain. The better one knows and defines the processing and accelerator mass spectrometers characteristics, detection limit and uncertainties, the better the analyst can define precise additions of biofuel to fossil fuel.

Recent Developments and Applications of *In Situ* Current Normalized PIGE Method Using Proton Beams for Quantification of Low Z Elements in Energy Materials

R. Acharya*

Radiochemistry Division, Bhabha Atomic Research Centre, Mumbai 400085, India

*E-mail: racharyabarc@gmail.com / racharya@barc.gov.in

1. Introduction

PIGE is an isotope specific nuclear analytical method capable of determining low Z elements (Li to S) using low energy proton beam (2-5 MeV). This technique involves measurement of prompt gamma-rays emitted from inelastic scattering ($p, p'\gamma$) and nuclear reactions like (p, γ), ($p, n\gamma$) and ($p, \alpha\gamma$). The present article deals with the development of an *in situ* current normalized PIGE method using 4-5 MeV proton beam from Folded Tandem Ion Accelerator (FOTIA), BARC for the determination of concentrations of low Z elements like Li, B, O and Ti and its applications to energy/nuclear energy materials. It includes analysis of boron based samples like B_4C and boron based refractory materials (meant for Indian fast breeder reactors like FBTR and PFBR and high temperature reactor control/shut-off materials) [1,2], Zr-based alloy, lithium based ceramics like Li_2TiO_3 and $LiAlO_2$ (D-T based fusion reactor blanket materials) [3,4] and lithium ion batteries [5].

2. Experimental

We have developed an *in situ* current normalized PIGE method in addition to conventional RBS method for measuring/normalizing the beam current variation during irradiation. A known amount of element (known as *in situ* current normalizer), not present in the matrix, having good sensitivity towards PIGE is added externally to the sample during the target preparation. Samples in pellet form in cellulose matrix along with *in situ* current normalizer were irradiated using 4 or 5 MeV proton beam at FOTIA and 8 MeV proton beam at BARC-TIFR Pelletron and prompt gamma-ray spectrometry was carried out by high resolution gamma-ray spectrometry using HPGe detector system (Table 1). PIGE facility at FOTIA is given in Figures. 1.

3. Results and Discussion

The current normalizers namely F for boron samples, lithium-based ceramics and Al for Zr-based alloy were used for quantification of low Z elements. The developed PIGE method was helpful for determination of total boron and $^{10}\text{B}/^{11}\text{B}$ atom ratio in boron-based neutron absorber including B_4C and boride based refractory materials, total B in Zr-based alloy, simultaneous quantification of Li, Ti and O in lithium titanate using 8 MeV proton beam from TIFR and total Li in Li-ion batteries. The results helped in chemical quality control (CQC) of these in-house prepared materials as well as optimizing the sol-gel synthesis procedure of lithium titanate (Li_2TiO_3) and its chemical quality control and ascertaining the isotopic composition of B ($^{10}\text{B}/^{11}\text{B}$ atom ratio) and its total concentration simultaneously in different boron-based neutron absorbers of carbide/alloy/refractory nature.

Table 1. Relevant reactions and gamma-rays in PIGE

Element	Nuclear Reaction	Energy (keV)
Li	$^7\text{Li} (p, p' \gamma) ^7\text{Li}$	478
	$^6\text{Li} (p, \gamma) ^7\text{Be}$	429
B	$^{10}\text{B} (p, \alpha \gamma) ^7\text{Be}$	429
	$^{10}\text{B} (p, p' \gamma) ^{10}\text{B}$	718
	$^{11}\text{B} (p, p' \gamma) ^{11}\text{B}$	2125
F	$^{19}\text{F} (p, p' \gamma) ^{19}\text{F}$	197
	$^{19}\text{F} (p, \alpha' \gamma) ^{16}\text{O}$	6129
Ti	$^{48}\text{Ti} (p, p' \gamma) ^{48}\text{Ti}$	983
O	$^{16}\text{O} (p, p' \gamma) ^{16}\text{O}$	6129



Figure 1. PIGE Setup at FOTIA

Acknowledgement: Author thanks Dr. P.K. Pujari, Associate Director, Radiochemistry and Isotope Group and Head, RCD, BARC and all co-workers for their contributions towards PIGE work.

References

- /1/ S. Chhillar, R. Acharya, S. Sodaye, et al., *Anal. Chem.* 86 (2014) 11167-11173.
- /2/ R. Acharya, S W. Raja, S. Chhillar, et al., *J. Anal. At. Spectrom.* 33 (2018) 784-791.
- /3/ S. Chhillar, R. Acharya, T.V. Vittal Rao, et al., *J. Radioanal. Nucl. Chem.* 298 (2013) 1597-1603.
- /4/ S. Chhillar, R. Acharya, R. Tripathi, et al., *J. Radioanal. Nucl. Chem.* 305 (2015) 463-467.

A Multitechnique Approach to Study Bioelements

A. Chatt, N. Bahroun, A. Lefsay, C.K. Jayackwreme, D.M. Chevrier, P. Zhang*

Trace Analysis Research Centre, Department of Chemistry, 6274 Coburg Road, Room 212,
PO BOX 15000, Halifax, Nova Scotia, B3H 4R2, Canada.

*E-mail: chatt@dal.ca

1. Introduction

Studies of biologically relevant elements, sometimes referred to as bioelements, have become increasingly important for understanding physiological functions of many organisms. It is now possible to do macro, micro and nano analysis of inorganic and organic compounds, speciation, enzymatic, kinetic, cellular, and structural analysis in conjunction with theoretical modelling to understand mechanism of interactions. We have pursued a multitechnique approach to study various aspects of bioelements. Emphasis will be placed in this lecture on the development and application of a number of methods for inorganic speciation analysis in water, organohalogen species in salmon oil, protein-bound trace element species in bovine kidneys, and selenolate-protected Au₂₅ nanoclusters.

2. Multielement Inorganic Species Analysis

In order to assess any effects, including synergistic and antagonistic effects, of co-contaminant species on the species of interest as well as to study the interconversion among the species of the same element, we have investigated a number of methods. For example, we have developed solvent extraction, high-performance liquid chromatography (HPLC), solid-phase extraction (SPE), and coprecipitation methods in conjunction with neutron activation analysis (NAA) to study speciation of As(III), As(V), Sb(III), Sb(V), Se(IV), Se(VI), the effects of Sb(III)/Sb(V) and Se(IV)/Se(VI) on As(III)/As(V), and interconversion among As(III)/As(V) [1-3].

3. Multielement Organic Species Analysis

Human exposure to persistent lipophilic halogenated organic compounds such as dioxins, PCBs, PBBs, etc., occurs mainly via food, especially fish. Salmon is considered to be a healthy food due to its high

omega-3 fatty acid content. However, organohalogen contaminants are of major concern in this type of fatty fish. We have studied extractable organohalogens (EOX), namely chlorine, bromine and iodine, in farmed Atlantic salmon tissue, skin and oil samples in detail by size exclusion, SPE and thin layer chromatography. Then we used ^{31}P , ^1H and ^{13}C NMR, positive-ion electrospray ionization (ESI+) and tandem MS/MS, and NAA to show that most of the EOX was present in triacylglyceride (TAG) fractions. We then developed GC/MS, both off-line and on-line 2D Ag-HPLC and RP-HPLC, off-line 2D RP-HPLC/GC/MS, off-line 2D Ag-HPLC/ESI(+)/MS, off-line 2D RP-HPLC/ESI(+)/MS, and a new off-line 3-D Ag-HPLC/ESI(+)/MS/GC/MS methods to characterize and identify 80+ TAGs in the salmon skin tissue oil for the first time [4,5].

4. Protein-bound trace elements

We developed biochemical methods for the separation, purification, and characterization of protein-bound trace element species. We have used dialysis, ammonium sulphate precipitation, gel filtration, ion exchange, hydroxyapatite chromatography, HPLC, chromatofocusing, isoelectrofocusing, isotachopheresis, sedimentation equilibrium and enzymatic assay in conjunction with NAA and detected new protein-bound Cd, Cr, Fe, Mn, Mo, Se and Zn species in bovine kidneys.

5. Thiolate- and Selenolate-Protected Nanoclusters

Interaction of metal nanoparticles (NP) and nanoclusters (NC) with proteins was also studied using EXAFS, XANES, and DFT computations. We have observed an intriguing bonding behavior of selenolate-protected Au_{25} nanoclusters ($\text{Au}_{25}(\text{SeR})_{18}$) compared to their thiolate counterparts using temperature-dependent XAS from both the metal (Au L_3 -edge) and ligand (Se K-edge) perspectives. We found that the Au_{13} core of $\text{Au}_{25}(\text{SeR})_{18}$ remains relatively unchanged at low temperature while aurophilic interactions on the surface are significantly longer compared to their thiolate-protected counterpart, $\text{Au}_{25}(\text{SR})_{18}$ [6].

References

- /1/ W. Menendez Sanchez, B. Zwicker, A. Chatt, J Radioanal Nucl Chem 282 (2009) 133-138.
- /2/ Y. Shi, A. Chatt, J Radioanal Nucl Chem 299 (2013) 867-877.
- /3/ Y. Shi, R. Acharya, A. Chatt, J Radioanal Nucl Chem 262 (2004) 277-286.
- /4/ N.H.O. Bahroun, MSc Thesis, Dalhousie University, Halifax, Canada (2007).
- /5/ A.M. Lefsay, PhD Thesis, Dalhousie University, Halifax, Canada (2016).
- /6/ D.M. Chevrier, X. Meng, Q. Tang, et al., J. Phys. Chem. C, 118(2014) 21730–21737.

Separation of Radio-cesium and Radio-strontium from Acidic Radioactive Wastes

*Prasanta K. Mohapatra**

Radiochemistry Division, Bhabha Atomic Research Centre, Trombay, Mumbai-400085, India.

*E-mail: mpatra@barc.gov.in

1. Introduction

In view of the large increase in energy demand and fast dwindling fossil fuel resources, nuclear power is emerging as one of the alternative sources of energy. However, one of the major issues affecting the public acceptance of nuclear energy programme is the generation of large volumes of highly radioactive wastes containing various fission and activation products. Most of the fission product radionuclides are short-lived and can be decayed to stable products within a short cooling period. However, ^{137}Cs and ^{90}Sr constitute the major radioactivity of the high level waste (HLW), a concentrate of the raffinate emanating from reprocessing operations and are responsible for many problems associated with waste management including severe MANREM issues. Separation of ^{137}Cs and ^{90}Sr from HLW facilitates the latter's safe disposal in the deep geological repositories by preventing the deformation due to high heat output in the glass matrices [1]. Also, the separated radionuclides, ^{137}Cs and ^{90}Sr can be used as source of gamma irradiation and power source, respectively [2]. A significant fraction of contemporary research is directed towards studies involving separation of radionuclides from wastes focus on these two radionuclides.

Radio-cesium recovery has been attempted by a variety of techniques such as precipitation, ion-exchange and solvent extraction. Out of these ion-exchange methods with AMP (ammonium molybdophosphate), CST (crystalline silicotitanate) and ferrocyanides have been thoroughly investigated. There have also been numerous reports on solvent extraction using Cs(I) ion selective extractants such as crown ethers and calix-crowns [3]. At ORNL, a thorough investigation has been done for the recovery of radio-cesium from alkaline wastes [4].

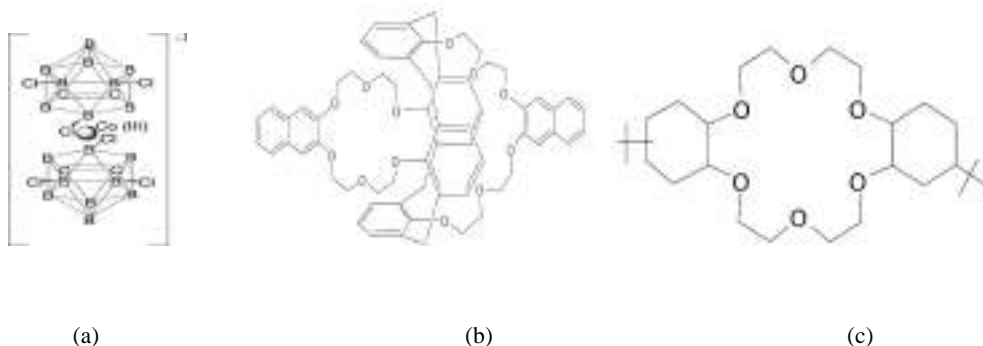


Figure 1. Structural formulae of (a) CCD, (b) calix-crown and (c) crown ether used for the separation of radio-cesium and radio-strontium

2. Results and Discussion

We have been working on the separation of radio-cesium and radio-strontium from acidic feed solutions using crown ether and calix-crown and chlorinated dicarbollide ligands (Figure 1). The solvent extraction studies have been promising in both molecular diluents as well as ionic liquids. Centrifugal extractor runs were carried out using a developed solvent system for radio-cesium recovery from acidic feeds.

Due to high cost of these ligands, separation methods such as supported liquid membrane (SLM), which require reduced ligand inventory, have become attractive alternatives. In this method, the two aqueous phases, i.e., the feed and the receiver are separated by a hydrophobic barrier. This barrier is a micro porous support containing the organic carrier solution (the extractant in a suitable diluent) absorbed by capillary action. Also, the flux can be increased by opting for the hollow fiber contactors. The present lecture will also summarize the liquid membrane transport of Cs(I) and Sr(II) using hollow fiber contactors. A mathematical model was used for the simulation of transport behaviour of metal through the membrane [5].

References

- /1/ IAEA Technical Report Series No. 356 (1993).
- /2/ W.W. Schultz and L.A. Bray, *Sep. Sci. Technol.*, 22 (1987) 191.
- /3/ J. F. Dozol, M. Dozol, R. M. Macias, *J. Incl. Phenom. Macrocyc. Chem.*, 38 (2000) 1.
- /4/ P.V. Bonnesen, L.H. Delmau, B.A. Moyer, R.A. Leonard, *Solv. Extr. Ion Exch.*, 18 (2000) 1079.
- /5/ P. Kandwal, S. Dixit, S. Mukhopadhyay and P.K. Mohapatra, *Chem. Eng., J.* 174 (2011) 110.

Chemical Properties of Flerovium (Element 114)

L. Lens^{1,2,3*}

for a HIM Mainz - GSI Darmstadt – U. Mainz – JAEA Tokai – U. Liverpool – LLNL Livermore – UNLV. – Lund
U. – RIKEN Wako – SINP Kolkata – IITR Uttarakhand – ANU Canberra – U. Oslo – U. Jyväskylä – ITE Warsaw
– collaboration
(The TASCA flerovium chemistry collaboration)

¹Helmholtz-Institut Mainz, 55099 Mainz, Germany

²GSI Helmholtzzentrum für Schwerionenforschung GmbH, 64291 Darmstadt, Germany

³Institut für Kernchemie, Johannes Gutenberg University, 55099 Mainz, Germany

*E-mail: L.Lens@gsi.de

Strong relativistic effects influence the chemical properties of transactinide elements [1]. Currently, the heaviest element ever studied chemically is element 114 (flerovium, Fl) and represents the limit of current day capabilities. Extrapolations in the periodic table [2] and early atomic calculations indicated that Fl would be chemically inert, thus potentially resembling a noble gas [3]. More recent relativistic calculations [4] agree on a lower reactivity than its lighter homolog, Pb, but suggest a distinct metallic character. Experimental studies on Fl are challenging due to low production rates of a few atoms per day at most and short half-lives in the range of only a few seconds. A successful chemistry experiment with Fl thus requires the detection and identification of single Fl atoms through their characteristic nuclear decays. Gas-phase chromatography studies have proven most successful; in current setups, elements as reactive and non-volatile as Pb, up to the inert noble gas Rn, can be studied under identical conditions.

A first experimental study to measure chemical properties of Fl was performed by a PSI/FLNR-collaboration [5]. Three observed radioactive decays were attributed to Fl; two thereof occurred after the Fl atoms passed an Au surface kept at room temperature. Hence, a rather weak physisorption on gold was inferred from these data [5]. At GSI Darmstadt, a first experiment using an improved setup providing much cleaner nuclear spectra was performed behind the gas-filled recoil separator TASCA. Two decay chains, observed under negligible background conditions and firmly attributed to Fl, were detected. Fl was unable to pass the gold surface kept at room temperature [6], pointing at the formation of a metallic bond of Fl with Au. Limited statistics and barely consistent results of these two experiments called for additional experimental studies to clarify the chemical properties of Fl. Further

experiments conducted by the PSI-FLNR collaboration did not lead to the observation of further FI events [7].

Prior to further investigations on FI at TASCA, several improvements to the experimental setup were performed, mainly to optimize the overall efficiency. This was assessed in multiple experiments with short-lived Hg, Pb, and Rn isotopes [8]. In the chromatography setup, the studied elements interact with SiO₂ as well as with Au surfaces, see Figure 1. This allows, e.g., differentiating between the two metals Hg and Pb.

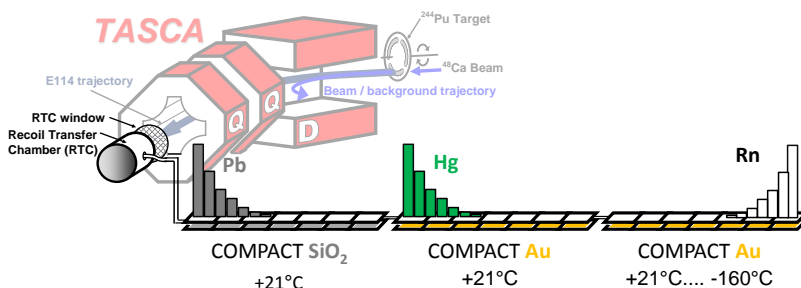


Figure 1. Deposition of Hg, Pb, and Rn in the COMPACT detector array setup, used in 2014.

Based on this, two additional FI experiments were performed at TASCA in 2014/2015. In this talk, the results and their interpretation will be presented and the current status of the chemical studies of FI will be discussed.

References

- /1/ P. Pyykkö *et al.*, Chem. Rev. 88 (1988) 563.
- /2/ B. Eichler, Kernenergie 19 (1976) 307.
- /3/ K. S. J. Pitzer *et al.*, Chem. Phys. 63 (1975) 1032.
- /4/ V. Pershina, Radiochim. Acta. 99 (2011) 459.
- /5/ R. Eichler *et al.*, Radiochim. Acta 98 (2010) 133.
- /6/ A. Yakushev *et al.*, Inorg. Chem. 53 (2014) 1624.
- /7/ Türlér, R. Eichler, A. Yakushev, Nucl. Phys. A 944 (2015) 640.
- /8/ L. Lens *et al.*, submitted to Radiochim. Acta.

Revisiting The Protocols for Low-level NORM Measurement in Environmental Samples

Nabanita Naskar^{1,2*}

¹Department of Environmental Science, University of Calcutta, Kolkata-700019, India

²Saha Institute of Nuclear Physics, Kolkata-700064, India

*E-mail: g.nabanitanaskar94@gmail.com

1. Introduction

Measurement of natural radioactivity is widespread globally in the present nuclear scenario not only to generate radiological baseline data but also to study their radiogenic. Only ~1-2 Bq activity might be present in experimental sample size, which is generally reported in per kg values. Therefore extreme care should be taken for such ultra-low level measurements. Unfortunately there is no universal protocol that to be followed. We have attempted to address different anomalies in NORM measurements through a series of publications in Journal of Radioanalytical and Nuclear Chemistry [1-4].

2. Addressing the rationales of NORM measurements:

2.1 Selection of photopeaks and minimum counting time: Majority of the daughter radionuclides of uranium and thorium series are γ -emitters and there are more than two hundreds photopeaks together. However, only few are acceptable as several of these peaks are either not resolvable or have poor intensities. Thus for narrowing down to a combination of photopeak for U and Th measurement; we introduced a new parameter; obvious but not used by the researcher earlier, ‘relative standard deviation’ (RSD) among the activity values of different photopeaks in $^{238}\text{U}/^{232}\text{Th}$ series. It has been observed that in many cases RSD value is greater than conventional “relative counting error” (RCE). In fact minimizing either RSD or RSD/photopeaks solves different ambiguities in low level NORM measurement. For example, in our set up only three photo-peak combinations either in ^{238}U series (295.22, 351.93 and 609.3

keV) or in ^{232}Th series (338.32, 583.19 and 911.20 keV) results minimum RSD values and therefore recommended as choice of photo-peaks for measurement of low level U or Th.

There are different practices by different research groups about fixing the duration of measurement. It is obvious that long duration would result minimum error, but in practice one cannot always count for long time. Therefore, the most pertinent question is how to choose the minimum counting time. It has been observed that RSD fluctuates around RCE in low counting time. It was also observed that the optimized counting time should be that point where RSD gets a regular trend and closer to RCE.

2.2 Efficiency calibration, essential or not: Efficiency calibration is an integral parameter of gamma-spectrometry. Again by minimizing RSD values, it has been observed for ultra low-level activity that comparator method provides mores reliable data for ^{238}U , ^{232}Th measurements, where known activity of standards are compared against unknown activity of the sample by the following the equation:

$$\frac{\text{Activity of Sample}}{\text{Activity of standard}} = \frac{\text{Count of sample under particular photopeak}}{\text{Count of standard under same photopeak}}$$

The same formula is also applicable to ^{40}K measurement. In an HPGe detector, the efficiency value at the 1460.83 keV photopeak of ^{40}K is very low. When the efficiency curve is fitted, value at this point depends on the fitting program. Therefore to get the reliable data it is recommended to use comparator method for determination of ^{40}K in environmental samples using a range of in-house prepared KCl standards.

At the end, we had successfully applied our rationale for the first report of NORM (^{238}U , ^{232}Th , ^{40}K) level in soil samples collected from the mangrove habitat of Indian Sundarbans [5]. Also the same was used to explore uranium concentration in paleosols and animal fossils from the Siwalik region [7].

Acknowledgement: Author is grateful to Professor Susanta Lahiri, SINP, and Dr. Punarbasu Chaudhuri, University of Calcutta for their support. Author also acknowledges UGC for providing her fellowship.

References

- /1/ N. Naskar, S. Lahiri, P. Chaudhuri, A. Srivastava. J Radioanal Nucl Chem 310 (2016) 1381-1396
- /2/ N. Naskar, S. Lahiri, P. Chaudhuri, A. Srivastava. J Radioanal Nucl Chem 312 (2017) 161-171
- /3/ N. Naskar, S. Lahiri, P. Chaudhuri, A. Srivastava. J Radioanal Nucl Chem 314 (2017) 507-511
- /4/ N. Naskar, S. Lahiri, P. Chaudhuri. J Radioanal Nucl Chem 316 (2018) 709-715
- /5/ P. Chaudhuri, N. Naskar, S. Lahiri. J Radioanal Nucl Chem 311 (2017) 1947-1952
- /6/ A. Srivastava, V. Chahar, V. Sharma et al. J Radioanal Nucl Chem 314 (2017) 1367-1373

Research using LBE Target at SINP

Dibyasree Choudhury^{1}, Susanta Lahiri^{1,2}*

¹Saha Institute of Nuclear Physics, 1/AF Bidhannagar, Kolkata-700064, India

²Homi Bhabha National Institute, 1/AF Bidhannagar, Kolkata-700064, India

*E-mail: dibyasree189@gmail.com

1. Introduction

Lead bismuth eutectic (LBE) having composition of 44.5% Pb and 55.5% Bi, has been proposed to use as converter targets for next generation radioactive ion beam (RIB) production. Besides its use as intense source of neutrons, high-energy proton-irradiated thick LBE targets may also be viewed as an alternative enormous source of clinically important radionuclides [1]. In this abstract, we will focus on recent works on LBE target carried out by the radiochemistry laboratory, SINP. Some of these works have been carried out in collaboration with CERN-ISOLDE group.

2. Inventory of Radionuclides

Impingent of high-energy proton beam on LBE targets initiates various nuclear reactions such as spallation, fission, fragmentation, etc., thereby produces huge numbers of radioisotopes. In 2014, for the first time total inventory of such radionuclides were attempted [2]. Six cylindrical LBE targets of varying lengths (1-8 mm) were bombarded with 1.4 GeV ¹H beam. Total 111 radionuclides from ⁷Be to ²⁰⁷Po were identified in the target of length 8 mm. As an extension to this experiment, the LBE target lengths were increased up to 50 mm and were irradiated with 1000 pulses of 1.4 GeV proton beam, delivering 5×10^{15} protons in 2455 s. [3]. The most notable difference with the earlier experiment, that this time, production of ²⁰⁹At was observed which was contributed by the secondary particle reactions like ³He, ⁴He or pion exchange reactions.

3. Radiochemical experiments with p/α bombarded LBE target

One of the key issues regarding use of LBE is the production of radiotoxic polonium radionuclides via ²⁰⁹Bi(p,xn) or ²⁰⁹Bi(p,γ) reactions. Accurate experimental measurement of Po production from LBE target is an important task from health physics view point. We reported a quantitative estimation of Po

produced in proton irradiated LBE targets from 8.95-21.95 MeV by liquid-scintillation counting (LSC)-TDCR technique [4]. TDCR is an excellent standardization approach of LSC which employs three photomultiplier tubes to experimentally measure the ratio of triple coincidences to the logical sum of double coincidences, which is a measure of its efficiency. For the first time, quantitative and qualitative estimation of no-carrier-added (NCA) Po radionuclides was carried out without any radiochemical separation of bulk Pb and Bi, which are trillion times more abundant than NCA Po radionuclides. Time resolved α -counts for 13 months from EOB identified a mixture of $^{208,210}\text{Po}$ in the target matrix. Production cross-sections of $^{207,208,210}\text{Po}$ were calculated.

The main challenges while dealing with radiochemistry of LBE is that the particular radionuclide of interest has to be separated from hundreds of radionuclides present in the target matrix as well as from bulk Pb and Bi. Moreover, presence of kilogram amount of bulk materials restricts use of complex chemical methods. Therefore, simple wet chemistry is of preference. The first chemistry attempted by us reported the separation of NCA $^{209,210}\text{At}$ radionuclides from α -irradiated LBE target by simple precipitation [5]. Ammoniacal AlCl_3 selectively precipitated bulk Pb, Bi and co-produced NCA Po, keeping astatine in the supernatant. We also developed method of separation of bulk Pb and Bi hoping that co-produced radionuclides would be lexically distributed between Pb or Bi fraction. The separation was carried out by selective precipitation of bismuth by de-ionised water from HNO_3 acid solution of Pb and Bi [6]. In line of the same approach, we also reported the use of liquid anion exchangers such as trioctyl amine (TOA), etc., to separate Pb and Bi [7].

Conclusion

There is enough scope and challenges left for exploring the radiochemical aspects of lead bismuth eutectic and to develop new radiopharmaceutical with the unconventional radionuclides produced in high-energy proton irradiated LBE target.

References

- /1/ D. Choudhury, S. Lahiri, Appl. Radiat. Isotopes 137 (2018) 33-40
- /2/ M. Maiti, K. Ghosh, T. Mendonca, T. Stora, S. Lahiri, J Radioanal Nucl Chem 302 (2014) 1003–1011.
- /3/ D. Choudhury, S. Lahiri, N. Naskar, et al., 9th International Conference on Isotopes (9ici), Doha, Qatar November 12- 16, 2017
- /4/ D. Choudhury, S. Lahiri, European Phys. J. A (accepted).
- /5/ M. Maiti, S. Lahiri, D. Kumar, D. Choudhury, Appl. Radiat. Isotopes 127 (2017) 227-230.
- /6/ D. Choudhury, S. Lahiri, N. Naskar, J Radioanal Nucl Chem 314 (2017) 2551–2555
- /7/ D. Choudhury, S. Lahiri, J Radioanal Nucl Chem (2018) doi.org/10.1007/s10967-018-6125-5

Contributed Papers

Hyperfine Interaction of Electron and Nuclear Spins in InSb Two-Dimensional Electron Gas Towards Quantum Information Processing

M. M. Uddin^{1,2}, H. W. Liu^{3,4}, K. F. Yang³, T. D. Mishima⁵, M. B. Santos⁵,
K. Nagase³, Y. Hirayama^{1,3,6}*

¹*Department of Physics, Tohoku University, Sendai, Miyagi 980-8578, Japan*

²*Department of Physics, Chittagong University of Engineering & Technology, Chittagong-4349, Bangladesh*

³*ERATO Nuclear Spin Electronics Project, Sendai, Miyagi 980-8578, Japan*

⁴*State Key Laboratory of Superhard Materials and Institute of Atomic and Molecular Physics,
Jilin University, Changchun 130012, People's Republic of China*

⁵*Homer L. Dodge Department of Physics and Astronomy, University of Oklahoma, 440 West Brooks, Norman,
Oklahoma 73019-2061, USA*

⁶*WPI Research Center, Advanced Institute for Materials Research, Tohoku University, Sendai 980-8577, Japan*

*E-mail: mohi@cuet.ac.bd

Nuclear spins in low-dimensional semiconductor structures have attracted growing interest because the long spin coherence time of nuclei facilitates the implementation of quantum information processing (QIP). The quadrupole splitting of ¹¹⁵In have been reported in a single InSb two dimensional electron gas (2DEG) that are of practical importance for the coherent control of the ten nuclear-spin quantum levels and for the implementation of multiple NMR-based quantum bits (≥ 2) [1]. The success of gate controlled InSb quantum wells [2, 3] allows us to perform pump and probe technique to investigate temperature dependent nuclear spin relaxation time T_1 at different filling factors (ν). Skyrmion like collective spin excitations in the domain walls enhance dynamic nuclear polarization in the quantum Hall ferromagnet around $\nu = 2$ characterized by a short (~ 60 sec) and temperature-independent T_1 . On the other hand, relatively long (~ 400 sec) and temperature dependent T_1 with following Korringa law have been demonstrated in the absence of the domains as well as collective spin texture at around $\nu = 3$. In addition, the large Zeeman, cyclotron and exchange energy scales of the InSb 2DEG favour to demonstrate the resistively detected NMR (RDNMR) signal at elevated temperature up to 6 K. Our results as shown in Fig (a) and (b) clearly show that the InSb 2DEG is a suitable candidate for implementation of the high temperature nuclear-spin based quantum information processing (QIP).

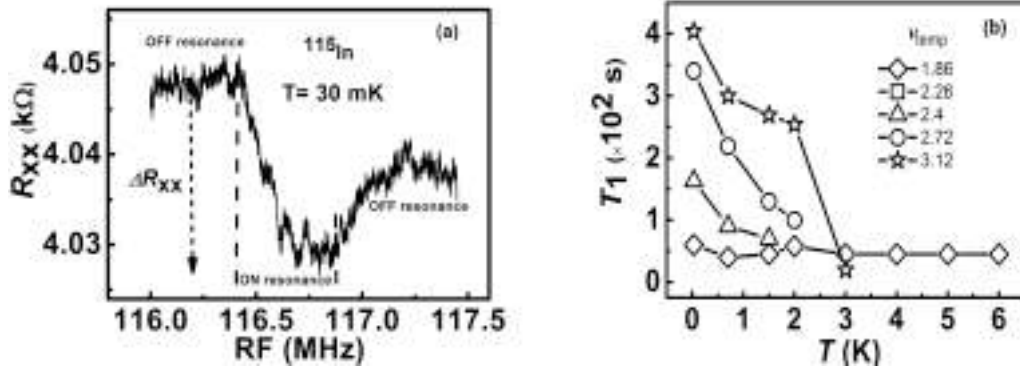


Figure 1. (a) The dispersive line shape of the RDNMR signal of ^{115}In at $I_{dc} = 760 \text{ nA}$ and $B_z = 5.58 \text{ T}$ with tilt angle $\theta = 63.5^\circ$. (b) Temperature dependence of nuclear spin relaxation time T_1 at different filling factors (ν)

References

- /1/ H. W. Liu, K. F. Yang, T. D. Mishima, et al., Phys. Rev. B 82 (2010) 241304(R).
- /2/ M. M. Uddin, H. W. Liu, K. F. Yang, et al., Appl. Phys. Lett. 98 (2011) 142109.
- /3/ M. M. Uddin, K. F. Yang, K. Nagase, et al., Appl. Phys. Lett. 101 (2012) 233503.
- /4/ M. M. Uddin, K. F. Yang, K. Nagase, et al., Appl. Phys. Lett. 103 (2013) 123502.

Radiotracer Application for Rapid Measurement of Contribution of Stem Assimilates Towards Grain Filling in Wheat

Bhupinder Singh, Sumedha Ahuja, Poonam Yadav*

Nuclear Research Laboratory, CESCRA, ICAR-Indian Agricultural Research Institute, New Delhi-110012, India

* E-mail: bhupindersinghiari@yahoo.com

1. Introduction

Photosynthesis during the grain filling period contributes about 60–100% of the final grain carbon content [1] while the remainder is realized through remobilization of stored carbohydrate laid down before anthesis in stem and leaf sheath [2]. Efficiency for translocation of photosynthates between source and sink is a critical determinant of grain filling. However, the source to sink relationship is known to change during the crop growth and also in response to biotic and abiotic stress. For higher economic yields, both the source and the sink efficiency are important and influence each other. We hypothesize that stem photoassimilate reserves can play a significant role in improving sink efficiency under condition of depleted source efficiency, i.e., during leaf senescence. Radiotracers and radiations have immense applications [3,4] and in this paper we report a method of stem injection of ^{14}C -sucrose to measure the contribution of stem reserves towards grain filling during induced leaf senescence in field grown wheat.

2. Experiment

Experiments were conducted using ^{14}C -sucrose to measure the contribution of pre-anthesis stem reserve to the developing sinks at different spikelet positions (apical, middle and basal) in wheat during induced flag leaf senescence. Internode feeding of ^{14}C -sucrose (10 μL volume, specific activity 5GBq/mmol) was executed at 20 days stage after anthesis in wheat plants at 24h after the foliar application of KI (0.3%) to induce leaf senescence. Decline in leaf chlorophyll was measured and taken as a signature of leaf senescence. Developing grains from different spikelet positions of the main

shoot ear were collected, oven dried, and ^{14}C accumulation at different spikelet positions was measured using liquid scintillation counter (TRICARB, USA).

3. Results and Discussion

We have earlier shown that sink demand in terms of the grain filling along the wheat ear is not uniform with the middle spikelets accumulating a larger share of assimilates than the apical and the basal spikelets (5). A rapid decline of photosynthesis after anthesis due to onset of leaf senescence limits the grain development if not compensated efficiently by stem photoassimilates. Radiotracer (^{14}C) aided in precise measurement of the contribution of stem assimilates towards grain filling in bottom, middle and apical sinks within a wheat spike. At the level of different spikelet position, a higher mobilization of 1st node stem reserves into the bottom spikelets was measured during leaf senescence (Fig 1). This shows that source limitation

created by leaf senescence appears to be compensated by translocation of stem reserves into the grains. This indicates that the translocation of photo-assimilates from the stem contributes particularly to the development of grains in the basal than the middle or the top position spikelets during the leaf senescence. These

results, obtained using radiotracer ^{14}C , strongly indicate that stem assimilates (^{14}C) are transported to basal grains in preference to middle and apical spikelet grains during the onset of flag leaf senescence in wheat.

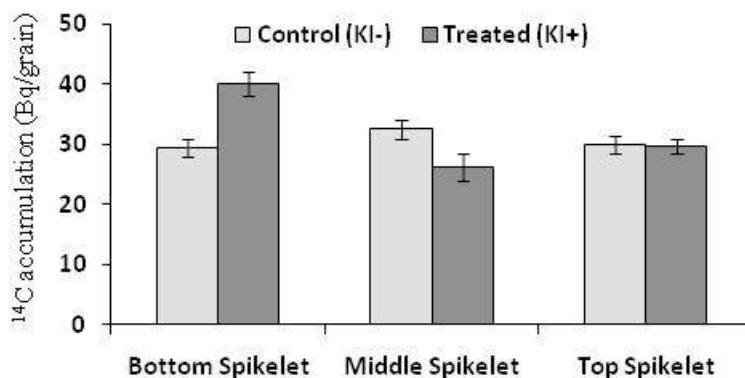


Figure 1. Mobilization of ^{14}C assimilates (Bq/grain) from stem to grains developing at different position spikelets in wheat.

References

- /1/ T. Inoue, S. Inanaga, Y. Sugimoto and K. El Siddig, *Photosynthetica* 42 (2004) 99-104.
- /2/ E.H. Murchie, J. Yang, S. Hubbart, P. Horton, S. Peng *J. Expt. Bot.* 53 (378) (2002) 2217-2224.
- /3/ B. Singh, S. Ahuja, R.K. Singhal, P.V. Babu *J. Radioanal. Nucl. Chem.* 298 (2013) 249-257.
- /4/ B. Singh, S. Ahuja, R. Pandey and RK Singhal *J. Radioanal. Nucl. Chem.* 302 (2014) 1315-1320.
- /5/ B. Singh, P.S. Datta, *Rad. Phys. Chem.* 79 (2010) 819-825

⁹⁹Mo / ^{99m}Tc Generator Based on Alumina ⁹⁹Mo-Molybdate (VI) Gel of High Radionuclidic Purity

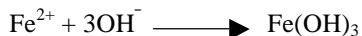
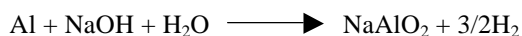
M.A. El-Absy,¹ T.W. Fasih^{1}, M.A. El-Garhy¹, M.A. El-Amir¹,
H.E.Ramadan¹, M.F. El-Shahat¹*

¹Radioactive Isotopes and Generators Department, Hot Laboratories Centre, Atomic Energy Authority, 13759, Cairo, Egypt

²Chemistry Department, Faculty of Science, Ain Shams University, Cairo, Egypt.

*E-mail: tharwatfaseih@yahoo.com

In this work high radionuclidic pure alumina ⁹⁹Mo-molybdate (VI) gel is synthesis for separation of the generated ^{99m}Tc (T_{1/2}= 6 h) radionuclide from small chromatographic columns. Unless otherwise stated for preparation of the starting radiotracer mixture solution, accurate amounts of MoO₃ powder (1.0 g tagged with 10 mCi ⁹⁹Mo (T_{1/2}=66 h)), 1.2 g Al thin pieces of Al foil (containing ~ 2.74 mg Fe) and 120 mg FeCl₃.6H₂O were dissolved in 30 ml ~ 5 M NaOH solution. The exothermic dissolution reaction was completed in ~ 15 min with evolution of H₂ gas. The final alkali concentration was found to be ~ 4 M NaOH. Dissolution of Fe from the Al foils and reduction of FeCl₃ by H₂ gas in hot concentrated alkali solution results in the formation of soluble Fe(II) species. Soluble sodium molybdate tagged with ⁹⁹Mo, sodium aluminate and hydroxy Fe(II) hydroxide may be the final dissolution products according to the following reactions:



The formed Fe(III) mineral and the co-precipitated radionuclide impurities and separated by centrifugation. Supernatant is acidified to pH 5.5 with concentrated HNO₃ acid to precipitate dissolved NaAlO₂. In situ precipitated pseudoboehmite incorporated the ⁹⁹Mo-molybdate (VI) anions from solution. Precipitation of Fe(III) minerals from aluminate/⁹⁹mo-molybdate mixture solution is a promising procedure for purification of neutron activated ⁹⁹Mo from a plenty of side-product trace impurities such as ⁹⁵Zr/⁹⁵Nb, ^{92m}Nb, ^{124,125}Sb, ¹²⁵Sn, ¹⁰³Ru, ⁵⁹Fe, ⁶⁰Co and ⁵¹Cr. Fig. 1 shows the elimination % of ⁹⁵Zr, ⁹⁵Nb, ¹⁰³Ru, ¹²⁴Sb, ¹²⁵Sb and ¹²⁵Sn from 33 ml aluminate/⁹⁹Mo-molybdate

mixture solution in ~ 4M NaOH via oxidation of different Fe(II) doses with 0.5 ml 30 % H₂O₂. The elimination % of ⁹⁵Zr, ⁹⁵Nb, ¹⁰³Ru, ¹²⁴Sb, ¹²⁵Sb and ¹²⁵Sn radionuclides were found to be Fe(III)/Fe(II) molar ratio dependent. The elimination % was gradually increased with increasing the total amount of fed iron dose in the system. There are two distinct elimination % sets namely ⁹⁵Nb, ¹⁰³Ru and ⁹⁵Zr and ¹²⁴Sb, ¹²⁵Sb and ¹²⁵Sn, respectively. It was found that ≥ 91, 84, ≥ 65, 8, 12 and 9 % of ⁹⁵Zr, ⁹⁵Nb, ¹⁰³Ru, ¹²⁴Sb, ¹²⁵Sb and ¹²⁵Sn were achieved at a total of 2.74 mg Fe from the Al wrapper, respectively. Elimination % of ⁹⁵Zr was increased from ~ 68 % at 0.146 x 10⁻² M Fe to ~ 94 % at 0.8 x 10⁻² M Fe.

Soluble sodium aluminate anions, remained in the supernatant together with 10 mCi ⁹⁹Mo-molybdate (VI) remained after precipitation of 120 mg FeCl₃.6H₂O, were transformed into an insoluble aluminum oxyhydroxide via acidification with concentrated HNO₃ at pH 5.5.

Meanwhile normal molybdate anions MoO₄²⁻ condense into paramolybdates, Mo₇O₂₄⁶⁻, and preferentially transferred from the solution via adsorption onto the surface of in-situ precipitated pseudoboehmite with a yield of ~ 97.5% ⁹⁹Mo at pH 5.5. The formed alumina ⁹⁹Mo-molybdate (VI) matrix was dried at 50°C for 1 day, crushed and sieved to ~ 0.15 - 0.8 mm particles size suitable for chromatographic column operations.

Purified gel matrices are separately conditioned and packed as elutable ⁹⁹Mo/^{99m}Tc generators. ^{99m}Tc radionuclide is eluted in 10 ml 0.9% saline solution at a flow rate of 1.0 mL/min with high elution yield, concentrated in 5 mL eluate and chemical, radiochemical and radionuclidic purity ≥ 99.99% suitable for use in nuclear medicine application.

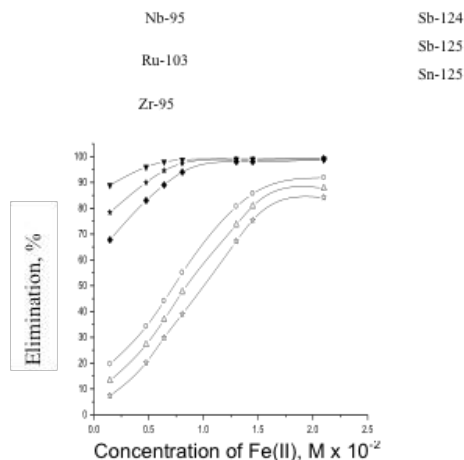


Figure 1. Effect of Fe(II) concentrations on elimination % of Nb-95, Ru-103, Zr-95, Sb-124, Sb-125 and Sn-125 radionuclides from ~ 33 mL aluminate/⁹⁹Mo- molybdate mixture solutions in ~ 4M NaOH via oxidation with 0.5 mL 30 (w/v)% H₂O₂.

Elemental Analysis of *Pterocarpus Santalinus* by PIXE and ICP-MS: Chemometric Approach

J. C. Rao¹, B. Gowri Naidu¹, S. Srikanth², P. Sarita¹, G. J. Naga Raju^{2*}

¹Department of Physics, GIT, GITAM University, Visakhapatnam-530 045, India

³Department of Physics, UCEV, JNTUK, Vizianagaram-535 003, India.

*E-mail: gjnraju@yahoo.com

1. Introduction

Since times immemorial, in every culture throughout the world herbal drugs constituting medicinal plant preparations have been used in the amelioration of various diseases ranging from common cold to cancer. Medicinal plants in particular have served as rich sources of many trace elements for man and it is suggested that this is an important factor in the curative effect of these plants [1]. Majority of the plant-based drugs prescribed by the local herbal practitioners do not undergo strict approval procedures and regulations, a certain amount of uncertainty is associated with their inorganic constituents, effective dose range and mechanism of action [2].

This study was undertaken with an aim to determine the levels of elements by PIXE and ICP-MS analytical techniques in bark samples of *Pterocarpus Santalinus* medicinal plant used in the treatment of Diabetes Mellitus (DM) and analyze the alteration with respect to the geographical region from where they are collected. Using the obtained elemental profile, principle component analysis (PCA) and hierarchical cluster analysis (HCA) classification techniques were performed to understand the association among the elements

2. Materials and Methods

Medicinal plant samples were collected from four different geographical regions of the state of Andhra Pradesh: (1) Vizianagaram, (2) Visakhapatnam, (3) Vijayawada and (4) Tadepalligudem. The processing and preparation of the samples in accordance with the two analytical techniques can be found in our earlier work [3]. The PIXE measurements were carried out using a 3 MeV collimated proton beam from the 3 MV Tandem Pelletron accelerator at the Ion Beam Laboratory of Institute of

Physics, Bhubaneswar, India. The ICP-MS analysis was carried out with an Agilent 7700 series ICP-MS system available at Centre for Studies on Bay of Bengal, Andhra University, Visakhapatnam, India. The accuracy of both these techniques was checked by analyzing National Institute of Standards and Techniques (NIST) certified reference materials, peach leaves (1547) and apple leaves (1515). The Guelph PIXE (GUPWIN) and IBM SPSS Statistics version 24 software packages were used to analyze PIXE spectra and chemometric techniques respectively

3. Results and Discussions

Significant levels of Mn are present in the bark of *Pterocarpus Santalinus* medicinal plant from all the four regions with concentrations ranging from 157 to 378 $\mu\text{g/g}$ (PIXE data) and 155 to 375 $\mu\text{g/g}$ (ICP-MS data). Samples from Tadepalligudem region had the lowest concentration while those from Visakhapatnam had the highest concentration of Mn. Among all the four regions, highest concentrations of Cu (37 $\mu\text{g/g}$) and Zn (46 $\mu\text{g/g}$) were found in *Pterocarpus Santalinus* bark from Tadepalligudem region. The concentration of Fe was observed to be very high (22000 $\mu\text{g/g}$) in the samples from Visakhapatnam region. Chromium was detected in samples from all the four regions with concentration ranging from 6.27 to 14.2 $\mu\text{g/g}$ (PIXE data) and 3.09 to 17.8 $\mu\text{g/g}$ (ICP-MS data). Visakhapatnam samples contained the highest concentration of Cr while the least concentration was exhibited in the Vijayawada sample.

As DM is a disease of metabolic abnormality, elements as such or as a component of enzymes may play a significant role in the development and control of DM. The elements K, Ca, Cr, Mn, Cu, and Zn are responsible for the secretion of insulin from beta cells of the islets of Langerhans and are involved in potentiating insulin action [4]. Supplementation of these elements through the consumption of this plant might help in the treatment of DM. For ICP-MS elemental profile, the PCA generated two principal components that explained 94% of the total variance in the data. HCA classified three significant groups based on the elemental concentrations.

4. References

- /1/ M Ebrahim, M. A., Etayeb, H. Khalid, M.Noun , M. Roumie , B. Michalke, Applied Radiation and Isotopes 90 (2014) 218-224.
- /2/ J.Chang, Biochemical pharmacology 59 (2000) 211-219.
- /3/ J. Chandrasekhar Rao, B.G. Naidu, P.S arita, S. Srikanth, G.J. Naga Raju Materials Science and Engineering Conference Series 225 (2017) 012235.
- /4/ J.D Kruse-Jarres, M. Rukguaer, J Trace Elem. Med. Biol. 14 (2000) 21–27.

Environmental Radioactivity Around the European Spallation Source facility

D. Ene^{1}, R. Avila², T. Hjerpe², B. Jaeschke², K. Stenberg²*

¹Environment, Health and Safety Department, European Spallation Source ESS-ERIC, Lund, Sweden

²Facilia AB, Gustavslundsvägen 151C, SE-167 51 Bromma, Sweden

*E-mail: Daniela.ene@esss.se

1. Introduction

A radiological assessment, based upon the actual status of the European Spallation Source ESS design, has been produced to demonstrate that the sum of the doses resulting from the exposure of any member of the public to ionizing radiation does not exceed the specified dose constraint of 50 $\mu\text{Sv}/\text{year}$. An approach was adopted in the assessment. The relative importance of the dose contributions was initially assessed by comparing doses calculated using the IAEA SRS19 screening approach against the predefined dose value of 0.1 $\mu\text{Sv}/\text{year}$. In the second step, for all radionuclides identified as having significant dose contribution, realistic dose factors were derived using dispersion and radio-ecological realistic models. The total dose rate was finally obtained by summing all the dose rates from the realistically-treated radionuclides and from the radionuclides which were screened out in the first step.

2. Radioactive releases to the surrounding environment

The evaluation of exposures to impacted environmental media considers three main pathways: i) airborne releases of radionuclides through ventilation, ii) liquid discharges of radionuclides to the sewage system and downstream surface water (rivers and sea), iii) migration of radionuclides with groundwater following activation of surrounding soil. The impact assessment has two main phases: i) estimation of the source term (ST), by means of calculation of radioactivity (Monte Carlo radiation transport simulations coupled with activation calculations by means CINDER'90 code) that can be released annually and taking into account the design parameters of abatement systems, e.g. ventilation system (HVAC), and ii) applying dispersion and radionuclide transport models to calculate concentrations in environment and dose models to calculate doses to reference groups of population

around the site. The considered land-use classes are: 1) residential building and garden plot, 2) cropland, 3) pastureland, 4) forest, 5) lake, 6) freshwater body, and 7) sea basins. In addition, sewage plant is considered as a type of land use. The calculation of effective doses to the reference population due to airborne releases was performed for two scenarios: i) a chronic constant 50 year long-term release with average atmospheric dispersion conditions and radionuclide accumulation in environment, and ii) short-term periodic atmospheric releases during which atmospheric dispersion conditions may significantly differ from the average conditions. Two main release points were accounted for: i) main stack, the exhaust of both continuous releases from the accelerator tunnel, target station and instrument systems as well as the periodic short-term releases from hot cell, and ii) waste stack, the point of releases from the waste facility, during short-term campaigns. The total annual dose obtained is below $1 \mu\text{Sv/a}$ and is dominated by ^{13}N , ^{11}C , ^{41}Ar , ^{15}O , ^3H and ^{125}I . The reduction effect of filtration system on the total doses from continuous releases is marginal, since the total doses are dominated by radionuclides that are released in gas form. All radioactive wastewater produced during the operation will be sent to the waste facility for treatment and further discharged to sewage plant. Radionuclides potentially contained in the wastewater originate from: i) activation of the water, and ii) contamination of water with corrosion products and dust. Realistic dose factors were used to derive discharge limits (Bq/a), for each radionuclide. The results show that doses will be formed practically 100% by ^3H . Tritium concentrations in well water are one order of magnitude below the admissible level of 100 Bq/L. Transport of other radionuclides is delayed by sorption, and their concentrations are negligible.

3. Stray radiation

Stray radiation fields were studied under the assumption of 5 MW beam power at 2 GeV and it was found that the maximum annual dose to members of the public is lower than $10 \mu\text{Sv/year}$.

4. Impact to non-human biota

Assessment of the dose for non-human biota required development of the ERICA computer code to address data and exposure pathways gaps relevant to the ESS site. The results indicate that no organisms are subjected to dose rates above the screening value of 10 mGy/h.

5. Conclusion

It was concluded from this assessment that during normal operation, the ESS facility will comply with the dose constraints imposed by the Swedish Authority.

Microarray Immunoassay for Thyrotropin on Track-Etched Membranes Using Radiotracers

Bharti Jain, Savita Kulkarni, S. Banerjee, M.G.R. Rajan.*

Radiation Medicine Centre, Bhabha Atomic Research Centre, Tata memorial Hospital, Parel, Mumbai 400012.
*E-mail: bharti.jain09@gmail.com

1. Introduction

Determination of serum level of thyroid stimulating hormone (TSH) or thyrotropin is an important biomarker for clinical assessment of thyroid status [1]. Microarray immunoassay (MI) or multianalyte immunoassay (MAIA), provides several advantages over conventional ones like lower sample and reagent consumption, higher through put, integration of multiple assay steps, assay automation and multiplexing capability [2]. Development of MI requires immobilization of antibodies at high spatial density in functionally active form on a suitable support to form “antibody-chip”. This work describes development and validation of MI for measuring human TSH using polycarbonate track-etched membranes (PC-TEM) as a novel solid support and radioisotopes for detection.

2. Experimental

PC-TEMs are highly microporous (10^5 - 10^8 pores/cm²) and thin (10-20 micron) membranes made through a combination of charged particle bombardment and chemical etching [3]. PC-TEMs were activated using 2.5% glutaraldehyde for 2 h and washed with phosphate buffer saline (PBS). Antibody-chip was prepared by spotting 0.5 μ L (1 mg/ mL) of anti-TSH monoclonal antibodies on the activated PC-TEM at pre-determined locations in duplicates and blocking remaining active sites using 4% BSA. Standards (S1-S8) were prepared by spiking recombinant human TSH in horse hormone free serum at concentrations of 0, 0.15, 0.5, 1.5, 5, 15, 50 and 100 μ U/mL. MI was performed by reacting the antibody-chip with 50 μ L of standards/ QC samples/ test serum sample and 100 μ L of ¹²⁵I-monoclonal anti-TSH antibodies (~100,000 cpm/100 μ L) for 2 h with gentle agitation and washed thrice with PBS containing 0.1% Tween-20. TEMs were imaged using PhosphorImager (Typhoon Trio+).

Background-subtracted mean spot intensity of duplicate spots was plotted against analyte concentration to provide standard curve. MI was validated using several parameters viz. sensitivity, range, reproducibility, linearity, recovery and comparison to IRMA.

3. Results

As shown in Figure 1(a), typical standard curves for TSH was generated using MI. Figure 1(b) shows corresponding autoradiogram. Developed MI achieved sensitivity of 0.01 $\mu\text{IU/mL}$ with upper limit of the working range of 100 $\mu\text{IU/mL}$. The intra-assay and inter assay %CV for two QC samples was less than 20%. Mean recovery for four serum samples spiked with three standards was 105.1 %, 110.6% and 115.7% respectively. Observed to expected ratio was determined for linearity studies varies from 85.5% to 112 %. Linearity and recovery show compatibility of standard matrix to human serum samples. 140 human serum samples were analysed by MI and showed excellent correlation to IRMA. ($\text{MI}=1.01*\text{IRMA}-0.36$, $r = 0.98$, $p < 0.001$, $n = 140$) as shown in Figure 1(c).

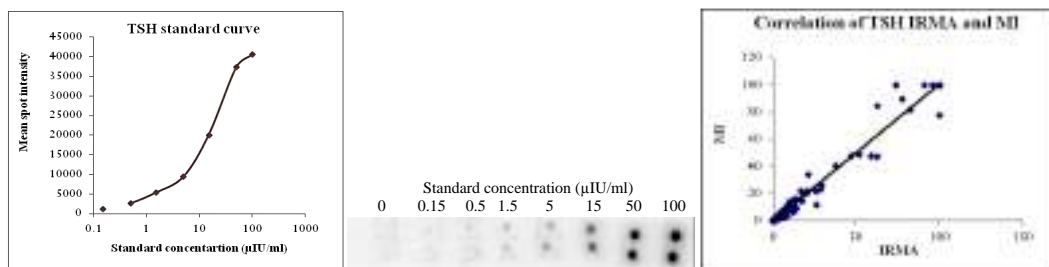


Figure 1. Autoradiogram (a), graph (b) showing standard curve for TSH MI. Graph (c) showing correlation of MI and IRMA.

4. Discussion and Conclusion

Here, we have developed a sensitive MI with acceptable accuracy and reproducibility on PC-TEM using ^{125}I -labeled antibodies. TEM being highly microporous provides high immobilization capacity and thereby high sensitivity. Isotopic tracer providing a convenient means of detection as compared to non-isotopic detection with no time bound readings, dust interference or auto-fluorescence. This sets a platform for further multiplexing for several analytes.

References

- /1/ D. Wild, *The immunoassay handbook*. 2005: Gulf Professional Publishing.
- /2/ R.P.Ekins, *J Pharm Biomed Anal*, 7 (1989) 155-168.
- /3/ P.Apel, *Radiat. Meas.*, 34 (2001) 559-566.

Assessment of Heavy Metals in Poultry Chicken Giblets Using ICP-MS

Mayeen Uddin Khandaker^{1,2,}, Nwokoma Oliver Chijioko¹*

¹Department of Physics, University of Malaya, 50603 Kuala Lumpur, Malaysia

²Center for Radiation Sciences, School of Healthcare and Medical Sciences, Sunway University, 47500 Bandar Sunway, Selangor, Malaysia

*E-mail : mu_khandaker@yahoo.com

Poultry chicken is playing a key role as a major component of daily diet to humans. It is a versatile and delicious choice - ready to grill, barbecue, roast, stir-fry, microwave, poach or sauté, and plays an important role from many international cuisines to our family table. It is also used in the production of several seasoning such as maggi and knorr chicken flavor grains globally. Therefore, the high demand of poultry chicken has also influenced their production and has been enhanced extensively by several technological contributions and inputs [1]. Poultry feeds are made from cereal and legume grain crops like corn, soya bean, rice, oat, wheat, barley, millet, bean, wild rice, teff, fonio, spelt, lentils, carob, peanuts, tamarind etc [2]. Soil is the main reservoir of heavy metals in the ecosystem, and all foodstuffs are grown in the soil [3]. Heavy metals are naturally occurring elements that have a high atomic weight and a density at least 5 times greater than that of water. Toxic heavy metals are found naturally in the earth, and become concentrated as a result of human caused activities [3]. They may enter into plant, then subsequently to animal and human tissues via air inhalation, diet and manual handling. Their multiple industrial, domestic, agricultural, medical and technological applications have led to their wide distribution in the environment; raising concerns over their potential effects on human health and the environment [4]. Their toxicity depends on several factors including the daily intake, route of exposure, chemical species etc.

Recognizing their potential hazards to human health, heavy metals concentrations in chicken giblets were assessed to determine their potential toxic level and impact to the human body upon their consumption. The concentration of 14 heavy metals such as; Fe, Cu, Mg, Zn, Al, Hg, Sb, As, Pb, Se, Ni, Sr, Cr and Sb were determined in 280 of poultry chickens giblets; liver, gizzard and heart samples that was collected from different local markets of Selangor Kuala Lumpur, Malaysia. The analysis was

performed using the Inductively Coupled Plasma-Mass Spectrophotometry (ICP-MS) and the obtained results were compared with the permissible limits set by World Health Organization (WHO) and The Australia Total Dietary Survey (ATDS). The result shows that all liver samples contain all toxic metals in ($\mu\text{g}/\text{kg}$) as Al (0.22), Cr (0.00508), As (0.00202), Se (0.00475), and Zn (0.4605), Cd (0.00204), Hg (0.03297), Pb (0.00187), Cu (0.047), and Sb (0.5187) followed by heart and with values of Al (0.19037), Cr (0.01725), Se (0.00414), Zn (0.620), Cd (0.01659), Hg (0.014658), Pb (0.0472), Cu (0.06476) and Sb (0.69076) with no As detected. The gizzard samples show no traces of Pb and Cd. The heart were found to have the highest concentration of Sb 0.690 $\mu\text{g}/\text{kg}$ and followed by the Zn 0.62 $\mu\text{g}/\text{kg}$ in the same sample.

The results indicated reasonable variation in the concentration of the measured metals among the studied samples. One-way analysis of variance (ANOVA) shows that, the concentrations of the heavy metals in the gizzard, liver and heart samples were statistically significant at $p < 0.05$, which indicates that the determined heavy metals are from the similar origin and/or similar feedstuffs. However, the concentration of all the metals was within the permissible limits set by the WHO and ATDS with the exception of Sb in all samples which is worthy for regular monitoring. Thus, the consumption of chicken livers, gizzards or hearts by the inhabitants of Selangor, Kuala Lumpur and its environs will not result to heavy metal toxicity. However, the anthropogenic factors that proliferate heavy metals in the environment should be discontinued and discouraged.

References

- /1/ J.S. Eales and L. J. Unnevehr, *Am. J. Agricultural Econ.* 70(3) (1988) 521-532.
- /2/ A.M. Amerah, V. Ravindran, R.G. Lentle, D.G. Thomas. *World's Poultry Sci. J.* 63 (2007) 439-455.
- /3/ S.Kärenlampi, H.Schat, J.Vangronsveld, et al., *Environ. Pollut.* 107 (2000) 225-231.
- /4/ Y. Guan, C. Shao, and M. Ju. *Int. J. Environ. Res. and Public Health* 11 (2014) 7286-7303.

Evaluation of Radon Concentration in Irrigation and Drinking Waters from Eastern Part of Oman Using Nuclear Track Detectors and Estimation of Corresponding Doses to Human Health

Saleh Mansoor Nasser¹, Mayeen Uddin Khandaker^{1,2,}*

¹Department of Physics, University of Malaya, 50603 Kuala Lumpur, Malaysia

²Center for Radiation Sciences, School of Healthcare and Medical Sciences, Sunway University, 47500 Bandar Sunway, Selangor, Malaysia

* E-mail : mu_khandaker@yahoo.com

The main source of radiation exposure to human life is Radon and its progeny. ²²²Rn is produced from the decay of ²²⁶Ra; a decay product of ²³⁸U, which is found in rocks, soil, natural gas and ground water. Recent study shows that the concentration of uranium in Earth's Crust ranges of 13.5–123 Bq/kg [1]. Most water sources in the Earth's crust have different levels of radon concentration depending on the local geological characteristics. ²²²Rn is soluble in water, and diffuse with water vapour and gases, subsequently building up in varying concentrations. For example, in underground water the ranges of radon concentration are from 1-50 kBq/m³ in aquifer and sedimentary rocks, from 10 to 300 kBq/m³ in deep wells, and from 100-50,000 kBq/m³ in crystalline rocks. While in surface water such as in lakes and rivers, concentration levels are often very low, they are in the range of a few kBq/m³ [2]. Ionizing radiation emitted from radon can easily damage chromosomes or other parts of a cell. Reasoned by the short half-life of radon decay products, alpha radiation is released and then it transfer large amount of energy to cells in lungs, thus leading to many health hazards. As a result, radon constitutes the principal leading reason of lungs cancer among non-smokers. According to UNSCEAR, radon inhalation dissolved in and released from water for human consumption accounts for 89% of estimated cancer risk, whereas radon ingestion from drinking water accounts for 11% [3].

Recognizing the vast uses of water in human life, assurance of radiological safety in respect to the level of radon in waterbody is very crucial for public health. This study concerns the determination of radon concentration and associated effective doses in drinking and irrigation water of Jalan BBH region of Oman as a means of water quality assessment of this region. Jalan BBH is generally an

agricultural area situated on the eastern part of Oman. Note that the interior plains of Oman are of young sedimentary rocks, wadi gravels, dune sands and salt flats. Beneath them is a several kilometer thick stack of older sedimentary rocks that host the country's hydrocarbon resources. People of this area fully dependent on the natural sources of water for their daily uses. Some desalination plants are also in operation to meet the water demand in this area. Large scale agricultural and some minor manufacturing/processing industries are also available in the vicinity of this area. The alteration of natural radioactive balance of this area via various known/unknown human activities may not be neglected, and thus the surrounding water body may be contaminated via various pathways. As a result, the water bodies could contain radioactive materials, which may affect the health of society in the long term. It is thus important to assess the water of this area to obtain information about the prevailing concentration of radon. Note that no other earlier study is available for an assessment of radon in the water of Jalan BBH area.

A total of 30 samples ($8 \times 2 = 16$ watercourse, $4 \times 2 = 8$ well water and $3 \times 2 = 6$ tap water) were collected from 15 different locations covering most types of water sources in the study region. The samples were collected following their principal uses as drinking and irrigation category/purposes. A passive and time integrated track etch detector (LR-115 type II) combined with high resolution optical microscope is used to obtain radon concentration in the studied samples. Present results show that all water samples contain radon concentrations much lower than the maximum contaminant level of 11 kBq/m^3 as recommended by ref. [2, 4]. The higher concentration of radon was found to be 349 Bq/m^3 in drinking water sample while the lower level was found in well water source using for irrigation with a value of 140.2 Bq/m^3 . The values of annual effective doses due to the inhalation of Radon varied from 0.35 to $0.9 \mu\text{Sv y}^{-1}$ with an average of $0.64 \mu\text{Sv y}^{-1}$. This mean value of effective dose is significantly less than the action level recommended as 0.1 mSv/y by WHO [5] and $3\text{-}10 \text{ mSv/y}$ by ICRP [6], which indicates that the water sources in Jalan BBH region of Oman are safe to use. The obtained data could serve as a reference for any future radiological study in waterbody of this region.

References

- /1/ O. Baykara, and M. Dogru, *Radiat. Measurements*, 41(2006) 362-367.
- /2/ Cosma, et al., *Radiat. Measurements*, 43 (2008) 1423-1428.
- /3/ N. Ahmad, M.S. Jaafar, and M.S. Alsaffar, *J. Radiat. Res. Appl. Sci.*, 8(2015) 294-299.
- /4/ US EPA, 1991. National primary drinking water regulations: radionuclides; proposed, EPA. Federal Reg. 56:33050-33127.
- /5/ Guidelines for drinking-water quality: recommendations. Vol. 1. 2004: World Health Organization.
- /6/ J. Valentin. The 2007 recommendations of the international commission on radiological protection. 2007: Elsevier Oxford, UK.

Comparative Study of $^{110m}\text{Ag(I)}$ Removal from Aqueous Media by Humic Substances

*Sabrina A. Shaikh, Hemlata K. Bagla**

Department of Nuclear and Radiochemistry, Kishinchand Chellaram College,
Vidyasagar Principal K. M. Kundnani Chowk, Churchgate, Mumbai – 400020.
*E-mail: hemlata.bagla@kccollege.edu.in

1. Introduction

The pollution of water resources due to the indiscriminate disposal of heavy metal ions has been causing worldwide concern. The main problem of heavy metal pollution is the possibility of significant and abrupt alterations in the ecosystem mainly due to the easy incorporation of those components in living beings. Therefore, the remediation of heavy metal ions from the industrial wastewaters is of great interest[1]. Silver is an extremely important heavy metal because of its industrial use and elevated economic value. Hence, the treatment of wastewater contaminated with silver is very relevant because, in high concentrations it may cause several negative health effects [2]. Humic substances have the ability to complex metal ions and are considered as important remediation agents for the immobilization of heavy metals in soils, thus the present research entails their application for the biosorption of silver from aqueous solutions.

2. Experimental

In this study, dry cowdung powder (DCP) and commercially available humic acid (HA) were used as sorbents. Interaction between effective variables like pH, adsorbent dose, agitation speed, contact time, temperature, metal ion concentration and capacity of sorbent were studied to enhance the removal efficiency of Ag(I), employing ^{110m}Ag radiotracer. Adsorption measurements were determined by batch experiments and residual of the metal ion concentration was measured using single channel NaI(Tl) well type gamma ray spectrometer (PEA GRS-301), at energy window 556-740 keV, peak value 625 keV with 88.53 keV FWHM.

3. Results & Discussions

This technique has proved its significance in optimizing the variables that influence the adsorption process in reducing both time and cost. Kinetic data was well represented by Ho & McKay Pseudo Second Order Model [3] as shown in Figure 1 & 2, indicating chemical adsorption as the rate limiting step. From the values of ΔH° , ΔG° and ΔS° , as shown in Table 1, biosorption for DCP and HA was spontaneous, favourable, exothermic and enthalpy controlled process. The maximum removal obtained at 303K (R.T.) was ~95% and ~77% for DCP and HA respectively. Results in Table 1, indicate that DCP is more liable than HA having maximum adsorption capacity of **19.42 mg/g** and can be considered alternative efficient, low cost and eco-friendly biosorbent for the removal and recovery of ^{110m}Ag from aqueous media.

Kinetic Modeling – Ho & McKay Pseudo Second Order

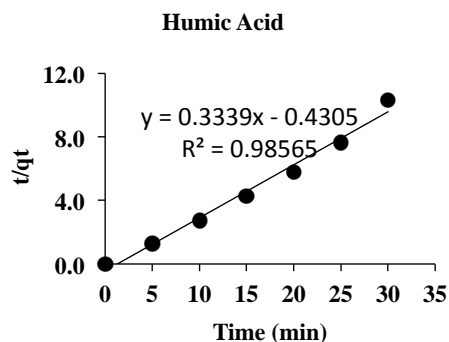
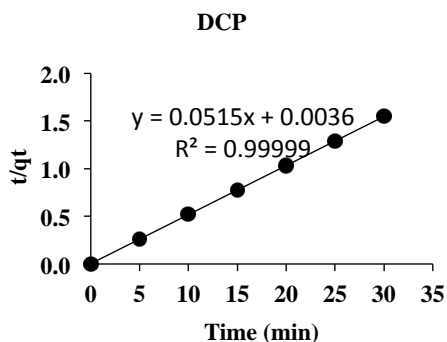


Figure 1. Kinetic profile of Ag(I) onto DCP

Figure 2. Kinetic profile of Ag(I) on Humic acid

Table 1. Comparison between DCP and Humic Acid

Biosorbent	Biosorbent Dose	%Biosorption	qe by graph	qe by calculation	ΔH° (kJ/mol)	ΔG° (kJ/mol)	ΔS° (J/molK)
DCP	50 mg	95.08 %	19.42 mg/g	19.00 mg/g	-8.18	-9.06	56.70
Humic Acid	200 mg	77.53 %	2.99 mg/g	3.88 mg/g	-7.44	-3.12	34.30

References

- /1/ T. Jintakosol and W. Nitayaphat, Materials Res. 19 (2016): 1114-1121
- /2/ M. L. C. A. F. N. Almeida and M. Vieira, Chem. Eng., 38 (2014) 109–114.
- /3/ Y. S. Ho and G. Mckay, Process Biochem. 34 (1999): 451-465..

Removal of $^{60}\text{Co}(\text{II})$ from Simulated Low Level Waste by an Eco-Friendly Biosorbent

*Sajida Sayed, Hemlata K. Bagla**

Department of Nuclear and Radiochemistry, Kishinchand Chellaram College,
Vidyasagar Principal K. M. Kundnani Chowk, Churchgate, Mumbai – 400020.
*E-mail: hemlata.bagla@kccollege.edu.in

1. Introduction

Nuclear industry is rising as an environmentally benign producer of reliable energy on a large scale. However, use of radioactive materials is bound to generate radioactive waste. In order to satisfy the demand for a safe and healthy environment, radioactive waste water must be treated prior to further disposal into nature, so as to meet national standards. Cobalt is present in the wastewater of nuclear power plants and many other industries such as mining, metallurgical, electroplating, paints, pigments and electronic industries [1] The treatment of this waste must be managed such that it is in accordance with the principles of Green Chemistry. Biosorption refers to the passive process of adsorption of metal ions by metabolically inactive biomass [2] It is one of the possible innovative techniques involved in the remediation of heavy metals and radionuclides from wastewaters and the subsurface environment.

2. Experimental

In the following investigation, 1000 ppm (1 mg/mL) Co(II) labelled with ^{60}Co tracer from simulated low level radioactive waste has been treated with dry cow dung powder (DCP) as a biosorbent. The influence of process parameters, such as effect of pH, amount of adsorbent, agitation, effect of temperature, and contact time, were evaluated. Percentage biosorption was calculated as:

$$\frac{A(i) - A(f)}{A(i)} \times 100$$

where A(i) and A(f) are the initial and final activity respectively. Langmuir, Freundlich and Dubinin-Radushkevich adsorption isotherms have been applied to further define the mechanism of sorption. Thermodynamic properties such as ΔG° , ΔH° and ΔS° were calculated.

3. Results & Discussions

Maximum uptake of 90% was observed at reactor pH 8.5, with a sorbent dosage of 20 g/L and contact time of 5 minutes at 303 K. From the comparison of different adsorption isotherm models, it was found that biosorption of Co(II) by DCP followed Freundlich model as shown in figure 1 and q_e value obtained was 3.02 mg of Co(II) per gram of adsorbent. Kinetic Modelling reveals that the reaction follows Pseudo Second Order Kinetics. Thermodynamic properties have been represented in figure 2, where negative value of ΔH° indicates the exothermic nature, negative ΔG° shows feasibility and spontaneity of reaction and positive value of ΔS° confirms the increase in randomness at the solid–solution interface during the adsorption process. Results have revealed that the presence of other metal ions influences co-operative sorption, and selectivity of DCP towards Co(II) can be improved by adjusting pH, time of contact, temperature and addition of chloride, bromide or nitrite salts. The ability of dry cow dung powder to adsorb Co(II) from aqueous solutions and the adsorptive capacity is comparable to the other high quality sorbents. Low cost and rapid adsorptive ability would offer a promising technique for industrial wastewaters clean-up and can be useful for optimizing the operating conditions for a large scale, economical process.

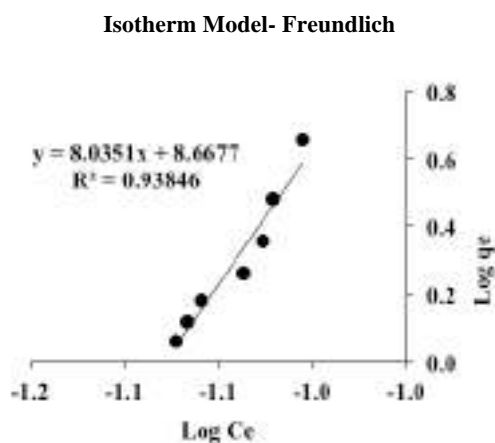


Figure 1. Slope ($1/n$) = 8.0351
Since $1/n > 1$, it indicates cooperative adsorption

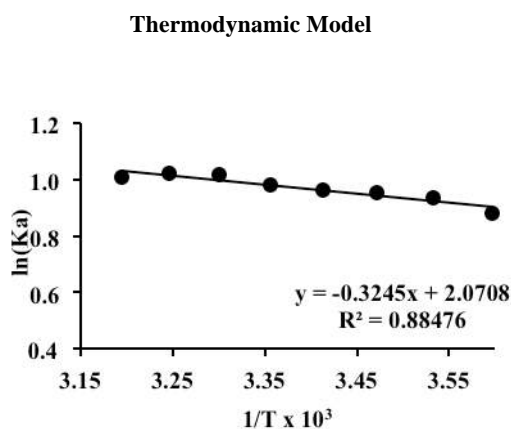


Figure 2. $\Delta G^\circ = -5219.34$ & $\Delta H^\circ = -2.70$
Therefore the reaction is exothermic, spontaneous and feasible

References

- /1/ S.S. Al-Shahrani, *Alexandria Eng. J.* 53 (2014) 205–211.
- /2/ A.H. Colagar, S. M. Hafeziyan, S. N. Azizi, and S. M. Hafeziyan, *J. Chem. Eng. Japan*, (2011) 1–8.

Application of Tracer Technique in Remediation of Sr(II) Polluted Waters

*Asma Khan, Hemlata K. Bagla**

Department of Nuclear and Radiochemistry, Kishinchand Chellaram College,
Vidyasagar Principal K. M. Kundnani Chowk, Churchgate, Mumbai – 400020.
*E-mail: hemlata.bagla@kccollege.edu.in

1. Introduction

Humic substances are ubiquitous in the environment, occurring in all soils, waters, and sediments of the ecosphere. One of their most striking characteristics is the ability to interact with metal ions, oxides, hydroxides, mineral and organic compounds, including toxic pollutants [1] to form water-soluble & insoluble complexes. Humic Acid as a metal chelator has been applied for the removal of Cr(VI), Cd(II), Al(III), Pb(II) and Zn(II) [2]. The present work explores the potentiality of humic acid in separation of Sr(II) from Low Level Radioactive Waste (LLRW) with a practical outlook to decontaminate such hazardous effluents. Literature survey reveals that Sr(II) and its radioactive counterparts have been separated from aqueous solutions employing seeds of *Ocimum basilicum* [3], eggshell waste, along with a diverse range of microbial cultures.

2. Experimental

Simulated reactor waste solution comprising of Sr(II), Cs(I), Co(II), NaI, NaNO₃ and reprocessing waste with Sr(II), Cs(I) and NaNO₃ were prepared. The effluent composition was obtained from Tarapur Power Plant. All chemicals and reagents used were of analytical grade. ⁸⁵⁺⁸⁹Sr radiotracer was added to the batch solutions in known amounts. Each batch was treated with commercially available Loba Humic Acid as a biosorbent at varying process parameters. After agitation, the solution was centrifuged and activity of the supernatant was quantified by Gamma ray NaI(Tl) scintillation detector. Kinetic and thermodynamic modelling have been applied to the data in order to understand the technical feasibility and nature of the process.

3. Results & Discussion

At optimized parameters, experiments were carried out in triplicate. It was noted that at pH 7, 33.33 g/L of humic acid, 3000rpm agitation speed and with contact time of 10 minutes at 303 K (R.T.), 84±1% of Sr(II) from reactor waste was adsorbed by humic acid. At pH 8, keeping other parameters constant, 75±1% biosorption was obtained from reprocessing waste. Thermodynamic calculations in figure 1 and Table 1, revealed that the process is exothermic, spontaneous, feasible and indicates an increase in entropy. In figure 2, Kinetic modelling indicates that the reaction follows Ho-McKay Pseudo Second Order, i.e., chemisorption is the rate limiting step.

Table 1. Thermodynamic variables of Sr(II) on Humic Acid

Effluent	ΔH°	ΔG°	ΔS°
Reactor	-0.96	-4.17	16.89
Reprocessing	-2.28	-2.39	15.21

Thus, the feasibility of Sr(II) removal was demonstrated as a time efficient, exothermic and spontaneous process. The effective outcome of scaling up will facilitate the utilization of humic acid as a potent material for treatment and processing of LLRW.

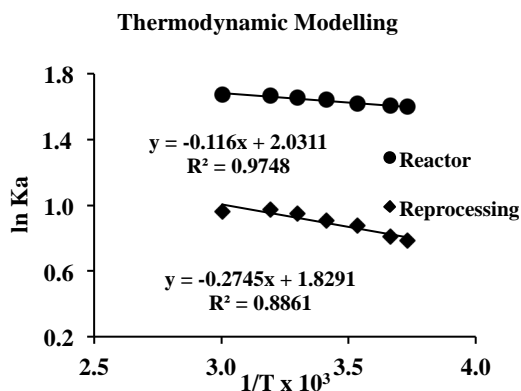


Figure 1. Thermodynamic studies of Sr(II) in reactor and reprocessing waste.

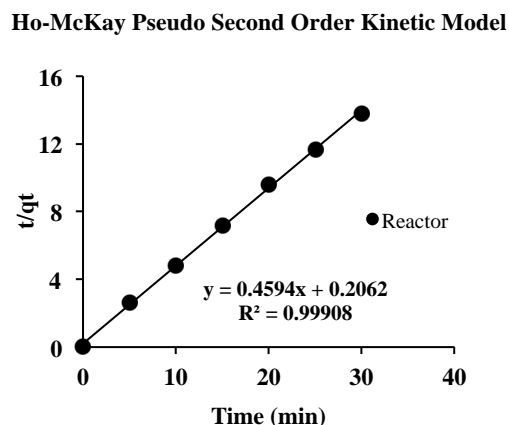


Figure 2. Kinetic Studies of Sr(II) in reactor waste. Similar results were obtained for reprocessing waste.

References

- /1/ S. Wang and C. N. Mulligan, *Chemosphere*, 74 (2009) 274–279.
- /2/ A. dos Santos, W. G. Botero, I. C. Bellin, et al., *J. Braz. Chem. Soc.*, 18 (2007) 824–830.
- /3/ D. Chakraborty, S. Maji, A. Bandyopadhyay, S. Basu, *Bioresour. Technol.*, 98 (2007) 2949.

Measurement of ^{40}K in Surface Soil Samples Collected from Sundarbans Biosphere Reserve, India

Nabanita Naskar^{1,2}, Susanta Lahiri^{2,3}, Punarbasu Chaudhuri¹*

¹Department of Environmental Science, University of Calcutta, Kolkata-700019, India

²Saha Institute of Nuclear Physics, 1/AF, Bidhannagar, Kolkata-700064, India

³Homi Bhabha National Institute, India

* E-mail: susanta.lahiri@saha.ac.in

1. Introduction

Naturally occurring ^{238}U , ^{232}Th , their decay products, ^{40}K , anthropogenic and cosmic radionuclides altogether comprise environmental radiation. Baseline radiological assessment is necessary in today's nuclear era, especially in unique and productive ecosystems like Indian Sundarbans as reference data for future radiological use. Sundarbans is world's largest contiguous mangrove ecosystem shared by India and Bangladesh. The present study attempts to assess ^{40}K activity in surface soil and sediment samples collected from different parts of Indian Sundarbans. Recently, ^{238}U and ^{232}Th measurement had been carried out in this region using γ -spectrometry [1,2].

2. Experimental

^{40}K was measured by 50% HPGe detector and resolution of 3.1 keV at 1.33 MeV energy, kept inside 10 cm thick Pb housing with graded shielding of Sn and Cu. Collected samples were air-dried, grinded and weighed 50 g kept in air-tight petri-dishes. Energy calibration was done using point sources. A set of in-house standards corresponding to 10, 20, 30, 40, 50, 60, 70, 80, 90 and 100 Bq ^{40}K activity were prepared, by mixing appropriate amount of KCl with silica gel. Following our recent paper [3], a calibration curve was obtained by plotting known activities of ^{40}K against their respective area counts.

3. Results and Discussion

The data obtained for the soil samples have been provided in Table 1 along with coordinates. K-40 activity varied from 532 ± 8.9 - 1043 ± 13.2 Bqkg⁻¹ with mean, median activities of 866 and 861 Bqkg⁻¹. Average ^{40}K activity is more than twice elevated than the world average of 420 Bqkg⁻¹ [4]. This

elevation may be attributed by the fact that the surface soil samples were collected from the reclaimed Islands (apart from reserved forest areas) of Sundarbans biosphere reserve where agriculture is a regular practice and use of fertilizers is common in these reclaimed zones. Also, tidal zone is situated at a strategic position with chances of upstream effluent accumulation. It is interesting to note that ^{40}K activity is somewhat lower in the western part of Sundarbans (mean, median activities 726.9 and 731.8 Bqkg^{-1} , six sampling sites) than that of eastern part of Sundarbans (mean, median activities 921.9 and 933.4 Bqkg^{-1} , thirteen sampling sites). This may be due to the fact that western part is more congested with industries, therefore contributions from agriculture is lesser. Also, the western part experiences appreciable mixing of freshwater influx from rivers Rupnarayan, Hooghly and Haldi with marine water influx of downstream of Bay of Bengal. Therefore, leaving a chance in washing out elemental K. In eastern part marine water influx predominates providing less opportunity for element leaching.

Table 1. Sample location and coordinates with ^{40}K activity, Bqkg^{-1} ; E= eastern, W=western

Sample location	^{40}K activity, Bqkg^{-1}	Sample location	^{40}K activity, Bqkg^{-1}
E1. Jhingakhali 22°10'47.35"N, 89°3'45.67"E	1022±15.1	E12. Canning 22°18'23.88"N, 88°40'40.56"E	988±14.9
E2. Shamshearnagar 22°12'26.96"N, 89°1'10.42"E	855±12.8	E13. Jamtala 22°6'41.81"N, 88°34'42.01"E	788±10.6
E3. Kumirmari 22°13'4.8"N, 88°55'27.0"E	988±17.4	E14. Baikunthapur 21°53'46.89"N, 88°30'9.68"E	820±19.5
E4. Satjelia 22°6'1.40"N, 88°51'57.90"E	1003±11.7	E15. Gajikhali 22°25'45.6"N, 88°50'45.1"E	950±21.4
E5. Amlamethi 22°5'45.01"N, 88°43'31.08"E	841±15.8	W1. Shibpur 22°33'11.7"N, 88°18'1.9"E	793±10.5
E6. Sonakhali 22°12'6.08"N, 88°42'53.79"E	802±12.0	W2. Birlapur 22°26'0.17"N, 88°08'27.42"E	695±11.3
E7. Uttar Mokamberia 22°14'49.0"N, 88°41'43.4"E	861±14.6	W3. Nayachar 22°1'31.7"N, 88°08'33.9"E	769±10.2
E8. Naliakhali 22°15'17.0"N, 88°40'25.8"E	933±18.2	W4. Kalinagar 21°53'33.81"N, 88°10'0.63"E	591±9.1
E9. Tetultala 22°15'31.83"N, 88°39'56.02"E	930±13.1	W5. Sagar Island 21°38'1.67"N, 88°5'4.93"E	532±8.9
E10. Jairamkhali 22°15'48.2"N, 88°38'29.3"E	1043±13.2	W6. Mousuni Island 21°38'8.70"N, 88°12'25.40"E	983±12.7
E11. Dabu 22°15'52.44"N, 88°39'26.60"E	1006±12.9		

References

- /1/ P. Chaudhuri, N. Naskar and S. Lahiri. J Radioanal Nucl Chem 311 (2017) 1947-1952
- /2/ N. Naskar, S. Lahiri, P. Chaudhuri and A. Srivastava. J Radioanal Nucl Chem 310 (2016) 1381-1396
- /3/ N. Naskar, S. Lahiri and P. Chaudhuri. J Radioanal Nucl Chem 316 (2018) 709-715
- /4/ United Nations Scientific Committee on the effects of atomic radiation report to the general assembly with scientific annexes, v. I. (2000). In UNSCEAR: sources and effects of ionizing radiation.

Uranium Intake by Population Around Upcoming BARC Facilities at Visakhapatnam, Andhra Pradesh – a Baseline Data

P. Padma Savitri, T. Sambamurty, J. Sudhakar, N.S. Krishna, A. Vinod Kumar*

Radiation Safety Systems Division, Bhabha Atomic Research Centre, Visakhapatnam- 530 012

*E-mail: ppsavitri@barc.gov.in

1. Introduction

The presence of uranium in the aquatic environment is due to leaching from natural deposits, combustion of coal and other fuels and the use of phosphate fertilizers. The upcoming R&D Centre of BARC is situated in Visakhapatnam district of Andhra Pradesh state and eastern part of India. As a part of baseline studies, water samples were collected in and around BARC, Visakhapatnam. The uranium intake was calculated using prescribed water intake rates for different group of people.

2. Experimental Procedure

Water samples from 25 bore/open wells were collected within BARC site and the surrounding villages up to 10 km radius of upcoming site. Estimation of uranium concentration in water was carried out by LED based fluorimeter supplied by Quantalase Enterprises Pvt. Ltd, Indore. Uranium intake was evaluated for water by using prescribed water intake rates for different age groups [2], e.g., The water intake rates for the infants (0–6 months old), (7–12 months old), children 1–3 y and 4–8 y old are 0.7, 0.8, 1.3 and 1.7 L d⁻¹, respectively [2,3]. Annual uranium intake through drinking water pathway was calculated by the relation.

$$\text{Uranium Intake } (\mu\text{g y}^{-1}) = \text{Uranium Concentration } (\mu\text{g L}^{-1}) \times \text{Water Intake } (\text{L d}^{-1}) \times 365 (\text{d y}^{-1})$$

3. Results and Discussion

Concentration of uranium varied from 0.2 to 19.31 $\mu\text{g L}^{-1}$ with mean of 5.01 $\mu\text{g L}^{-1}$ which is well within the guideline value given by WHO (15 $\mu\text{g L}^{-1}$), United States Environmental Protection Agency (USEPA) (30 $\mu\text{g L}^{-1}$) [4] and Atomic Energy Regulatory Board (AERB), India (60 $\mu\text{g L}^{-1}$) [4]. Table

1, shows the estimated range of uranium intake for various age groups. Uranium intake in the case of males is estimated to be higher when compared with females, due to high water intake values. In case of females, uranium intake will be higher during lactation due to higher water intake values. Uranium intake through drinking water pathway is estimated to be in the range of 0.05 to 26.77 mg y⁻¹ with a mean of 4.23 mg y⁻¹ for all age groups.

Table1. Age dependent uranium intake through drinking water pathway for public

Life stage group	Age	Annual uranium intake (mg y ⁻¹)	
		Minimum	Maximum
Infants	0-6month	0.05	4.93
	7-12month	0.06	5.64
Children	1-3year	0.10	9.16
	4-8year	0.12	11.98
Male	9-13year	0.18	16.91
	14-18year	0.24	23.25
	Adult	0.27	26.06
Female	9-13year	0.15	14.79
	14-18year	0.17	16.20
	Adult	0.20	19.02
Pregnancy	Adult	0.22	21.13
Lactation	Adult	0.28	26.77

4. Conclusion

In the present study, annual uranium intake to the public residing around upcoming BARC facilities at Visakhapatnam, AP, India, through drinking water pathway has been evaluated. Uranium concentration in ground water was found to be in the range of 0.2 to 19.31 µg L⁻¹ with a mean of 5.01 µg L⁻¹. This is well within the prescribed limits set by different agencies. Estimated mean annual uranium intake through drinking water pathway is estimated to be 4.23 mg y⁻¹ considering all age groups in and around upcoming BARC site.

Acknowledgement: The authors are grateful to Dr. K.S.Pradeepkumar, Associate Director Health, Safety and Environment Group, BARC for his keen interest in this work. Shri D.Venkateswarulu is gratefully thanked for the facilities extended.

Reference

- /1/ S.K. Sahoo, S. Singh, A. Chakrabarty, et al., Proc. Eighth DAE-BRNS National Laser Symposium, Cat.11-2-1-2 (2009).
- /2/ M. Bronzovic and G Marovic, Health Phys. 88(5), 480–485 (2005).
- /3/ United States Environmental Protection Agency. National Primary Drinking Water Regulations; Radionuclides. Final Rule. 40 CFR Parts 9, 141, and 142 (USEPA) (2000).
- /4/ AERB. Atomic Energy Regulatory Board Directive for limit on uranium in drinking water, India (2004).

Dual Displacer-Gamma Ray System for Level Measurement of Fluids-Interface in Oil Separator

*Nader M. A. Mohamed**

Atomic Reactors Department, Atomic Energy Authority, Abo Zaabal, 13759, Cairo, Egypt
*E-mail: mnader73@yahoo.com

1. Introduction

Improving the performance of gravity oil separators depends on accuracy and speed of measurement of the level between different materials. Horizontal oil separators have usually 2-3 m in diameter and 5 to 10 m in length and receive crude oil for multi-phase separation [1]. A typical separator contains layers of sand, water, emulsion, oil, foam and gas from bottom to top, respectively. The differences between the densities of the materials are used for the separation of these materials. A displacer is a submerged body, which commonly used to detect oil-water interfaces and in this case it has density between the densities of the two fluids. The presence of emulsion between water and oil in the separator disturbs the measurement of the interface between water and oil using displacer techniques [2,3].

2. Methodology

We propose inserting a gamma-ray attenuation measurement system that can be moved automatically in the vertical direction around a displacer to measure the levels of interfaces of the fluids around the displacer as shown in Figure 1. Monte Carlo calculations were carried out to calculate the sensitivity of a gamma-ray detection system. For energies below 35 keV, the attenuation will be strongly dependent on the composition and the system will be very sensitive to differentiate between water, emulsion and oil. When the system is coupled with the displacer technique, the measurements process will be fast since the displacer will define the area of scanning.

3. Experimental

In order to validate the performance of the designed system, an experiment was conducted using three different fluids.

These are water, engine oil and kerosene with densities of 1, 0.9 and 0.81 g/cm³, respectively. A bottle was filled with water and kerosene, the water in the bottom half of the bottle and the kerosene in the top and another bottle was filled with the three fluids: water, engine oil and kerosene such that each fluid had the same volume in the bottle. A displacer was put in each bottle with density slightly lower than the water density. In the both cases, the displacer was located in the interface between the water and the next fluid (Figure 2). In the two cases, the displacer defined the level of water but it could not detect the type of the fluid that interferes with water. The presence of a third fluid (engine oil) between the water and the kerosene results in a false measurement of the kerosene level by the displacer. When the gamma-ray system started the scan from the displacer position, the levels of the interfaces between the different fluids were measured as shown in figure 3. The measurements show the number of counts is sharply changed when the system was moved from one fluid to another as shown in the figure.

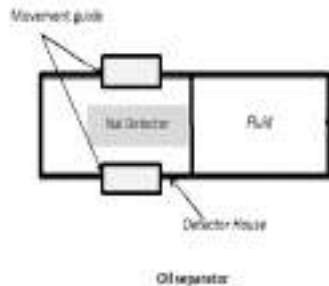


Figure 1. A gamma-ray system in the oil separator setup

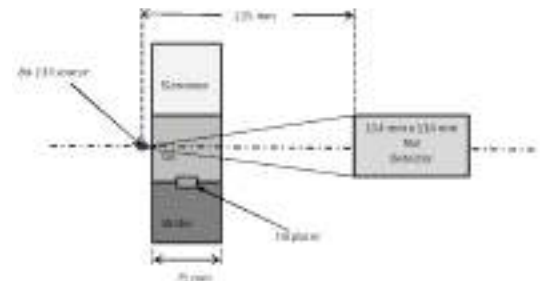


Fig 2. Experimental setup

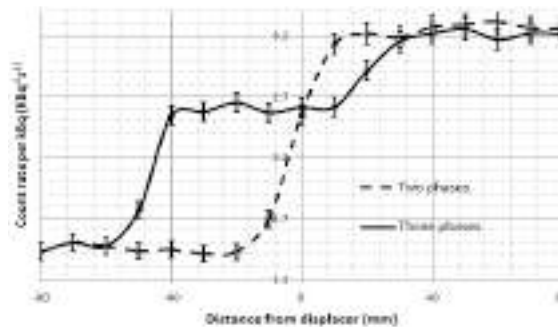


Fig 3. Experimental results

References

- /1/ D. Havard, Oil and gas production handbook; an introduction to oil and gas production, ABB oil and gas, Edition 3.0 Oslo, August 2013.
- /2/ E. M. Akhneifer, Development of a multi-interface level measurement system, MSc dissertation, Dept. of Electrical Engineering and Electronics, UMIST, 1999.
- /3/ S. F. A. Bukhari, W. Q. Yang, Proc. of 3rd Int. Symp. on Sensor Science, 18-21 July Juelich, Germany, (2005) 179-184

Cross Section Calculations of (n, p) and (n, 2n) Nuclear Reactions on Zn, Mo and Pb Isotopes with ~14 MeV Neutrons

A. Gandhi^{1*}, *Y. Sawant*², *B. J. Roy*^{2, 3}, *B. K. Nayak*^{2, 3}, *A. Saxena*^{2, 3}, *S. Ganesan*²,
*S. Kailas*², *Yu. N. Kopatch*⁴, *I. N. Ruskov*^{4, 5}, *D. N. Grozdanov*^{4, 5},
*N. A. Fedorov*⁴, *A. Kumar*¹

¹Department of Physics, Banaras Hindu University, Varanasi - 221005, India

²Nuclear Physics Division, Bhabha Atomic Research Centre, Mumbai - 400085, India

³Homi Bhabha National Institute, Anushakti Nagar, Mumbai - 400094, India

⁴Joint Institute for Nuclear Research (JINR), Dubna- 141980, Russia

⁵Institute for Nuclear Research and Nuclear Energy (INRNE- BAS), Sofia-1784, Bulgaria

*E-mail: gandhiaman653@gmail.com

1. Introduction

Fast neutron-induced cross-section data are needed to estimate the main nuclear parameters such as nuclear heating, nuclear transmutation rates, neutron-induced radioactivity, and to study radiation damage effects [1]. Despite of the relatively big number of experimental data sets in IAEA-EXFOR library, there is a need for new, more accurate measurements, in order to solve the discrepancies between experimental data and various evaluations around 14 MeV neutron energy [2]. We report the theoretical calculations of the reaction cross-sections, using TALYS 1.8 [3] and EMPIRE-3.2 [4] computer codes for $^{67}\text{Zn}(n,p)^{67}\text{Cu}$, $^{100}\text{Mo}(n,2n)^{99}\text{Mo}$ and $^{208}\text{Pb}(n,p)^{208}\text{Tl}$ reaction around 14 MeV.

2. Calculations

In EMPIRE 3.2 calculations, we used the standard Hauser-Feshbach formalism for the compound nucleus decay, the exciton model for the pre-equilibrium emission and the EMPIRE specific level density model for the level densities. The sensitivity of the cross section for different values of the parameters, such as: nuclear level density, nuclear reactions model, nucleon potential, etc., were also checked. In TALYS-1.8, the compound nuclear reaction was accounted using Hauser-Feshbach model including a width fluctuation correction for the binary compound reactions.

The two-component exciton model, developed by Kalbach, was used for calculating the particle evaporation contribution. The optical model potentials (OMP_s) of Koning and Delaroche were used for parameterization of the proton and neutron. There are 6 level density models (ldmodel 1-6) defined in TALYS-1.8, 3 of them are phenomenological and 3 are microscopic level densities dependent.

3. Results and Discussion

From Table 1 one can conclude that the obtained data, using the TALYS 1.8 with level density default option (ldmodel-2), gave a very good agreement with the experimental data for all 3 reactions. The experimental data from the IAEA-EXFOR and the evaluation data from the ENDF/B-VIII.b4, JENDL-4.0, and TENDL-2015 are shown in Figures 1 and 2 in comparison with our results. It is seen that the calculated values are in good agreement with the literature data and evaluation libraries data.

Table 1. Cross sections estimated by different level density model options of TALYS-1.8

Reactions	Energy (MeV)	Experimental Data (mb)	ldmodel1 (mb)	ldmodel2 (mb)	ldmodel3 (mb)	ldmodel4 (mb)	ldmodel5 (mb)	ldmodel6 (mb)
$^{67}\text{Zn}(n,p)^{67}\text{Cu}$	14.5	43.1±4.1	33.36	41.83	22.14	72.11	51.44	65.73
$^{100}\text{Mo}(n,2n)^{99}\text{Mo}$	14.5	1505.7±96.0	1536.30	1524.60	1323.00	1518.70	1537.30	1309.10
$^{208}\text{Pb}(n,p)^{208}\text{Tl}$	14.8	0.87±0.10	1.06	0.83	184.00	1.19	1.39	1.24

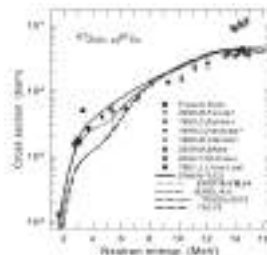
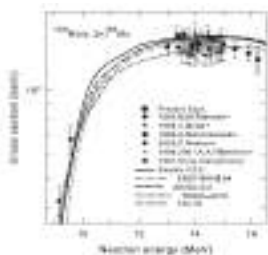


Figure 1. Excitation function for $^{100}\text{Mo}(n,2n)^{99}\text{Mo}$ reaction Fig 2. Excitation function for $^{67}\text{Zn}(n,p)^{67}\text{Cu}$ reaction

4. Conclusion

The results obtained with the both codes, are in good agreement with the existing data for neutron energies around 14 MeV. Such nuclear model calculations of excitation functions can enhance the basic understanding of the mechanism of nuclear reaction induced by fast neutrons.

References

- /1/ N. Dzysiuk, A. J. Koning, D. Rochman, U. Fische Fusion Science and Technology, 73.1(2018): 13-24.
- /2/ TALYS-1.8 -software for simulation of nuclear reactions, at <http://www.talys.eu/download-talys/>
- /3/ EMPIRE-3.2 -system of codes for nuclear reaction calculations, at <https://www-nds.iaea.org/index-meetingcrp/EmpireWorkshop2013/downloadEmpire322win.htm>

New Dates from The Site of Erenda, East Medinipur District, West Bengal: Implications for Indian Protohistory

Nabanita Naskar^{1,2}, Kaushik Gangopadhyay^{3}, Susanta Lahiri^{2,4}, Ahana Ghosh³, Punarbasu Chaudhuri¹, Rajveer Sharma⁵, Pankaj Kumar⁵, S. Ojha⁵, S. Chopra⁵*

¹Department of Environmental Science, University of Calcutta, 35 Ballygunge Circular Road, Kol-700019, India

²Saha Institute of Nuclear Physics, 1/AF, Bidhannagar, Kolkata-700064, India

³Department of Archaeology, University of Calcutta, 1 Reformatory Street, Kolkata 700027, India

⁴Homi Bhabha National Institute, India

⁵Inter-University Accelerator Centre (IUAC), New Delhi, India

* E-mail: k.gongo@gmail.com

1. Introduction

The archaeological sites in West Bengal, India belonging to the time period of 4500-2600 BP has been placed in the 'protohistoric' period. The published dates in this geographical area fall between 4500 - 3000 BP and some of the sites have conventional radiocarbon dates of 2700 BP [1]. For the first time in coastal West Bengal, we have carried out ¹⁴C-Accelerator Mass Spectrometry (AMS) dating at Inter-University Accelerator Centre (IUAC), Delhi on recently excavated archaeological site (Erenda, East Medinipur district, (21°55'4.8" N, 87°34'42.4" E). This site is located between 5-10 m above present mean sea level [MSL] and in the context of a geological formation which is known as Panskura formation dated between 5850-120 BP. Below this formation lies the 'Sijua' formation, which is dated in the time-frame of upper Pleistocene to Lower Holocene period [2]. However, these geological studies did not address the question of archaeology. It is therefore imperative that the archaeological sites and the cultural layers should be dated independently as the coarse resolution dating of quaternary geological formations is not applicable.

2. Experimental

2.1 Sample collection: At the excavation site of Erenda, the total deposit of the archaeological layer was 1.65 m from the datum points and reference pegs. Out of this total deposit the thickness of the protohistoric phase was approximately 1 m whereas the later phase deposits consists of ~ 60 cm. The excavations revealed evidence of human habitation in form of floors. The floors were full of charcoals

which resulted from burning activities. Soil samples containing these charcoals were collected from two adjacent trenches named A1 and ZA1 of depths 1.69 m and 1.39 m respectively. Charcoal pieces were segregated from burned floor materials excavated out from these trenches.

2.2 Chemical treatment and AMS measurement: 5 mg of charcoal samples were subjected to acid-base-acid treatment prior to AMS measurement and combusted in oxygen environment. Thus produced CO₂ was purified and reduced to graphite involving hydrogen gas in the presence of catalyst Fe powder by the help of Automated Graphitization Equipment (AGE). Graphite powder was packed in a capsule and loaded in ion source of AMS machine based on 500kV Tandem ion accelerator.

OX II (Oxalic acid) sample procured from NIST, USA was used as reference material. Background value during the measurement was (0.503±0.0144) pMC (Percentage modern carbon) and that corresponds to ¹⁴C/¹²C ratio (5.3698± 0.1536) x 10⁻¹⁵. Data quality was monitored with secondary standard sample (IAEA-C8). Its consensus values (pMC = 15.03±0.17) was matching with its experimental result (pMC= 14.95±0.09). Data was collected for about 30 minutes (in 10 runs) from each sample and obtained ratio of ¹⁴C/¹²C was background corrected, normalized to reference material and finally corrected for δ¹³C, which is considered (-25.00±2.000) ‰ for all the samples. Libby age was calibrated to calendar age using online calculator Calib7.1 [3] for results interpretation.

3. Result and Discussion

Excavation at the site of Erenda and the consequent dating of the site using AMS has now largely altered some of the present views of archaeological dates. ¹⁴C dating of charcoal samples from various trenches showed an acceptable pattern as shown in Table 1. The trend of dates obtained from depth layers provided an insight and idea about the age of the excavation site in this study.

Table 1. Dates obtained in two tranches of Erenda, East Medinipur district, India

Trench	Lab Code	Depth	LAYER	Dig	Median Calendar age (Cal BP), 2sigma
ZA1	IUACD#17C1305	26 cm	2	Dig-3	126 cal BP
ZA1	IUACD#17C1304	122.5 cm	4	Dig-19	2593 cal BP
ZA1	IUACD#17C1303	130.5 cm	4	Dig-20	2899 cal BP
A1	IUACD#17C1317	45 cm	2	Dig-2	1580 cal BP
A1	IUACD#17C1316	160 cm	3	Dig-17	2581 cal BP
A1	IUACD#17C1315	160 cm	3	Dig-17	3929 cal BP

References

- /1/ G. Sengupta , B.D Chattopadhyaya and S. Chakrabarty (ed) An Annotated Archaeological Atlas of West Bengal, Vol 1, Pre and Protohistory, Manohar, New Delhi, pp 83-102 (2005)
- /2/ R.K Roy and Chattopadhyay. Indian J. Geol. 69, 177-269 (1997)
- /3/ M. Stuiver and P.J. Reimer, 1993, Radiocarbon, 35, 215-230

Production of $^{190-193}\text{Au}$ Radionuclides through ^{11}B Induced Reactions on Natural Tungsten Target

Dibyasree Choudhury¹, Susanta Lahiri^{1,2}*

¹Chemical Sciences Division, Saha Institute of Nuclear Physics, 1/AF Bidhannagar, Kolkata-700064, India

²Homi Bhabha National Institute, 1/AF Bidhannagar, Kolkata-700064, India

*E-mail: susanta.lahiri@saha.ac.in

1. Introduction

The neutron deficient $^{190-193}\text{Au}$ radionuclides offer high intensity auger electrons for their possible clinical applications. The range of the low energy auger electrons is short and allows targeted therapy in DNA level. Earlier reports reveal the use of ^1H , ^2H or ^4He particles for production of neutron deficient $^{190-193}\text{Au}$ radioisotopes from Au, Pt and Ir targets respectively [1-3]. Indirect production routes of $^{190-193}\text{Au}$ through spallation reaction on Pb target by 660 MeV protons [4] or as a decay product of Hg isotopes were also reported [5]. The aim of this work is to investigate an alternate production route of the $^{190-193}\text{Au}$ by the use of heavy ion beam ^{11}B on $^{\text{nat}}\text{W}$ target.

2. Experimental

Five WO_3 targets ($936 \mu\text{g}/\text{cm}^2$) were irradiated each at a time with 41.5-62.5 MeV ^{11}B at BARC-TIFR Pelletron, Mumbai, India. The beam intensity varied from $(1.1-1.7) \times 10^{10}$ at all energies while it was 3.4×10^{10} at 57 MeV. Series of γ - spectra were taken in a p-type HPGe detector of 2.35 keV resolution at 1.33 MeV. The radionuclides were identified from their corresponding photo peaks and decay data. The energy and efficiency calibration of the detector were performed using ^{152}Eu standard source of known activity. The production cross section of $^{190-193}\text{Au}$ was measured and compared with theoretical codes PACE4 and EMPIRE3.2.2. Total error in experimental cross sections were estimated $\sim 17\%$.

3. Results and discussions

$^{\text{nat}}\text{W}$ has five stable isotopes: $^{180,182-184,186}\text{W}$, therefore the production of Au radioisotopes is possible from different reaction channels.

Time resolved gamma-ray spectroscopy of ^{11}B irradiated WO_3 target indicated the presence of $^{190-193}\text{Au}$ radioisotopes in the matrix. The excitation functions obtained experimentally and theoretically were plotted against incident energy (Figure 1). PACE4 and EMPIRE predicted results similar to experiment measurements. However, at 56.5 and 51.5 MeV, the theoretical results over predicted the experimental results for Au-191. This discrepancy necessitates repetition of the experiment at those energies. The excitation plots reveal that the maximum target thickness for isotope production should be 18 mg/cm^2 .

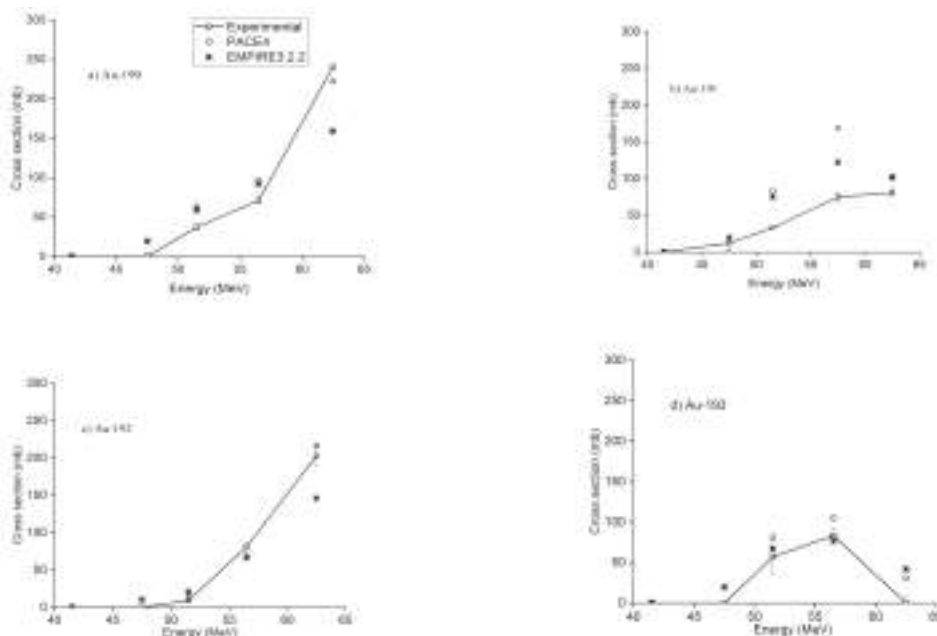


Figure 1(a-d). Production cross sections of $^{190-193}\text{Au}$ and comparison with PACE4 and EMPIRE3.2.2

The report offers a feasible production pathway for the neutron deficient no-carrier-added $^{190-193}\text{Au}$ radioisotopes of clinical significance with high production cross section. The experiment leaves further scope to modify the irradiation parameters and maximize the production yield.

References

- /1/ W.B. Ewbank, H.A. Shugart, Phys. Rev. 135 (1964) A358-A361.
- /2/ F.Ditrói, F.Tárkányi, S.Takács, A.Hermanne, Appl. Radiat. Isotopes 113 (2016) 96.
- /3/ F. Tarkanyi, S. Takacs, F. Ditroi, A. Hermanne, Yu.N. Shubin, A.I. DityukNucl. Instr. Meth. Phys. Res. B 226 (2004) 473–489
- /4/ M.Majerle et al. J. Phys.: Conf. Ser. 41 (2006) 331.
- /5/ J. Streib, H.J.Kluge, H. Kremmling, R.B. Moore, H.W. Schaaf, K.Wallmeroth, CERN/EP 85-32 (1985)

Investigation of Radon Concentration in Drinking Water to Assess the Whole Body Dose and Excess Lifetime Cancer Risk along Coastal Kerala, India

Prakash V, Divya P V*

Department of Studies & Research in Physics, Payyanur College, Kannur, Kerala - 670 327

* E-mail: prakashmv@gmail.com

1. Introduction

Radon is a radioactive gas, which is easily soluble in water and the second leading cause of lung cancer [1] as per various reports. Chavara- Neendakara at Kollam District in Kerala has got second position in the ranking of HBRA in the world and it has a significant position in case of number of cancer patients. Potential carcinogenic effects that are considered by estimating the probability of cancer incidence in a population of individual for a specific lifetime from projected intakes and chemical-specific dose-response data are expressed in terms of excess lifetime cancer risk (ELCR) [2]. Hence, the objective of the study is radiological protection of population from the enhanced level of activity in the selected region of coastal Kerala by understanding the radionuclide enrichment and evaluating the excess lifetime cancer risk.

2. Experiment

Sampling stations were identified in selected locations on the basis of radiation intensity (scintillometer UR 705) along the coastal parts of Kerala; Kovalam (S1), Varkala (S2), Neendakara (S3), Chavara (S4), Alappuzha (S5), Cherai (S6), Chavakkad (S7), Padinjarekkara (S8), Kappad (S9) and Kannur (S10). Water samples were collected and treated following standard procedure [3]. In each region three sets of samples and in total 30 samples were collected for the analysis. The concentration of ^{222}Rn in aqueous samples was determined by the emanometry method [4].

3. Results and Discussions

Radon concentrations in water samples collected along coastal parts of Kerala are presented in Table 1. Comparatively higher concentration of radon was found in samples collected from the Varkala region and lower concentration was found in samples collected from Chavakkad region. The result indicates that, the radionuclide concentration in water was influenced by the activity of nearby soil. The higher activity observed in the samples collected from Varkala region may be attributed to the presence of coloured granite soil in the region [5]. Presence of hot spring, which carry high amount of radium and its decay products to the surface may also be influenced the concentration of activity in the region [6].

Table 1. The ^{222}Rn concentration, whole body dose and ELCR parameter

Location	^{222}Rn con. (Bq l^{-1})	Dose to stomach ($\mu\text{Sv y}^{-1}$)	Dose to lungs ($\mu\text{Sv y}^{-1}$)	Whole body dose ($\mu\text{Sv y}^{-1}$)	ELCR ($\times 10^{-3}$)
Kovalam (S1)	2.11	22.18	5.90	28.08	0.1
Varkala (S2)	4.35	45.72	12.18	57.9	0.2
Neendakara (S3)	0.23	2.41	0.64	3.05	0.01
Chavara (S4)	3.00	31.53	8.4	39.93	0.13
Alappuzha (S5)	0.60	6.30	1.68	7.98	0.02
Cherai (S6)	0.62	6.51	1.73	8.24	0.03
Chavakkad (S7)	0.12	1.26	0.33	1.59	0.005
Padinjarekkara (S8)	0.20	2.10	0.56	2.66	0.009
Kappad (S9)	0.40	4.20	1.12	5.32	0.02
Kannur (S10)	1.12	11.77	3.13	14.9	0.05

The enhanced level of radon concentration in water in turn leads to significant radon exposure to the human beings through ingestion. The results were also compared with the values recommended by the WHO (100 Bq L^{-1}) and EU council (100 Bq L^{-1}) and found that, the values from the present study were well within the permissible limit. The ELCR parameter at different locations varies in the range 0.005×10^{-3} - 0.2×10^{-3} . It is observed that, ELCR parameters also well within the reported world average value of 0.29×10^{-3} .

References

- /1/ C. Sainz, A. Dinu, T. Dicu, et al., *Sci Total Environ*, 407 (2009) 4452-4460.
- /2/ V. Ramasamy, M. Sundarajan, K. Paramasivam, et al., *Appl. Radiat. Isotopes* 73 (2013) 21-31.
- /3/ L. Herbert, *EML Procedure manual*. In: Volchok and Gail de Planque. 26th Environmental Monitoring Laboratory; New york (1983).
- /4/ Primal D'Cunha, Y Narayana, N Karunakara, I Yashodhara, S. Kumara. *Radiat. Protec. Environ.* 34, 2012.
- /5/ S. R. Soniya, S. Monica, A. K. Vishnu Prasad, P. J. Jojo. *Int J Pure Appl Phys* 13(2017) 209-14.
- /6/ A.K. Gopinathan, M.T. Derin, P. Vijayagopal, et al., *pLos One*, 7 (2012) e 5046.

Distribution of Natural Radionuclides and Assessment of Excess Lifetime Cancer Risk Along Coastal Areas of Varkala in Kerala

*Divya P V, Prakash V**

Department of Studies & Research in Physics, Payyanur College, Kannur, Kerala- 670 327

*E-mail: prakashamv@gmail.com

1. Introduction

High natural background radiation areas (HBRA) are given emphasis while studying the distribution and enrichment of natural radionuclides. Monazite, the rich source of radioactive uranium and thorium, becomes an important component in the sand from HBRA. Further, the possible impact of natural radiation on the biota (including the human) has been a matter of serious concern from societal and biological stand-points. Potential carcinogenic effects that are considered by estimating the probability of cancer incidence in a population of individual for a specific lifetime from projected intakes and chemical-specific dose-response data are expressed in terms of excess lifetime cancer risk (ELCR) [1]. In view of this, an attempt has been made to understand radionuclides enrichment in Varkala coast, a known HBRA in Kerala. Further, excess lifetime cancer risk parameters were evaluated and possible conclusions are drawn.

2. Experiment

Sampling stations were identified in selected locations along the coastal areas of Varkala on the basis of radiation intensity (Micro-R Survey Meter UR-705 having range 0 - 10000 $\mu\text{R h}^{-1}$). Sand samples were collected following standard procedure [2]. Sample analysis was done using a high efficiency 2" x 2" NaI(Tl) detector and the activity of radionuclides viz. ^{40}K , ^{226}Ra and ^{232}Th was estimated from the counts obtained[3]. The ELCR parameter was evaluated from the activity following equation $\text{ELCR} = \text{AEDE} \times \text{DL} \times \text{RF}$, where AEDE is annual effective dose equivalent (mSv y^{-1}), DL is average lifespan (70 years) and RF is risk factor (Sv^{-1}) [1].

3. Results and Discussion

Table 1 gives the activities of ^{40}K , ^{226}Ra and ^{232}Th in sand samples and associated radiological parameters evaluated from these activities. The values obtained from the present study indicate that, the activities in sand samples were high compared to the world average values [4]. It can be attributed to the presence of coloured granite soil, which is a rich source of monazite in the region. Presence of hot spring, which carry high amount of radium and its decay products to the surface may also be influenced the concentration of activity in the region. There exists a good correlation between the activity of ^{232}Th and external gamma absorbed dose with correlation coefficient $r = 0.9$, which confirms ^{232}Th is the major contributor to the external gamma dose rate in air. Average value of ELCR at Varkala region is 7.9×10^{-3} which is higher than the world average value 0.29×10^{-3} . The higher values of ELCR from the present study indicate that, potential carcinogenic effects may be significant in the region and remedial measures should be implemented accordingly. Further, detailed investigation on the health problems of inhabitants from the region is also required to get a clear picture on adverse effects of enhanced level of background activity.

Table 1. Activity of ^{40}K , ^{226}Ra and ^{232}Th and associated radiological parameters

Sample	Activity (Bq kg ⁻¹)			Absorbed dose (nGyh ⁻¹)	Annual effective dose (mSv)	ELCR (x10 ⁻³)
	⁴⁰ K	²²⁶ Ra	²³² Th			
S1	3691.3	643.9	968.4	897.8	1.1	3.8
S2	1433.1	1021.6	3009.4	2295.6	2.8	9.8
S3	996.7	107.1	313.0	242.7	0.2	1.0
S4	3976.9	581.8	1340.9	1095.3	1.3	4.7
S5	4827.1	196.2	6238.1	3878.7	4.7	16.6
S6	216.0	32.2	1310.3	807.2	0.9	3.4
S7	110.3	236.5	1516.8	1025.8	1.2	4.4
S8	286.1	567.1	1331.0	1067.1	1.3	4.5
S9	905.5	425.3	8134.5	5113.5	6.2	21.9
S10	47.3	325.0	3332.7	2163.2	2.6	9.2
Range	47.3 – 4827.1	32.2 – 1021.6	313.0 – 8134.5	242.6 - 3878.5	0.2 – 6.2	1 – 21.9
Mean	1649.0	413.6	2749.5	1858.7	2.2	7.9

References

- /1/ V. Ramasamy, M. Sundarajan, K. Paramasivam, et al., Appl. Radiat. Isot., 73 (2013) 21-31.
- /2/ L. Herbert, EML Procedure manual. In: Volchok and Gail de Planque. (26th) Environmental Monitoring Laboratory; New York (1983).
- /3/ N. Venunathan, C. S. Kaliprasad and Y. Narayana, Radiation Prot. Dosimetry, 171 (2016) 1-6.
- /4/ UNSCEAR, Sources and Effects of Ionizing Radiation. United Nations Scientific Committee on the Effects of Atomic Radiation, United Nations, New York, (2000).

Production and Separation of No-Carrier Added $^{43,44,44m}\text{Sc}$ from ^{12}C Irradiated BaCl_2 Target

Kousiki Ghosh^{1,2}, Dibyasree Choudhury³, Susanta Lahiri^{3,2}*

¹Bhabha Atomic Research Centre, Trombay, Mumbai-400085, India

²Homi Bhabha National Institute, India

³Saha Institute of Nuclear Physics, Block-AF, Sector-1, Bidhan Nagar, Kolkata-700064

*E-mail: susanta.lahiri@saha.ac.in

1. Introduction

Sc radioisotopes are now studied extensively as the alternate PET radioisotopes along with ^{18}F , ^{68}Ga , ^{60}Cu etc. First PET image using ^{44}Sc -DOTATOC has been safely conducted recently [1]. Relatively longer half-life of ^{44g}Sc ($T_{1/2} = 3.97$ h) and ^{43}Sc ($T_{1/2} = 3.89$ h) are the added advantages over other common PET isotopes. Common production routes include proton, deuteron and alpha induced reactions on $^{\text{nat}}\text{Ca}$ [2, 3]. For the first time chloride targets have been used to produce $^{43,44,44m}\text{Sc}$ via the reactions $^{35,37}\text{Cl}(^{12}\text{C},\text{xpyn})^{43,44,44m}\text{Sc}$ reactions followed by development of an effective separation procedure of no-carrier added (NCA) Sc radionuclides.

2. Experimental

2.1. Irradiation details: Four BaCl_2 targets of thickness 3 mg/cm^2 were deposited on Al foil of thickness 1.8 mg/cm^2 . The targets were irradiated with 64, 56, 47 and 38 MeV ^{12}C beam with maximum 60 nA beam intensity.

2.2. Radiochemical separation: The irradiated BaCl_2 targets were collected from the Al foil by careful scratching with spatula and 2 mL 0.1 M HCl was added followed by sonication and slight heating. The stock solution was spiked with ^{133}Ba . Di-(2-ethylhexyl) phosphoric acid (HDEHP) dissolved in cyclohexane and various concentration of HCl solutions were used as organic and aqueous phase in liquid liquid extraction (LLX) studies. The back extraction of NCA Sc radionuclides was carried out by 0.1 M DTPA in 1 M NaOH.

3. Result and discussion:

The yield of $^{43,44,44m}\text{Sc}$ at EOB has been presented in table 1. The maximum target thickness for maximum production of NCA Sc radionuclide would be 19 mg/cm^2 as revealed from excitation function and SRIM data.

Table 1. Yield of $^{43,44,44m}\text{Sc}$ at different projectile energies at EOB

Target	Incident energy, MeV	Exit energy, MeV	Projectile energy at mass center, MeV	Integrated charge (μC)	Yield of ^{43}Sc at EOB (kBq)	Yield of ^{44}Sc at EOB (kBq)	Yield of ^{44m}Sc at EOB (kBq)
Target 1	38	32.5	35.2	1405	36 ± 0.34	157.5 ± 0.3	17.1 ± 0.1
Target 2	47	42.8	44.9	1405	7 ± 0.25	96.3 ± 0.2	14.3 ± 0.1
Target 3	56	51.7	53.8	1405	37 ± 0.2	35.8 ± 0.1	7.1 ± 0.0
Target 4	64	59.9	61.9	1405	40.6 ± 0.18	15.76 ± 0.1	3.5 ± 0.0

The extraction profile of Ba and Sc at 10% HDEHP as a function of various concentration of HCl has been presented in figure 1. No extraction of Ba was found in organic phase irrespective of acid concentration. Whereas maximum extraction of Sc was obtained at 10^{-4} M HCl concentration after which extraction percentage decreased with increasing HCl concentration followed by a further increasing trend after 1M acid concentrations. At lower acid concentration $[\text{Sc}(\text{H}_2\text{O})_n]^{3+}$ species is present whereas at higher concentration Sc^{3+} state is preferred. On the other hand in aqueous phase Ba remains in +2 oxidation state. Hence HDEHP was selective to either $[\text{Sc}(\text{H}_2\text{O})_n]^{3+}$ or Sc^{3+} over Ba^{2+} .

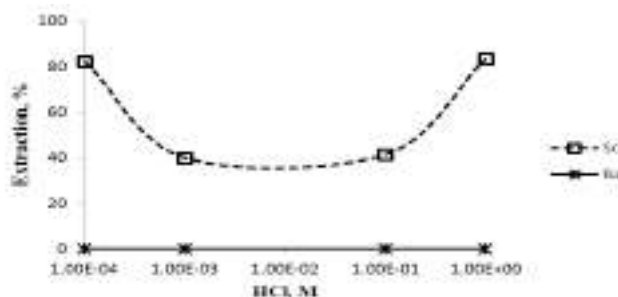


Figure.1. Extraction profile of NCA scandium and bulk barium at 10% HDEHP as a function of HCl concentration

References

- /1/ A. Singh, R. Baum, I. Klette, et al., J. Nucl Med. 56 (2015) 267-267.
- /2/ S. Katarzyna, M. Sitarz, R. Walczak, et al., Appl. Radiat. Isotopes 118 (2016) 182-189.
- /3/ H.F. Valdovinos, R. Hernandez, T. E. Barnhart, et al., Appl. Radiat. Isotopes 95 (2015) 23-29.

Alpha Track Detection Employing Tetraethyl Ammonium Bromide (TEAB) as New Chemical Etchant of CR-39

Sushma S. Chavan¹, Amol M. Mhatre², Ashok K. Pandey², Hemlata K. Bagla^{1}*

¹Department of Nuclear & Radiochemistry, Kishinchand Chellaram College, Vidyasagar Principal K.M. Kundanani Chowk, Churchgate, Mumbai-400020.
²Radiochemistry Division, Bhabha Atomic Research Centre, Mumbai-400085, India
*E-mail: hemlata.bagla@kccollege.edu.in

1. Introduction

Solid state nuclear track detection technique to recognize incident ionizing particles utilizing their latent tracks in target CR-39 detector, has been developed enthusiastically and used widely in many fields of science [1,2]. When an ionizing radiation passes through a polymer it produces extensive ionization of the detector material and dissociates the chemical bonds in the polymer forming permanent tracks of the radiation path in the detector. Different chemical etching techniques has been used to enlarge the primary latent tracks by which they grow slowly and become visible [3]. The motivation behind this work is to understand the various aspects of alpha track registration from solution medium and to find the outcome of new chemical etchant on CR-39 nuclear track detector.

2. Experimental

CR-39 detectors were exposed with alpha particle from different uranyl nitrate ($\mu\text{g/mL}$) solutions. Chemical etching was carried with 6 N NaOH and new chemical etchant solution, which includes 5% Tetraethyl ammonium bromide (TEAB) with 6 N NaOH (w/w). The analysis of the alpha tracks registered on CR-39 requires the standardization and characterization of some specific parameters such as the concentration range, etching time, exposure time, bulk etch rate, normality, amount of TEAB with NaOH and temperatures of etchant. In this present work the effect of different parameters and performance of new chemical etching method has been studied by comparing the results from the

parameters of CR-39 with those determined by NaOH etching. Etched CR-39 detectors were scanned under an optical microscope on higher magnification (40X) and data were further analyzed.

3. Results and Discussion

Variations of alpha track density were studied with respect to different parameters in order to obtain the optimum etching conditions. Figure 1 & Figure 2 indicates track density as a function of etching time and bulk etch rate respectively. Highest track density (31 mm^{-2}) was obtained employing new etching method (5% TEAB with 6 N NaOH) with 12 h exposure and 6 h of etching at 60°C . Concentrations more than 6 N and temperatures above 60°C the detector film tends to form cracks and become hazy. The newly introduced chemical etchant helps to enhance the interaction of etchant with latent damage on CR-39 in a reduced etching time of 90 min, hence obtained results clearly indicates that it is highly effective for the alpha track revelation from solution medium.

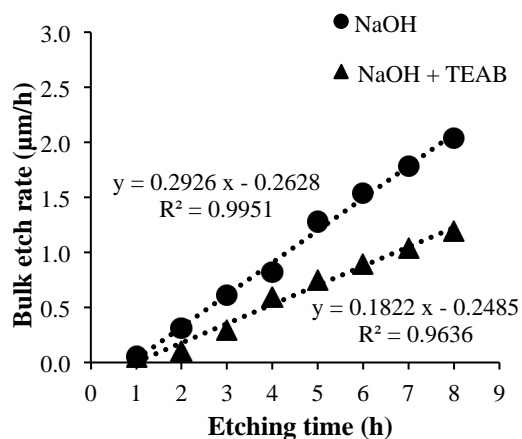
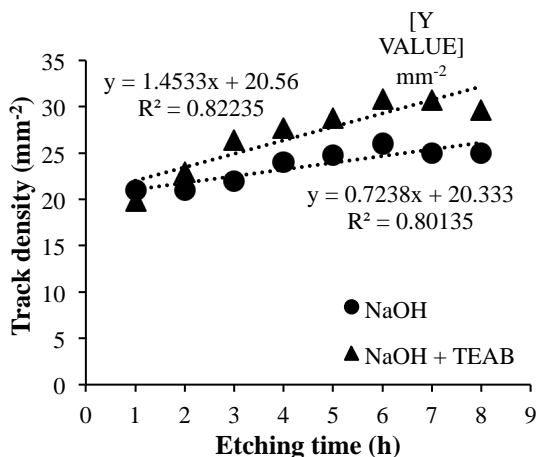


Fig 1. Track density (T_d) variation as a function of etching time

Fig 2. Bulk etch rate (V_b) as function of etching time

References

- /1/ R. L. Fleischer, P. B. Price, and R. M. Walker, Nuclear Tracks in Solids: Principles and Applications. University of California Press, 1975.
- /2/ S.A.Durrani and R. K. Bull, Solid State Nuclear Track Detection: Principles, Methods and Applications. Pergamon Press, Oxford. 1987.

Preparation and Evaluation of Freeze-dried Kits of BPAMD Suitable for Labelling with ^{68}Ga Eluted from Different Commercial Generators

Mohini Guleria¹, Tapas Das^{1*}, Jeyachitra Amirdhanayagam¹, Haladhar D. Sarma²,
Ajit S. Shinto³, K.K. Kamaleshwaran³, Arun Pandian³, Ashutosh Dash¹

¹Radiopharmaceuticals Division, Bhabha Atomic Research Centre, Trombay, Mumbai - 400085, India

²Radiation Biology & Health Sciences Division, Bhabha Atomic Research Centre, Mumbai - 400085, India

³Department of Nuclear Medicine & PET, Kovai Medical Center and Hospital,
Coimbatore - 641014, Tamil Nadu, India

*E-mail: tdas@barc.gov.in

1. Introduction

^{68}Ga -BPAMD has recently emerged as one of the preferred radiopharmaceuticals for imaging of bone lesions due to its ability to produce high resolution images and uncomplicated availability of ^{68}Ga , a PET radionuclide, from commercial $^{68}\text{Ge}/^{68}\text{Ga}$ generators [1,2]. The objective is to develop freeze-dried BPAMD kit, for the easy, single-step and convenient formulation of ^{68}Ga -BPAMD patient dose at the hospital radiopharmacy. Additionally, the kit should be compatible with ^{68}Ga , eluted with HCl of various molarities from the $^{68}\text{Ge}/^{68}\text{Ga}$ generators sourced from different suppliers [3,4].

2. Experimental

Freeze-dried BPAMD kits, comprising 50 μg of BPAMD and 150 mg of HEPES, were prepared and evaluated using ^{68}Ga eluted from three different $^{68}\text{Ge}/^{68}\text{Ga}$ generators. Radiochemical purity of ^{68}Ga -BPAMD was determined by both TLC and HPLC studies. The biological behaviour of ^{68}Ga -BPAMD, prepared using freeze-dried kit, was evaluated by both *in vitro* and *in vivo* studies. Clinical studies were also performed in limited number of patients suffering from metastatic bone cancer.

3. Results and Discussion

^{68}Ga -BPAMD could be prepared with > 95 % radiochemical purity using the freeze-dried BPAMD kit and ^{68}Ga , eluted from three different commercial generators. ^{68}Ga -BPAMD, prepared using the freeze-

dried kit, exhibited adequate serum stability and ~91 % binding with the hydroxyapatite particles. Biodistribution studies in normal Wistar rats exhibited selective uptake of the agent in skeleton (2.22 ± 0.43 , 2.10 ± 0.75 and 2.50 ± 0.28 % IA/g at 30 min, 1 h and 2 h, respectively. IA stands for Injected Activity) and fast clearance of the non-accumulated activity through urinary route. The results of the biodistribution studies are shown in Figure 1. Clinical studies in cancer patients showed excellent accumulation of the agent in bone lesions (Figure. 2).

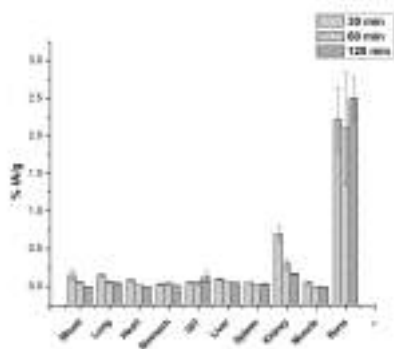


Fig 1. Bio-distribution pattern of ^{68}Ga -BPAMD in normal Wistar rats (n=3).



Fig 2. Whole-body scans of a patient recorded after 30 min of administration of ^{68}Ga -BPAMD

4. Conclusions

The preliminary studies exhibited the potential of developed BPAMD kit towards its utilization for the PET scanning of skeletal metastases. The methodology standardized during the course of the present work can be exploited for the preparation of freeze-dried kits, suitable for formulation of ^{68}Ga -based radiopharmaceuticals, using ^{68}Ga obtainable from any commercial $^{68}\text{Ge}/^{68}\text{Ga}$ radionuclide generator.

Acknowledgement

Authors gratefully acknowledge Dr. P.K. Pujari, Radiochemistry and Isotope Group, BARC for his encouragement. Authors thank the staff members of the Animal House Facility, Radiation Biology and Health Sciences Division, BARC and Department of Nuclear Medicine & PET, Kovai Medical Center and Hospital for the help received during animal experimentations and clinical studies, respectively.

References

- /1/ M. Fellner, B. Biesalski, N. Bausbacher, et al., Nucl. Med. Biol. 39 (2012) 993.
- /2/ N. Pfannkuchen, M. Meckel, R. Bergmann, et al., Pharmaceuticals 10 (2017) 45.
- /3/ I. Velikyan, Theranostics 4 (2014) 47.
- /4/ F. Rosch, Appl. Radiat. Isotopes 76 (2013) 24.

Synthesis and Evaluation of a Novel ^{99m}Tc Labelled Folic Acid Derivative for Targeting Folate Receptor Positive Cancers

Soumen Das*, Navin Sakhare, Anupam Mathur, Shubhangi Mirapurkar, Sheela M., S.S. Sachdev

Radiopharmaceuticals Program, Board of Radiation and Isotope Technology

*E-mail: soumen.das@britatom.gov.in

1. Introduction

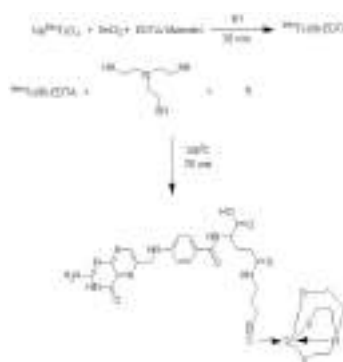
Folate receptor (FR) is an important biomarker in cancer [1]. Folic acid derivatives can serve as vectors for target specific delivery of radioisotopes either for non-invasive imaging or for delivering cytotoxic dose. In the present work an isonitrile bearing folic acid derivative has been synthesized and evaluated in FR positive KB cell line after labelling with ^{99m}Tc through the well-established '4+1' chemistry.

2. Experiment

The folic acid isonitrile derivative (1) was synthesized following a three step reaction scheme (Scheme 1). The formation of the final product was confirmed by FT-IR spectroscopy. This isonitrile derivative was then labeled with ^{99m}Tc through a reported two step process [2] with ^{99m}Tc (III)-EDTA as intermediate to yield the final ^{99m}Tc -4+1 complex (Scheme 2).



Scheme 1: Synthesis of folic acid isonitrile



Scheme 2. Radiolabelling

Formation of the product was established using analytical HPLC equipped with a radioactivity detector and the HPLC purified ^{99m}Tc labeled complex was used for *in vitro* cell study in folate receptor positive KB cell line. The cell uptake experiments of ^{99m}Tc -4+1 folic acid complex was carried for different concentrations of ^{99m}Tc complex with time.

3. Results and Discussion

The radiolabelled complex eluted out of the HPLC column with a retention time of ~ 19 min (Figure 1). The radiolabelling yield was found to be greater than 85%. *In vitro* biological evaluation of the HPLC purified radiolabelled complex was carried in FR positive KB cell line. Figure 2(a) shows the cell uptake results of the prepared ^{99m}Tc radiotracer in KB cell lines for different periods of 1, 2 and 24 h. The tracer was found to have significant uptake in the cells and an increase in uptake was observed upon increase in incubation upto 2 h (~7%ID/ 10^6 cells). The uptake observed was found to be specific as cold folic acid could nearly inhibit ~90% of the tracer uptake. Figure 2(b) shows the cell internalization at various concentrations of the tracer, each incubated for 2 h. On increasing the tracer concentration, specific cell internalization increases with increase in tracer concentration.

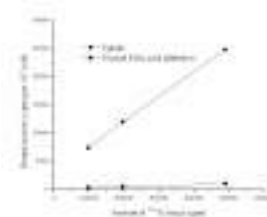
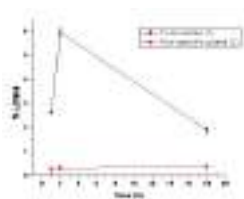
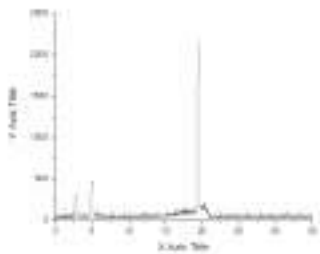


Figure 1. HPLC profile of the final radiolabelled complex Figure 2. Variation of cell uptake with (a) time and (b) concentration

4. Conclusion

^{99m}Tc -Folic acid isonitrile conjugate was synthesized in ~ 85% yield. Preliminary evaluation of ^{99m}Tc complex in KB cell line showed affinity towards folate receptors. Further experiments in nude mouse xenografts are planned to evaluate the *in vivo* imaging potential of the present ^{99m}Tc labeled derivative.

References

- /1/ C. P. Leamon, P. S. Low, Drug Discov Today. 6 (2001) 44-51.
- /2/ S. Seifert, J.U. K nstler, E. Schiller, et al., Bioconjug Chem. 15 (2004) 856-863.

Studies on Indoor and Outdoor Radon/Thoron Concentration and Estimation of Radiological Parameters from Gamma Dose Rates along the Coastal Regions of Trivandrum and Kollam Districts, Kerala, India

K. Nadira Mahamood, V. Prakash*

Department of Studies & Research in Physics, Payyanur College, Kannur, Kerala, India 670 327
*E-mail: nadirasufaid@gmail.com

1. Introduction

Large scale indoor and outdoor radionuclides concentration surveys assume significance in high background radiation areas (HBRAs) due to high air-kerma rate and presence of thorium rich monazite in the soil. About the half of radiation exposure to population comes from inhalation dose in which radon, thoron and their progenies are major contributors and when the decay products entered into the lungs increases the risk of lung cancer [1,2]. The present study includes estimation of indoor and outdoor radon/thoron concentration & measurement of gamma exposure rates in selected regions of Trivandrum and Kollam district, south-west coast of Kerala. Assessment of annual effective doses, lung dose and excess lifetime cancer risk were also done since these are the important radiological parameters used to determine the radiological protection of general public.

2. Experiment

Gamma radiation level measurements were made using Micro-R Survey Meter UR-705. Radon and thoron concentrations were measured using pin-hole dosimeter which is a cylindrical plastic chamber consists of two equal compartments separated by a central disc. The first compartment SSNTD films give radon concentration while the second gives both radon and thoron. Dosimeters were suspended in indoor and outdoor for a period of 3 months and after the retrieval, the films were chemically etched using 2.5 N NaOH at a temperature of 60°C for 90 minutes. After etching, the track densities were counted using spark counter.

3. Results and Discussion

Figure 1 shows variation of indoor and outdoor gamma exposure rates in different types of dwellings. Maximum indoor and outdoor dose rates were observed in Kovalam (Varkala) region due to the difference in air-kerma rate and soil composition. Figure 2 shows average values of radon and thoron concentration in different types of houses. The concentrations were varied according to the change in building materials and ventilation conditions. A comparison of annual effective doses due to radon, thoron and gamma exposure rates were shown in figure 3. The higher concentration of thoron may be attributed to high thorium content in the soil of the studied area.

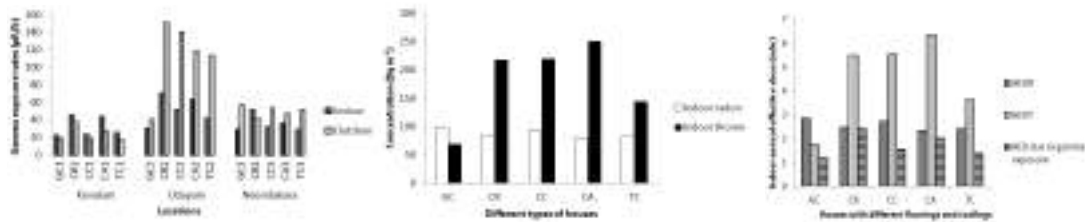


Figure 1, 2, 3: Indoor and Outdoor Gamma exposure rates, Indoor radon and thoron concentration, Annual effective dose due to indoor radon, thoron and gamma exposure

4. Conclusion

Indoor radon concentration was observed to be varying with different building materials, ventilation conditions while thoron varies irrespective of these reasons. Measured indoor thoron concentration is relatively higher as compared to indoor radon concentration. This may be attributed to relatively high concentration of thorium as compared to radium in the studied locations. Effective dose of tracheo-bronchial (D_{T-B}), pulmonary + Pulmonary lymph region (D_{P+PL}) and lung (D_{RL}) due to indoor radon exposure was within the safe limit. The health hazards related to radon exposure are negligible in the studied area while resulting average ELCR values emphasis the requirement of further studies.

Acknowledgement: Corresponding author wishes to acknowledge the University Grand Commission for providing Maulana Azad National Fellowship.

References

/1/ Y. Omori, S. Tokonami, S.K. Sahoo, et al., J of Radio. Protect. 37 (2017) 111-126.
 /2/ S. Mittal, A. Rani, R. Mehra . Indoor and built environment 0 (2017) 1-14.

Design, Characterization and Evaluation of ^{99m}Tc Labeled Functionalized Gold Nanoparticles for Imaging FR Positive Cancers

Dheeraj Kumar, Navin Sakhare, Pooja Kale, Soumen Das, Anupam Mathur, Shubhangi Mirapurkar, Sheela M., S.S. Sachdev*

Radiopharmaceuticals Program, Board of Radiation and Isotope Technology
*E-mail: dheeraj.kum@britatom.gov.in

1. Introduction

Cancer nanotechnology is one of the fastest growing fields. This the present work is a novel approach to functionalize gold nanoparticle (NP) with folic acid so as to target folate receptors present on several cancers such as ovarian, breast, etc. These NPs have been radiolabeled with ^{99m}Tc (technetium) and evaluated for its potential towards Folate receptor (FR) positive cancer imaging.

2. Experiment

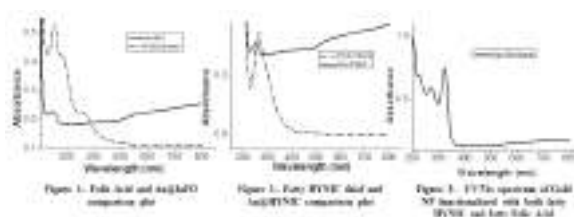
Methods: 11-Bromoundecanoic acid was synthetically modified with either folic acid or HYNIC (Hydrazino Nicotinamide) chelator at carboxylic acid end of fatty acid via 1, 3-propoyldiamino linker in a three step synthetic procedure. The bromo terminal of Folic acid/HYNIC conjugated fatty acid derivatives was converted to thiol group using potassium thioacetate in DMF followed by deprotection under acidic conditions. All the intermediates were characterized by NMR and MS. Gold NPs of three different functionalities namely i) Au@fatty acid-HYNIC ii) Au@fatty acid-Folid Acid and iii) Au functionalized with both fatty acid-HYNIC and fatty acid-Folic acid, were synthesized by a two phase synthesis method as reported in literature by Brust et al [1]. The NPs were then characterized by UV/Vis spectroscopy and were investigated for their labelling efficiency by ^{99m}Tc .

^{99m}Tc labeling was carried following the conventional HYNIC chemistry approach. Briefly, $^{99m}\text{TcO}_4^-$ (10-25 mCi, 0.5 mL) was added to a vial containing folic acid/HYNIC functionalized gold nanoparticle in ethanol (500 μL sample), $\text{SnCl}_2 \cdot 2\text{H}_2\text{O}$ (100 μg) in 0.1 N HCl (100 μL) and tricine (40 mg) in water (0.5 mL).

The reaction mixture heated in boiling water for 30 min and brought to room temperature. The formation of labeled gold nanoparticle was characterized by PC using saline as eluent. Yield: >90%. However, fatty acid-folic acid conjugate was evaluated as preliminary step towards evaluating the functionalized gold nanoparticle towards FR positive KB cancer cell lines.

3. Results and Discussion

Gold nanoparticles functionalized with folic acid and HYNIC were synthesized on incubating the above two thiolated long fatty acid chain conjugates of folic acid/ HYNIC with either or together with gold (III) chloride in presence of sodium borohydride as reducing agent. UV spectrums of the three functionalities of Gold NPs are shown in Figures 1, 2 and 3. Figure 3 is the UV/Vis spectrum of gold NPs where they are functionalized with both fatty acid- HYNIC and fatty acid-Folic acid conjugates. The attachment of both ligands on the surface of gold was deduced from the above UV patterns, where attachment of two conjugates on the gold surface shows signature of both folic acid and HYNIC and there is a blue and red shifts in comparison to peaks observed in Figures 1 and 2. ^{99m}Tc radiolabeling further confirmed (paper chromatography) the presence of HYNIC chelate on the gold nanoparticle. The specificity towards FR positive cancer cell line of inactive fatty acid-folic acid conjugate was ascertained by recording the fall in uptake of ³H-folic acid by varying the concentration of the conjugate. Preliminary inhibition experiment with inactive folic acid established IC₅₀ of 50 nM whereas the synthesized fatty acid-folic acid conjugate showed an IC₅₀ value around 550 nM.



Conclusion

Folic acid/HYNIC functionalized gold nanoparticles were successfully synthesized and labeled with ^{99m}Tc via HYNIC chelate in > 90% yield. Preliminary biological evaluation of fatty acid-Folic acid conjugate showed reduced affinity towards FR positive cancer cell lines. Further experiments are underway to evaluate the folic acid functionalized gold nanoparticles and its ^{99m}Tc labeled derivative towards FR positive KB cancer cell lines.

4. References

/1/ M. Brust,, M. Walker, D.Bethell, D.J.Schffrinand R.J. Whyman, J.Chem. Soc., Chem. Commun., 801 (1994)

Effect of γ -Irradiation on Ruthenium-Morin Nanocomposite for Trace Detection of Ce(IV), Ce(III) and Dy(III)

*Pritam Singh, Kamalika Sen**

Department of Chemistry, University of Calcutta, 92, A. P. C. Road, Kolkata 700009, India

*E-mail: kamalchem.roy@gmail.com

1. Introduction

Transition metal nanoparticles show unique electrical, optical and catalytic properties which attract attentions of modern science community [1]. Amidst this, ruthenium nanoparticles are gaining special interest due to their huge application in fuel cells, energy storage and most importantly in electrochemical sensing [2]. Recently lanthanides have captured a vast industrial application field which demands their associated pollution monitoring and regeneration studies. In this work we opt to synthesize ruthenium nanoparticles using a biogenic polyphenol, morin which has both reducing and stabilizing effect for the synthesis of nanoparticles in a green approach. These nanoparticles were then γ -irradiated for sensing and analysis of trace concentrations of Ce(IV), Ce(III) and Dy(III) in water.

2. Experiment

$\text{RuCl}_3 \cdot \text{XH}_2\text{O}$ and morin hydrate were mixed at equimolar concentrations (10 mM each) to synthesize the nanocomposite. Two similar sets were synthesized of which one set was synthesized under γ -irradiation for 24 h, with a dose rate of 1.594 kGy/h. The particles were deposited at the bottom of the container. They were washed with water-alcohol mixture for two to three times and finally collected after drying under IR lamp and characterized.

For sensing of lanthanides, the nanoparticles were first re-dispersed in water and then used for spectral detection of lanthanides. Measured aliquots of 1 mM aqueous solutions of the lanthanides were gradually added to the nanoparticle solution and the resulting absorption spectra were analyzed.

3. Results and Discussion

We have characterized the nanoparticles with transmission electron microscopy (TEM) which confirms its dimensions and crystallinity as can be seen in the lattice fringes in the image shown in figure 1. The average particle size of the nanoparticles is about 10 nm.

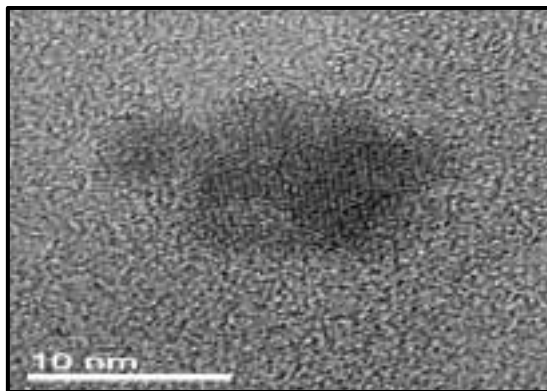


Figure 1. TEM image of gamma irradiated nanocomposite

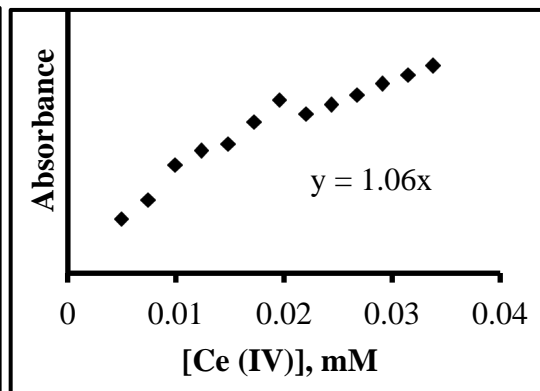


Figure 2. UV-vis calibration plot of Ce(IV) in nanocomposite solution

Table 1. Limit of detection (LOD) of different lanthanides by gamma irradiated nanoparticles

Parameters	Ce(IV)	Ce(III)	Dy(III)
λ_{\max} (nm)	290	253	297
LOD ($\mu\text{M/L}$)	7.9	10.39	13.16

Only the γ -irradiated nanocomposite solution was found to be active towards sensing of Ce(VI), Ce(III) and Dy(III). This can be explained on the basis of the fact that, in presence of γ -irradiation free electrons and free radicals are generated in the nanocomposite, which make them reactive species and hence become prone to be oxidized by lanthanide ions. However, for non-irradiated samples, the nanoparticles are quite stable and resistant towards such phenomena. The γ -irradiated nanocomposite can help in detection of Ce(IV), Ce(III) and Dy(III) down to 7.9 μM , 10.39 μM and 13.16 μM concentrations respectively. Table 1 summarizes the results along with the detection limit and wavelength of maximum absorption for the different lanthanides. Figure 2 describes the calibration of Ce(IV) detection at 290 nm.

References

- /1/ B. Thirumalraj, C. Rajkumar, S.M. Chen, et al., Sens. Actuator B 257 (2018) 48.
- /2/ A. Chen, C. Ostrom, Chem. Rev. 115 (2015) 11999.

^{210}Po and Uranium Sequential Analysis By Extractive Liquid Scintillation Spectrometry

Vandana Pulhani^{1*}, Priyanka J. Reddy², Moushumi Chaudhury¹, R M Tripathi¹

¹Health Physics Division, Bhabha Atomic Research Centre, Trombay,

²Radiation Safety Systems Division, Bhabha Atomic Research Centre, Trombay

*E-mail: vanpulh@barc.gov.in

1. Introduction

^{210}Po ($t_{1/2} = 138$ days) is a decay product in the ^{238}U decay series and widely distributed in the earth's crust and environment. Natural concentration of polonium in environment can be enhanced due to human activity and contributes around 8% to internal dose to human. The most widely used technique is the spontaneous deposition of Po on a silver disc but is subject to interferences from oxidants, organic materials, and other matrix elements that also deposit on the silver disc. These interferences can be removed by co-precipitation of Po and its chemical separation from interfering radionuclides and matrix elements. Extractive scintillation cocktails, POLEX, TOPO and TNOA have been reported for ^{210}Po analysis from groundwater samples [1], but could not be validated due to co-extraction of uranium from real ground waters. In the present study, Polonium separation methodology using extractive agents 75 g L^{-1} HDEHP and TOPO in toluene scintillator, followed by counting using liquid scintillation spectrometry was optimized and validated using various types of materials, including IAEA certified reference material viz., IAEA-385: Irish Sea sediment and IAEA-447: Moss-soil.

2. Materials and methods

Standard solution of uranium (30 Bq mL^{-1}) and ^{210}Po (90 Bq mL^{-1}) in equilibrium with ^{210}Pb obtained from BIPM, France were used for spiking experiments. Toluene based scintillator was prepared by dissolving 7 g PPO, 0.5 g POPOP and 200 g naphthalene in 1 L toluene. Extractive scintillator was prepared with two different extractants 75 g HDEHP and 75 g TOPO in toluene scintillator (7.5 % V/V). Extraction recovery of ^{210}Po spiked in aqueous solutions with varying HCl concentrations (0.1-1.2 M) using two different extractants 0.75M TOPO and HDEHP in toluene scintillator and was

studied as shown in Figure 1. The sequential separation of U and Po was carried out based on previous studies [2] and suitable extractant as observed from the current study.

3. Results and Discussion

Uranium is expected to interfere in the measurement of Po along with its daughters like Ra, Pb, Rn etc. Fig.1 indicates that extraction of Po by HDHEP is negligible whereas TOPO has superior extraction capability (95%) for ^{210}Po at 1 M HCl. The sequential separation methodology (Figure 2) was standardized using two stages, extracting U with HDHEP-Toluene in 0.01 M DTPA first and holding back Ra, Rn and Po in the aqueous phase. The second stage was extraction of Po with TOPO-Toluene extractant, where Ra was left in the aqueous phase. But Rn gets extracted and was observed to interfere with the alpha spectrum. Preheating the sample before extraction and sparging with Argon gas removes this interference totally. Polonium and uranium were then estimated using LSA. The methodology was validated with IAEA certified reference material and results are reported in Table 1, indicating good agreement within 7% deviation. The MDA obtained using this method 1.2 mBq for 10 ml aqueous samples and 0.7 Bq/kg for 1.74g of solid sample for a 1000 min counting time.

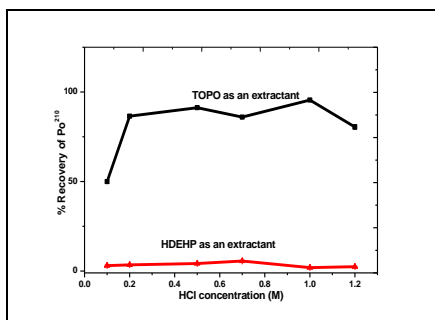


Figure 1. Efficiency of ^{210}Po extraction by 0.75M TOPO and HDEHP extractant in toluene scintillator

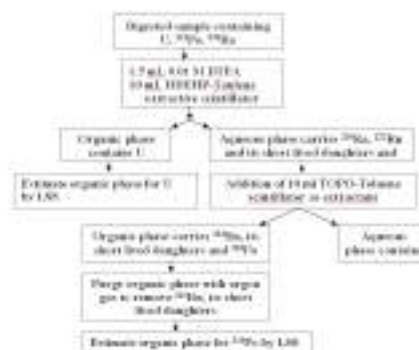


Figure 2. Flow Chart of the Separation Scheme standardized for U and Po separation

Table 1. ^{210}Po certified and experimental activity in certified reference materials

Sample ID	Certified Activity (Bq Kg^{-1})	Experimental $\pm \sigma$ (Bq Kg^{-1})
IAEA-385, Irish Sea sediment	31.2 - 35.3 (32.9)	35.02 ± 1.6
IAEA-447, Moss-soil	413 - 433 (423)	395 ± 7.8

4. References

- /1/ L. Jokelainen., P Vesterbacaka, and J Lehtol, Radiochimica Acta, 98 (2010) 91-97.
- /2/ P. J. Reddy, V. Pulhani, S. D. Dhole, et al, J. Radioanal. Nucl. Chem. 309 (2016) 1049-1057.

Physico-Chemical Investigation of Gamma Irradiated Guanidine Nickel(II) Sulphate

T A Jayashri¹, G Krishnan², K Viji¹*

¹Department of Chemistry, University of Kerala, Thiruvananthapuram 695581, Kerala, India

²Department of Chemistry, University college, Thiruvananthapuram 695034, Kerala, India

*E-mail: drjayashrita@yahoo.co.in

1. Introduction

Effect of gamma irradiation on physico-chemical characteristics of various materials have been studied while the same is scarce in transition metal complexes [1,2]. The present investigation reports effect of gamma irradiation on spectral characteristics, PXRD pattern, surface morphological features and antifungal properties of guanidine nickel(II) sulphate, a polymerization catalyst.

2. Experiment

The complex was prepared by known method and characterized. Pure sample was irradiated to 900 kGy at 6 kGy/h. Various studies of un-irradiated and irradiated samples were performed within one week of irradiation.

3. Results and Discussion

Radiolytic products, ammonia and sulphite were detected and estimated (table1). IR spectral studies showed significant changes in shape, position and intensity, suggesting hydrogen bonding interactions in the irradiated sample. From UV spectra Racah parameters were evaluated (table2). Irradiated sample has a higher LFSE and also the metal ligand covalent interaction is increased. Results of PXRD (figure1, table3) revealed that the hexagonal crystal system retained after irradiation, but the unit cell parameters, cell volume, lattice constants and average crystallite size were changed upon irradiation. Results of AFM (table 4, figure 2) showed that particle size and roughness were decreased upon irradiation. Similar results are obtained from SEM. Enhanced antifungal activity is exhibited by the pre-treated sample. Reduced crystallite size improves catalytic activity.

Table 1. Radiolytic fragments of $[\text{Ni}(\text{CH}_5\text{N}_3)_2]\text{SO}_4$

Radiolytic fragments	900kGy
SO_3 (ppm)	396
NH_3 (ppm)	2373

Table 2. spectral parameters of $[\text{Ni}(\text{CH}_5\text{N}_3)_2]\text{SO}_4$

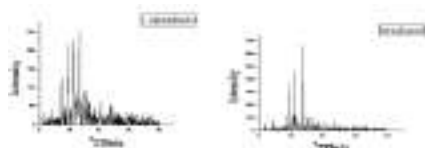
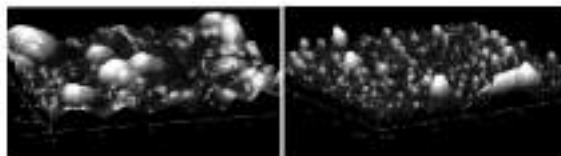
Sample	B' (cm^{-1})	$LFSE$ (cm^{-1})	β
Un-irradiated	895	15221	0.829
Irradiated	854	15383	0.791

Table 3. X-ray diffraction data of $[\text{Ni}(\text{CH}_5\text{N}_3)_2]\text{SO}_4$

Sample	Lattice Constants			Unit cell parameters (\AA)			Average crystalline size(nm)	Crystal system	Cell volume (\AA^3)
	A	B	C	a	b	c			
Unirradiated	0.0092	0.0092	0.0138	8.01	8.01	6.54	48.33	Hexagonal	419
Irradiated	0.0161	0.0161	0.0053	6.06	6.06	10.52	36.32	Hexagonal	386

Table 4. AFM data of unirradiated and irradiated $[\text{Ni}(\text{CH}_5\text{N}_3)_2]\text{SO}_4$

Sample	Surface Roughness (Rq) (nm)	Height (nm)	Particle Size(nm)
Un-irradiated	17.2	37.25	51.8
Irradiated	7.11	32.05	45.8

Figure 1 .XRD pattern of unirradiated and irradiated $[\text{Ni}(\text{CH}_5\text{N}_3)_2]\text{SO}_4$ Figure 2. AFM images of (a) unirradiated and (b)irradiated $[\text{Ni}(\text{CH}_5\text{N}_3)_2]\text{SO}_4$

References

- /1/ N. M. Thomas, H. Mathew, S. Sebastian, et al., Int. J. Sci. Res. Publ., 4 (2014) 1-7.
- /2/ T.A. Jayashri, G. Krishnan, K. Viji, J. Radioanal. Nucl. Chem. 302 (2014) 1021-1026.

Graphene Quantum Dots Prepared From Glucose as a Fluorescent Sensor Of Uranium in Environmental Samples

Pradeep Kumar Dewangan¹, Fahmida Khan^{1}, Kamlesh Shrivastava², Vinayak¹*

¹National Institute of technology Raipur , Raipur(C.G) 492010

²School of Studies in Chemistry Pt. Ravishankar shukla University Raipur (C.G.) 492010

E-mail: fkhan.chy@nitrr.ac.in

1. Introduction

In this work GQDs are prepared by direct pyrolysis method using glucose as precursor. The fluorescence property of GQDs is used for qualitative and quantitative analysis of uranium. The fluorescence of GQDs is intensively quenched by uranium via forming non luminescence complex of GQDs-U⁶⁺. Synthesized GQDs were characterized by uv-visible spectroscopy, FTIR, XRD, scanning electron microscopy and fluorescence spectrophotometry. Single layered, small in size and independently photoluminescent GQDs were recorded with maximum excitation and emission wavelength at 290 and 341nm respectively.

2. Experiment

2.1. Material: GQDs were prepared by pyrolysis of glucose. 2g glucose was heated at 250°C on a hot plate. After 5 min, glucose was liquefied and color changed from colorless to yellow and then to orange after 20 minutes. Then the orange liquid was added drop wise into 100 ml of 12.5% ammonia solution with constant stirring. The solution was heated at 70°. The pH of the solution was maintained at 7.

3. Result and Discussion

The high selectivity of GQDs to U⁶⁺ may be attributed to the fact that the interaction between ions and carboxylate or hydroxyl groups facilitated GQDs and U⁶⁺ close to each other which accelerated the non-

radiative recombination and excitations through an effective electron transfer process, leading to a substantial decrease of the fluorescence of GQDs. Hydroxyl group acts as a hard base and U^{6+} as a hard acid, so these are well interacted.

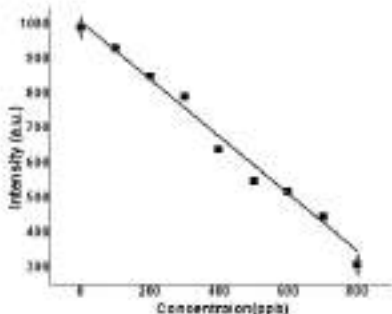


Figure a. Linear plot of PL peaks intensity quenching of GQDs as a function of uranium concentration

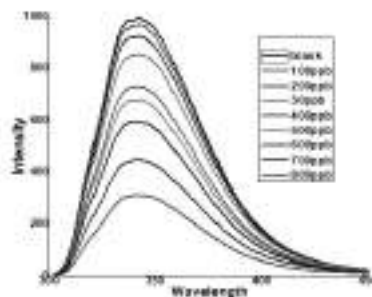


Figure b. PL spectra of GQD's in U(VI) aqueous solution of different concentrations(excited at 290 nm)

It is seen that an increase of the pH lead to gradual decrease of fluorescence intensity up to 7 pH but further increase resulted in gradual increase of fluorescence intensity. Optimum pH is 7 for uranium detection and up to 1.5 ppb is accurately determined. UV-Visible absorption spectrum of GQDs shows two absorption bands at 230 nm and at 280 nm of which are characteristics for GQDs and are very selective and sensitive for uranium. Calibration curve is plotted between the concentration of uranium and fluorescence intensity. UV-Visible spectra and fluorescence spectra show excellent fluorescence properties of GQDs with excitation at 290 nm. A range of linear 0 – 800 ppb with recovery of 96 – 110% is obtained for uranium determination in different ground water samples. The glucose based GQDs nano-sensing probe is successfully applied for detection and determination of uranium in ground water.

Acknowledgement: The authors are thankful to Dr A. M. Rawani, Director NIT Raipur for laboratory and library facilities. One of the author Pradeep Kumar Dewangan gratefully acknowledges the JRF awarded by CSIR.

References

- /1/ B. Xue, K. Li, L. Feng, J.Lu, L. Zhang, *Electrochimica Acta*. 239 (2017) 36-44
- /2/ W.Zhe, Y. Lu, H. Yuan, Z. Ren, C.Xu and J. Chen, *Nanoscale*. 7.48 (2015) 20743-20748.

Tritium Analysis in Radioactive Waste Solution using Liquid Scintillation Counter

*B. Arun**, *Y. Ramani*, *I. Vijayalakshmi*, *S. Viswanathan*

Radiological Safety Division, Indira Gandhi Center for Atomic Research, Homi Bhabha National Institute,
Kalpakkam, Tamilnadu, India

*E-mail: arunhcu09@igcar.gov.in

1. Introduction

For analysis of tritium in the low quenched samples and in the absence of other radionuclides, direct addition of sample to cocktail method is used. Distillation technique is used for separation of tritiated water in presence of impurities (high quenched samples) and other radionuclides. In this paper effect of distillation for measurement of tritium in presence of other radionuclides is discussed.

2. Materials

Hidex Make 300SL liquid scintillation counter (LSC) was used for tritium measurement. The efficiency of the system is found from quench curve, which is correlation between Triple to double coincidence ratio (TDCR) and efficiency values. Quench curve is obtained from 10 standards having a constant tritium activity of 4350Bq but quenching levels are increased by addition of nitro methane.

3. Results and Discussions

Gross alpha, gross beta and ^{137}Cs activities in the three samples were measured using ZnS (Ag), GM counter and HPGe detector. Tritium was measured using LSC by direct addition of 8mL sample and 12mL of cocktail. The three samples are distilled by taking 100 mL of the original samples in alkaline medium in presence of potassium permanganate [1] to oxidize the organic matter. The distillate collected was analyzed for gross alpha, beta, ^{137}Cs and tritium activities. Figure 1 shows the comparison of LSC spectrum

with and without distillation. After distillation the high-energy beta emitters (Sr^{90} - Y^{90}) disappeared. Figure 2 Shows gamma ray spectra for ^{137}Cs with and without distillation. The ^{137}Cs peak disappeared in the later method. Table 1 compares gross alpha, gross beta, ^{137}Cs and ^3H activities with and without distillation.

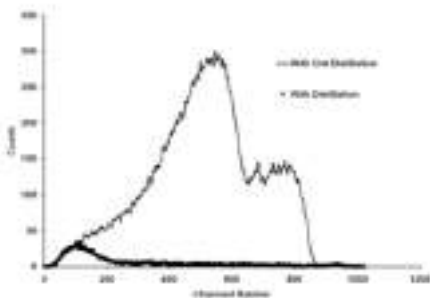


Figure 1. Comparison of LSS Spectra before and after Distillation

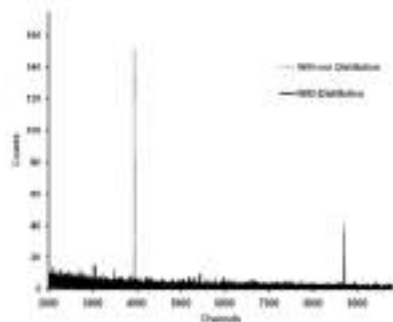


Figure 2. Comparison of HPGe Spectra before and After Distillation

Table 1. Comparison of Tritium values with and without distillation

	Without Distillation				With Distillation			
	Gross Alpha (Bq/L)	Gross Beta (Bq/L)	Tritium Bq/L	^{137}Cs Bq/L	Gross Alpha (Bq/L)	Gross Beta (Bq/L)	Tritium Bq/L	^{137}Cs Bq/L
S-1	3.0	146.78	161.03	129.16	BDL	BDL	BDL	BDL
S-2	12.76	1825.35	456.36	594.78	BDL	BDL	144.89	BDL
S-3	25.76	7387.12	1633.07	1728.5	BDL	BDL	628.86	BDL

4. Conclusions

The Study, experimental verification of distillation method for measurement of tritium in presence of other radionuclides shows that absence of other radioactive elements in the distillate samples. So to avoid the overestimation by direct analysis of tritium, it is better to distillate the sample and measure the tritium activity.

Acknowledgement: The authors are grateful to Dr. B.Venkatraman, Director, HSEG, IGCAR, Dr. R. Baskaran, Head, RSD, Dr. K.Sivasubramanian, Head, RAMS for their support and encouragement.

References

- /1/ ISO, 9698- Water quality: determination of tritium activity concentration, Liquid Scintillation Counting Method, 2nd edn.

Highly Selective Removal of Pertechnetate by Donnan Dialysis through Supported Liquid Membrane

Sanhita Chaudhury^{1}, V. G. Mishra², D. J. Shah²*

¹Radiochemistry Division, ²Radioanalytical Chemistry Division,
Bhabha Atomic Research Centre, Mumbai-85, India,
*E mail: sanhita.poi@gmail.com

1. Introduction

⁹⁹Tc is of major concern to the environmentalist because of its long half life (2.11×10^5 years) and significant (6.05%) yield in the fission of ²³⁵U [1]. In aqueous nuclear waste streams, ⁹⁹Tc is mostly present as Pertechnetate (TcO_4^-) form and this species is having high mobility in the environment. Till date, ion exchange based extraction methods using different materials [1], as well as precipitation based methods have been used to remove this species from nuclear waste streams [1]. The advantages of the membrane based separation methods over these conventional separation methods are well established. Till date, only a few literatures [2-3] are available on the use of membrane based (using amines or aza-crowns) separation method for TcO_4^- removal. On the other hand, literature reports [4-5] indicate the possibility of using tetraphenyl arsonium chloride as a selective extractant for TcO_4^- . However, till date, there is no report on separation of TcO_4^- using this reagent in polymer membranes. With this in view, in the present work, the transport selectivity of TcO_4^- over nitrate (major competing anion in nuclear waste) has been studied in detail using tetraphenyl arsonium perchlorate (TAP) in polypropylene based supported liquid membrane. The transport of TcO_4^- from feed to receiver is based on the principle of Donnan dialysis using high concentration of another anion in the receiver compartment. Initially, experiments have been carried out to optimize the receiver composition to obtain fast and complete transport of the ion of interest.

2. Experimental

The commercially available polypropylene membrane (dia 0.2 μm , thickness 90 μm) was soaked with the ligand solution (0.015 g TAP in 1 mL nitrobenzene). Two compartment (each of 13.5 mL) Donnan

dialysis based permeation experiments using these membranes for different feed and receiver compositions have been carried out. In order to optimize the receiver composition, experiments have been carried out for TcO_4^- (0.1 mCi/ L) in deionised water in feed and 0.1 M of other salt solutions (NaNO_3 / LiClO_4 / NaCl / Na_2SO_4) in receiver. The transport selectivity of TcO_4^- over nitrate has also been studied for TcO_4^- (0.1 mCi/ L) in varying conc. of (0.1- 1 M) NaNO_3 in feed. The transport of TcO_4^- and NO_3^- has been monitored by gamma spectroscopy and ion chromatography respectively.

3. Results and Discussions

The Pertechnetate transport profiles from deionised water in feed and different salt solutions in receiver compartment are shown in Figure 1. It can be seen that the transport is fastest for ClO_4^- and slowest for SO_4^{2-} .

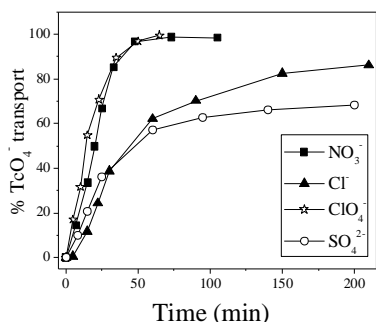


Figure 1. Comparison of TcO_4^- transport profiles for different anions (0.1 M) in receiver phase.

With ClO_4^- , within ~50 minutes, ~100% TcO_4^- was transported to the receiver phase. The transport rate for NO_3^- is almost comparable to that for ClO_4^- . However, with 0.1 M NaNO_3 in receiver compartment, it will be impossible to determine the selectivity factor of TcO_4^- over nitrate. Henceforth, all the selectivity studies have been done with 0.1 M LiClO_4 in receiver compartment. Further

results indicated that in this work, in presence of varying conc. of NaNO_3 in feed, TcO_4^- was transported to the receiver compartment with high degree of selectivity over NO_3^- . In all the cases, more than 90% TcO_4^- was transported to the receiver compartment with a selectivity factor >70 . The selectivity increased as nitrate conc. decreased and for 0.1 M NaNO_3 , the factor was 88. These interesting results indicate that the membrane can further be explored for selectivity studies from simulated nuclear waste solutions.

References

- 1/ D. Banerjee, D. Kim, M. J. Schweiger, et al., Chem. Soc. Rev., 45 (2016) 2724-2739.
- 2/ R.Chiarizia. J. Membr. Sci, 55(1991) 39-64.
- 3/ J. D. Lamb, C. A. Morris, J. N. West, et al., J. Membr. Sci. 321 (2008) 15–21.
- 4/ T. Omori, Y. Muraoka, H. Suganuma, J. Radioanal. Nucl. Chem., 178 (1994) 237-243.
- 5/ A.Srivastava, A. Goswami, B. K. Srivastava, et al., Phys. Rev. C, 33 (1986) 969-973.

Size Dependent Ion Exchange Property of Nanosilica As Green Inorganic Exchanger in Radiochemical Separations

Rajesh Chakraborty, Pabitra Chattopadhyay*

Department of Chemistry, The University Burdwan, Golapbag, Burdwan-713104, India

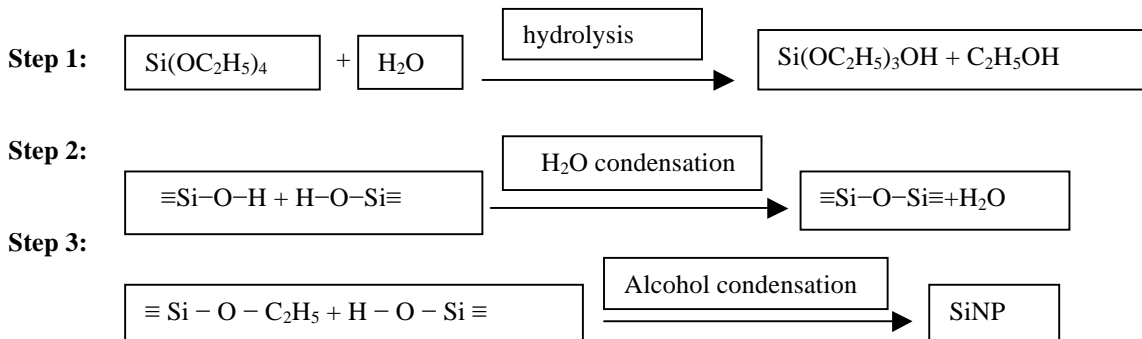
*E-mail: pabitracc@yahoo.com

1. Introduction

The present investigation attempts to employ silica nanoparticle in radiochemical separation of ^{90}Sr - ^{90}Y pair. The synthesis and employment of nanosilica as exchanger material keeps space with modern day's green chemical approach which says things to be done to get close to the Environment.

2. Experimental

2.1. Preparation of Si nanosilica: SiNP was prepared following earlier report [1].



2.2. Size modification using different concentration of TEOS: We made an attempt to produce SiNP with different size distribution by varying concentration of precursor TEOS (Figure 1).

3. Results and discussion

3.1. Characterization of SiNP: The figure 2 shows the SEM image for SiNP. The particles are mostly spherical in shape as shown in SEM. TEM images show the different ways of aggregation for the

spherical particles in different scale. TEM images also helps to calculate the size of particles ranging from 30-50 nm.

3.2 Studies of separation of ^{90}Sr - ^{90}Y : Separation of ^{90}Sr - ^{90}Y parent-daughter pair was done by a column method. A glass column of length 10 cm and 1 cm internal diameter was packed with the air-dried acidic form of the exchanger material and thoroughly washed with water to remove any traces of adhered acid and preconditioned at pH 7. Equilibrated mixture of ^{90}Sr - ^{90}Y (100 L) maintaining a neutral pH was loaded over the column. Then ^{90}Y was eluted with 1.0% EDTA solution. ^{90}Y thus comes out as in complexed form with EDTA. Purity of the eluted solution was checked by calculating half-life of ^{90}Y from the eluted solution with the help of the decay curve and the presence of the no-carrier added ^{90}Y in the elute was confirmed by Feather analysis [3]. Feather analysis is a technique for determining the range in aluminium of the beta rays of a species by comparing the absorption curve of that species with the absorption curve of a reference species. The decay curve is shown in Figure 3.

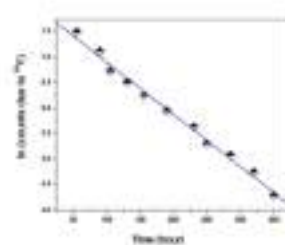
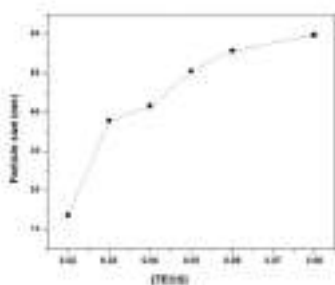


Figure 1. Increase in particle size with [TEOS]

Figure 2. SEM image

Figure 3. Elution profile of ^{90}Y loaded with a 1.0 % aq. EDTA

4. Conclusion

Size modification of nano materials along with the investigation on size dependent properties and also greener approach to the synthesis have emerged as a fascinating area of modern materials research. This exchanger can also be used in separating a promising positron-emitting radionuclide ^{86}Y which is capable of serving as a PET imaging surrogate for ^{90}Y , from its mixtures with ^{86}Sr .

References

- 1/ W. Ostwald, Lehrbuch der Allgemeinen Chemie, 2 (1896), Leipzig, Germany.
- 2/ I.A. Rahmana, P. Vejayakumaran Sipaut, C.S. Ismai, et al., Colloids and Surfaces A, 294 (2007)102–110.
- 3/ R. Chakraborty, P. Chattopadhyay, J. Radioanal. Nucl. Chem. 294 (2012) 31–35.

Fission Analysis of Z=114 Superheavy Isotopes Formed Via Heavy-ion Induced Reactions

Gurjit Kaur^{1}, Kirandeep Sandhu², Manoj K. Sharma¹*

¹School of Physics and Materials Science, Thapar Institute of Engineering & Technology, Patiala-147004, India

²Department of Physics, GSSDGS Khalsa College, Patiala-147001, India.

*E-mail: gurjitsaini2505@gmail.com

1. Introduction

Recent experimental and theoretical developments have enriched our knowledge regarding fusion-fission (FF), symmetric fission, and quasi-fission (QF) processes. The relative contribution of QF to the capture cross-section becomes dominant in the superheavy mass region and hence hinders the compound nucleus formation to a reasonable extent. The different characteristics such as shell effects, deformations, orientations of nuclei, collision energies, Coulomb factor etc. strongly influence the relative emergence of compound nuclear (CN) and non-compound nuclear (nCN) processes. To explore the relative contribution of CN and nCN-processes we have investigated the different binary reaction channels of superheavy isotopes within Z=114.

2. The Methodology

The dynamical cluster decay model (DCM) [1] works on the coordinates of mass asymmetry, relative separation R, deformations, and orientations, which gives adequate description of different decay mechanisms. In terms of above mentioned co-ordinates, the symmetric fission decay cross-sections are calculated using partial wave analysis as defined in [1]. The Preformation probability (P_0) used to estimate the fission cross-sections is obtained via solution of stationary Schrödinger wave equation and is defined as: $P_0 = \sqrt{B_{\eta\eta}} |\psi[\gamma(A_i)]|^2 \left(\frac{2}{A}\right)$, where $B_{\eta\eta}$ are hydrodynamical mass parameters.

3. Results and Discussion

The symmetric fission cross-sections ($\sigma_{A/2\pm 20}$) of $^{48}\text{Ti}+^{238}\text{U}$ and $^{48}\text{Ca}+^{244}\text{Pu}$ reactions [2] leading respectively to $^{286}\text{Fl}^*$ and $^{292}\text{Fl}^*$ nuclei, are calculated using DCM [1]. The DCM based results are shown in Table 1 for both channels using quadrupole (β_2) deformations with hot optimum approach.

Using these parameters the preformation probabilities (P_0) of $^{286}\text{Fl}^*$ and $^{292}\text{Fl}^*$ nuclei are compared at near barrier energies to explore the relative contribution of symmetric and asymmetric fission for spherical as well as deformed choice of fragmentation. The preformation structures for given nuclei are significantly modified while shifting from spherical to deformed as shown in Figure 1. There is also evident modification in structure of preformation profile of different isotopes of $Z=114$ namely $^{286}\text{Fl}^*$ and $^{292}\text{Fl}^*$. Relatively symmetric yield is observed for $^{286}\text{Fl}^*$ nucleus which becomes highly asymmetric in nature for $^{292}\text{Fl}^*$ superheavy system. For heavier isotope of $Z=114$, both symmetric fission and asymmetric quasi-fission processes seems to operate for deformed choice of fragments. Also the contribution of HMF region, giving asymmetric quasi-fission, increases with the inclusion of deformations. It will be of further interest to explore the dynamics of quasi-fission phenomenon under the influence of different parameters such as deformations, Coulomb factor, orientations etc.

Figure 1. Preformation probability (P_0) plotted as a function of fragment mass for decay of (a) $^{286}\text{Fl}^*$ and (b) $^{292}\text{Fl}^*$ nuclei.

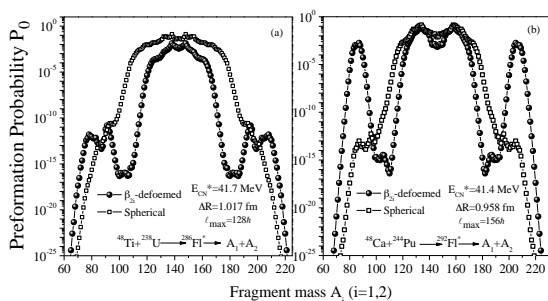


Table 1. DCM fitted symmetric fission cross-sections for $^{286}\text{Fl}^*$ and $^{292}\text{Fl}^*$ superheavy systems using hot optimum approach with β_2 -deformations.

E_{CN}^* (MeV)	$E_{c.m.}$ (MeV)	ΔR (fm)	l_{max} (h)	$\sigma_{DCM}^{A/2\pm 20}$ (mb)	$\sigma_{Exp.}^{A/2\pm 20}$ (mb)
$^{48}\text{Ti} + ^{238}\text{U} \rightarrow ^{286}\text{Fl}^*$					
33.3	207.0	0.983	125	0.058	0.060
41.7	215.5	1.017	128	2.040	1.980
52.4	226.2	1.036	132	9.980	9.720
$^{48}\text{Ca} + ^{244}\text{Pu} \rightarrow ^{292}\text{Fl}^*$					
29.5	191.0	0.927	148	0.276	0.280
37.2	198.7	0.952	154	6.940	6.760
41.4	203.0	0.958	156	14.60	14.40

4. Conclusion

The DCM based fission cross-sections shows decent agreement with experimental data [2] for both the reactions. The variation of preformation yield suggest that symmetric fission is the prime decay mode for $^{286}\text{Fl}^*$ nucleus, whereas for $^{292}\text{Fl}^*$, both symmetric fission and asymmetric quasi-fission processes contribute with each other.

Acknowledgement: Assistance from DST, New Delhi, for INSPIRE-fellowship (grant no. DST/INSPIRE/03/2015/000199).

References

- /1/ G. Kaur, K. Sandhu, and M. K. Sharma, Phys. Rev. C 94 (2016) 014615.
- /2/ Y.T. Oganessian, Phys. Rev. C 69 05 (2004) 4607.
- /3/ E. M. Kozulin, G. N. Knyazheva, K. V. Novikov, et al., Phys. Rev. C 94, (2016) 054613.

Role of Biomolecules in Extraction of U(VI) using An Aqueous Biphasic System

*Rajib Karmakar, Kamalika Sen**

Department of Chemistry, University of Calcutta,
92, A. P. C. Road, Kolkata 700009, India
*E-mail: kamalchem.roy@gmail.com

1. Introduction

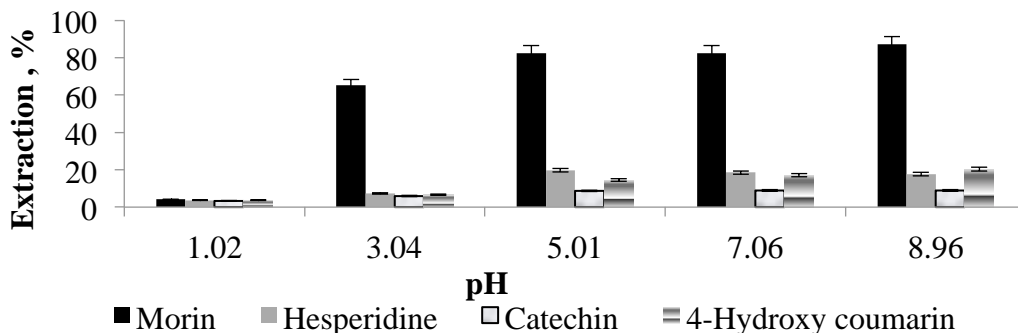
Radiological contaminations are becoming a major concern due to unwanted discharge of nuclear reaction products in the environment. Contamination of drinking water by uranium has documented nephrotoxicity [1]. Therefore, the detection and remediation of radioactive elements is very significant. There are many techniques for the removal of radioactive elements e.g., electrocoagulation [2], emulsion liquid membrane (ELM), using zero-valent iron, etc., which are often time consuming and involve toxic reagents. Recently, aqueous biphasic systems (ABSs) have shown to offer an environment friendly tool for extractions of several analytes. Here we report the extraction of trace uranium by ABS using morin hydrate as a polyphenolic extractant which forms a strong complex with UO_2^{2+} .

2. Experimental

The ABS was formed by 50% (w/v) PEG#6000 and 2 M Na_2SO_4 solution. Four different polyphenolic compounds viz., morin hydrate, catechin, 4-hydroxy coumarin and hesperidin were used as extractants. 0.1 mL of 10 mM polyphenol solution and 0.05 mL of 10.5 mM uranyl nitrate were added to a 3 mL PEG#6000 solution taken in a centrifuge tube. The mixture was shaken for 10 mins and kept for 10 mins. Then 3 mL of 2 M Na_2SO_4 solution was added to form a biphasic system. Na_2SO_4 solution of different pH were taken to obtain the best extraction efficiency of U(VI). The PEG-rich phase was then taken from ABS and acidified with HCl. Arsenazo III was used as spectrophotometric reagent to detect and estimate uranium by absorption spectrometry.

3. Results and Discussion

Among all four extractants, maximum removal of U(VI) from aqueous solution was found in case of morin hydrate. Best removal (~88%) of uranium was obtained at ~pH 9 of 2 M Na₂SO₄ solution. Figure 1 shows the extraction profile of uranium using different extractants at different pH of salt solution.



The result may be explained on the basis of the binding constant of each of the extractants with U(VI) calculated using Benesi Hildebrand method. The values were found to be 13503, 3349, 1408 and 375 mol⁻¹L for morin, catechin, hesperidin and 4-hydroxy coumarin respectively. At the acidic pH the -OH moieties of morin get protonated and the lone pair on O atom becomes unavailable for chelate formation which is reflected in low extractions at lower pH.

References

- /1/ P. Kurttio, A. Auvinen, L. Salonen, H. Saha, J. Pekkanen, I. Mäkeläinen. *Env. Health Persp.* 4 (2016) 337.
- /2/ E. Nariyan, M. Sillanpää, C. Wolkersdorfer. *Sep. Pur. Tech.* 193 (2018) 386.

An Analysis of The Production of Neutron Deficient Platinum Radionuclides

*Rinku Prajapat, Moumita Maiti**

Department of Physics, Indian Institute of Technology Roorkee, Roorkee-247667, Uttarakhand, India

*E-mail: moumifph@iitr.ac.in

1. Introduction

The production cross-sections of the neutron deficient platinum radionuclides have been studied from the different projectile-target combinations. The production routes of $^{184-191}\text{Pt}$ consist of both light and heavy-ion induced reactions at the energy range from threshold to 95 MeV. The half-lives of $^{184-191}\text{Pt}$ cover a range from 17.3min to 10.2d, and they have suitable decay radiation. Therefore, one may choose these isotopes for various applications, in the field of medicine, agriculture, etc. The cross-sections of the platinum radionuclides populated via xn -channel have been calculated using the statistical nuclear reaction models: Hauser-Feshbach (HF) and Weisskopf-Ewing (WE) for equilibrium (EQ) and the exciton model and hybrid Monte-Carlo simulation (HMS) for the preequilibrium (PEQ) processes. The combined effect of EQ and PEQ are compared with the available measured data. The contribution of PEQ and equilibrium (EQ) reactions is analyzed through the comparative study.

2. Results and discussion

The following reactions have been explored to study the production of Pt-radionuclides: $\alpha+^{188}\text{Os}$, $^7\text{Li}+^{185}\text{Re}$, $^9\text{Be}+^{186}\text{W}$, $^{11}\text{B}+^{181}\text{Ta}$. The following reaction model codes were used in this study: PACE4, considers the HF model with Gilbert-Cameron (GC) level density; ALICE14: based on the WE and HMS models with Fermi gas level density; and EMPIRE3.2: considers the HF and EM with a phenomenological version of Generalized Superfluid Model (GSM) characterized by a phase transition from superfluid behavior at low energy, where pairing correlations influence the level density, to a Fermi gas state. The value of the mean free path parameter for the EM is chosen as 1.5. However, only the production cross-sections of ^{187}Pt (2.35h, 104.6 keV γ -rays) and ^{191}Pt (2.8d, 538.9 keV γ -rays) are shown in Fig. 1 from the $^{185}\text{Re}(^7\text{Li},5n)^{187}\text{Pt}$ and $^{186}\text{W}(^9\text{Be},4n)^{191}\text{Pt}$, respectively. An enhancement in the

cross-section is observed for both ^{187}Pt and ^{191}Pt due to the PEQ emissions at the high energy tail of the excitation function compared to the pure HF calculation of PACE4. In the case of ^{191}Pt , it is observed that ALICE and EMPIRE are in good agreement with the experimental data [1] available in the range of compound reaction process compared to PACE4. The difference of the cross-section in different nuclear models can be explained in terms of different level density. Being weakly bound, fragmentation/nucleon transfer followed by the breakup of ^7Li and ^9Be in the nuclear force field is also possible, which will eventually reduce the production of Pt-radionuclides [2]; however, the extent of those reactions needs to be checked experimentally. With a maximum cross-section of $\sim 900\text{-}1000\text{mb}$, the feasible production of both the radionuclides is observed in the $40\text{-}65\text{MeV}$ energy range, which is mostly dominated by the EQ process. PEQ emission starts around 65 and 55MeV for ^{187}Pt and ^{191}Pt , respectively, with a maximum contribution of $\sim 20\text{-}30\%$ of the total cross-section.

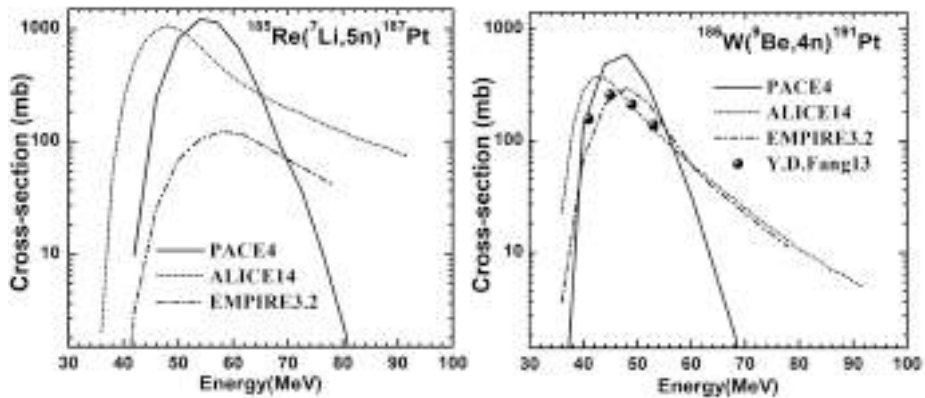


Figure 1. Comparison of excitation functions of ^{187}Pt and ^{191}Pt from PACE4, ALICE14 and EMPIRE3.2.

3. Conclusion

The comparative study of the theoretical models suggests that the compound reaction mechanism is the favorable way for the production of residues. The experimental cross-sections of ^{191}Pt are in good agreement with theoretical estimations. However, more experiments are required to validate the study.

The MHRD research fellowship is highly acknowledged.

References

- /1/ Y. D. Fang et al, Phys. Rev. C 87 (2013) 024607.
- /2/ D. Kumar, M. Maiti, Phys. Rev. C 96 (2017) 014617.

Experimental Investigation of Soil to Grass Transfer Factor for ^{137}Cs and ^{60}Co using Lysimetry Facility

S.S.Wagh^{1,*}, A. K. Patra¹, Jaison T. John¹, J. S. Mistry², P.M.Ravi^{3,4}, R.M. Tripathi^{3,4}

¹ESL (ESS, HPD, BARC), Kakrapar Gujarat Site, P.O. Anumala, Surat District, Gujarat-394651

²WMP, Kakrapar Atomic Power Station, P.O. Anumala, Surat District, Gujarat-394651

³Health Physics Division, Bhabha Atomic Research Centre, Mumbai-400 085

⁴Homi Bhabha National Institute (HBNI), Mumbai-400094

*E mail: sswagh@npcil.co.in

1. Introduction

Uptake of radionuclides from soil to plant is characterized using a transfer factor (TF), the ratio of radionuclide concentration in plant to radionuclide concentration in soil per unit mass [1]. TF for a given type of plant and for a given radionuclide can vary considerably from one site to another, with season and with time after contamination. This paper presents the results of estimation of soil to grass transfer factor for ^{137}Cs and ^{60}Co in an in-house developed lysimeter facility.

2. Experimental

The lysimeter consist of a 12 mm thick mild steel cylinder, 1200 mm in diameter and 1500 mm in length (Figure 1). 10 L de-mineralized water was spiked with stable salts and radiotracers. The specific activity in the solution was ^{137}Cs : 55 Bq/mL; ^{60}Co : 40 Bq/mL; Amount of $\text{Cs}(\text{NO}_3)$ and $\text{Co}(\text{NO}_3)_2 \cdot 6\text{H}_2\text{O}$ added: 15 mg/mL and 45 mg/mL respectively. Total volume was sprinkled over the surface soil within Lysimeter. Natural growth of grass was allowed. Surface soil (up to 10 cm) and grass samples were collected at different time interval, pre-processed and counted by HPGe detector.

3. Results and Discussion

3.1 Physico-chemical parameter of soil samples: Physical properties of soil sample collected from lysimetry facility namely bulk density, porosity and organic matter was observed to be in the range of 1.08-1.45 g/cc , 35.9-49.5 % and 9.7-12.2% respectively. Distribution Coefficient (K_d) estimation of the soil sample was carried out for ^{137}Cs and ^{60}Co using batch sorption method. Site-specific K_d for 7

days of ^{60}Co and ^{137}Cs was observed to be 3256 mL/g and 2600 mL/g respectively. K_d of ^{60}Co is comparatively higher than that of ^{137}Cs . Uptake of radionuclide by plant largely depends on the K_d value of the corresponding soil [2]. A higher K_d value attributes a lower transfer.

3.2 Soil to grass Transfer Factor for ^{137}Cs and ^{60}Co : Soil to grass transfer factor (TF) was estimated using the activity estimation in soil and grass samples based on the following equation;

$$\text{TF} = [\text{Activity in Grass (Bq/kg dry weight)}] / [\text{Activity in soil (Bq/kg dry weight)}] \text{ ---(1)}$$

Soil and grass samples (6 nos. each) collected from Lysimeter experimental facility at different occasions and analysed for ^{137}Cs and ^{60}Co . ^{137}Cs and ^{60}Co activity in soil samples was found to be in the range of 114-596 and 125-461 Bq/kg dry wt. respectively (Table-1). ^{137}Cs and ^{60}Co activity in grass samples was found to be in the range of 3.7-62.8 and 7.0-156.6 Bq/kg dry wt. respectively. Soil-to-grass transfer factor for ^{137}Cs and ^{60}Co was found to be in the range of 1.26E-02 - 3.6E-01 and 1.52E-02 - 1.26E+00 respectively (Table-1). IAEA, TECDOC-1616 (2009) [3] reported the TF for ^{137}Cs and ^{60}Co from soil to grass ranged 4.8E-03 - 9.9E-01 & 4.0E-02 – 1.7E-01 respectively. The site-specific TF data will be used for the prediction of radionuclide distribution pattern in soil and vegetation in case of a hypothetical air contamination.



Figure 1. Lysimeter experimental facility within SWMF, Kakrapar Site

Table 1. ^{137}Cs and ^{60}Co activity in soil and grass & Soil-to-Grass Transfer Factor

Sr. No.	Soil (Bq/Kg of Dry wt.)		Grass (Bq/Kg of Dry wt.)		TF	
	^{137}Cs	^{60}Co	^{137}Cs	^{60}Co	^{137}Cs	^{60}Co
1	596±2	403±2	43.0±1.0	22.3±0.8	7.21E-02	5.53E-02
2	363±3	164±2	41.2±1.6	21.5±1.3	1.13E-01	1.31E-01
3	377±6	284±8	62.8±2.5	48.4±2.5	1.67E-01	1.71E-01
4	265±4	125±3	56.0±4.0	156.6±7.6	2.11E-01	1.26E+00
5	291±5	461±7	3.7±0.6	7.0±0.8	1.26E-02	1.52E-02
6	114±2	165±3	41.2±1.6	21.5±1.3	3.61E-01	1.30E-01

References

- /1/ T. Yassine, M. Al-Odat, I. Othman, J. Food Phys. XVI (2003) 73-79.
- /2/ A. Gommers, T. Gafvert, E. Smolders, et al. J. Environ. Radioact, 78 (2005) 267-287.
- /3/ IAEA, Tecdoc-1616 (2009).

Uptake and Distribution of Ceria Nanoparticles in Plants Using Radiotracer Techniques

Zhiyong Zhang*, Xiao He, Yuhui Ma

Key Laboratory for Biomedical Effects of Nanomaterials and Nanosafety, Institute of High Energy Physics, Chinese Academy of Sciences, Beijing 100049, China

* E-mail: zhangzhy@ihep.ac.cn

1. Introduction

With the fast development of nanotechnology, manufactured nanoparticles (NPs) are being increasingly used in a wide range of areas including cosmetics, medicine, food and food packaging, paints, electronics, fuel catalysts and water treatment, etc. The unique properties of these materials, such as large specific surface area and high reactivity, have raised questions concerning potential adverse effects on human and environmental health. To support the sustainable development of nanotechnology, possible risks have to be evaluated based on sound research that elucidates all relevant aspects of the concern.

Assessing the impacts of NPs on terrestrial plants will provide insight into the risk of ecological exposure to these materials, as well as to the potential human exposure through food chain contamination. Phytotoxicity of some types of nanoparticles has been observed for higher plants in the seed germination and root elongation test, but there are few published studies on uptake, translocation and accumulation of NPs in plants [1].

2. Experiment

Cerium-141 [$T_{1/2}=32.5$ d, $b_1=580.4$ keV (30%), $b_2=435.0$ keV (70%), $g=145.4$ keV (48 %)] was produced by thermal neutron bombardments of ^{140}Ce (CeO_2) in a swimming pool reactor. Then $^{141}\text{CeO}_2$ was chemically transformed into $^{141}\text{Ce}(\text{NO}_3)_3$ with H_2O_2 and HNO_3 .

Radioactive ceria NPs with the sizes of ca. 7 nm and 25 nm were prepared by a precipitation method using $^{141}\text{Ce}(\text{NO}_3)_3$ as the starting material as reported previously [2].

Cucumber seedlings were treated with these ceria NP suspensions at 2, 20, and 200 mg/L for 2 weeks. Then the radioactivities of plant tissues were measured. Two-dimensional distribution patterns of 7 and 25 nm ceria NPs in cucumber leaves were obtained by autoradiography.

3. Results and Discussion

With increasing concentration of the nanoparticles, concentration dependent absorption by the plant roots was noticed (Figure 1). The seedlings treated with 7 nm ceria particles showed significant higher ceria contents in both roots and shoots than those exposed to 25 nm ceria particles at all test concentrations (2, 20, and 200 mg/L). Only very limited amounts of ceria NPs could be transferred from the roots to shoots because the entry of nanoparticles into the roots was difficult. However, the results of tissue distributions of ceria nanoparticles in the plants and 2-D distributions of the particles in the leaves imply that once entered into the vascular cylinder, ceria nanoparticles could move smoothly to the end of the vascular bundle along with water flow. To the best of our knowledge, this is the first detailed study of uptake and distribution of metal oxide nanoparticles in plants.

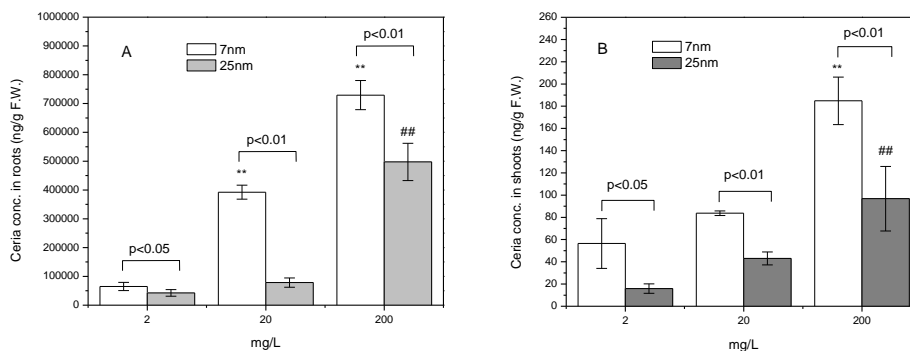


Figure 1. Ceria NP concentrations in the cucumber root (A) and shoot samples (B) after treatments with 2, 20, and 200 mg/L of ceria NPs for 7 d.

References

- /1/ S.K.Verma, A.K. Das, Patel, M.K., A. Shah and G.V Kumar .S. Sci Total Environ. 630 (2018) 1413.
- /2/ Z. Zhang, X.He, H. Zhang, Y. Ma, P. Zhang, Y.Ding and Y. Zhao, Metallomics 3 (2011) 816.

Sources and Tracer Significance of Radionuclide ^{210}Po in The Atmosphere of Beijing, China

Jie Ouyang^{1,2}, Li-Juan Song³, Ling-Ling Ma^{1*}, Min Luo¹, Xiong-Xin Dai^{3,4},
Dian-Dou Xu^{1**}

¹Beijing Engineering Research Center of Radiographic Techniques and Equipment, Institute of High Energy Physics, Chinese Academy of Sciences, Beijing 100049, China

²School of Nuclear Science and Technology, University of Chinese Academy of Sciences, Beijing 100049, China

³China Institute for Radiation Protection, Taiyuan 03000, China

⁴Collaborative Innovation Center of Radiation Medicine of Jiangsu Higher Education Institutions, Suzhou 215000, China

*E-mail: malingling@ihep.ac.cn

**E-mail: xudd@ihep.ac.cn

1. Introduction

Polonium-210 (^{210}Po), an α -emitter with a half-life of 138 days, is of great concern due to its high toxicity. ^{210}Po is a highly volatile radionuclide, which could enter into the atmosphere through natural activities and human activities [1], and then suffer a long distance transport with air masses [2]. ^{210}Po is also an effective indicator for tracing air pollutants and has been widely used in investigating some atmospheric processes. In this paper, temporal variations in polonium-210 (^{210}Po) and its potential sources were characterized in the atmosphere of Beijing, China to investigate its tracer applications in atmosphere environmental sciences.

2. Experiment

2.1. Analysis of ^{210}Po , selenium and aluminum: For leaching of ^{210}Po , 6 M HCl was added to the total suspended particle (TSP) and CCPs samples. The leachate was filtrated through a 0.1- μm membrane. The Po in the solution was first coprecipitated with hydrous titanium oxide (HTiO) by TiOCl_2 , followed by microprecipitation with tellurium. After that, the Te precipitate on the filter was then rinsed with ultrapure water, followed by anhydrous ethanol. Finally, the prepared ^{210}Po alpha counting source was counted by alpha spectrometry. Se and Al were analyzed by digesting sample with concentrated acid and then determined by inductively coupled plasma-mass spectrometry.

3. Results and Discussion

As presented in Figure 1, compared to the significant correlation between ^{210}Po and Se in the TSP samples ($r^2 = 0.705$), there was a weak correlation between ^{210}Po and Al in TSP samples ($r^2 = 0.168$), indicated the insignificance of the soil resuspension as a source of ^{210}Po in the atmosphere of Beijing. Figure 2 shows the strong correlation between ^{210}Po and Se (an indicator of coal combustion) in both the TSP samples and coal fly ash samples, which indicated that coal combustion was a primary source of atmospheric ^{210}Po in Beijing and could be an indicator of coal combustion.

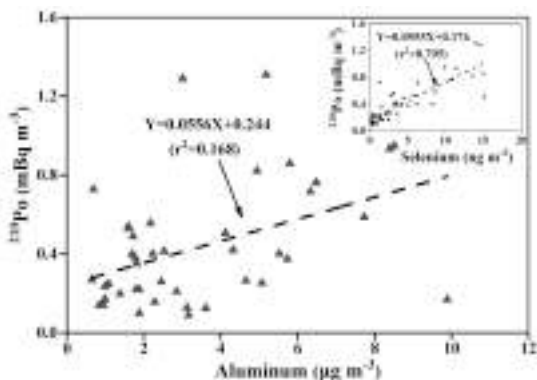


Figure 1. Correlation between concentrations of ^{210}Po and Al in the TSP samples.

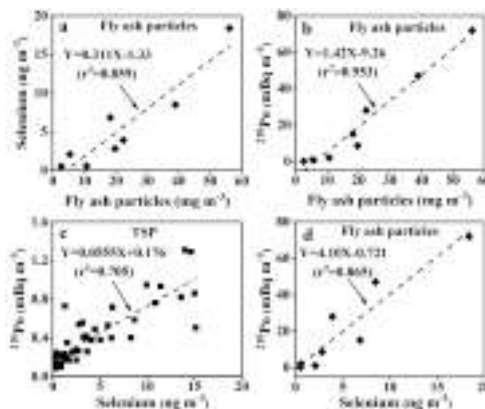


Figure 2. Correlation between concentrations of ^{210}Po and Se in the TSP samples and coal fly ash samples

4. Conclusion

Coal combustion emission was a primary source of ^{210}Po in the TSP of Beijing. ^{210}Po could be an indicator of the contribution of coal combustion to air pollution.

References

- /1/ M. Baskaran, J. Environ. Radioactiv. 102 (2011) 500.
- /2/ G. Yan, H.M. Cho, I. Lee, G. Kim, Atmos. Environ. 54 (2012) 80.

Generation of Site Specific Washout Parameters Using ^7Be as A Tracer at Kakrapar Gujarat Site

T.J. Jaison^{1*}, *A. K. Patra*¹, *D. P.Nankar*¹, *A. Jain*¹, *P.M. Ravi*^{2,3}, *R.M. Tripathi*^{2,3}

¹ESL (ESS, Health Physics Division, BARC), KAPS, P.O. Anumala, Surat District, Gujarat-394651

²Health Physics Division, BARC, Mumbai-400 085

³Homi Bhabha National Institute, Anushaktinagar, Mumbai

*E-mail: jaisontjohn@npcil.co.in

1. Introduction

^7Be is a natural radionuclide of cosmogenic origin. It is produced in the atmosphere by spallation when secondary cosmic rays hit nitrogen and oxygen atoms. Several studies show that ^7Be is one of the most important environmental radionuclide and can be used as a tracer of environmental processes such as cloud scavenging and precipitation or as a tracer for a transport and residence time of aerosols in the atmosphere. Once formed it diffuses through the atmosphere and is electrostatically adsorbed in atmospheric aerosol particles. It reaches the soil surface via two mechanisms: wet and dry deposition. It is assumed that the wet deposition is the main path leading to the ^7Be input (90%) into the soil, dry deposition being negligible [1]. Correlation between temporal changes of ^7Be and the meteorological parameters, mainly precipitation, were investigated by many authors. Studies have shown that for different regions and dissimilar environmental conditions, ^7Be wet deposition was dependent on rain precipitation volume [2]. This study investigates the influence of precipitation on ^7Be deposition from the atmosphere at Kakrapar environment, Gujarat.

2. Experiment

Rainwater samples were obtained using seven 15 L capacity plastic collector of 755 cm² surface area, placed at the terrace of ESL Kakrapar Gujarat site, to avoid soil derived contributions. The samples were cumulated. ^7Be activity in rainwater samples were scavenged by $\text{Fe}(\text{OH})_3$ precipitation using standard procedure. Total 16 nos. of such rain water samples were collected, processed and analysed for ^7Be (Cw, Bq m⁻³) using Gamma spectrometry in the pre-calibrated geometries using 100% RE, p-type HPGe from 477.6 keV gamma photon.

This covered all rain events during the monsoon season of 2017. Using high volume air sampler (flow rate: $1\text{ m}^3\text{ min}^{-1}$), surface air samples were also collected during corresponding period and the concentration of ^7Be in air (Ca , Bq m^{-3}) was estimated. Decay correction for ^7Be activity is applied in each case. Corresponding rainfall (RF, cm) of each sampling period (D, days) of rain samples were also measured.

3. Results and Discussion

Wet deposition (WD, Bq m^{-2}), deposition rate (DR $\text{Bq m}^{-2}\text{ d}^{-1}$), deposition velocity (DV m d^{-1}) and washout ratio (WR) were estimated for each of the sixteen rain events from corresponding Cw, Ca, RF, D and ρ – the air density (1.2 kg m^{-3}) based on the standard methods. The wet deposition of ^7Be was found to be in the range of 5 to 243; deposition rate was found to be in the range of 0.5 to 12.6; deposition velocity was in the range of 99 to 4193; washout ratio was in the range of 61 to 571. The default value for the total deposition velocity reported by IAEA is 1000 m d^{-1} [3]. The data of ^7Be activity in rain, WD, DR, DV and WR were subjected for correlation analysis. Good +ve correlation was observed between Cw & WD (R-0.97), Cw & WR (R-0.97), WD & DR (R-0.74), WD & WR (R-0.96), DR & DV (R-0.92) as well as DR & WR (R-0.75). Various studies have established strong linear relationship between ^7Be deposition and amount of rainfall, with R^2 varying from 0.46 to 0.93 as mentioned in [4]. This study also found such a relationship but with $R^2 = 0.56$ (Figure 1). Further studies are in progress such as rain drop diameter, rain intensity, liquid water content, fall velocity to find out the exact reason of wet deposition on different rain events.

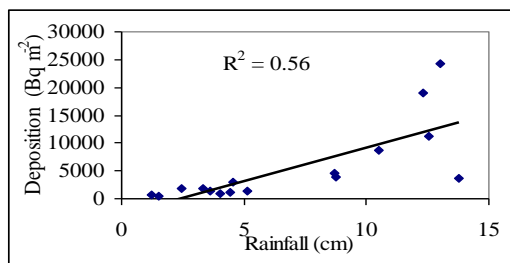


Figure 1. Relation of ^7Be wet deposition with Rainfall

4. References

- /1/ R.T. Salisbury, J. Cartwright, 2005. J. Environ. Radioact. 78, p353-361.
- /2/ J.M. Kaste, S.A. Norton, C. Hess, 2002.. Rev. Mineral.Geochem. 50, p271–289.
- /3/ IAEA.. Safety Reports Series No. 19 (Vienna: IAEA) p. 27, 60, 61 (2001).
- /4/ D.E.L. Alexander, M.M. Rubens, P.G.M. Roberto, et al., J. Environ. Radioactivity 169-170 (2017) 56-63.

Production of Polonium Isotopes in p -induced Reaction on the LBE Target up to 150 MeV

Moumita Maiti^{}, Deepak Kumar, Rinku Kumar Prajapat*

Department of Physics, Indian Institute of Technology Roorkee, Roorkee-247667, Uttarakhand, India,
*E-mail: moumifph@iitr.ac.in

1. Introduction

Lead-bismuth eutectic (LBE) has the ability to be used as a converter target in radioactive ion beam facility [1], as a spallation target in an accelerator driven sub-critical system, as a coolant in a nuclear reactor [2] etc. Therefore, it is important to study the possible production of radionuclides and the associated reaction dynamics such as preequilibrium (PEQ) and equilibrium (EQ), observed in the low/moderate energy p -induced reactions on the LBE targets. In this quest, extensive theoretical analysis using the nuclear reaction model codes ALICE14, ALICE91, and TALYS1.8 has been carried out for the p -induced reactions in the LBE target over a wide energy range to predict the production cross-section of neutron-deficient toxic $^{208,207,206,205}\text{Po}$ radionuclides and compared with the available measured data [3-6] in order to check the reliability of the upgraded model codes.

2. Results and Discussion

Theoretical excitation functions of $^{208,207,206,205}\text{Po}$ in the p +LBE reaction are shown in Figure 1(a),(b),(c),d). Further, in order to compare with the experimental results [3-6], the measured data from p + ^{209}Bi system are scaled to an isotopic abundance of Bi (55.5%) in LBE. In the model calculations, Weisskopf-Ewing model and Blann's hybrid model is used for EQ and PEQ processes, respectively, in ALICE14 as well as ALICE91. Hybrid Monte Carlo simulation is implemented in ALICE14 contrary to ALICE91. On the other hand, TALYS1.8 utilizes Hauser-Feshbach model and exciton model for EQ and PEQ emissions, respectively. Most of the experimental observations are satisfactorily reproduced by theoretical model estimations. The deviation of the excitation functions from its traditional shape of the compound process reveals the PEQ emission towards the high energy tail of excitation function.

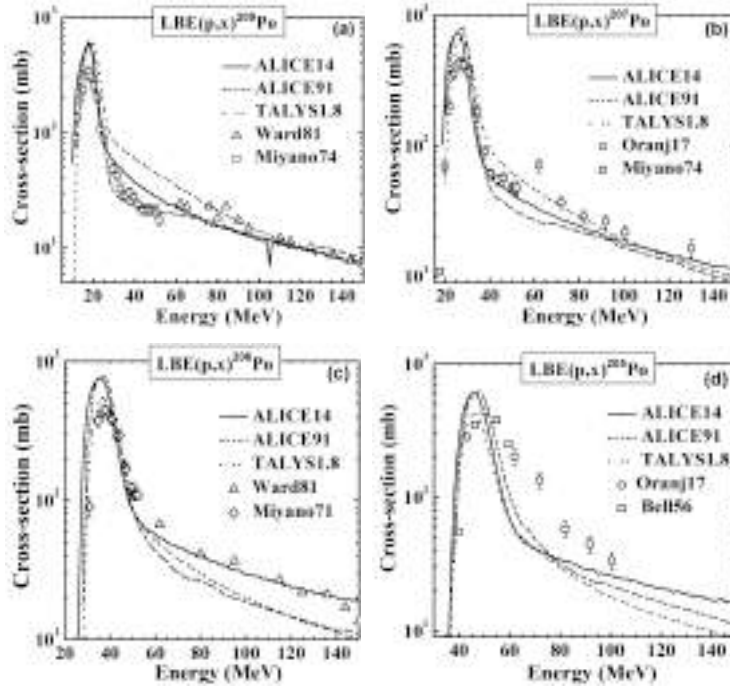


Figure 1. Theoretical excitation function of $^{208,207,206,205}\text{Po}$ for p -induced reaction on LBE target.

3. Conclusion

Theoretical model calculations of $^{208,207,206,205}\text{Po}$ radionuclides populated via neutron emitting channels are consistent with each other as well as with the experimental results. Therefore, theoretical model calculations could be used to predict the quantity of some important radionuclides, having relevance in various applications, in the p -induced reaction on the LBE target. Moreover, the high energy tail of the excitation functions indicates the PEQ emissions of neutrons over compound evaporation.

Acknowledgement: - Financial support of SERB project SR/FTP/PS-111/2013 is acknowledged.

References

- /1/ M.Maiti, S.Lahiri, D. Kumar, et al., Proc. DAE-BRNS Symp. on Nucl. Phys. 61 (2016).
- /2/ Final report of EURISOL design study, J.C. Cornell (ed.), GANIL, France (2009).
- /3/ T. E. Ward, P. P. Singh, D. L. Friesel, et al., Phys. Rev. C 24 (1981) 588.
- /4/ K.Miyano, M.Sekikawa, T.Kaneko, et al., Nucl. Phys. A 230, 98 (1974).
- /5/ L. Mokhtari Oranj, N. S. Jung, M. Bakhtiari, et al., Phys. Rev. C 95, 044609 (2017).
- /6/ R. E. Bell, H.M. Skarsgard, Can. Jour. Phys. 34, 745 (1956).

Determination of Boron in In-house Graphite Reference Material by Instrumental Charged Particle Activation Analysis

S. Dasgupta^{1}, J. Datta¹, K. K. Swain²*

¹*Analytical Chemistry Division, Bhabha Atomic Research Centre, Variable Energy Cyclotron Centre, Bidhannagar, Kolkata 700064, India*

²*Analytical Chemistry Division, Bhabha Atomic Research Centre, Trombay, Mumbai 400085, India*

* E-mail: sdasgupta@vecc.gov.in

1. Introduction

Carbon in the form of graphite is extensively used in nuclear technology [1]. Boron (B) content in graphite is an important parameter that decides its acceptability for nuclear applications due to its high thermal neutron absorption cross section. Reliable analytical methods are essential for determination of B in graphite at ppm to sub ppm levels. In view of the importance of boron determination in graphite and unavailability of graphite reference material (GRM), an In-house GRM for B has been prepared at Analytical Chemistry Division, Bhabha Atomic Research Centre, Mumbai [2] and analyzed in this work for B content by Charged Particle Activation Analysis (CPAA). This GRM can be used for quantification of B in unknown graphite samples, validation of existing analytical methods or developing new methodologies.

2. Experiment

Pellets of 10 mm diameter and varying thickness depending upon the range (calculated by SRIM–2008) for 10 MeV protons(p) were prepared. Standards were prepared by mixing B₂O₃ powder and spec pure graphite. The nuclear reaction, ¹⁰B(p,α)⁷Be (T_{1/2}=53.4 d; 477.6 keV) was used to quantify B. Due to unavailability of matrix matched reference material, IAEA RM 155 (WP) and synthetic B standard in spec pure graphite (B50: 50 mg kg⁻¹) were analyzed. The irradiations were done with 10 MeV p-beam, in 300-400 nA current at Variable Energy Cyclotron Centre (VECC), Kolkata.

Radioactivity measurements were carried out with a high resolution γ -ray spectrometer using HPGe detector (relative efficiency: 40%) coupled to PC based MCA.

3. Results and Discussion

Fe and Ni present in the matrix undergoes (p, γ) and (p, α) reactions respectively to produce ^{55}Co ($T_{1/2}=17.4$ h; 477.2 keV), which can cause spectral interferences. Judicious choice of p-beam energy can minimize these interferences. Use of a 10 MeV p-beam, can restrict higher production of ^{55}Co . Also, as the half life of ^{55}Co (17 h) is much less than ^7Be (53 d), samples can be cooled post-irradiation for a longer period of time, e.g., 10 half lives of ^{55}Co before counting for the analyte activity of ^7Be .

The concentrations of analytes have been computed using comparator method as follows:

$$C_x = C_s \frac{A_x}{A_s} \cdot \frac{I_s}{I_x} \cdot \frac{R_s}{R_x} \cdot \frac{S_s}{S_x}$$

where, subscripts x, s denote sample and standard; A- Activity; C- Concentration; I- Beam current; R- Effective range; S- Saturation factor. In CPAA, the matrix effect is taken care of by using the respective effective ranges of ions having same energy in samples and standards. Heating of samples during irradiation was taken care of by using a recirculation chillier (ALPHA RA8, Lauda). The concentrations of B are represented in Table 1. Detection limit for B in GRM by CPAA is 1.3 mg kg^{-1} .

Table 1. Concentrations of boron (mg kg^{-1}) in In-house graphite RM and other standards

Sample	B by CPAA	B (Reported)
B50	51 ± 3.4	-
WP	5.2 ± 0.32	5.1 ± 0.85 [3]
In-house GRM	7.2 ± 0.52	7.3 ± 0.46 [2]

Rounding off as per ASTM E-29 13 guidelines

4. Conclusion

Analysis of refractory materials, metal alloys and various other matrices require the samples to be digested for most of the analysis techniques. Boron being a volatile element may be lost during digestion and non-destructive approaches like CPAA is advantageous. The instrumental approach of CPAA is simple and suitable for quantification of boron in varied matrices including graphite.

References

- /1/ T. Burchell, R. Bratton and W. Windes. "NGNP Graphite Selection and Acquisition Strategy" *ORNL/TM-2007/153 Oak Ridge National Laboratory, Oak Ridge, Tennessee, United States 2007.*
- /2/ S. A. Kumar, K. Venkatesh, K K. Swain, et al., BARC/2016/E/005
- /3/ https://nucleus.iaea.org/rpst/Documents/rs_iaea-155.pdf accessed on 15.06.2018.

Production Estimates of $^{101,100}\text{Pd}$ Radionuclides in Lower Energy Region: An Indirect Route of $^{101\text{m}}\text{Rh}$ Isomer

*Amit Chauhan, Moumita Maiti**

Department of Physics, Indian Institute of Technology Roorkee, Roorkee-247667, Uttarakhand, India

*E-mail: moumitaph@iitr.ac.in

1. Introduction

The neutron-deficient palladium radionuclides ($^{100,101,103}\text{Pd}$) and $^{101\text{m}}\text{Rh}$ have a range of applications in medical science, industry, etc. The ^{100}Pd (84 keV, 52%) has a half-life of 3.63 d and decays through EC (100%), while the half-life of ^{101}Pd (296.2 keV, 19%) is 8.47 h and decays to $^{101\text{m}}\text{Rh}$ (306.9 keV, 81%, half-life 4.34 d), which acts as a potential diagnostic agent and a good anti-tumor agent for radiotherapeutics. The production of $^{100,101}\text{Pd}$ has been reported from the light-ion induced reactions in the literature [1]. However, at present, very few data are available from the heavy-ion induced reactions for the optimization of production route for those radionuclides [2]. The production estimates of $^{100,101}\text{Pd}$ from the heavy-ion induced reactions at the lower energy range, starting from the threshold to maximum up to 85 MeV, have been investigated in this article from the $^9\text{Be}+^{95}\text{Mo}$, $^{12}\text{C}+^{92}\text{Zr}$, and $^{11}\text{B}+^{94}\text{Mo}$ reactions.

2. Results and Discussion

The production cross-sections of the evaporation residues from the $^9\text{Be}+^{95}\text{Mo}$, $^{12}\text{C}+^{92}\text{Zr}$, and $^{11}\text{B}+^{94}\text{Mo}$ reactions have been estimated using the statistical compound nuclear model code PACE4 within a wide energy range. The excitation functions of the radionuclides from the $^{12}\text{C}+^{92}\text{Zr}$ reaction are plotted in Figure 1 along with estimated yield of ^{101}Pd , assuming unit parameters like target thickness (mg/cm^2), irradiation time (h), and beam current in (μA). It is noticed that an appreciable amount of ^{101}Pd could be produced below 50 MeV energy with a relatively small quantity of ^{101}Rh , most of which is $^{101\text{m}}\text{Rh}$, directly produced in this reaction. Pure production of $^{101\text{m}}\text{Rh}$ is possible by (1) the chemical separation of ^{101}Pd , which will decay to $^{101\text{m}}\text{Rh}$, from the trace Rh and bulk Zr, (2) allowing

^{101}Pd to decay to long lived $^{101\text{m}}\text{Rh}$ followed by the separation of Rh from Zr. Similarly, the production cross-sections of ^{101}Pd , ^{101}Rh and the yield of ^{101}Pd from the $^9\text{Be}+^{95}\text{Mo}$ reaction are shown in Figure 2. The yield of ^{101}Pd is similar to that of previous reaction, but produced relatively in the low energy range. The $^{101\text{m}}\text{Rh}$ is also expected to be produced in a considerable quantity in the $^{11}\text{B}+^{95}\text{Mo}$ reaction.

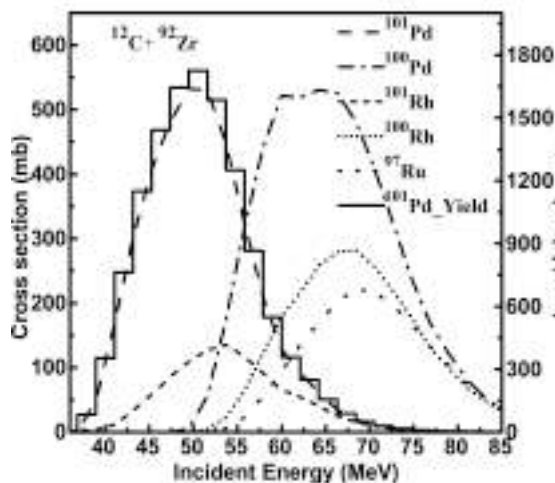


Figure 1. Excitation functions of residues from the $^{12}\text{C}+^{92}\text{Zr}$ (dotted lines) using PACE4 and estimated yield of ^{101}Pd (histogram, dark line).

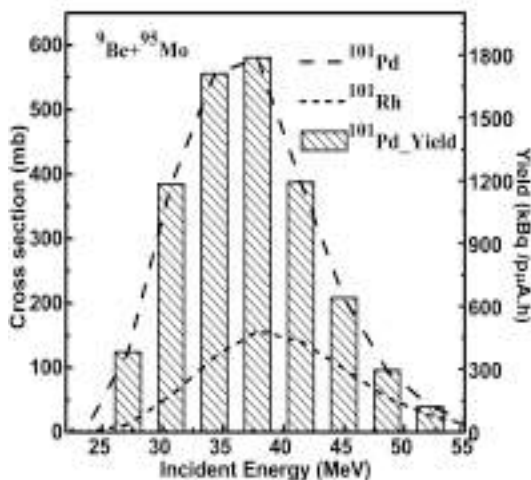


Figure 2. Theoretical excitation function (dotted lines) and estimated yield (dark line) of ^{101}Pd from the $^9\text{Be}+^{95}\text{Mo}$ reaction.

3. Conclusion

The study reports mainly the production of ^{101}Pd through the xn -channels from the two different target-projectile combinations. The maximum yield of ^{101}Pd is observed at relatively higher energy ~ 50 MeV for the $^{12}\text{C}+^{92}\text{Zr}$, while that observed at ~ 38 MeV for the $^9\text{Be}+^{95}\text{Mo}$. The investigation of the $^{11}\text{B}+^{94}\text{Mo}$ system commends an alternative approach for the production of ^{101}Pd . The theoretical model calculation shows that the compound nuclear mechanism is a major contributor for the production of $^{101,100}\text{Pd}$. The $^{101\text{m}}\text{Rh}$ radionuclide could be produced through the decay of ^{101}Pd .

Acknowledgement: - The fellowship from the MHRD is highly acknowledged.

References:

- /1/ F. Tarkanyi *et al.*, Appl. Radiat. Isotopes 114 (2016) 128.
- /2/ D. Kumar, M. Maiti, S. Lahiri, J. Radioanal. Nucl. Chem. 313 (2017) 655.

The Alpha+LBE Reaction up to 37.5 MeV/A

*Gayatri Sarkar, Deepak Kumar, Moumita Maiti**

Department of Physics, Indian Institute of Technology Roorkee, Roorkee-247667, Uttarakhand, India,
*E-mail: moumifph@iitr.ac.in

1. Introduction

The use of lead-bismuth eutectic (LBE, Pb-44.5%, Bi-55.5%) alloy is a fascinating choice because of its several attractive physicochemical properties in applications like, accelerator driven subcritical system (ADSS), converter target in the next generation high-power RIB facility, etc. Since no experimental report is available for α +LBE, the aim of the present work is to obtain an estimate of cross-sections of the radionuclides produced in the α +LBE reactions from the threshold to a maximum of 150MeV, which is the primary reaction range. The available measured cross-sections of the residues from the α +Bi/Pb reactions are used to validate the model calculations using TALYS1.8 and ALICE14; however, it is difficult to use most of those data to validate the model estimations for α +LBE as multiple reactions contribute to the production of residues.

2. Results and discussion

A large number of radionuclides are expected to be produced in the α +LBE reaction up to 150 MeV. The code TALYS1.8 uses the Hauser-Feshbach formalism to account the compound nuclear evaporation (EQ), and the exciton model for the pre-equilibrium (PEQ) process, while ALICE14 uses the Weisskopf-Ewing and hybrid Monte-Carlo simulation method for EQ and PEQ processes, respectively. The Fermi gas and back shifted Fermi gas level density are used in ALICE and TALYS calculations, respectively. Excitation functions of all the residues are calculated considering the natural abundance of Pb and Bi isotopes and their proportional contribution in LBE. Considerable cross-sections of $^{202-211}\text{Po}$, $^{205-211}\text{At}$, $^{201-208, 210}\text{Bi}$, $^{201-203, 209}\text{Pb}$, $^{206,207, 200, 201}\text{Tl}$ are observed. A representative comparison of neutron-deficient ^{211}At , ^{209}At , ^{206}Po , ^{207}Po is shown in Fig 1. Further, theoretical excitation functions have been compared with the experimental cross-sections of ^{211}At , ^{209}At from the α + ^{209}Bi reactions [1-5] by scaling the abundance proportion of Bi (55.5%) in LBE. The measured data

are well reproduced by both the model codes in the lower energy region where pure evaporative emissions are favored. However, none of the PEQ models could reproduce the cross sections of the At-radionuclides; exciton model underpredicts the data and hybrid Monte-Carlo method overpredicts them in all the xn -channels showing the deviation of ~ 70 -95% in the PEQ emission process.

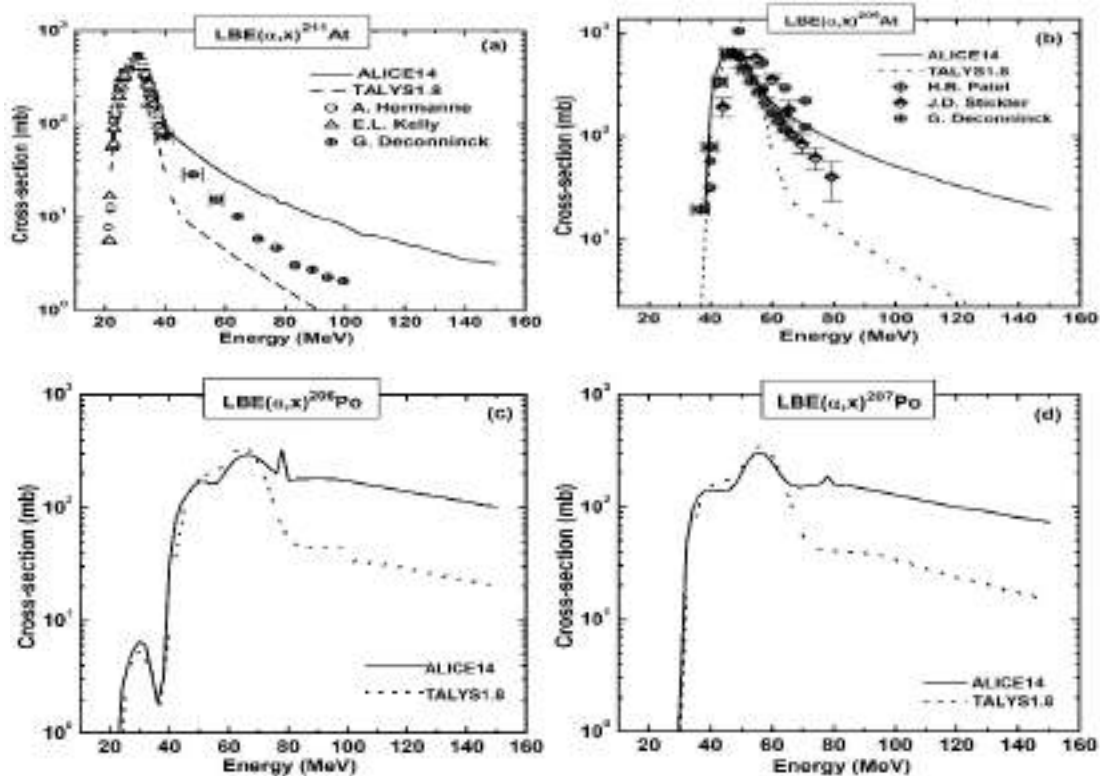


Figure 1. (a,b) Comparison of theoretical excitation functions of $^{211,209}\text{At}$ from the α +LBE reactions with the measured data [1-5]; (c,d) Computed excitation functions of $^{206,207}\text{Po}$ from the α +LBE.

This study indicates that the compound reaction process is dominating mechanism in the lower energy range.

References

- /1/ A. Hermanne, F. Tarkanyi, S. Takacs, et al., Appl. Radiat. Isotopes 63 (2005) 1.
- /2/ E.L. Kelly, E. Segre. Phys. Rev. 75 (1949) 999.
- /3/ G. Deconninck et al., Annales de la Societe Scientifique de Bruxelles, 88 (1974) 341.
- /4/ J.D. Stickler, K.J. Hofstetter. Phys. Rev. C 9 (1974) 1064.
- /5/ H.B. Patel, D.J. Shah, N.L. Singh. Nuovo Cimento A 112 (1999) 1439.

Pertraction of Americium(III) Through Supported Liquid Membranes Containing Benzene Centered Tripodal Diglycolamides

Bholanath Mahanty¹, Prasanta K. Mohapatra^{1*}, Willem Verboom^b

¹Radiochemistry Division, Bhabha Atomic Research Centre, Mumbai-400085, India

²Laboratory of Molecular Nanofabrication, MESA⁺ Institute for Nanotechnology, University of Twente, P.O. Box 217, 7500 AE Enschede, The Netherlands

*E-mail: mpatra@barc.gov.in

1. Introduction

N,N,N',N'-tetra-*n*-octyl diglycolamide, (TODGA) has shown high efficiency for extraction of trivalent actinides and lanthanides from acidic feeds [1]. Generally 3 to 4 TODGA molecules participate in the formation of the reverse micellar structure, which facilitate metal ion extraction [2]. We have been investigating multiple DGA – functionalized ligands, containing 3-4 DGA arms, for actinide extraction from acidic feeds [3,4]. In order to study the effect of substituents and also that of the spacer length, two new benzene centred tripodal diglycolamide (Bz-T-DGA) ligands were synthesized with iso-amyl groups and also with methylene and ethylene spacers termed as TPAMTEB (Figure 1a) and TPAETEB (Figure 1b), respectively and were studied for the supported liquid membrane transport of Am³⁺.



Figure 1. Structural formulae of TPAMTEB (left) and TPAEPEB (right) used in the present study
Experimental

TPAMDGA and TPAEDGA were synthesized at University of Twente and characterized by NMS and HR-MS. ²⁴¹Am was used from laboratory stock solutions. The supported liquid membrane studies were

carried out using polypropylene (PP) membrane whose pores were filled with the carrier ligand solution (6.6×10^{-4} M ligand in 5% iso-decanol-95% n-dodecane).

2. Results and Discussion

Solvent extraction studies indicated relatively fast extraction (10 minutes) of Am³⁺ with both the Bz-T-DGA ligands. On the other hand, the stripping kinetics was slow for TPAMTEB (20 minutes) and slower for TPAETEB (60 minutes). The transport of Am(III) was studied at two different feed HNO₃ concentrations viz., 3 and 6 M using 6.6×10^{-4} M solutions of TPAMTEB and TPAETEB in 5% isodecanol + 95% n-dodecane as the carrier solvent. The transport profiles are given in Figure 2.

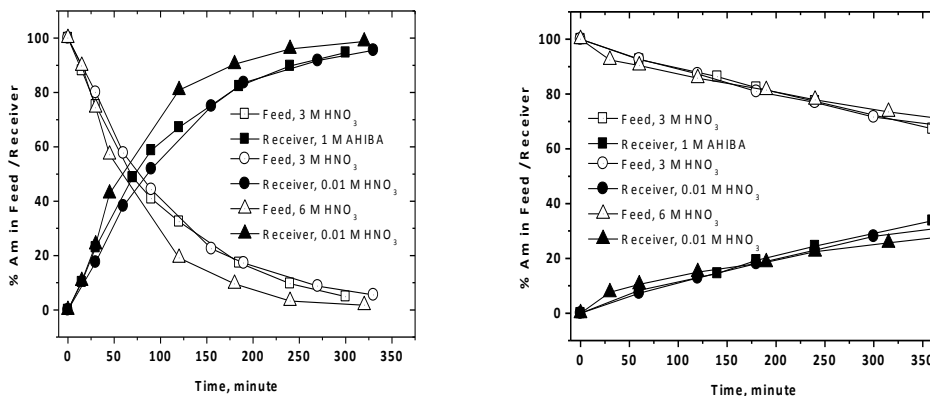


Figure 2. Transport profiles of Am³⁺ with TPAMTEB (left) and TPAETEB (right) from 3 M and 6 M HNO₃ feed solutions

As seen from the figure, around 93.8% and 98.8% transport of Am(III) was observed after 5 h for the feed HNO₃ concentrations of 3 M and 6 M, respectively when TPAMTEB was the carrier ligand. However when with TPAETEB, the respective Am(III) transport rates were found to be 28.3% and 25.2%. It is expected that the concentration of the diffusing species will increase at 6 M HNO₃ as compared to that at 3 M HNO₃ and hence, the data with TPAMTEB conform to this. The slower transport in case of TPAETEB could be attributed to steric factors, slow diffusion of the complexed species, difference in the ligand structure, etc. The transport efficiency of the ligand appeared to be significantly higher as compared a C-pivot [3] or N-pivot [4] tripodal ligands used previously.

References

- /1/ S. A. Ansari, P.N. Pathak, P. K. Mohapatra, and V. K. Manchanda, *Chem. Rev.* 112 (2012) 1751–1772.
- /2/ M.P. Jensen, T. Yaita, R. Chiarizia, *Langmuir*, 23 (2007) 4765–4774.
- /3/ P. K. Mohapatra, M. Iqbal, D. R. Raut, et al., *J. Membr. Sci.* 375 (2011) 141-149.
- /4/ B.N. Mahanty, S.A. Ansari, P.K. Mohapatra, et al., *J. Hazard. Mater.* 347 (2018) 478–485

Estimation of Uranium in Water and Urine by Liquid Scintillation Spectrometry

Priyanka J. Reddy, Sonal M. Wankhede, Pramilla D. Sawant*

Radiation Safety Systems Division, Bhabha Atomic Research Centre, Mumbai-400085, India

* E-mail: pjreddy@barc.gov.in

1. Introduction

Rapid estimation of uranium in urine and water is required for assessment of internal dose of radiation workers working in nuclear facilities and members of the public in case of any radiological or nuclear emergency. The commonly used technique for estimation of U in bioassay and environment samples is ion exchange method followed by α spectrometry or LED based fluorimetry. Both these techniques require extensive processing of sample and homogenous source preparation. The present study is aimed to optimize the parameters for solvent extraction of U coupled with LSS in water and urine samples using HDEHP as an extractant in toluene based scintillation cocktail.

2. Experiment

2.1. Materials and method: U stock solution was prepared by dissolving known weight of U turnings in nitric acid ($S1-596 \pm 4.8 \text{ Bq mL}^{-1}$) and working standards of 50-100 mBq mL^{-1} were prepared by diluting S1. Toluene scintillator was prepared by dissolving 7 g PPO, 0.5 g POPOP and 200 g naphthalene in 1 L toluene [1]. Extractive scintillator was prepared by adding 60 g HDEHP to 1 L toluene based scintillator. Ultra low level Quantulus 1220 LSS system was used for measurement of U.

2.1.1 Effect of equilibration time and pH on U extraction in urine: The effect of equilibrium time (5-20 mins) on the extraction of U was studied using (6% v/v) HDEHP in toluene based scintillator at optimized pH for urine samples with 1:1 scintillator : sample ratio [2]. 10 mL urine samples (in duplicates) were spiked with U standard ($\sim 100 \text{ mBq mL}^{-1}$). The mixtures were shaken using for 10 min. Under these conditions U was quantitatively transferred to the organic phase. Following phase separation, known ($\sim 10 \text{ mL}$) aliquot of the organic phase containing U was counted in LSS at various

time intervals viz., 10, 20, 30 and 60 minutes at the optimized Pulse Shape Analyzer. Experiments were also carried out by spiking U standard ($\sim 100 \text{ mBq mL}^{-1}$) in 10 mL distilled water. Extraction of U in these samples was studied at pH 1-5. Sample : extractive scintillator ratio was maintained at 1:1.

3. Results and Discussion

82 % of U was extracted from urine in 5 min and it improved to 85% when extraction time was increased to 10 min, which is optimum time for extraction of U from urine and water samples. The extraction recovery of U in water reached a maximum of 98-99.6% between pH 2.0 – 3.0 whereas the maximum recovery of 85% was observed in case of urine samples between pH 1.5 - 2.0 where the formation of an ion pair complex in nitrate media is favorable. Solvent extraction recovery for urine is comparatively less than water. With further increase in pH, U extraction decreased for water as well as urine mainly due the possibility of hydrolysis of U ion pair complex [3]. Hence, pH of 1.5-2.0 and 2.0-3.0 was optimized for solvent extraction of U in urine and water samples, respectively. Minimum Detectable Activity (MDA) for water and urine was calculated at different counting times. MDA of 0.3 mBq mL^{-1} (12 ng) and 0.9 mBq mL^{-1} (36 ng) is obtained for water and urine samples respectively for 30 min counting time. The time taken for complete extraction (20 mins) and counting (30 mins) of a single sample is 1 h and solvent extraction can be performed for 5 samples at a time. Thus, in a day more than 50 samples can be processed and counted as compared to 3 days for alpha spectrometry method (with a minimum counting time of 24h) required to achieve the sensitivity. By the method standardized in the present study nearly 50 water / urine samples can be analyzed in a day increasing the sample throughput which is a main requirement in case of any nuclear / radiological emergency.

4. Conclusion

Extraction recovery of about 98–99.6 % and 85% in the pH range of 2.0–3.0 and 1.5-2.0 was obtained for water and urine matrices, respectively using the present solvent extraction method followed by LSS counting. The overall time required for analysis by this method is 1hr. as compared to the ion exchange α spectrometry technique (2–3 days). Hence the method standardized is simple, fast and can be used for analysis of U in bioassay/environment samples in case of radiological/ nuclear emergency.

References

- /1/ J. Aupiais. J Anal Chim Acta (2004) 517:221–228.
- /2/ K. Kiegiel, A. Abramowska, P. Bieluszka, et al., J Radioanal Nucl Chem 311 (2017) 589–598.
- /3/ Sato. J. Inorg. Nucl. Chem. 6 (1958) 334-337.

Radiochemical Studies and Pre-clinical Evaluation of ^{111}In -Pentetreotide using Indigenously Produced $^{111}\text{InCl}_3$, Via ^{109}Ag (α , 2n) Nuclear Reaction

A. Chakraborty¹, A. Mitra², S. Lad¹, T. Upadhye¹, M. Tawate¹, S. Satamkar¹, R. Bhoite¹, S. S. Das³, L. Barua³, S. Chattopadhyay³, S. Banerjee^{1,2,3*}

¹RMC, BARC, Parel, Mumbai 400 012, India.

²MCF, RMC, BRIT, Parel, Mumbai 400 012, India

³Regional Centre, BRIT, Kolkata 700 064, India.

*E-mail: avikbarc@gmail.com

1. Introduction

^{111}In -Pentetreotide, Octreoscan is an established diagnostic radiopharmaceuticals for detection of overexpressed somatostatin receptor (subtype 2), in patients with neuroendocrine tumors. Most of the nuclear medicine centers use imported and costly $^{111}\text{InCl}_3$ and lyophilized kits of DTPA-octreotide (DTPA-OC) consisting of antioxidants, buffers, bulking agents, etc., for formulation of ^{111}In -octreotide. We made an attempt to radiolabel pentetreotide with indigenously sourced $^{111}\text{InCl}_3$. In-house radiolabeled ^{111}In -Pentetreotide efficacy towards clinical use was proved by performing different physicochemical and biological quality control studies. Also various *in-vitro* and *in-vivo* studies were performed to prove its pharmacological behavior.

2. Experiment

2.1 Radiolabeling and Quality Control: ^{111}In was produced via ^{109}Ag (α , 2n) ^{111}In nuclear reaction, purified by sephadex column and obtained as $^{111}\text{InCl}_3$ in 0.1M HCl. $^{111}\text{InCl}_3$ (10mCi in 0.7mL) was mixed with FeCl_3 (3.5 $\mu\text{g/mL}$ of $^{111}\text{InCl}_3$) in Tube-A. In another tube (Tube-B) 4.9mg $\text{C}_6\text{H}_5\text{Na}_3\text{O}_7 \cdot 2\text{H}_2\text{O}$, 0.4mg $\text{C}_6\text{H}_8\text{O}_7 \cdot \text{H}_2\text{O}$, 2mg $\text{C}_7\text{H}_6\text{O}_4$ and 10mg $\text{C}_6\text{H}_{12}\text{O}_6$ were taken. The mixture in Tube-A was aseptically transferred to Tube-B (reaction tube). Further, 30 μg of DTPA-OC (1 $\mu\text{g}/\mu\text{L}$) was added to the Tube-B and incubated at pH:4 for 30 min at 25°C. The ^{111}In -Pentetreotide was purified by SPE column (C18, 360 mg) and product was passed through 0.22 μm filter. Radiochemical purity (RCP) was assessed by TLC and HPLC. Radionuclidic purity was assessed by HPGe detector.

The endotoxin limit was quantified by gel-clot BET assay; sterility test was done by direct inoculation. Stability of the product at -20°C was evaluated by HPLC at 24h, 48h & 72h post radiolabeling.

2.2 In-vitro Cell Binding & In-vivo Bio-distribution Studies: Human colon carcinoma cell-line HCT-116 expressing SSTRII, used for the *in vitro* evaluation, was grown in IMDM medium with 10% FBS in 5% CO₂ at 37°C. *In vitro* cell-binding studies was performed by incubating HCT-116 cells in 1mL of internalization buffer (IMDM, 0.2% BSA) containing radioligand ($\sim 5 \times 10^{-12}$ mol peptide) for 15, 30, 60 & 120 min followed by washing with PBS. Non-specific internalization was assessed by addition of cold DTPA-OC (5×10^{-9} mol). For membrane receptor binding assay, HCT-116 cells homogenates were incubated for above time points, followed by washing with PBS. *In vitro* cytotoxicity was studied by incubating ¹¹¹In-Pentetreotide for 24h with the cell-line followed by colorimetric MTT assay. Biodistribution studies was carried out in Wistar rats by injecting ¹¹¹In-Pentetreotide (0.74 MBq) and sacrificed at 2h, 24h, 48h & 72h intervals. For comparison, Planar scintigraphy images were obtained from Wistar rat using γ -camera with pinhole collimator.

3. Results and Discussion

3.1 Radiolabeling and Quality Control: The radiochemical yield (RCY) of the ¹¹¹In-Pentetreotide (n = 3) was >80%. The RCP of ¹¹¹In-Pentetreotide was >98% with R_f : 0.01-0.04. The RCP derived by HPLC was also >98% with R_t at 30.5 min. γ -spectrum of ¹¹¹In-Pentetreotide, only two γ peaks (171 and 246 keV) were observed. EL was <6 EU/mL and the product was sterile. Retention of RCP on storage at -20°C, at 72h post-preparation was confirmed by the single radioactive peak (R_t : 30.4 minutes).

3.2 Cell Binding and Bio-distribution: ¹¹¹In-Pentetreotide showed rapid Internalization (25-30%) in HCT-116 cells, reaching a plateau after 15-30 min. In the bio-distribution study, radioactivity in the blood and most of the organs decreased after 24h post-injection. High uptake and long-term retention of radioactivity were found in the kidney (3.36% dose/gm), which is in concordance with our scintigraphy studies.

4. Conclusions

The in-house radiosynthesis of clinical grade ¹¹¹In-Pentetreotide was achieved using indigenously produced ¹¹¹InCl₃. Preclinical study through biodistribution, cell binding assay and scintigraphic imaging ascertains the potential of the in-house developed ¹¹¹In-Pentetreotide as a diagnostic radiopharmaceutical.

Study of Pre and Post Edge Structure Effect on Mass Attenuation Coefficients

Anand B C¹, Sharanabasappa^{1*}, B. R. Kerur²

¹Department of Physics, JSSATE Bangalore-560060, India.

²Department of Physics, Gulbarga University, Gulbarga-585105, India.

*E-mail: sharanabasappa@jssateb.ac.in.

1. Introduction

In this paper total mass attenuation coefficient (MAC) for compounds Lanthanum oxide and Lanthanum sulphate, at different X-ray energies were measured. The results compared with theoretical values, agreement found to be good when the incident photon energy is far below and away from the L edge, disagreement is observed near L absorption edges. The mass attenuation co-efficient for a compound is computed using the mixture rule, is given by $\mu/\rho = \sum \omega_i (\mu/\rho)_i$. Where ω_i is the proportion by weight if the i^{th} element present in the compound and $(\mu/\rho)_i$ is the mass attenuation co-efficient of the i^{th} constituent element of the compound. For a chemical compound ω_i can be written as, $\omega_i = a_i A_i / \sum (a_j A_j)$. A_i is the atomic weight of the i^{th} element and a_j is the number of formula units.

2. Experimental Procedure

The MAC was determined by measuring transmission intensity of the X-ray arranged vertically over an n-type HPGe detector. ¹⁰⁹Cd, ²⁴¹Am, ⁵⁵Fe and ⁵⁷Co each of 25 μ Ci were used as X-ray sources.

3. Results and discussion

The experimental μ/ρ value along with their associated error were calculated by the least-squares fit (Table -1). The theoretical values were calculated by WinXCom programme. The uncertainty involved in the theoretical value is about 1-2%, while overall experimental was estimated of about 4%. There is a good agreement between theoretical and experimental results for the energies between 8.041 to 14.39 keV. On the other hand the mixture rule is not in agreement for the compound with $\Delta E = (E_x - E_{L_i})$ from 0.415 to 1.061 for L_I , L_{II} and L_{III} edges. In some compounds the incident X-ray energy is

sufficient to knock out L_{II} and L_{III} edge electrons only but not L_I edge electron and in some cases only L_{III} edge electron knock out but not L_{II} and L_{III} edge electrons as it can be seen from all the tables particularly at 5.895 keV X-rays. Hence the experimental value deviates from the theoretical value by -20.2, -35.8, -24.8 and -7.8.

Table 1. Comparison between theory and experimental MAC in Lanthanum oxide [La₂O₃] for different energies.

X-ray energy, keV, E _x	E _{Li}	ΔE=E _x - E _{Li} in keV	Experimental, cm ² /g	Theoretical value cm ² /g	P.D
5.895 K _α Fe	6.266	-0.371	448.1 ± 3.2	561.4	-20.2
	5.891	-0.004			
	5.483	+0.412			
6.404 K _α Fe	6.266	+0.224	339.6 ± 5.6	529.5	-35.8
	5.891	+0.599			
	5.483	+1.007			
6.490 K _β Fe	6.266	+0.138	384.9 ± 1.4	512.0	-24.8
	5.891	+0.513			
	5.483	+0.921			
7.05 K _β Co	6.266	+0.784	383.0 ± 2.2	415.7	-7.8
	5.891	+1.159			
	5.483	+1.567			
8.041 K _α Cu	6.266	+1.775	289.1 ± 1.5	298.5	-3.1
	5.891	+2.150			
	5.483	+2.558			
8.900 K _β Cu	6.266	+2.639	235.7 ± 1.1	228.4	+3.1
	5.891	+3.014			
	5.483	+3.422			
14.390 Co	6.266	8.214	62.21±0.27	64.34	-3.3
	5.891	8.499			
	5.483	8.907			

4. Conclusion

The observed deviation between the experimental and theoretical μ/ρ values may be attributed to the effects of the resonance scattering of X-rays near absorption edges, extended X-ray absorption fine structure [1]. Our results clearly call for the theoretical recalculations of the mass attenuation coefficient near absorption edge.

Acknowledgment: BRNS Project sanctioned by DAE (No. 2004/37/23/BRNS).

References

/1/ B. R. Kerur, S. R. Thontadarya and B. Hanumaiah, Appl.Radiat. Isotopes 45 (1994) 159-3.

A New Sephadex Based Separation of ^{43}Sc from Alpha Irradiated $^{\text{nat}}\text{CaCO}_3$ Target

S. S. Das¹, S. Chattopadhyay^{1}, L. Barua¹, Md. N. Alam¹, Madhusmita¹, A. K. Pal¹, U. Kumar¹, A. K. Hudait¹, S. Banerjee^{2*}*

¹RPL, Regional Centre, BRIT, VECC, Kolkata 700064, India

²Radiation Medicine Centre, BARC, Parel, Mumbai-400 012, India

*E-mail: sharmila@barc.gov.in, sankha@vecc.gov.in

1. Introduction

The promising PET radionuclide ^{43}Sc with nuclear property ($\beta^+ = 88.1\%$, $T_{1/2} = 3.9$ h) is similar to those of other commonly used PET radionuclides including ^{68}Ga ($\beta^+ = 88.9\%$, $T_{1/2} = 68$ min), ^{64}Cu ($\beta^+ = 17.6\%$, $T_{1/2} = 13$ h), ^{89}Zr ($\beta^+ = 22.7\%$, $T_{1/2} = 3.3$ d), or ^{124}I ($\beta^+ = 22.7\%$, $T_{1/2} = 4.2$ d). ^{43}Sc can be produced by $^{43}\text{Ca}(p,n)$, $^{42}\text{Ca}(d,n)$ or $^{46}\text{Ti}(p,\alpha)$ reactions, using costly enriched Ca or Ti targets [1]. A more promising method of ^{43}Sc production is alpha irradiation of natural calcium target via $^{40}\text{Ca}(\alpha,p)$ and $^{40}\text{Ca}(\alpha,n)$ channels. The aim of this study is to investigate the suitability of sephadex as a novel column matrix for recovery of no-carrier-added ^{43}Sc from alpha irradiated $^{\text{nat}}\text{CaCO}_3$ target.

2. Experiment

Pellets targets were prepared from $^{\text{nat}}\text{CaCO}_3$ powder (~150 mg, 0.5mm thick, dia 10mm) by pressing in dice plunger at 10 ton pressure. The pellet was placed on an aluminum target holder and was irradiated with 26 MeV external α - beam of about 0.8 μA current for 4 h. The irradiated target was dissolved in iron-free dilute HCl. Radiochemical separation of ^{43}Sc from irradiated CaCO_3 target was carried out by sephadex-based column chromatography method. The dissolved target solution was made ammoniacal with NH_4OH and loaded on a small sephadex column (1mL) where ^{43}Sc was selectively retained by sephadex, leaving behind bulk Ca as a waste during loading and washing steps. ^{43}Sc was then eluted with dilute HCl and loaded on a tiny dowex-50 column (20 mg) for further purification. Finally, ^{43}Sc was eluted from the dowex column in 0.25M ammonium acetate solution which was directly used for radiolabeling with DOTA-TATE and PSMA-617 ligands.

The schematic representation of separation process is shown in Fig 1. The co-produced radionuclidic impurities in ^{43}Sc were determined by HPGe.

3. Results and Discussion

Sephadex, a cross-linked dextran gel is used for size-exclusion chromatography. Sephadex G-25 has been used earlier to separate nca ^{68}Ge from bulk Ga target [2] and ^{89}Zr from Y target [3]. The separation of ^{43}Sc from $^{\text{nat}}\text{CaCO}_3$ target matrix has been carried out using a small sephadex column. ^{43}Sc was recovered in 25 min with recovery yield of 83% (n=6). The respective radiochemical and radionuclidic purities of ^{43}Sc were >95% and >99.9% (determined by TLC and γ -spectroscopy). The ^{43}Sc was labeled with DOTA-TATE and PSMA-617 with a yield of 80% in each case (n=4).

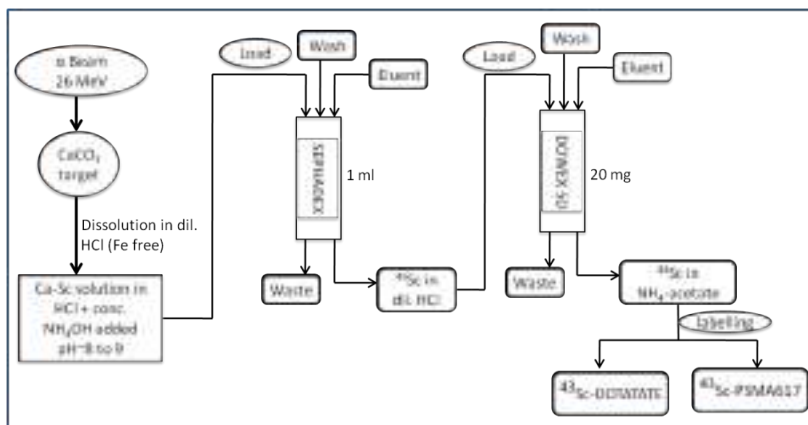


Figure 1. Schematic process diagram of radiochemical separation of ^{43}Sc from $^{\text{nat}}\text{CaCO}_3$ target

4. Conclusion

The newly developed sephadex column chromatography technique is found to be novel for separation of ^{43}Sc from $^{\text{nat}}\text{CaCO}_3$. This method would offer high separation yield of ^{43}Sc in a high radioactive concentration having suitability for direct radiolabeling in radiopharmaceutical applications.

Acknowledgement: - The authors acknowledge Shri G. Ganesh, Chief Executive, BRIT and Shri Amitava Roy, Director, VECC for their support in the work.

References

- /1/ K.A. Domnanich, R.Eicher, C. Muller. EJNMMI. Radiopharm. Chem. 2(2017) 14.
- /2/ J.M. Fitzsimmons, L. Mausner. Radiochim. Acta. 103 (2015) 117.
- /3/ S.S. Das, S. Chattopadhyay, L. Barua, et al., J. Radioanal. Nucl. Chem. 313 (2017) 641.

Simulation Study on Purification of Spent ^{100}Mo and $^{99\text{m}}\text{Tc}$ from Nb, Zr, Y and Ru Traces

S. Chattopadhyay¹, S.S.Das², Madhusmita¹, Md. N. Alam¹, S. Banerjee^{2*}

¹RPL, Regional Centre, BRIT, VECC, Kolkata 700064, India

²Radiation Medicine Centre, BARC, Parel, Mumbai-400 012, India

*E-mail: sharmila@barc.gov.in; sankha@vecc.gov.in

1. Introduction

Molybdenum-99 production and direct $^{99\text{m}}\text{Tc}$ production can be achieved through $^{100\text{nat}}\text{Mo}(\gamma, n)$ reaction, using high-power electron linear accelerator (LINAC) and $^{100}\text{Mo}(p,2n)$ reaction in medical cyclotron, respectively, where various non-isotopic impurities like Nb, Y, Zr, Ru and various isotopic impurities are co-produced [1,2]. We report here sephadex column method for removal of Nb, Zr and Y isotopes from Mo and a versatile MEK solvent extraction method for removal of Nb, Zr, Y, Ru and Mo isotopes from $^{99\text{m}}\text{Tc}$.

2. Experiment

The ^{99}Mo activity was produced in the Dhruva reactor of BARC. The radiotracers of ^{97}Ru , ^{95}Tc , $^{91\text{m}},^{92\text{m}}\text{Nb}$ and $^{89/88}\text{Zr}$ / ^{88}Y were produced from Mo, Y target foils by irradiation with alpha and proton beam, respectively, in VECC Cyclotron, Kolkata, India. An aliquot of the samples before and after separations were taken and counted in a HPGe detector coupled with a MC analyzer.

2.1. Simulation study to remove radioisotopes of Nb, Y & Zr from Mo: A solution of inactive Mo (made in NH_3 solution) was doped with trace quantities of radioactive isotopes (pre-load solution). 20mL of the test solution in 6% NH_3 solution, was loaded on a pre-conditioned sephadex G-25 column (2mL) and the column was washed with 5mL 6% NH_3 solution (Figure 1).

2.2. Simulation Study to remove radioisotopes of Mo, Nb, Y, Zr & Ru from $^{99\text{m}}\text{Tc}$: An inactive Mo solution (10 mL) in $\text{NaOH/KOH/NH}_4\text{OH}$ doped with trace quantities of radioactive isotopes of $^{99}\text{Mo}/^{99\text{m}}\text{Tc}$, Nb, Y, Zr and Ru were taken in a 25mL centrifuge tube and neutralized to pH-7. Five

milliliter methyl ethyl ketone (MEK) solvent was added to this solution and mixed thoroughly for 1min. ^{99m}Tc extracted in MEK was passed through a pre-conditioned alumina column (1g) (Figure 2).

3. Results and Discussion

Simulation experiments were carried out to eliminate Nb, Y, Zr and Ru radioisotopes using a small sephadex column and MEK solvent extraction methods to mimic the actual experimental condition while using irradiated ^{100}Mo . There was a complete adsorption of non-isotopic impurities on the column (99.99%; n=3) based on size-exclusion principle. The recovery yield of ^{99}Mo (99.98%) and ^{99m}Tc (98%) was almost quantitative (n=3). The extraction efficiency of pure ^{99m}Tc - from various Mo solution was 97% (n=3). The RN Purity of ^{99m}Tc using solvent extraction method was 99.99% (n=3).

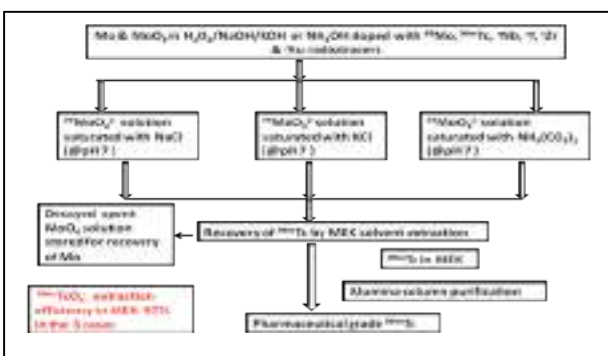
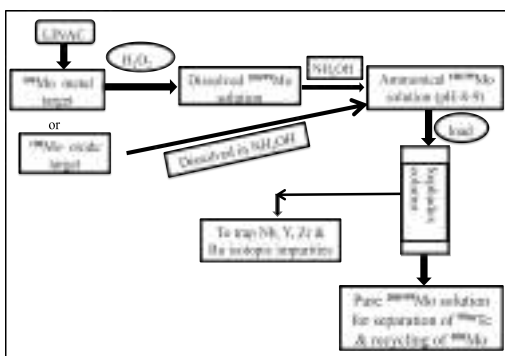


Figure 1. Spent Mo purification using sephadex column Figure 2. Extraction of pure ^{99m}Tc using MEK

4. Conclusion

The simulation studies reveal that the newly developed sephadex column and MEK solvent extraction purification systems are very effective to remove non-isotopic impurities from Mo and ^{99m}Tc . These methods may be applied in purification of spent ^{100}Mo used in the production of ^{99}Mo and ^{99m}Tc .

Acknowledgement: The authors acknowledge the IAEA (Contract no. 22475) and Shri G. Ganesh, Chief Executive, BRIT and Shri Amitava Roy, Director, VECC for their support in the work.

References

/1/ T. M Martin, T. Harahsheh, B. Munoz, et al., J Radioanal Nucl Chem 314 (2017) 1051–1062.
 /2/ M K Das, S Saha Das, Madhusmita, et al., J Radioanal Nucl Chem. 311 (2017) 643–647.

Estimation of ^{14}C in Irradiated Graphite using CO_2 Gasification Method

Susheela Sivakumar^{1}, Sanjay Singh¹, K. S Babu¹, D. Banerjee²,
R. K. Gopalkrishnan¹*

¹Radiation Safety Systems Division, ²Process Development Division
Bhabha Atomic Research Centre, Trombay Mumbai-400085, India

*E-mail: susheela@barc.gov.in

1. Introduction

Nuclear Reactor uses graphite as moderator or a reflector. ^{14}C produced in reactor graphite is primarily by neutron activation of $^{14}\text{N}(\text{n,p})^{14}\text{C}$, $^{13}\text{C}(\text{n},\gamma)^{14}\text{C}$ and $^{17}\text{O}(\text{n},\alpha)^{14}\text{C}$. Most commonly adopted techniques for quantitative analysis of ^{14}C in graphite involves gasification of graphite to CO_2 followed by its trapping into suitable solvent and radiometric using Liquid Scintillation Analyser (LSA) [1]. The commonly used solvent for CO_2 trapping are NaOH, Ethanolamine and Carbo-sorb E [2]. A simple assembly, as depicted in this paper, can be used for estimation of ^{14}C in low active graphite samples.

2. Materials and Method

Experimental set-up consists of a top loading tubular furnace. A quartz tube containing graphite sample in platinum crucible, is placed inside the furnace. The glass tube has a provision for inlet and outlet port. The outlet is connected to series of three bubblers and inlet port is kept open for air to enter due to suction created by pump. The bubblers contain ethanolamine ($\text{C}_2\text{H}_7\text{NO}$) for trapping CO_2 evolved during combustion of graphite. The solvent ($\text{C}_2\text{H}_7\text{NO}$) containing ^{14}C was spiked with Aqua light scintillation cocktail and analysed using PerkinElmer Make LSA (Tri-carb 2910 TR).

3. Results and Discussion

The effect of temperature and time for complete gasification of graphite was studied with a known amount (1 gm) of inactive graphite and the results are presented in Figure-1. Results show that at least 2 hours is required for complete gasification of graphite at 900°C . These conditions were therefore used for analysis of all samples.

Further experiments were carried out with inactive sample spiked with ^{14}C tracer. More than 95% of ^{14}C was found to be trapped in first two bubblers indicating that the assembly can be used for analysis of ^{14}C in graphite samples.

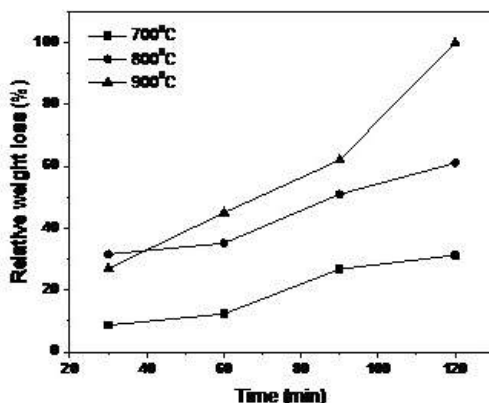


Figure 2. Relative weight loss profile of graphite sample as a function of time at different temperature

Table 1 depicts the analysis of eight active samples. It was observed that about 90% of total activity was present in first bubbler and the remaining in second bubbler. As no measurable amount of activity was present in third bubbler, total of activity present in the first two bubblers was considered as the sample activity. Though each sample carries different identity, specific activity of the sample was found to be very close and in the range of 1.3×10^5 Bq/gm to 4.8×10^5 Bq/gm. It can be noted that tritium content of the samples were very low. In case of high tritium bearing sample, HNO_3 should be used in the first bubbler. Finally it can be concluded that this simple system can reliably be used for analysis of ^{14}C in graphite samples.

Table 1. Measured ^{14}C activity in graphite using LSA

Sr. No.	Sample Weight (mg)	Specific activity (Bq/gm)
1.	414.7	3.6×10^5
2.	175.0	3.1×10^5
3.	230.0	4.8×10^5
4.	248.0	3.4×10^5
5.	260.0	1.9×10^5
6.	522.3	2.3×10^5
7.	353.8	1.7×10^5
8.	480.0	1.3×10^5

References

- /1/ J. Pageot, J. N. Rouzaud, L. Gosmain, et al., Progress in Nuclear Energy 105(2018) 279-286.
- /2/ G. K. Young, K. Chang-Jong, H.C. Young, et al., J. Hazardous Materials 331 (2017) 13-20.

Study on Thermoluminescence Properties of Commercial Glasses Used in Bangladeshi Dwellings for Accidental Dosimetry

Sabina Yasmin¹, Bijoy Sonker Barua², Mayeen Uddin Khandaker^{3},
Z.Siti Rozaila⁴, Md. Abdur Rashid¹, Faruque-Uz-Zaman Chowdhury¹*

¹Department of Physics, Chittagong University of Engineering and Technology, 4349 Chittagong, Bangladesh

²Department of Civil Engineering, Southern University Bangladesh, 4000 Chittagong, Bangladesh

³Center for Radiation Sciences, School of Healthcare and Medical Sciences, Sunway University, 47500 Bandar Sunway, Selangor, Malaysia

⁴Department of Physics, University of Malaya, 50603 Kuala Lumpur, Malaysia

* E-mail: mu_khandaker@yahoo.com

1. Introduction

Commercial glasses used in Bangladeshi dwellings were analyzed by the thermoluminescent (TL) technique, to verify the prospect of their use as dosimeters for measurements of environmental and accidental radiation exposures, due to their easy handling, low cost and moisture protection. Therefore, the investigated samples were studied in terms of their dosimetric characteristics: energy and dose response, glow curve and reproducibility in typical irradiation procedures.

2. Experiment

All the powdered glass samples and TLD-100 were annealed for a period of 1 hour and irradiations were made using X-ray and gamma beams, from an ERESO 200 MF4 and a conventional Gamma cell-220 ⁶⁰Co respectively. X-ray mean photon energies from 20 keV to 185 keV and gamma dose of range 10 Gy to 50 Gy were used in this study. The sample TL measurements have been carried out using a Harshaw 3500 TLD reader (USA) supported by WinREMS software. The TLD reader was set up as following the preheat temperature of 50 °C, heating rate of 10 °C.s⁻¹ and maximum temperature for data acquisition of 400 °C.

3. Results and Discussion

The energy-response of both investigated Glass samples and TLD-100 shows a comparable pattern of variation, though differing in magnitude as a direct consequence of the effective atomic number. TLD-100 showed significantly superior energy-response compared to the studied samples. Dose response implies the functional dependence of the intensity of the measured TL signal upon the absorbed dose [1]. The linearity of the TL response over a wide range or dose is one of the important characteristics for the ideal dosimeter. In this study the dose response of the glass samples [A (Osmania, Normal white); B (PHP, Normal white); C (Nasir, Normal white); D(Rider, Normal white) & E(Rider, Black ambush)] and TLD-100 subjected to a range from 10 Gy to 50 Gy of mean ^{60}Co source are shown in Table 1.

Table 1. TL response of the collapsed glass samples and TLD-100 subjected a range from 10Gy to 50Gy of mean ^{60}Co source.

Dose (Gy)	TL_A (nC/g)	TL_B (nC/g)	TL_C (nC/g)	TL_D (nC/g)	TL_E (nC/g)	TLD-100
10	1650.5	1716.7	1436.9	1623.0	943.7	1400224.1
20	3328.9	3428.0	3698.8	3684.7	2331.7	3215667.1
30	5816.6	4799.4	5963.3	5478.3	4094.1	5481501.7
40	8112.4	6925.7	8055.1	7504.8	5583.5	8677491.5
50	9407.8	9257.7	10243.9	9631.8	7702.5	11578594.2

The glow curves of the investigated samples are composed of a broad, dominant peak with a maximum between 180 to 250 $^{\circ}\text{C}$, and the integrated area indicating the particular sensitivity to the amount of absorbed dose. The general structure of the TL glow curve remains unchanged by repeating the cycles of annealing and irradiation at various doses. The reproducibility of the glass samples was determined and showed repeatable response in successive cycles of annealing, irradiation and read out.

4. Conclusion

These results demonstrate the potential use of commercial glass as TL dosimeters to determine radiation dose (for both the ‘emergency’ and ‘retrospective’ case) following catastrophic, large-scale radiological events.

5. References

/1/ C. Furetta, (2003) Handbook of thermoluminescence, World Scientific.

Evaluation of Excitation Function for The Productions of Polonium-207 and Polonium-208 Isotopes from Bismuth-208 Nucleus

Idris Ahmad, Yahaya Ibrahim Yola*

Department of Physics, Faculty of Physical Sciences, Bayero University, Kano, Nigeria

* E-mail: manidris37@yahoo.com

1. Introduction

Nuclear reactors, cyclotrons and accelerators are used for the production of radionuclides for both diagnostic and therapeutic purposes in nuclear medicine by using neutron induced nuclear reactions or charged particles nuclear reactions [1]. The physical basis of their production routes is described through the interaction of neutrons and charged particles with matter. These processes have to be well understood in order to produce radionuclide of high purity radionuclide in an efficient manner.

The present study investigated the possibilities of production artificially radionuclide by particles induced nuclear reactions through ^{208}Bi using EXIFON code [2].

2. Experiment

EXIFON code is a nuclear reaction software which provides continuous and smooth description of nuclear reactions over a wide energy and mass range, which is based on an analytical model for statistical multistep direct and multistep compound reactions (SMD/SMC model). Theoretical calculations of Cross-section were performed by nuclear model code EXIFON the program was run and the input and output directory were defined, and then the target nucleus is specified. The incident particle and target nucleus were selected and excitation function in the general option section for this calculation was chooses. The number of incident energy was specified followed by the first incident energy, and then the incident energy step is also specified. The Cross-section correspond to each particular energy was obtained.

3. Results and Discussion

The results of the excitation function calculations are plotted in figures 1 and 2. The Evaluated Nuclear Data File (ENDF) data used in this work are from the nuclear data section of the IAEA available at <https://www-nds.iaea.org> (IAEA-NDS, 2016).

Figure 1 shows the excitation function for the productions of polonium isotopes from Bismuth 208 nucleus. The excitation function typically resembles a Gaussian bell curve. Mathematically, it is described as a Breit-Wigner function, owing to the resonant nature of the production of the compound nucleus. Figure 2 shows the excitation function of $^{208}\text{Bi}(p,2n)^{207}\text{Po}$ along with evaluated nuclear data libraries (ENDL) for the production of polonium-207 isotope.

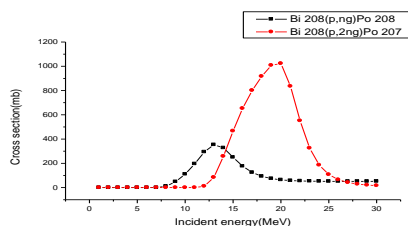


Figure 1. Excitation function (EXIFON)

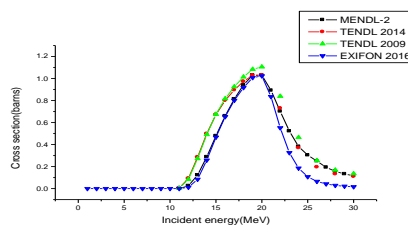


Figure 2. Excitation function (EXIFON & ENDF)

Table 1. Maximum cross section for the productions of polonium isotopes and energy at maximum cross section from figure 1

Reaction	Reaction product	Max. Cross section(mb)	Energy provides Max. Cross section (MeV)
$^{208}\text{Bi}(p,n)$	^{208}Po	353.4	13
$^{208}\text{Bi}(p,2n)$	^{207}Po	1023	20

4. Conclusion

In the present work, the excitation functions of artificially produced radioisotopes of polonium from naturally occurrences isotope of ^{208}Bi were investigated. Obtained results show that the maximum cross sections are 353.4mb and 1023mb at the energy of 13MeV and 20MeV for Po-207 and Po-208 respectively, and are in good agreement with the other results on evaluated nuclear data library.

Acknowledgement This research was founded by Bayero University, Kano. Nigeria and is highly acknowledged

References

- /1/ M. Al-Abyad, J. Nucl. Radiation Phys. 6 (2011) 43–53.
- /2/ I. Ahmad, F. S. Koki, Int. J. Med. Physics, Clin. Eng. Radiat. Oncol. 6 (2017) 344-359.

Sequential Separation of Pu, Am and U in Urine Using Solid Extraction Chromatography Technique

Rupali Dubla^{1}, Ranjeet Kumar¹, J.R. Yadav¹, P.D. Sawant²*

¹Health Physics Laboratory, RSSD, Bhabha Atomic Research Centre, Tarapur – 401502, India

²Radiation Safety Systems Division, Bhabha Atomic Research Centre, Mumbai – 400085, India

*E-mail: gamre.rupali@gmail.com

1. Introduction

This paper deals with the standardization of sequential radiochemical separation for determination of plutonium, americium and uranium in urine samples using solid extraction chromatography technique (TRU resin). Radiotracers, ²⁴²Pu, ²⁴³Am and ²³²U were used to establish chemical recovery. Method involves sample oxidation followed by Ca₃(PO₄)₂ co-precipitation of actinides and separation of each radionuclide through TRU (Eichrom) column. Average radiochemical recovery observed for 1 L urine sample matrix was 71.6%, 73.7% and 75.1% (n=8) of ²⁴²Pu, ²⁴³Am and ²³²U, respectively.

2. Experiment

Eight urine samples of 1 L volume were spiked with ²⁴²Pu, ²⁴³Am and ²³²U tracer and oxidized with conc. HNO₃ and H₂O₂, followed by co-precipitation with Ca₃(PO₄)₂. The precipitate was separated from supernatant by centrifuging, dissolved in conc. HNO₃ with occasional addition of H₂O₂ and evaporated to dryness. The white residue was dissolved in 15mL 1M Al(NO₃)₃ prepared in 3M HNO₃, and about 500 mg of NaNO₂ was added to adjust the valency of Pu to +4 state. The sample was loaded on TRU resin column, preconditioned with 30mL of 3M HNO₃, at the rate of 0.3-0.4 mL/minute. Trivalent Am was eluted first from the column with 3 mL of 9M HCl and 30mL of 2.5M HCl leaving behind Pu & U on the column. Subsequently Pu(IV) was eluted using 30 mL of 0.075M oxalic acid prepared in 1M HCl [1] followed by U(VI) elution using 30mL of 0.1M ammonium bioxalate solution. Eluted Pu, Am and U-fractions were electrodeposited on stainless steel planchette in ammonium sulphate medium at 2.2 pH. Activity estimation was done by alpha spectrometry. Extraction equilibria for Am⁺³, Pu⁺⁴ & UO₂⁺² in CMPO extractant (TRU resin) can be given as follows:

- a) $Am^{+3} + 3NO_3^- + \overline{3E} \leftrightarrow \overline{Am(NO_3)3.E3}$
 b) $Pu^{+4} + 4NO_3^- + \overline{2E} \leftrightarrow \overline{Pu(NO_3)4.E2}$
 c) $UO_2^{+2} + 2NO_3^- + \overline{2E} \leftrightarrow \overline{UO_2(NO_3)2.E2}$

3. Results and Discussion

Analytical results are given in Table 1. The average radiochemical tracer recovery obtained for ^{242}Pu , ^{243}Am and ^{232}U tracer was 71.6%, 73.7% and 75.1%, respectively. Earlier, sequential separation of Pu, Am & U in urine samples [2] was demonstrated using TEVA-TRU resin column in tandem whereas in the present study only single column comprising TRU resin was used. This method has yielded clear separation of actinides with acceptable chemical recovery in case of routine monitoring of radiation workers and monitoring members of the public in case of any radiological / nuclear emergency.

Table 1. Radiochemical recovery of urine samples spiked with ^{242}Pu , ^{243}Am and ^{232}U tracers

S. No	Sample No	^{242}Pu recovery (%)	^{243}Am recovery (%)	^{232}U recovery (%)
1	TP-1	70.3	43.7	89.8
2	TP-2	75.6	77.6	84.7
3	TP-3	87.2	92.2	99.2
4	TP-4	80.7	74.0	78.3
5	TP-5	62.4	74.8	59.6
6	TP-6	70.6	70.9	59.9
7	TP-7	52.4	78.3	50.1
8	TP-8	73.9	77.9	79.4
Aver. recovery (%)		71.6 ± 10.7	73.7 ± 13.6	75.1 ± 16.9

4. Conclusion

Advantage of the method standardized in the present study for sequential actinide separation is the reduction in overall analysis time as compared to the tandem column operation used for mixed actinide separation. This method is very useful for handling incidental/accidental exposure cases of radiation workers. Further improvements in the method can be pursued to obtain consistent higher recovery.

Acknowledgement: The authors are thankful to Dr. K.S.Pradeepkumar, Associate Director, HS&EG, BARC for his constant encouragement in carrying out this work.

References

- /1/ S. Quidelleur, M. Granet, I. Laszak, et al., J. Radioanal. Nucl. Chem., 280 (2009) 507.
 /2/ S.L.Maxwell, III and D.J.Fauth, J. Radioact. Radiochem. 11 (2000) 28.

He⁺ Ions Induced Effects in Nd-doped Zirconolite

Merry Gupta^{1}, S. S. Ghumman¹, R. Kumar², P. K. Kulriya²*

¹Sant Longowal Institute of Engineering and Technology, Longowal, Sangrur, Punjab 148106, India

²Inter-University Accelerator Centre, Aruna Asaf Ali Road, New Delhi 110067, India

*E-mail: g41merry@gmail.com

1. Introduction

Zirconolite is known to be a potential candidate for the immobilization of nuclear high level wastes especially under the induced effects of α -recoil events simulated with low energetic heavy ions [1]. Some studies have also been reported for the material durability under the effects of α -particles using 200 keV He⁺ ion beam irradiation [2]. Zirconolite remained crystalline even at the highest dose of 1×10^{17} He⁺ ions/cm², but found to have a band of He accumulation in the material. To investigate in deep, 30 keV He⁺ ions was used in our previous work to study such effects in CaZrTi₂O₇ examined through XRD and XPS techniques [3]. Surface damage was observed in terms of reduction and increase in covalency. Here, the same study of ion beam irradiation with 30 keV He⁺ ions has been employed to investigate the structural behavior of Nd-doped zirconolite (Ca_{0.8}Nd_{0.2}ZrTi_{1.8}Al_{0.2}O₇). Neodymium acts as a good surrogate for the actinides as Pu, Cm and Am due to their similar charges and ionic radii. So α -particles effects have been studied in Nd-zirconolite through XRD in the present work.

2. Experimental

Samples of Ca_{0.8}Nd_{0.2}ZrTi_{1.8}Al_{0.2}O₇ were prepared using solid state technique through thorough homogenization of CaCO₃, Nd₂O₃, ZrO₂, Al₂O₃ and TiO₂ added in their stoichiometric proportions. Ion beam irradiation was performed with 30 keV He⁺ ions using Tabletop 50 kV ion accelerator, indigenously designed and installed at IUAC, New Delhi. Samples were exposed to irradiation for different fluences as 1×10^{13} , 1×10^{14} , 1×10^{15} , 1×10^{16} and 1×10^{17} He⁺ ions/cm². Characterization of as prepared samples (virgin) and thus examination of irradiated samples were employed using XRD. The detailed methods regarding sample preparation, ion beam irradiation and XRD examination have been used the same as done previously in case of CaZrTi₂O₇ [3].

3. Results and discussion

XRD patterns of irradiated samples have been shown in Figure 1a. Intensity of all the peaks observed to be decreased with increasing fluence, while the peak intensity of the sample irradiated with 1×10^{16} He^+ ions/cm² was increased slightly. The zoom view of the main peak at 2θ of around 30.4° for all the irradiated samples is also presented in Figure 1b, showing a clear picture of fluence dependent decrease in peak intensity with an exceptional behavior of 1×10^{16} He^+ ions/cm² irradiated sample. Full width at half maximum (FWHM) also increased with increasing fluence. Sample retained its crystallinity behavior even at the highest fluence of 1×10^{17} He^+ ions/cm².

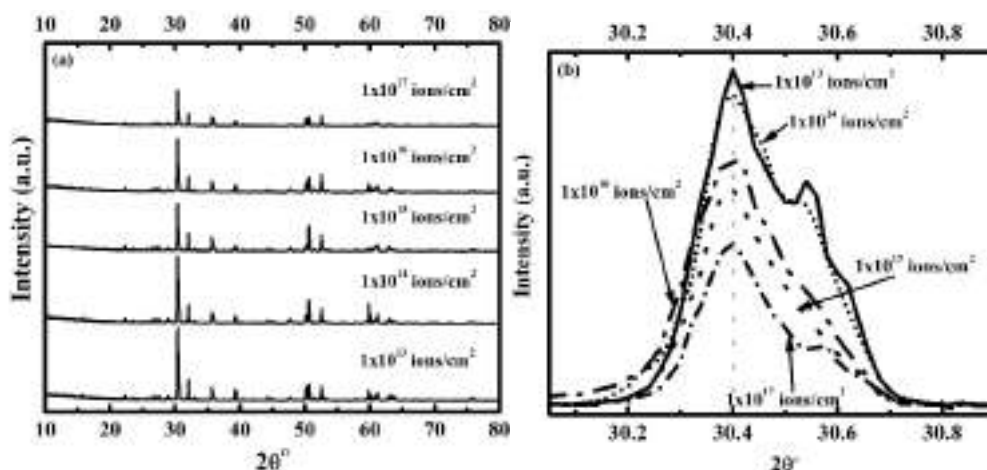


Figure 1. Fluence dependent XRD patterns of irradiated samples ranging from 2θ (a) $10\text{-}80^\circ$ and (b) $30\text{-}31^\circ$

4. Conclusions

Nd-doped zirconolite samples prepared through solid state technique were analyzed for 30 keV He^+ ion irradiation effects through XRD. Surface damage was observed while keeping the crystal and structural integrity of the material. XRD showed the fluence dependent defects in terms of decrease in peak intensity and increase in FWHM with an exception of the sample irradiated with fluence of 1×10^{16} He^+ ions/cm².

References

- /1/ S.X Wang, G.R. Lumpkin, L.M. Wang, R.C. Ewing. Nucl. Instr. Meth. B. 166-167 (2000) 293.
- /2/ M. Gilbert, C. Davoisne. M. Stennett, et al., J. Nucl. Mater. 416 (2011) 221.
- /3/ M. Gupta, P.K. Kulriya, R. Shukla, et al., Nucl. Instr. Meth. B. 379 (2016) 119.

Assessment of Radiological Hazards in Indian Sundarbans

Nabanita Naskar^{1,2}, Susanta Lahiri^{2,3}, Punarbasu Chaudhuri¹*

¹Department of Environmental Science, University of Calcutta, 35 Ballygunge Circular Road, Kolkata-700019, India

²Saha Institute of Nuclear Physics, 1/AF, Bidhannagar, Kolkata-700064, India

³Homi Bhabha National Institute, India

*E-mail: susanta.lahiri@saha.ac.in

1. Introduction

Environmental radiation comprises of primordial ^{238}U , ^{232}Th , their decay products, ^{40}K , anthropogenic and cosmic radionuclides. Radio-ecological assessment provides knowledge on any harmful radiological effects on humanity during long-time exposure. Hence dose assessment through different radiological indices is essential in today's nuclear era, especially in pristine and productive ecosystems like Sundarbans. It is the world's largest contiguous mangrove ecosystem shared by India and Bangladesh. The unique and rare species biodiversity has made it a natural heritage site. Present study attempts to assess radiological hazards confronted by human population of Indian Sundarbans through various radiological indices like absorbed dose rate (D), annual effective dose rate (AEDE), radium equivalent activity (R_{eq}), annual gonadal dose equivalent (AGDE) and hazard indices (H_{ex} and H_{in}).

2. Assessment of radiological indices

Earlier, we have assessed for the first time, baseline activity of ^{238}U and ^{232}Th in Indian Sundarban. Samples were counted for 75000s in 50% HPGe detector [1, 2, 3]. Also we have measured ^{40}K level in twenty-one surface soil samples collected from different areas of Indian Sundarbans [4]. ^{238}U activity ranged between 40 ± 2.4 to 58 ± 2.5 Bq kg^{-1} with mean, median activity of 48.7 ± 2.8 and 46.7 Bq kg^{-1} . ^{232}Th varied from 47 ± 2.4 to 65 ± 3.1 Bq kg^{-1} with mean, median activity of 58.3 ± 3.3 and 59.9 Bq kg^{-1} [1]. ^{40}K activity varied from 532 ± 8.9 to 1043 ± 13.2 Bq kg^{-1} with mean and median activity of 860.6 and 855.4 Bq kg^{-1} [4]. Activity of ^{238}U , ^{232}Th were found to be slightly elevated compared to world average of 35 and 45 for ^{238}U , ^{232}Th respectively. However, ^{40}K in Sundarban area is much higher than

the world average of 420 Bq kg⁻¹. This data prompted us to calculate various radiological risk indices from the obtained activities [1]. For assessing radiological hazard, radiological parameters including D, AEDE, Ra_{eq}, Hazard indices (External: H_{ex} and Internal: H_{in}), AGDE, etc., have been calculated from the measured activities of ²³⁸U, ²³²Th and ⁴⁰K using following equations [5] and provided in table 1.

$$D = (0.462A_U + 0.604A_{Th} + 0.0417A_K) \text{ nGy h}^{-1};$$

$$\text{AEDE } (\mu\text{Svy}^{-1}) = D \text{ (nGy h}^{-1}) \times 365 \times 24 \times 0.2 \times 0.7 \text{ SvGy}^{-1} \times 10^{-3}$$

$$\text{Ra}_{\text{eq}} \text{ (Bq kg}^{-1}) = A_U + 1.43A_{Th} + 0.077A_K$$

$$H_{\text{ex}} = \frac{A_U}{370} + \frac{A_{Th}}{259} + \frac{A_K}{4810} \leq 1 \text{ and } H_{\text{in}} = \frac{A_U}{185} + \frac{A_{Th}}{259} + \frac{A_K}{4810} < 1$$

Here, A_U, A_{Th}, A_K are specific activities of ²³⁸U, ²³²Th and ⁴⁰K in Bq kg⁻¹ respectively in sediments.

3. Result and discussion

Table 1. Data of the radionuclides and associated radiological parameters

Activities in Bq/kg	Range	Arithmetic Mean	Standard deviation	Geometric mean	Median	Global averages*
²³⁸ U activity,	40±2.2 – 58±2.5	48.7	5.5	48.5	47.2	33-35
²³² Th activity,	47±2.4 – 65±3.1	58.5	4.9	58.3	59.9	45
⁴⁰ K activity,	532±8.9 – 1043 ±13.2	866.2	140.9	853.8	860.9	420
D, nGy/h	82 – 101	93.6	6.5	93.4	95.4	59
AEDE, μSv/y	101 – 124	114.8	8.0	114.5	116.9	70
Max Permissible limit						
Raeq, Bq/kg	201 – 214	198.3	13.1	197.9	202.1	370
Hex	0.47 – 0.58	0.54	0.04	0.53	0.55	≤1
Hin	0.59 – 0.72	0.67	0.04	0.67	0.67	≤1
AGDE, mSv/y	0.58 – 0.72	0.66	0.05	0.66	0.67	1

The radiological indices viz AGDE, H_{ex} and H_{in} are ≤1, indicating towards insignificant health troubles from natural radiation in the area. D and AEDE are higher than recommended value but not alarming. For all the parameters, mean and median values are in close proximity, which indicates towards normal distribution pattern. This report is significant from the view-point that no such radiological studies have been documented from this region and may serve as future reference data.

References

- /1/ P. Chaudhuri, N. Naskar, S. Lahiri. J Radioanal Nucl Chem 311 (2017) 1947-1952
- /2/ N. Naskar, S. Lahiri, P. Chaudhuri, A. Srivastava. J Radioanal Nucl Chem 312 (2017) 161-171
- /3/ N. Naskar, S. Lahiri, P. Chaudhuri, A. Srivastava. J Radioanal Nucl Chem 310 (2016) 1381-1396
- /4/ Naskar et al., 4th International conference on Applications of Radiotracers and Energetic Beams in Sciences (ARCEBS 2018), 11-17 Nov, 2018, Kolkata, India.
- /5/ United Nations Scientific Committee on the effects of atomic radiation report to the general assembly with scientific annexes, v. I. (2000). In UNSCEAR: sources and effects of ionizing radiation.

Importance of Voxel Size in Localizing Defect Using Gamma Ray Scattering

Akash Tondon^{1*}, Mohinder Singh², B. S. Sandhu¹, Bhajan Singh¹

¹Department of Physics, Punjabi University, Patiala, 147002, India

²Department of Basic and Applied Sciences, Punjabi University, Patiala, 147002, India

*E-mail: akashtondonnsl@gmail.com

1. Introduction

Among different non-destructive methods, gamma-ray scattering method proves to be the valuable method for characterization of wood in terms of wood density and also for localization of inhomogeneity present in it. In the experimental study of localizing defect using gamma ray spectroscopy the knowledge of exact size and location of the voxel is indispensable. In the present work gamma rays emitted from ¹³⁷Cs radioactive source (having strength 222 GBq) are scattered from various regions of the wooden sample. The scattered gamma flux is detected by an NaI(Tl) scintillation detector placed at 110° to primary gamma ray beam. By restricting the photon beam to narrow region i.e. making the voxel sufficiently small then even small changes in the electron density of the material inside the voxel are detectable [1]. The present work describes the importance of voxel size in localizing the defect (decay) in given wood matrix by employing gamma ray backscattering method.

2. Experiment

Materials and method: In the present experiment for the detection of defect in wood, a wooden block (*Dalbergia sissoo*) having uniform density and dimensions 17 × 3.5 × 7.0 cm prepared by axing. Two cylindrical voids having diameter 0.8 cm and 1.2 cm are drilled. A uniform mixture of saw-dust and glue is filled in these two voids to create artificial defect. Further, a numerical method given by Balogun et al. [2] is used to estimate the common volume (voxel), which is the intersection between two cones representing detector and source field of view. An algorithm has been encoded in FORTRAN and the scattering volume is calculated at various scattering angles as shown in Figure 1 for different combinations of source and detector collimators keeping other parameters fixed.

3. Results and Discussion

A significant difference in the scattered counts is observed under the full energy peak of the recorded spectra for three voxel sizes (16.13, 25.65 and 38.36 cm³). This is due to the fact that the intensity of scattered gamma flux depends on the quantity of available electrons inside the sensitive volume. The plot for the variation of measured % SD (Standard deviation) versus scan position is shown in Figure 2. An unexpected change in the SD is indicated by two peaks, one of these corresponds to smaller defect (SD ~ 39.9 %) and other to bigger defect (SD ~ 69.5 %). A relatively low contrast (10.80 % for 1.2 cm and 5.24 % for 0.8 cm defect) is observed for the voxel size of 25.65 cm³.

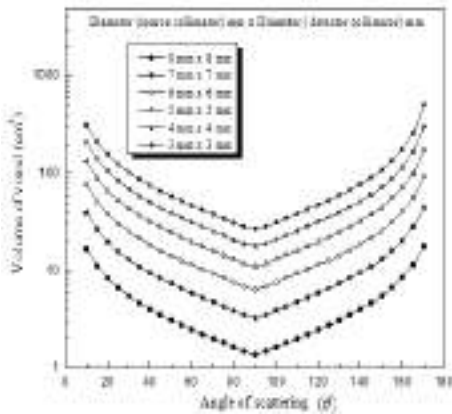


Figure 1. Variation of scattering volume (voxel) as a function of scattering angle for collimators of different diameters for source and detector.

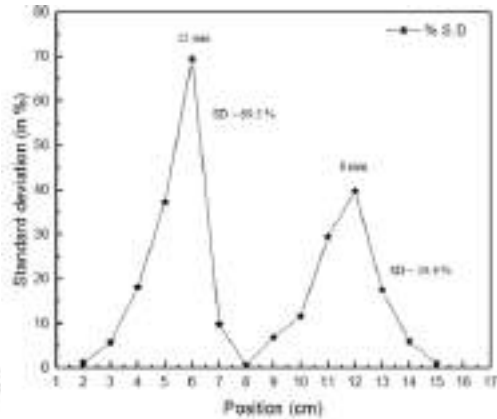


Figure 2. Measured percentage standard deviation (SD) as a function of scan position for two defects for voxel size

4. Conclusion

The objective of the present experiment is to examine the importance of voxel size in order to estimate internal defects (decay) in the given wooden sample. We conclude that with increase in the voxel volume the ability of the system to distinguish between regions of high density (wood) and low density (decay) decreases. For the present experimental set-up smaller defect (3.52 cm³) can be detected more precisely if finer beam collimation (smaller voxel size) is used. The present system shows high degree of contrast of the order of 29.43% between defect and wood phases for voxel size of 16.13 cm³.

References

- /1/ Mullin, S.K., Hussein,E.M.A., Nucl. Instrum. Meth. A.353 (1994) 663-667.
- /2/ Balogun,F.A., Brunetti,A., Cesareo,R., Radiat. Phys. Chem. 59 (2000) 23-30.

Study on Groundwater Quality in Parts of Rajasthan with Special Reference to Uranium Contamination

Diksha Pant^{1,4}, Tirumalesh keesari^{1}, A.Roy¹, U.K.Sinha¹, Manveer Singh², S.K.Jain², R.M.Tripathi^{3,4}*

¹Isotope and Radiation Application Division, Bhabha Atomic Research Centre, Mumbai 400085, India
²Central groundwater board, western region, Ministry of water resources, Government of India, Jaipur 302004, India

³Health Physics Division, Bhabha Atomic Research Centre, Mumbai 400085, India

⁴Homi Bhabha National Institute, Bhabha Atomic Research Centre, Mumbai 400085, India

*E-mail: tirumal@barc.gov.in

1. Introduction

Groundwater is an important source of drinking water in most part of India, especially in arid and semi-arid regions. Groundwater situation in Rajasthan is deteriorating at an alarming level with respect to both quality and quantity. The rainfall and water level depletion in many aquifers forced people to depend on deep groundwater and the situation is becoming grave with time. Among the major contaminants fluoride, nitrate was found to be very high in groundwater of state. With the reports on high uranium in southwest Punjab, there is a likelihood of the presence of uranium in the neighboring states. In this study assessment of groundwater quality was carried out including uranium.

2. Experiment

The study area consists of Jaipur and Dausa districts located in the eastern part of Rajasthan. It stretches between 26°26'08.11" to 27°51'52.11" north latitude and 74°54'52.59" to 76°17'34.36" east longitude. Jaipur district has a semi-arid climate. The average annual rainfall is 823.2 mm. Groundwater in the districts is contained in several different lithologic units ranging in age from younger alluvium to old Gneisses. Important aquifers are alluvium, Gneiss, Schist, Quartzite and partly in Granite. Physicochemical parameters (temp., pH, DO, TDS and EC) were measured by Hanna handheld meter while dissolved uranium was measured using laser fluorimeter (UA1, Quantalase). Environmental isotopes ($\delta^2\text{H}$, $\delta^{18}\text{O}$) are analyzed by an isotope ratio mass spectrometer.

3. Results

The electrical conductivity of the collected samples varies from 740 to 6600 $\mu\text{S}/\text{cm}$. U concentration of the samples varies from 5 $\mu\text{g}/\text{L}$ to 145 $\mu\text{g}/\text{L}$ with an average value of 48.6 $\mu\text{g}/\text{L}$. Stable isotope value varies from -5.2‰ to -3‰. Out of the thirty-three samples collected twelve samples have the concentration above the AERB stated limits (60 ppb) [1] for drinking water and twenty samples above the suggested WHO limit (30 ppb) [2].

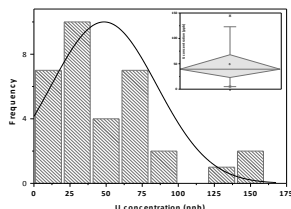


Figure 1. Total uranium distribution

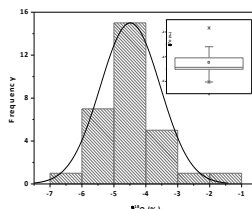


Figure 2. $\delta^{18}\text{O}$ distribution

On comparing the electrical conductivity and uranium, it is interpreted that there is a positive linear correlation between EC and uranium concentration in groundwater at lower concentrations of uranium but at the higher concentration, the linearity is not observed. On comparing $\delta^{18}\text{O}$ vs uranium it's seen that there is no correlation with respect to $\delta^{18}\text{O}$ values between low or high concentration regions. The depth profile of uranium in the study area shows that with increasing depth there is a decrease in concentration. This suggests that there are factors working in the shallow zones that are leading to leaching of uranium into the groundwater while these factors may be absent or low at the deeper aquifer i.e. alkalinity [6].

Acknowledgment: - Authors sincerely acknowledge the constant support and encouragement by Dr. K.S.S.Sarma, Head, Isotope and Radiation Application Division and Dr. P.K.Pujari, Associate Director, Radiochemistry and Isotope Group, Bhabha Atomic Research Centre, Mumbai.

References

- /1/ AERB, Directive for Limit on Uranium in Drinking Water, India. Mumbai: Atomic Energy Regulatory Board,2004.
- /2/ Uranium in Drinking-water Background document for development of WHO Guidelines for Drinking-water quality World Health Organization 2011 http://www.who.int/water_sanitation_health/dwq/chemicals/uranium_forcomment_20110211_en.pdf

Determination of ^{90}Sr in Environmental Samples Using Solid Extraction Chromatography

Amar D. Pant^{1*}, R. Ruhela², B. S. Tomar³ and Anilkumar S.¹

¹Radiation Safety Systems Division, Bhabha Atomic Research Centre, Mumbai-85, India

²Material Processing and Corrosion Engineering Division, Bhabha Atomic Research Centre, Mumbai-85, India,

³Homi Bhabha National Institute, Bhabha Atomic Research Centre, Mumbai-85, India,

*E-mail: amarp@barc.gov.in

1. Introduction

^{90}Sr is one of the main components of fallout activity and accidental release from nuclear facilities Sr is accumulated in bone tissue and the high energy beta particles from its daughter ^{90}Y cause damage to bone marrow. Earlier, Horwitz et al developed a solid extraction chromatography (SEC) method using crown ether for the selective extraction of strontium [1]. Sr resin (Sr-spec resin, Eichrom Industries) consists of the crown ether 4, 4' (5')-bis(tert-butylcyclohexano)-18-crown-6 dissolved in 1-octanol sorbed on an inert polymeric support. It possesses selectivity of solvent extraction, the ease of column chromatography. The present paper describes the determination of ^{90}Sr in environmental samples using Sr spec resin based solid phase extraction method.

2. Experiment

2.1 Column capacity for Sr: Solutions containing $^{85+89}\text{Sr}$ tracer in nitrate form was obtained from BRIT, Mumbai, India and 100 mg of $\text{Sr}(\text{NO}_3)_2$ dissolved in 3M HNO_3 was used as a carrier. Solution was loaded onto the column (3 g of Sr spec resin) and washed with 3M HNO_3 . Fractions were collected and gamma activity of ^{85}Sr was measured using High Purity Germanium (HPGe) detector.

2.2 Sample Preparation: Five sediments samples were taken up in duplicates, dried at 110 °C and then ashed in a furnace at 450°C. 10 g of ash sample was then used for the analysis. To each sample, 20 mg of stable Sr^{2+} carrier and known amount of $^{85+89}\text{Sr}$ activity was added for determination of recovery. Samples were wet ashed with conc. HNO_3 solution, heated and centrifuged. 8 M HNO_3 was added to the residue and solution was again heated, centrifuged and supernatant was collected in another beaker. 500–600 mL of deionized water was added to the extract and $\text{Fe}(\text{OH})_3$ was precipitated at pH >8.0 by

addition of liquid ammonia. To the supernatant 25% ammonium carbonate was added to precipitate SrCO₃. The carbonate precipitate was centrifuged, washed with water and dissolved in 3 M HNO₃.

2.3 Strontium separation by SEC: Sr-spec resin column was preconditioned with 3 M HNO₃ and strontium was stripped from the column with 0.05 M HNO₃. Eluted Sr solution was made alkaline (pH >8.0) using liquid ammonia and Sr was precipitated as SrCO₃ by adding of 25% (NH₄)₂CO₃. The precipitate after proper treatment was counted using a low background gas flow GM counter.

3. Results and Discussion

The capacity of Sr-spec resin column was observed to be 12.2 ± 0.5 mg of Sr per g of Sr spec resin. The capacity of the column decreased with use but not linearly. Before analysis the actual sediment samples, five sediment samples were spiked with known activity of ⁹⁰Sr to compare both the methods viz. conventional gravimetric method with the SEC method. Table 1 gives the results of ⁹⁰Sr activity obtained from sediment sample using two methods. The radiochemical recoveries obtained by both these methods were observed to be in good agreement, thus validating the SEC method.

Table 1. Comparison of ⁹⁰Sr activity estimated using conventional and SEC methods

S.No.	Sediment Samples	
	Conventional method (mBq/g)	SEC method (mBq/g)
1	2.4 ± 0.1	2.2 ± 0.1
2	3.2 ± 0.1	3.5 ± 0.1
3	4.9 ± 0.2	5.3 ± 0.2
4	6.4 ± 0.4	6.1 ± 0.5
5	7.8 ± 0.5	7.7 ± 0.4

4. Conclusion

The studies showed that Sr spec resin can be successfully used for separation of strontium from environmental samples. The method standardized is relatively simple and fast for assessment of Sr contamination in large number of environmental samples which is presently not possible with conventional gravimetric method.

Acknowledgement: The authors express their sincere thanks to Dr. Pradeepkumar K.S., Associate Director, HS&E Group for his constant encouragement and support in this work. Authors are also thankful to Smt. Narayani K. and Shri Amit K. Verma for co-operation during the work.

References

/1/ E.P. Horwitz, M.L. Dietz, D.E. Fisher, Solvent Extraction and Ion Exchange (1990), 8, 199-208.

Certification of Iodine Filters NPP Using ^{131}I and ^{127}I

*Volodymyr Levenets**, *Oleksiy Lonin*, *Oleksandr Omelnik*, *Volodymyr Sokolenko*,
Andrey Shchur

National Science Center “Kharkov Institute of Physics and Technology”, Kharkiv, Ukraine
*E-mail: levenets@kipt.kharkov.ua

1. Introduction

The basic radioactive components of atmospheric emissions from nuclear power plants include isotopes of xenon, krypton, and also vapors of radioactive iodine and its various compounds. Of particular danger is ^{131}I and its organic compounds, which are actively accumulated in the human body [1]. Basically for the certification of iodine sorbents radioactive iodine is used and measurement the intensity of gamma rays of 365 keV energy in upstream and downstream air [2]. We used a method to measure the concentration of stable iodine in beds of the absorber.

2. Experiment

2.1. Generation air with vapor: an air flow of $0.48 \text{ m}^3/\text{s}\cdot\text{m}^2$ is created. Relative humidity resulting from H_2O evaporation was above 50%. The amount of iodine vapor admixture is determined by the flow of air through the iodine vapor generator and the temperature of the thermostat.

2.2. Measurement: in each beds of the absorber the iodine concentration was determined from the radiation intensity K - shell of iodine atoms (energy $\sim 28 \text{ keV}$) excited by gamma ray with energy of 59.6 keV from a radioactive source of ^{241}Am . The x-ray emission was recorded by HpGe detector with energy resolution of 250 eV for the line of 13.8 keV. The measurement time was about 20 minutes.

3. Results and Discussion

The results were compared for activated carbon (such as Norit 2 (Belgium)). For radioactive iodine (^{131}I) the intensity distribution of gamma radiation was determined as a function of bed absorber [3]. Figure 1 shows distributions the intensity of gamma radiation of 365 keV energy (p/s – pulse/second).

For stable iodine (^{127}I) the distribution of iodine concentration in the beds absorber is determined by our method. (Iodine concentration was obtain from the radiation intensity K - shell of iodine atoms) According to the obtained data, the sorption ability indices were determined and the correlation coefficient was calculated. Figure 2 shows distributions the intensity of gamma radiation and iodine concentration.

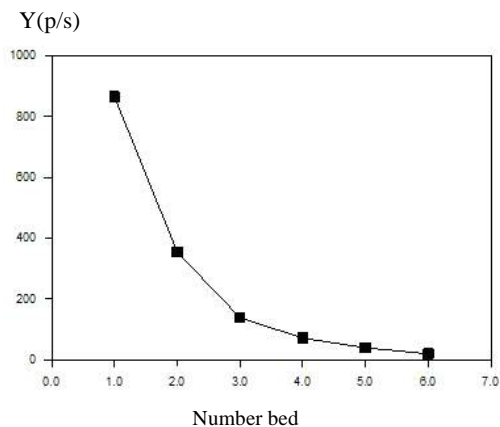


Figure 1. Distributions of gamma ray

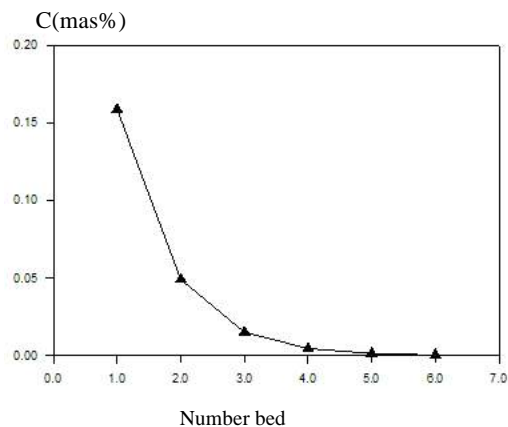


Figure 2. Distributions of concentration

4. Conclusion

Technique for determination of purification coefficient of sorbent on iodine using nonradioactive materials has been developed.

References

- /1/ D.S.Riggs Pharmacological Reviews, 4 (1952) 284
- /2/ Testing and Monitoring of Off-Gas Cleaning Systems at Nuclear Facilities. Technical Report, Series N 247, IAEA, Vienna, 1984.
- /3/ Wilhelm J.G. Iodine filters in nuclear installations. Contract No. 1175-80-12L/V (1982) 209 pg.

Natural Radioactivity in Alluvial soil of Indo-Gangetic Plain

*Rupali Karpe**, Ajay Kumar, Y.P. Gautam, M.K.Mishra, V.M.Joshi, Vandana Pulhani and R.M.Tripathi

Health Physics Division, Bhabha Atomic Research Centre, Trombay, Mumbai, India

*E-mail: chakor@barc.gov.in

1. Introduction

In the earth's crust, the most commonly encountered naturally occurring radionuclides are ^{238}U , ^{232}Th , their decay products and ^{40}K . These are also a source of natural external radiation exposure due to their gamma-ray emissions. Their concentration in soil, sand and rocks depends upon their geological and geographical origin [1]. The widely varying content of such radionuclides, prevalent in soils is an essential input for understanding the natural radiation background and any changes in it. During the past decades, agricultural activities in the Indo Gangetic plains of India have widely expanded causing an escalation in the application of inorganic fertilizers and pesticides to increase crop production. Inorganic, especially phosphate (P) fertilizers, contain hazardous elements including, heavy metals (Cd, Cr, and Pb) and radioactive elements (U, Th and their daughters), which are considered to be toxic to human and animal health [2]. These anthropogenic activities can impact the distribution and bioavailability of radionuclides in the terrestrial environment. In this context, the present work will provide a reference data for estimating the change in environmental radiation levels as these radionuclides can also serve as excellent biochemical and geochemical tracers in the environment.

2. Experiment

2.1. Materials and Method: A total of 100, representative, agricultural surface soil samples were collected from 32 locations of northwestern part of India. The samples were processed and sealed for a month to ensure equilibrium between uranium, thorium & their daughters respectively. Radioactivity measurement was performed by employing a coaxial p-type HPGe (50% relative eff.) gamma spectrometer.

The activity of ^{238}U was determined by taking a weighted mean of separate photopeaks of two radon daughters: ^{214}Pb (352 keV) & ^{214}Bi (609 keV), and for ^{232}Th , weighted mean of: ^{212}Pb (238.39 keV), ^{228}Ac (911 keV) & ^{208}Tl (583, 2614 keV) for counting the sample for 60,000 sec.

2.2 Radium equivalent activity: External exposure due to natural occurring radionuclides can be quantified in terms of Radium equivalent activity, which is a weighted sum of activities (A) of ^{238}U (^{226}Ra), ^{232}Th , & ^{40}K .

$$\text{Ra}_{\text{eq}}(\text{ex}) = A^{226}\text{Ra} + 1.429A^{232}\text{Th} + 0.077A^{40}\text{K} \text{ ----- (Eq.1)}$$

2.3 Outdoor gamma radiation air absorbed dose rate (OADR): OADR due to distribution of radionuclides (^{238}U , ^{232}Th and ^{40}K) in soils was calculated as proposed by UNSCEAR, 2000

$$\text{D}(\text{nGyh}^{-1}) = 0.462C_{\text{U}} + 0.604C_{\text{Th}} + 0.042C_{\text{K}} \text{ ----- (Eq.2)}$$

Where, 0.462, 0.604 and 0.042 are dose conversion factors in terms of nGyh^{-1} per Bqkg^{-1} . C_{U} , C_{Th} and C_{K} are the average activity concentrations of ^{238}U (^{226}Ra), ^{232}Th and ^{40}K respectively.

3. Results and Discussion

The activity concentrations of ^{238}U (^{226}Ra), ^{232}Th & ^{40}K in soil were found to vary from 32 to 68 Bqkg^{-1} (mean: $47 \pm 3 \text{ Bqkg}^{-1}$), 48 to 93 Bqkg^{-1} (mean: $67 \pm 2.0 \text{ Bqkg}^{-1}$) and 512 to 878 Bqkg^{-1} (mean: $638 \pm 18 \text{ Bqkg}^{-1}$) respectively. The measured mean radioactivity contents of ^{238}U , ^{232}Th and ^{40}K in soil of studied area were within the nationwide range although some extreme values were observed. The corresponding OADR due to ^{238}U (^{226}Ra), ^{232}Th & ^{40}K in soils ranged from 85–104 nGyh^{-1} with mean value of 89 nGyh^{-1} . According to UNSCEAR, 2000, the corresponding worldwide average values range from 18 to 93 nGyh^{-1} and typical range variability for measured absorbed dose rates in air outdoors is from 10 to 200 nGy h^{-1} . The mean equivalent radium [$\text{Ra}_{\text{eq}}(\text{ex})$] was found to be 197 Bq kg^{-1} , which is well below the defined limit of 370 Bq kg^{-1} by UNSCEAR, 2000.

4. Conclusion

Results reveal that the average dose rates do not exceed the average world recommended values and do not pose a significant health hazard. The data presented can be used as a reference data for monitoring possible radioactivity pollutions in future as well as for preparing a radiological map of the area.

References

- /1/ S. Singha, A. Rania, R.K. Mahajan. Radiat. Meas. 39 (2005) 431 – 439.
- /2/ K. Brigden, R. Stringer R, D. Santillo. Greenpeace Research Laboratories Technical Note (13/2002), 16
- /3/ United Nations Scientific Committee on the Effect of Atomic Radiation). Report to the general assembly. Annex B: exposures from natural radiation sources United Nations, New York 2000.

Effect of Electron Irradiation on Optical, Thermal and Electrical Properties of Polymer Electrolyte

B. K. Mahantesha¹, V. Ravindrachary^{1}, R. Padmakumari¹, R. Sahanakumari¹,
Pratheeka Tegginamata¹, Ganesh Sanjeev¹, V. C. Petwal², V. P. Verma²*

¹Department of Physics, Mangalore University, Mangalagangotri 574199, India

²Raja Ramanna Centre for Advanced Technology, Department of Atomic Energy, Indore 452012, India

*E-mail: vravi2000@yahoo.com

1. Introduction

Solid polymer electrolytes (SPE) have attracted the scientific community due to their potential uses in optoelectronic and other electrochemical devices [1]. These devices require SPE with good mechanical and thermal stability, electrical conductivity with high dielectric strength and better optical parameters with narrow band gap. Among the techniques used to improve these properties of SPE, irradiation of polymers with electron beam has shown some promising results. Thus, here we tried to improve the optical, thermal and electrical properties of KBr/PVA polymer electrolytes by electron irradiation.

2. Experimental

2.1 Materials and sample preparation: 5 wt% KBr/PVA films were prepared by solution casting method using double distilled water. Films were irradiated with 10 MeV Linac-based electron beam at RRCAT, Indore, India. Here 3×3 cm² sized films were sealed in a thin transparent polyethylene sachets and stacked in conveyor belt perpendicular to the electron beam direction at room temperature. The films were irradiated with 0, 50, 100, 150, 200, 250 and 300 kGy doses of electron beam of power 235 mA. Pure and irradiated films were characterized using different techniques.

3. Results and Discussion

FTIR spectra (Figure 1(a)) show that the peaks are shifted slightly with change in the peak intensity upon irradiation indicating the chemical modification of KBr/PVA due to electron irradiation. Splitting

of 2919 cm^{-1} into 3945 cm^{-1} and 2915 cm^{-1} upon radiation etching of electron irradiated films. UV-Vis spectra (figure 1(b)) show two absorption bands along with the red-shifted bands upon irradiation.

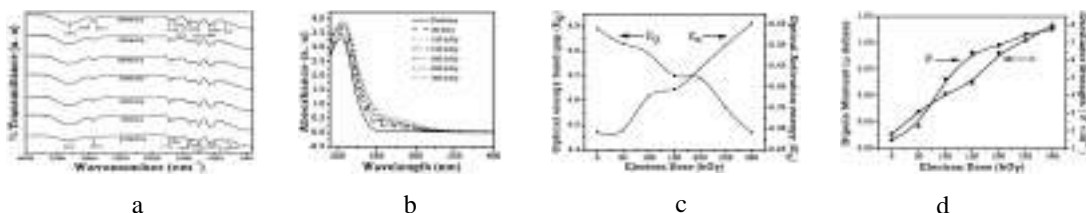


Figure 1 a) FTIR, b) UV-Vis, c) band gap and activation energy and d) dipole moment and oscillator strength of pristine and electron irradiated KBr/PVA polymer electrolyte films.

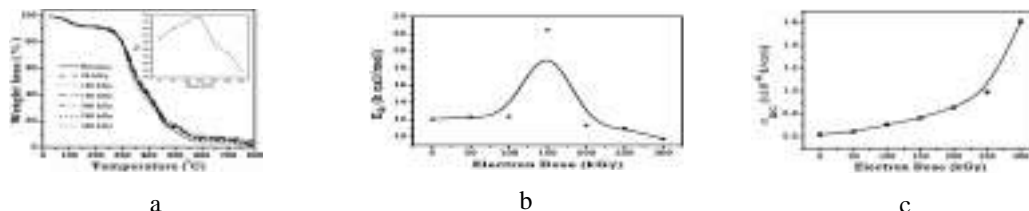


Figure 2 a) TGA, b) activation energy of thermal decomposition, c) DC conductivity plot with varying electron irradiation dose

These changes are indicative of formation of charge transfer complexes and the presence of defects within the band gap created upon irradiation. The presence of the complexes are also modifies the dipole moment and the oscillator strength of the composite figure 1(d) [2]. Here the electron irradiation creates new molecular levels near the conduction band and the dipoles lives longer as a result the electrical conductivity increases (figure 2(c)) with dose. The enhancement of conductivity with irradiation dose are mainly due to the fact that the crosslinking of polymer chains (below 150 kGy) and then due to chain scission (after 150 kGy) [2]. From the TGA study, it is clear (figure 2(a)) that the crosslinking produced upon irradiation enhances the onset temperature (T_0) at lower dose, further the degradation temperature increases with irradiation dose. The estimated activation energy of thermal decomposition (figure 2(b)) is in good agreement with the value of onset temperature.

Acknowledgment: A part of research was carried out using facilities at CeNSE, Indian Institute of Science, Bengaluru, funded by Ministry of Electronics & Information Technology (MeitY), GOI.

References

- /1/ N. Ahad, E. Saion, E. Gharibshahi, Journal of Nanomaterials 2012 (2012) 94
- /2/ Ismayil, V. Ravindrachary, R. Bhajantri, et al, Nucl. Instrum. Methods Phys. Res. B, 342 (2010) 29

Accumulation of ^{210}Po in Medicinal Plants in the Environment of Mangalore, Southwest Coast of India

V. Prakash^{1*}, K. M. Rajashekara², Y. Narayana³

¹Department of Physics, Payyanur College, Edat - 670327, India, Email: prakashamv@gmail.com

²Department of Physics, SJC Institute of Technology, Chickballapur - 562101, India

³Department of Physics, Mangalore University, Mangalagangothri - 574 199, India

*E-mail: prakashamv@gmail.com

1. Introduction

Mangalore is a major industrial hub in the southwest coast of India with industrial activities like oil refineries, petrochemical complexes, chemical and fertilizer factories, thermal power stations and a host of other industries. Though the information on the radiation level and radionuclide distribution in different environmental matrices of the region is available in literature, systematic studies on uptake of radionuclides by plants from soil are sparse. The mobility and availability of radionuclides in soil and plants depend on several factors such as geochemical, biological and climatic conditions. The risk to both the environment and human health of a given radionuclide is a function of its mobility and phytoavailability. Therefore, studies on behavioural properties of radionuclides in soils and medicinal plants have gained importance during environmental studies. In view of the above, twelve ayurvedic medicinal plants and associated soils were collected from Moodabidri, near Mangalore, were analysed for the concentration of ^{210}Po . Radionuclide ^{210}Po is one of the most toxic alpha emitting natural radionuclides of ^{238}U series and an important contributor to the internal exposure of human population.

2. Materials and methods

In the present study, twelve medicinal plants and associated soils were collected from Moodabidri were subjected to ^{210}Po analysis. Standard techniques were followed in the collection of samples [1]. The electrochemical deposition method was employed for the determination of ^{210}Po activity [2]. Counts were noted using ZnS (Ag) alpha counter of 0.4 cpm background and 30% efficiency.

3. Results and Discussions

The results of the activity concentration of ^{210}Po in plant species and associated soils are given in Table 1. It can be seen from the table that, the activity concentration of ^{210}Po in plant species vary from 6.3 Bq kg⁻¹ to 56.9 Bq kg⁻¹ with a mean value of 27.8 Bq kg⁻¹ and that of soil vary from 2.2 Bq kg⁻¹ to 19.6 Bq kg⁻¹ with a mean value of 8.3 Bq kg⁻¹. The maximum activity of 56.9 Bq kg⁻¹ and 19.6 Bq kg⁻¹ was observed for the plant *Barringtonia acutangula* (Samudraphalam) and associated soil respectively. The minimum activity of 6.3 Bq kg⁻¹ and 2.2 Bq kg⁻¹ was measured for the plant *Ficus benghalensis* (Vatavrksam) and associated soil respectively. This clearly indicates that soil is one of the main sources of radionuclides in plants. The ^{210}Po concentration was found to vary widely among the plant species and with soil type. The plant to soil ratio of ^{210}Po indicates that, in addition to natural decay of ^{238}U in soil, ^{210}Po also comes from atmospheric deposition due to the decay of ^{222}Rn . The ^{210}Po activity concentration varied with soil structure and soil type. The activity concentration ^{210}Po in plants is almost certainly depends on the physicochemical parameters of the corresponding soil.

Table.1 Activity of ^{210}Po in plants and soils, activity ratio and dose rate

Botanical Name	Common Name	Activity (Bq kg ⁻¹)		Ratio plant/soil	Dose Rate (nGy hr ⁻¹)
		Plant	Soil		
<i>Putranjeeva roxburgii</i>	Putranjeeva	25.2±2.2	7.4±1.8	3.4	34.8
<i>Mesua nagassarium</i>	Nagakesara	15.7 ± 1.7	3.7 ± 1.4	4.2	43.5
<i>Mamia suregia</i>	Punnaga	13.5 ± 1.6	4.4 ± 1.5	3.1	52.2
<i>Saracaasoca pappilionaceae</i>	Ashoka	16.3 ± 1.8	7.0 ± 1.8	2.3	34.8
<i>Syzygium jambolanum</i>	Jambo	23.5 ± 2.1	3.7 ± 1.4	6.4	43.5
<i>Garcinia indica</i>	Amalavetasa	53.7 ± 3.2	16.3 ± 1.7	3.3	43.5
<i>Ficus benghalensis</i>	Vatavrksam	6.3 ± 1.1	2.2 ± 1.2	2.9	34.8
<i>Flacartia montana</i>	Abluka	25.2 ± 2.2	3.3 ± 1.3	7.6	52.2
<i>Nyctanthes arbor-tristis</i>	Parijatam	29.6 ± 2.4	7.4 ± 1.8	4.0	52.2
<i>Morinda citrifolia</i>	Manjanathi	50.9 ± 3.1	15.2 ± 1.6	3.3	34.8
<i>Ficus recemosa</i>	Atti	16.3 ± 1.8	8.9 ± 2.0	1.8	52.2
<i>Barringtonia acutangula</i>	Samudraphalam	56.9±3.3	19.6±2.0	2.9	43.5
Mean		27.8	8.3	3.8	43.5
Median		24.4	7.2	3.3	43.5
Range		6.3 -56.9	2.2 -19.6	1.8 -7.6	34.8 -52.2

References

- /1/ L.V. Herbert and Gail de Planque, *EML Procedure manual* 26th Edn., Environmental Measurement Laboratory, New York (1983).
- /2/ M.A.R. Iyengar, S. Ganapathy, S.V. Kannan, M.P. Rajan and S. Rajaram, *Procedure manual*, Workshop on Environmental Radioactivity held at Kaiga, India, April 16-18 (1999).

Distribution and Enrichment of ^{210}Po and ^{210}Pb in The Environment of Mangalore, Southwest Coast of India

V. Prakash^{1}, V. Vineethkumar¹, K. M. Rajashekar², Y. Narayana³*

¹Department of Physics, Payyanur College, Edat - 670327, India.

²Department of Physics, SJC Institute of Technology, Chickballapur - 562101, India

³Department of Physics, Mangalore University, Mangalagangothri - 574 199, India

*E mail: prakashamv@gmail.com

1. Introduction

Mangalore, is one of the major industrial area of south-west coast of India. Detailed studies on radiation level and distribution and enrichment of radionuclides in environment of the region have relevance in understanding the radiation effects on environment and human health. In view of this, studies on radiation level and radionuclide distribution have been carried out in the environment of the region. As part of the program, soil samples collected from the region were analyzed for ^{210}Po and ^{210}Pb activity concentration to understand the distribution and enrichment of these radionuclides in the region. The results of these investigations are presented and discussed in this paper.

2. Materials and methods

In the present study, sixteen soil samples were collected from Mangalore in a radius of about 5 km using standard methods [1]. Soil samples were dried in an oven at 110°C till a constant dry weight is obtained and calculated the moisture content. Electrochemical deposition method was employed for determination of ^{210}Po and ^{210}Pb activity [2]. Activity of the samples was measured using ZnS (Ag) alpha counter.

3. Result and discussion

The activity concentration of ^{210}Po and ^{210}Pb in soil samples of Mangalore region are given in Table 1. The activity of ^{210}Po varies from 1.5 Bq kg⁻¹ to 26.9 Bq kg⁻¹ with a mean value of 12.6 Bq kg⁻¹ and that of ^{210}Pb varies in the range 7.6 Bq kg⁻¹ to 67.5 Bq kg⁻¹ with a mean value of 38.9 Bq kg⁻¹.

The maximum activity for both ^{210}Po and ^{210}Pb was found at Urva Store and the minimum activity for both ^{210}Po and ^{210}Pb at Padil. The highest ^{210}Po and ^{210}Pb activity at Urva store is due to high organic matter in the soil sample of the region. Both ^{210}Po and ^{210}Pb activity in soil was found to increase with increasing organic matter. ^{210}Po and ^{210}Pb concentration in soil varied from place to place and with soil type. The present results show that the radionuclides ^{210}Po and ^{210}Pb are not in equilibrium and the accumulation of ^{210}Pb in soil is much more compared to ^{210}Po . The correlation study clearly indicates that, it is due to organic matter present in the samples. A good correlation observed between the ^{210}Po activity and organic matter in the soil with correlation coefficient $r = 0.8$.

Table 1. The activity of ^{210}Po and ^{210}Pb in Mangalore environs

Sampling station	Activity (Bq kg ⁻¹)		$^{210}\text{Po}/^{210}\text{Pb}$ Ratio	Dose Rate (nGy hr ⁻¹)	Organic Matter (%)
	^{210}Po	^{210}Pb			
Bejai	06.4 ± 1.2	31.5 ± 3.3	0.2	43.8	9.8
Kottara	24.1 ± 2.4	33.3 ± 4.0	0.4	39.4	14.0
Kodialbail	06.7 ± 1.2	10.0 ± 1.9	0.7	48.2	6.7
Urva store	26.9 ± 2.5	67.5 ± 5.6	0.4	39.4	14.9
Car street	07.3 ± 1.3	14.5 ± 2.4	0.5	56.9	9.5
Kudroli	16.6 ± 1.7	62.2 ± 4.7	0.3	52.6	10.0
State Bank	09.2 ± 1.3	37.8 ± 3.5	0.2	56.9	8.5
Bunder	23.9 ± 2.1	56.5 ± 4.6	0.4	39.4	14.0
Attavar	10.5 ± 1.4	32.0 ± 3.2	0.3	48.2	10.5
Mugaru	12.0 ± 1.8	43.9 ± 4.5	0.3	39.4	12.0
Jeppu	03.7 ± 0.9	14.0 ± 2.4	0.3	39.4	8.3
Ekkur	22.9 ± 2.6	60.5 ± 5.8	0.4	39.4	13.1
Pumpwell	15.4 ± 1.9	42.9 ± 4.5	0.4	65.7	13.5
Padil	01.5 ± 0.7	07.6 ± 1.7	0.2	39.4	7.5
Kadri	07.5 ± 1.0	52.1 ± 3.7	0.1	43.8	9.8
Nanthoor	07.8 ± 1.3	56.1 ± 4.5	0.1	78.8	10.3
Mean	12.6	38.9	0.3	48.2	11.2
Median	9.8	40.4	0.3	43.8	10.2
Range	1.5 - 26.9	7.6 - 67.5	0.1 - 0.7	39.4 - 78.8	7.5 - 14.9

References

- /1/ L.V. Herbert and Gail De Planque, *EML Procedure Manual*, 26th Edn., Environmental Measurement Laboratory, New York (1983).
- /2/ M.A.R Iyengar, S. Ganapathy, S.V. Kannan, M.P. Rajan and S. Rajaram, *Procedure Manual, Workshop On Environmental Radioactivity Held At Kaiga, India*. April 16-18 (1999).

The Behavior of Neptunium In Natural Objects

A.M. Emelianov, E.A. Lavrinovich, T.A. Goryachenkova, A.P. Novikov*

Vernadsky Institute of Geochemistry and Analytical Chemistry, Russian Academy of Sciences, Moscow, Kosygin Street, 19, 119991 Russian Federation
*E-mail: Ksander93@mail.ru

1. Introduction

Artificial radionuclides and, first of all, the most dangerous isotopes of transuranium elements (TUE) became constant and irreversible components of the biosphere because of the experimental nuclear explosions performed, the wrong concept of the disposal of radioactive wastes to open water reservoirs, and also process upsets and emergency situations at NFC enterprises.

It is known that many radionuclides can accumulate by biogeocenosis components and incorporate into food chains. However, only behavior of γ -emitting short-lived isotopes has been studied comprehensively at present. Bioaccumulation of α -emitting and the most toxic isotopes of actinide elements have been studied less due to methodological difficulties of radiochemical analysis. However, laboratory researches show a high degree of actinide sorption, primarily of neptunium, by microorganisms and plants.

The main problem of determining the coefficients of actinide accumulation by biota is the impossibility of direct detection of their content and the significant influence of organic substance on the yield of the analyte during alpha-spectrometric determination. A method for determining actinides according to luminescence of crystallophosphors was developed and tested in the Vernadsky Institute of Geochemistry and Analytic Chemistry of the Russian Academy of Sciences. A photometer and membrane modules for separation of actinides in physicochemical forms, as well as for their concentration, were created. The method is particularly useful when analyzing natural objects, because it doesn't require prior separation of actinide elements, as well as cleaning the sample from alkali and alkali-earth elements. Actinide luminescence is induced by the ultraviolet radiation of the

crystallophosphor located at room temperature. Detection limit of the photometer for determining the neptunium contents in simulated groundwater is 3 pg/ml (0.3 pg of Np in a quartz crucible).

2. Experiment

The present research studies the processes of bioaccumulation and biotransformation (changing of speciation) of the most toxic, alpha-emitting actinides on real biological objects, selected in the areas of Krasnoyarsk Mining and Chemical Combine (KMCC), and in the impact zone of the Kraton-3 underground nuclear explosion (Yakutia). The procedure of the direct luminescence determination of actinides consisted in the application an aliquot portion of a test solution onto the crystal phosphor (0.02 to 0.1 mL) put into a quartz beaker, drying under an IR lamp, calcination of the sample on an electric hot plate within 45 min, and final calcination in a muffle furnace within 1 h at 900°C. As crystal phosphor matrices, we used PbMoO_4 (200 mg). Amounts of actinides were determined by the luminescence of crystal phosphors activated by analytes recorded by an LFF-5 analyzer.

3. Results and Discussions

It has been established that relative content of water-soluble and exchange forms of neptunium is 5-10 times higher than the relevant values for plutonium and americium. Among long-lived radionuclides only ^{90}Sr has similar solubility. It was found that, for all of the studied soil types, the concentration of radionuclides in water-soluble and exchange forms, which are most mobile and determine in the series ^{237}Np (39.1-75.4%) > ^{241}Am (3.9-21.7%) > ^{239}Pu (4.1-20.1%). In poorly soluble forms (acid-soluble and residues) irrespectively of the soil type, the Concentration of radionuclides changed in the inverse order: ^{239}Pu (68.4-85.7%) > ^{241}Am (19.6-36.2%) > ^{237}Np (9.7-31.8%). In the soil organic matter the main content of neptunium was found in the fulvic acids fraction and low molecular weight acids (below 43%), and moreover, up to 25% of neptunium is directly bonded to the low molecular weight substances of non-specific nature. This, apparently, provides its high bioavailability.

Neptunium is found in the aquatic vegetation of Yenisei River. The water plant *Fontinalis antipyretica* (water moss), in the dry biomass of which the maximum specific activity of neptunium amounts up to 10 Bq/kg, accumulates it most actively. The content of neptunium in the vegetation in the impact zone of the Kraton-3 underground nuclear explosion increases in the line: lingonberry (*Vaccinium vitis-idaea*) < mountain ash (*Sorbus aucuparia*) < sedge (*Carex riparia*) < lichen (*Hypogymnia physodes*) < larch needles (*Larix sibirica*) < moss (*Cladonia rangiferina*).

This work is supported by the Russian Science Foundation project 219 №17-17-01212

Development of Radiolabeled Chemotherapeutics for Tumor Theranosis: A Preliminary Study with ⁶⁸Ga- and ¹⁷⁷Lu-labeled Gemcitabine

Subhajit Ghosh^{1,2}, Tapas Das^{1,2}, Haladhar D. Sarma³, Ashutosh Dash^{1,2}*

¹Radiopharmaceuticals Division, Bhabha Atomic Research Centre, Mumbai 400085, India

²Homi Bhabha National Institute, Anushaktinagar, Mumbai 400094, India

³Radiation Biology and Health Sciences Division, Bhabha Atomic Research Centre, Mumbai 400085, India

*E-mail: tdas@barc.gov.in

1. Introduction

Gemcitabine (2'-deoxy-2',2'-difluorocytidine), a nucleoside analogue, is a well-established chemotherapeutic drug and used alone or with other agents for the treatment of various types of cancers, such as bladder, pancreas, lung, ovary, breast [1,2]. Therefore, radiolabeled gemcitabine is expected to have a serious potential for diagnosis as well as treatment of a variety of cancers [3]. The objective of the present study is to radiolabel gemcitabine with ⁶⁸Ga, and ¹⁷⁷Lu, and evaluate the potential of radiolabeled agents towards theranostic applications.

2. Experiment

Gemcitabine was coupled with a bifunctional chelating agent, *p*-NCS-benzyl-DOTA. The conjugate was characterized by ¹H-NMR and mass spectrometry. Radiolabeling was done by incubating the gemcitabine-*p*-NCS-Benzyl-DOTA conjugate dissolved in NH₄OAc buffer (pH=5) with either ⁶⁸GaCl₃ or ¹⁷⁷LuCl₃ [1 mCi] in a boiling water bath, 20 min for ⁶⁸Ga and 1 h for ¹⁷⁷LuCl₃. The radiolabeled products were characterized by HPLC. The radiolabeled agents had adequate stability in normal saline and human blood serum. Biological distribution and pharmacokinetic behaviour of both the agents were studied in Swiss mice bearing fibrosarcoma tumors. Biological distribution was studied at ½ h, 1 h and 2 h post-administration time points for ⁶⁸Ga-gemcitabine, while for ¹⁷⁷Lu-gemcitabine distribution was studied at 3 h, 1 d, 2 d and 6 d post-injection time points.

3. Results and Discussion

Evidence towards formation of gemcitabine-*p*-NCS-benzyl-DOTA conjugate was obtained from the $^1\text{H-NMR}$ and mass spectrometry. Both the radiolabeled complexes had $> 95\%$ radiochemical purity. In HPLC studies, radiolabeled gemcitabines exhibited a retention time of more than 10 min, while uncomplexed $^{68}\text{Ga}/^{177}\text{Lu}$ eluted from the column within 5 min. Bio-evaluation studies showed good tumor uptake with rapid renal clearance and a high tumor to muscle ratio. The results of the biodistribution studies are shown in Figure 1 and 2, respectively.

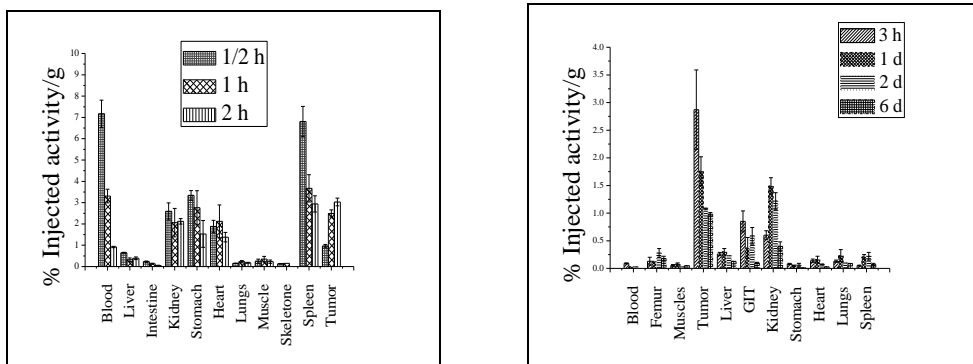


Figure 1. Biodistribution pattern of ^{68}Ga -gemcitabine Figure 2. Biodistribution pattern of ^{177}Lu -gemcitabine

4. Conclusion

Gemcitabine, was radiolabeled with ^{68}Ga and ^{177}Lu with high radiochemical purity and adequate in-vitro stability. Both the agents exhibited good tumor specificity with high tumor to background ratios and fast clearance from non-target organs. The present study demonstrated the potential of ^{68}Ga and ^{177}Lu -labeled gemcitabine as a theranostic pair for tumor diagnosis and targeted therapy.

Acknowledgement: The authors gratefully acknowledge Dr. P.K. Pujari, Radiochemistry and Isotope Group, BARC for his support, staff members of the Radiochemicals Section, Radiopharmaceuticals Division, BARC for providing the $^{177}\text{LuCl}_3$. Authors also acknowledge staff members of the Animal House Facility, Radiation Biology and Health Sciences Division, BARC.

References

- /1/ A.B. Ibrahim, T.M. Sakr, O.M.A. Khoweysa, et al., J. Radioanal. Nucl. Chem. 302 (2014) 179
- /2/ M. Barton-Burke, Cancer Nursing, 22, (1999) 176.
- /3/ S. Ghosh, T. Das, H.D. Sarma, A. Dash, Cancer Biother. Radiopharm. 32 (2017) 239.

Regulating Energetic Beams for Medical Isotope Production in Canada

Abdul Alwani^{1}*

¹Canadian Nuclear Safety Commission, 280 Slater Street, Ottawa, Ontario, Canada, K1P 5S9,
*E-mail: abdul.alwani@canada.ca

1. Introduction

The Canadian Nuclear Safety Commission is the federal regulator of nuclear power and materials in Canada. Under the Nuclear Safety and Control Act, the CNSC's mandate includes regulating the development, production and use of nuclear energy in Canada to protect health, safety and the environment and regulating the production, possession, use and transport of nuclear substances, and the production, possession and use of prescribed equipment and prescribed information.

The use of particle accelerators for medical isotope production has grown significantly during the past thirty years. This is both in terms of quantity and in terms of the variety of isotopes produced. The upward trend is expected to continue steadily in the future.

2. PET Cyclotrons

Small cyclotrons have always been the source for the four main short-lived Positron Emission Tomography isotopes namely, Fluorine 18, Oxygen 15, Nitrogen 13, and Carbon 11. A large number of new cyclotrons have been deployed in the country recently. Research has also increased in many research centres on new radiopharmaceuticals using the now more available PET isotopes.

3. Technetium 99m from Energetic Beams

The Technetium-99m supply has been through a world crisis in 2008. The shortage or the looming risk of shortage of supply of this essential isotope traditionally produced from reactors has impacted the evolution and the focus of the nuclear industry. The particle accelerators and the cyclotrons have

presented themselves as potential solutions to this supply security issue. Several projects have been launched in Canada toward this objective.

4. CNSC Oversight

An overview of the CNSC oversight functions to ensure that the production and use of the medical isotopes as well as the construction and operation of the associated facilities meet the safety requirements are presented. In addition, whether at the time of introducing new techniques or technologies or even exploring new ideas for producing medical isotopes the CNSC has been present to provide the appropriate consultations and input.

5. Conclusion

The CNSC has offered and continue to offer the required regulatory guidance, has performed and continue to perform safety monitoring to the nuclear industry embarking on the various stages of medical isotope production.

References

/1/ Nuclear Safety and Control Act and Regulations <http://www.cnsccsn.gc.ca/eng/>

Monte Carlo Simulation Approach to Evaluate Radon Suppression in Low Background Gamma-ray Spectroscopy

Sy Minh Tuan Hoang^{1}, Gwang Min Sun², Hoai-Nam Tran¹, Ngoc-Thiem Le³, Manh-Dung Ho⁴, Tuan-Anh Tran⁴*

¹Institute of Fundamental and Applied Sciences, Duy Tan University, Ho Chi Minh City 700000, Vietnam

²Korea Atomic Energy Research Institute, 111, Daedeok-Daero, 989 Beon-Gil, Yuseong-gu, Daejeon, Republic of KOREA

³Institute for Nuclear Science and Technology - VINATOM, 179 Hoang Quoc Viet, Hanoi, Vietnam

⁴Dalat Nuclear Research Institute-VINATOM, 01 Nguyen Tu Luc, Dalat, Lam Dong, Vietnam

*E-mail: hsmtuan@gmail.com

1. Introduction

Low-background gamma-ray spectrometry has been developed for many years and widely applied in different fields such as fundamental physics researches and conventional sample investigations [1]. Low-background HPGe gamma spectrometers are playing an increasingly important role in material selections for rare event experiments and measurements of environmental samples [2-4]. One of the main challenges of all ultra-low background germanium spectroscopy is the presence of radon isotopes in air. In order to reduce the effects of radon isotopes inside the spectrometry volume, there are several approaches and flushing the spectrometry volume with nitrogen to actively remove the radon isotopes is one of its. Maintain constant overpressure by continuous flushing to suppress radon diffusion. In this study, Monte Carlo simulation based on MCNP6 code [5] has been applied to perform this approach with several configurations of the HPGe spectrometry in the NAA lab (KAERI, Republic of KOREA).

2. Method

A series of measurements of radon activity levels and gamma background counting rates been performed to quantify and understand the evolution of these background components. To quantify the gamma background a set-up was prepared, consisting of a coaxial ORTEC HPGe detector (model number - GMX40-76) and the energy of events up to ~3 MeV was continuously registered.

The simulated background source can be modeled based on the advantaged features of MCNP6 that introduced a generic background source of neutrons and photons from a background.dat source file. The background.dat file consisting of generic terrestrial soil emission spectra (from K, U, Th, etc. decay) include not only air to ground transport effects but also ground reflection effects (Ref. 5). The simulation backgrounds with and without nitrogen flushing are shown in Figure 1.

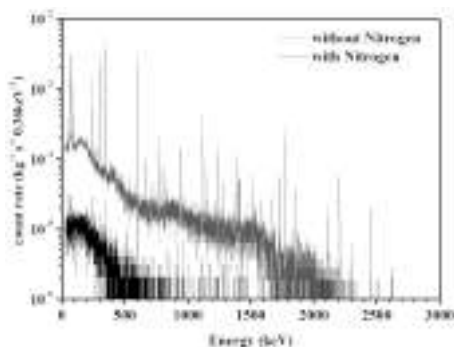


Figure 1. Background spectra of HPGe spectrometry with (blue) and without (red) N₂ flushing by simulation

3. Conclusion

²²²Rn in the air around the detector contributes significantly to the remaining background and attention will be paid to the radon concentration, especially inside the sample chamber. The reduction of ²²²Rn contributions was performed by using Monte Carlo simulation with some distinct conditions and showed significant improvements were possible by its removal.

Acknowledgement: This work was funded by National Foundation for Science and Technology Development (NAFOSTED), Vietnam under grant 103.04-2018.70.

References

- /1/ M. Hult. Metrologia 44, (2007) S87-S94.
- /2/ C. Arpesella, H. Back, M. Balata, et al., Astroparticle Phys. 18, (2002) 1-25.
- /3/ D. Budjáš, A. Gangapshv, J. Gasparro, et al., Appl Radiat Isotopes 67, (2009) 755-758.
- /4/ M. Kohler, D. Degering, M. Laubenstein, et al., Appl Radiat Isotopes 67, (2009) 736-740.
- /5/ D. B. Pelowitz, MCNP6 User's Manual, Los Alamos National Laboratory, New Mexico, USA (2013).

The Innovative PIXE/PIGE Facility at the 2-MV KIST Tandem Ion Accelerator: Design and Calculation

Sy Minh Tuan Hoang^{1}, Gwang Min Sun², Hoai-Nam Tran¹, Ngoc-Thiem Le³, Manh-Dung Ho⁴, Tuan-Anh Tran⁴*

¹Institute of Fundamental and Applied Sciences, Duy Tan University, Ho Chi Minh City 700000, Vietnam

²Korea Atomic Energy Research Institute, 111, Daedeok-Daero, 989 Beon-Gil, Yuseong-gu, Daejeon, Republic of KOREA

³Institute for Nuclear Science and Technology - VINATOM, 179 Hoang Quoc Viet, Hanoi, Vietnam

⁴Dalat Nuclear Research Institute-VINATOM, 01 Nguyen Tu Luc, Dalat, Lam Dong, Vietnam

*E-mail: hsmtuan@gmail.com

1. Introduction

Particle Induced X-ray Emission (PIXE) is a method in which X-ray emission is used for analysis. The high energetic proton beam excites, due to inner-shell ionization, the emission of characteristic X-rays from the sample target atoms [1]. Besides, PIGE (Proton Induced Gamma Emission) is based on the detection of prompt gamma rays emitted from nuclei that are excited state following the nuclear reactions (p, γ) , $(p, p'\gamma)$, $(p, n\gamma)$ in the sample [2]. Gamma rays and X-rays emit simultaneously when the samples are bombarded with high energetic protons. The PIGE is utilized in the analysis of light elements as lithium, boron, and fluorine, which are often difficult to determine by other analytical methods. In addition, The PIGE complements to PIXE that is a powerful yet non-destructive elemental analysis technique.

The Korea Institute of Science and Technology has a Tandem Ion Accelerator, which has been installed in 2011, consisting of mainly four ion accelerators as 6-MV, 2-MV, 0.5-MV, and 400-keV [3]. This study has carried out the design and simulations of a PIXE/PIGE system at the reserved location of the 2-MV output port where is available for standard analysis.

2. Method

A target vacuum chamber that will be installed at the end of the 2-MV beam line was designed for a high throughput of samples, ensured by a tight geometry of its components. The appropriate materials

for chamber walls, components and especially collimators were carefully chosen for rendering a low intrinsic chamber background. The schematic diagram of the vacuum chamber, as well as collimators, detectors and standing table, is shown in Figure I. The design of the PIXE/PIGE systems has been done using the CAD program and can be easy to export to the simulation packages.



Figure 1. Schematic view of the vacuum chamber, collimator, and detectors will be installed at KIST Tandem Ion Accelerator

Simulation of PIXE/PIGE in context of MCNP6/PHITS/TRIM must deal with the constraints imposed by condensed-random-walk schemes adopted for charged particle transport, as well as with the limitations of theoretical calculations, which are currently available in this problem domain.

3. Conclusion

The PIXE/PIGE system has been designed and predicted the performance by using the CAD program and Monte Carlo simulation codes. Based on the simulated results, the PIXE/PIGE systems will be turned compatibly with the proposed requirements before manufacturing and installing at the available position of the KIST Tandem Ion Accelerator.

Acknowledgement: This work was funded by National Foundation for Science and Technology Development (NAFOSTED), Vietnam under grant 103.04-2018.70.

References

- /1/ S. A. E. Johansson, J. L. Campbell, Wiley and Sons, New York, USA, (1998).
- /2/ M. B. H. Breeses, D. N. Jamieson, P. J. C. King, Wiley and Sons, New Yourk, (1996).
- /3/ D. H. Park, S. Y. Le, K. H. Chae, J. W. Choi, J. Korean Phys. Soc., 54, (2009) 52.

Solid State Synthesis and Phase Confirmation of Ce-Doped Zirconolite

Rajveer Kaur¹, M. Gupta¹, P. K. Kulriya², S. S. Ghumman^{1}*

¹Sant Longowal Institute of Engineering & Technology, Longowal 148106 Punjab, India

²Inter-University Accelerator Centre, Aruna Asaf Ali Marg, New Delhi 110067, India

*E-mail: ssghumman@sliet.ac.in

1. Introduction

The immobilization of high level wastes (HLWs) is one of the biggest challenges in nuclear energy industry for energy production and environment protection. Various studies over glasses and ceramics as hosts have been investigated. Titanate based ceramics, known as SYNROC's being more advantageous over glasses have been well studied under the effects of α -decay events. Among various waste forms, zirconolite, a fluorite based structure has been considered as a stable and chemically durable matrix for the desired purpose due to their specific properties such as waste loading, radiation stability, chemical flexibility and aqueous resistant [1]. Zhang et al. [2] found the solubility of CeO₂ in zirconolite of about 17.5 wt% of the raw material. Recently, Clark et al. [3] have studied the transition from 2M- to 4M-zirconolite by increasing the Ce substitution while targeting zirconium site.

Keeping in view the importance of lanthanides to be used as surrogates of minor actinides, Ce-doped zirconolite (Ca_{0.8}Ce_{0.2}ZrTi_{1.8}Al_{0.2}O₇) has been chosen to study the ion beam induced effects in the present work, concerning plutonium surrogacy by Ce. For the said purpose, samples were prepared by conventional solid state reaction method using their oxide reagents. Single phase matrix is an essential property for a compound to be radiation resistant and prepared samples were found to be almost single phase as characterized through X-ray diffraction (XRD) confirming their phases.

2. Experimental

The Ce-doped Zirconolite Ca_{0.8}Ce_{0.2}ZrTi_{1.8}Al_{0.2}O₇ in stoichiometric proportions was synthesized by conventional solid-state reaction of high purity binary oxides CaCO₃, ZrO₂, TiO₂, Al₂O₃, and Ce₂O₃ from sigma Aldrich. The appropriate amount of these reactants were mixed and homogenized in acetone media using agate mortar and pestle. The mixture was pelletized using hydraulic press die into

pellets of 10 mm diameter and about 1-2 mm thickness. Pellets were then sintered at 1350°C for 16 hrs in air. Characterization of sintered samples was done using Bruker Advanced D8 X-ray diffractometer with the radiation source Cu K α ($\gamma = 1.5406\text{\AA}$) and step size 0.02° and scan speed 2.4 s/step over the 2-theta range of 10-80°. The XRD pattern was examined by comparing with the reported data.

3. Results and Discussion

The XRD pattern of Ce-doped zirconolite (Ce-CZT) (Figure 1) was in monoclinic (2M) structure with almost single phase. Ce can be doped easily in the structure with its 20% concentration to keep zirconolite in its main 2M single phase. Unit cell parameters were calculated using JCPDS-PDF 84-0164 and refined parameters are given as: $a = 12.4440(2)\text{\AA}$, $b = 7.2699(4)\text{\AA}$, $c = 11.4222(4)\text{\AA}$, $\beta = 100.54(1)^\circ$. The obtained parameters are in accordance with the reported ones [4]. With the doping concentration of 20%, Ce³⁺ mostly gets substituted on Ca²⁺ site [2], favouring the zirconolite in 2M monoclinic phase, due to the incorporation of charge compensating ion Al³⁺ in the structure.

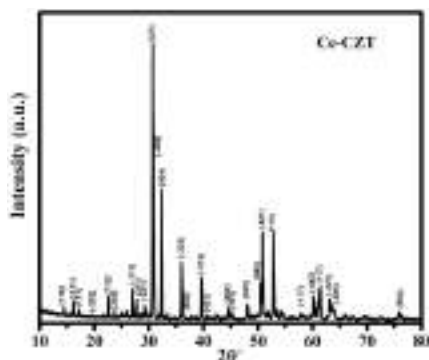


Figure 1. XRD pattern of $\text{Ca}_{0.8}\text{Ce}_{0.2}\text{ZrTi}_{1.8}\text{Al}_{0.2}\text{O}_7$ composition

4. Conclusions

The aim of this work is to design single phase waste form which remains crystalline under irradiation effects too. The XRD pattern showed that the Ce-doped zirconolite, $\text{Ca}_{0.8}\text{Ce}_{0.2}\text{ZrTi}_{1.8}\text{Al}_{0.2}\text{O}_7$ was in monoclinic (2M) phase. Zirconolite can accommodate Ce (20%) and retains its structural integrity.

References

- /1/ W.J. Weber, R.C. Ewing, C.R.A. Catlow, et al., J. Mater. Res. 13 (1998) 1434-1478.
- /2/ K. Zhang, G. Wen, D. Yin and H. Zhang, J. Am. Ceram. Soc., 99 [6] (2016) 1894-1901.
- /3/ B.M. Clark, S.K. Sundaram, S.T. Mixture, Scientific Reports.7 (2017) 5920.
- /4/ P. Pöml, T. Geisler, J. Cobos-Sabaté, et al., J. Nucl. Mater. 410 (2011) 10-23.

Surface Properties of Neutron-rich Thermally Fissile Nuclei at Finite Temperature

*Abdul Quddus¹, M. Bhuyan², ¹Shakeb Ahmad, and S. K. Patra^{*3,4}*

¹Aligarh Muslim University, Aligarh-202002, India

²Instituto Tecnológico de Aeronáutica - ITA, 12228-900, São José dos Campos, Sao Paulo

³Institute of Physics, Bhubaneswar-751005, India.

⁴Homi Bhabha National Institute, Training School Comple, Anushakti Nagar, Mumbai-400085, India

*E-mail: patra@iopb.res.in

1. Introduction and formalism

Apart from ^{233,235}U and ²³⁹Pu, Satpathy et al [1] predicted some neutron-rich U and Th thermally fissile isotopes, which have the efficiency in the yield more than that of known fissile nuclei. These nuclei may be a better fuel for the production of nuclear energy. For neutron-rich nuclei, the symmetry energy coefficient S_0 , neutron pressure P_0 , and nuclear incompressibility K_0 play crucial role to understand various phenomena such as heavy ion collision, supernovae explosion, neutron star and the fission properties of thermally fissile nuclei. The aim of our study is to calculate these surface properties for the neutron-rich thermally fissile U and Pu isotopes. Here, we have presented the results of ²⁵⁰U along with the known compound nuclei ^{234,236}U and ²⁴⁰Pu. To our knowledge, this is the first such calculation at finite temperature within the effective field theory motivated relativistic mean field (E-TRMF) approach using coherent density fluctuation method (CDFM).

It is worthy to mention that presently, the E-RMF theory is a well-defined approach, which is successfully used in almost all nuclear systems starting from finite nuclei to infinite nuclear matter [2]. Densities of the nuclei ^{234,236,250}U and ²⁴⁰Pu at finite temperature are calculated within E-TRMF model, which further used to calculate temperature dependent S_0 , P_0 and K_0 using CDFM by the relations [2]:

$$S = \int_0^{\infty} dx |f(x)|^2 S^{NM}(x), \quad P = \int_0^{\infty} dx |f(x)|^2 P^{NM}(x), \text{ and } K = \int_0^{\infty} dx |f(x)|^2 K^{NM}(x)$$

where $|f(x)|^2$ is the weight function. $S^{NM}(x)$, $P^{NM}(x)$, and $K^{NM}(x)$ are the temperature dependent symmetry energy coefficient, neutron pressure and incompressibility of infinite symmetric nuclear matter obtained within E-TRMF model.

2. Results and discussions

To see the predictability of the E-RMF model, we have compared the ground state properties obtained with various parameter sets (NL3, IOPB-I, FSUGarnet) with the experimental data. The binding energy per particle B/A , charge distribution radius R_{ch} and quadrupole deformation parameter β_2 for the known nuclei ^{208}Pb , $^{234,236}\text{U}$ and ^{240}Pu are shown in Table 1. From the table, it is clear that the obtained results are in excellent agreement with the data and give confidence enough to proceed further for the neutron-rich ^{250}U nucleus at finite temperature. The surface properties S_0 , P_0 and K_0 as a function of temperature T for the parameter sets are calculated. As a representative case, the results of S_0 obtained by IOPB-I are shown in Figure 1. From the figure, it is clear that the magnitude of S_0 is decreased almost monotonously with increase of T . Similar pattern obtained for the other quantities like P_0 and K_0 (which is not shown).

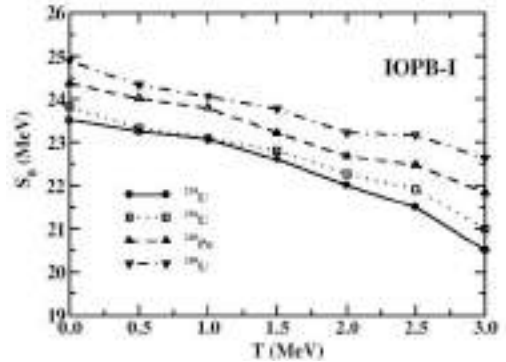


Figure 1. The S_0 of $^{234,236}\text{U}$, ^{240}Pu , and ^{250}U with IOPB-I parameter set.

Table 1. The ground state B/A , β_2 and R_{ch} for the nuclei corresponding to the parameter sets

Temperature	^{208}Pb			^{234}U			^{236}U			^{240}Pu			^{250}U		
	B/A	R_{ch}	β_2	B/A	R_{ch}	β_2	B/A	R_{ch}	β_2	B/A	R_{ch}	β_2	B/A	R_{ch}	β_2
FSUGarnet	7.88	5.55	0.00	7.60	5.84	0.20	7.57	5.86	0.22	7.56	5.91	0.24	7.41	5.95	0.22
IOPB-I	7.88	5.58	0.00	7.61	5.88	0.20	7.59	5.90	0.22	7.57	5.95	0.25	7.43	5.99	0.23
NL3	7.88	5.52	0.00	7.60	5.84	0.24	7.58	5.86	0.25	7.55	5.90	0.27	7.42	5.94	0.22
Experimental	7.87	5.50	0.00	7.60	5.83	0.27	7.59	5.84	0.27	7.56	5.87	0.29	-	-	-

In summary, we have investigated temperature dependent bulk and surface properties for $^{234,236,250}\text{U}$ and ^{240}Pu within E-TRMF models. After verifying the validity of E-TRMF model we proceeded for the study of temperature dependent surface properties of the thermally fissile ^{250}U . These properties are very sensitive to temperature, which may have consequences to energy production and astrophysical process.

The authors are thankful to B. K. Agrawal and Bharat Kumar for fruitful discussion. A Q would like to thank IOPB for their hospitality and DST for partial support.

References

- /1/ A. Quddus, K. C. Naik, and S. K. Patra, J. Phys. G: Nucl. Part. Phys. 45, 2018, 075102, and references therein.
- /2/ A. Quddus, M. Bhuyan, and S. K. Patra, to be communicated and references therein (Personal communication)

The Study of Natural Radioactivity Levels in Beach Sand Samples of Kollam, Kerala, India

Ramsiya M^{1}, Antony Joeph¹, Vishnu Prasad AK², Eappen KP³, Vishnu CV¹*

¹Department of Physics, University of Calicut, Kerala 673635, India

²Department of Physics, Fatima Mata National College, Kollam, Kerala, India

³Ex- BARC and Consultant, IEC - New Delhi

*E mail: ramsiyaashraf@gmail.com,

1. Introduction

Terrestrial radioactivity is mainly caused by primordial radionuclides such as ²²⁶Ra, ²³²Th and ⁴⁰K in various geological matrices. Primordial radionuclides are non uniformly distributed in Earth crust and some areas on Earth show high radioactivity. Preta and Dois Rios beach, Brazil, Southwest coast of India, Ramsar and Mahallat in Iran, Yangjiang in China [1] are well known high background radiation areas (HBRA). South-west coast of Kerala is enriched with monazite sand- a rich source of radioactive thorium, and uranium. The main objective of the present study is assessment of the primordial radionuclides and the radiological hazard parameters along the Coastal belt of Kollam district, Kerala.

2. Experiment

A total of 43 sand samples were collected from 5 locations along the coastal areas of Kollam district. The samples collected were then dried in an oven at 110 °C for 24 hours to remove the moisture content. The samples were then counted for gamma activity, for a period of 36000 seconds to get a reasonable area under the photo-peaks, corresponding to various gamma energies. HPGe detector (ORTEC, GMX10P4-70) having a relative efficiency of 21% with an energy resolution of 1.7 keV for 1.33 MeV peak of ⁶⁰Co was used for gamma ray spectrum analysis of the samples. The energy calibration was done using the ⁶⁰Co, ¹³⁷CS, ²²Na, and ¹³³Ba sources. The efficiency calibration of the system was carried out using the IAEA reference standard ore samples RGU-1, RGTh-1, taken in containers having same geometry as that of the samples. The activities of radium was estimated by measuring the area under the photo peaks of ²¹⁴Pb (351.9 keV) and ²¹⁴Bi (609.3 keV). The thorium

activity was determined from the ^{228}Ac (911.2 keV), ^{212}Pb (238.6 keV) and ^{208}Tl (583.2 keV) photo peaks. The ^{40}K was measured directly from the full energy photo peaks of 1460 keV.

3. Results and Discussions

The activity of ^{226}Ra , ^{232}Th and ^{40}K in the superficial beach sand obtained from the present study is listed in Table 1. Activity of ^{226}Ra and ^{232}Th in the analysed samples are higher than the worldwide population weighted average of 32 Bq/kg for radium and 45 Bq/kg for thorium. The radium equivalent activity values in all beach sand samples are higher than the recommended limit of 370 Bq kg⁻¹ [1]. The radiological hazard parameters like Absorbed dose rate, Annual effective dose rate, Radium equivalent activity, and External hazard index were estimated and presented in this table.

Table 1. Summary of the radionuclides concentrations and radiological parameters.

Location (No. of samples)	Radium (Bq/kg)	Thorium (Bq/kg)	Potassium (Bq/kg)	Absorbed dose rate (nGyh ⁻¹)	Annual effective dose rate (mSvy ⁻¹)	Radium equivalent activity (Bq/kg)	External hazard index
Neendakara Jyothi(8)	507±188	1311±598	151±32	1058±457	1.29±0.56	2394±1039	6.46±2.80
Neendakara(10)	513±226	1365±687	166±17	1094±533	1.34±0.65	2477±1209	6.69±3.26
Parimanam(5)	545±24	1570±998	148±10	1236±362	1.51±0.44	2801±834	7.56±2.25
Chavara ((10)	326±174	888±594	180±22	71±24	0.87±0.55	1609±1024	4.3±2.76
Chavara IRE(5)	204±108	933±343	175±13	390±222	0.47±0.27	877±504	2.36±1.36
Karithura(5)	1089±80	1818±837	363±52	1651±590	2.02±0.67	3715±1259	9.97±3.51

4. Conclusion

Natural radioactivity levels in sand samples along the coastal areas of Kerala, India was measured and the exposure rates have been estimated. The study reveals that the heavy mineral deposits confined in the coastal areas of Kollam district causes the enhanced radioactivity in beach sands. External hazard index values are greater than unity. This study indicates that beaches in Kollam district Kerala can be regarded as HBRA and a more elaborate radiometric study is required for a conclusive finding with respect to population dose and dose effects to humans in the living areas of HBRA .

References

/1/ UNSCEAR (2000) Sources and effects of ionising radiation, vol 1.

Gamma ray Irradiated Ni-Hesperidin Nanocomposite for Selective Trace Level Sensing of Sulfide Ions

*Zarina Ansari, Kamalika Sen**

92, A. P. C. Road, Department of Chemistry, University of Calcutta, Kolkata 700009, India
*E-mail: kamalchem.roy@gmail.com

1. Introduction

Hesperidin is a polyphenol commonly found in citrus fruits. Polyphenols are naturally occurring polyhydroxylated compounds which undergo tautomeric transformations to release reactive hydrogen atoms that can reduce metal ions to their nano states.[1] The role of γ -irradiation during nanoparticle (NP) formation is well established. It leads to faster production of these particles due to the formation of free radicals and solvated electrons generated by the virtue of radiolysis of water. Sulfide is one of the environmentally obnoxious ion at trace level, due to several health impacts including irritation of the mucous membranes, unconsciousness and respiratory paralysis. Out of many available techniques to measure the ion, spectral detection is preferred owing to its simplicity, sensitivity and selectivity.

In this work, hesperidin is used for the synthesis of nickel nanocomposites (NiNC). These particles were well characterized by several analytical techniques. A similar synthesis is repeated in presence of γ -irradiation. The NCs thus synthesised with and without irradiation was compared for their sensing ability towards the sulfide ions spectroscopically.

2. Experiment

For synthesis of NiNCs, 10 mL of 8 mM $\text{NiSO}_4 \cdot 6\text{H}_2\text{O}$ solution was added to 10 mL of hesperidin (set A). The solution was kept overnight at 40 °C. A similar set of solution was γ -irradiated for 24 h (set B). A γ radiation chamber with ^{60}Co source (obtained from BRIT, India) of strength 3.7 kCi and cylindrical sample chamber with diameter of 10.6 cm and height 14.2 cm was used for the irradiation (dose rate 2.249 kGy/h). For the sensing experiment aliquots of solutions containing various sulfur based anions (SO_4^{2-} , SO_3^{2-} , $\text{S}_2\text{O}_3^{2-}$, $\text{S}_2\text{O}_8^{2-}$ and S^{2-}) were added to the solution of NiNC to observe any spectral changes.

3. Results and Discussion

The results of sensing experiment reveal a prominent increase in the absorbance ($\lambda_{\text{max}} = 360 \text{ nm}$) only in presence of S^{2-} ions out of all the sulphur containing anions and that too only with the γ -irradiated NiNC solution (figure 1a). The linear range of detection was found to be 7-85 μM . The TEM image of NiNC shows spherical particles of diameter 5 nm (inset of figure 1a). The NiNC formation has been confirmed by FTIR spectral studies (figure 1b) together with a new peak at 760 cm^{-1} in the S^{2-} treated sample. The peak corresponds to a C-S stretching frequency. This behavior may be attributed to the enhancement of surface reactivity of the NCs in presence of γ -irradiations. Out of the five sulphur containing anions all others excepting S^{2-} are oxyanions, which are of bulkier disposition and S in positive oxidation state. S^{2-} being a smaller species with an available lone pair of electrons, show higher mobility to attack the hesperidin cage thereby showing selective sensing.

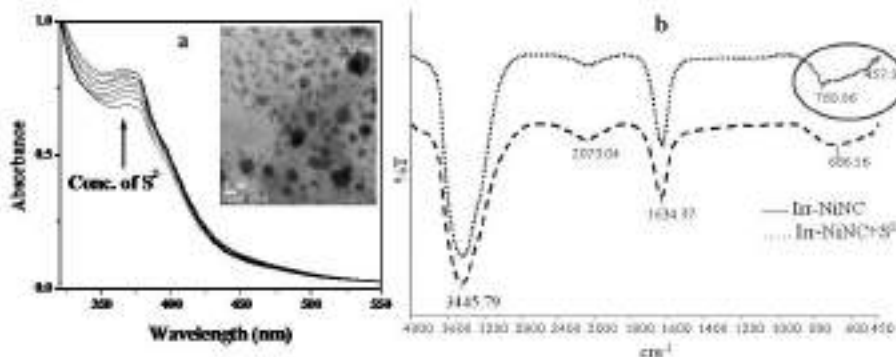


Figure 1. (a) Interaction of S^{2-} with irradiated NiNCs (TEM image inset) (b) FTIR spectrum of S^{2-} treated NiNCs

4. Conclusion

A simple approach for generating NiNCs was designed. The NiNCs were prepared in presence of γ -irradiation to obtain favorable spectral changes upon addition of trace S^{2-} ions out of a series of other sulphur containing anions. The proposed method is therefore apt for sensing sulfide ions.

Acknowledgement: ZA acknowledges CSIR SRF No:09/028(1022)/2118-EMR-I for funding.

Reference

/1/ V.V Makarov, A.J. Love, O.V. Sinitsyna, et al., Acta Naturae 6 (2014) 35

Radiation Dosimetry of ^{99m}Tc -DTPA-bis-choline based on Mice Data

Aruna Kaushik^{1}, Puja Panwar Hazari¹, Ambika Parmar Jaiswal¹, Anil K. Mishra¹*

¹Institute of Nuclear Medicine & Allied Sciences, Brig. S.K. Mazumdar Marg, Timarpur, Delhi 110054, India
*E-mail: kaushik_aruna@rediffmail.com

1. Introduction

^{99m}Tc -DTPA-bis-choline is a choline analog designed for the purpose of imaging neoplasms. Any novel radiopharmaceutical needs to be evaluated for associated radiation exposure. Accordingly, in the present study, we estimated the effective dose to humans from ^{99m}Tc -DTPA-bis-choline based on the bio-distribution data in mice.

2. Material and Methods

The biodistribution of ^{99m}Tc -DTPA-bis-choline was evaluated ex-vivo in balb-c mice (n=5 per group) by measuring the amount of radioactivity in excised organs. Absorbed dose was calculated using OLINDA software (Version OLINDA/ EXM 1.0, Vanderbilt University, USA) [1]. The software uses MIRD (Medical Internal Radiation Dose) method for calculation of doses from internally administered radiopharmaceuticals. The residence time in various source organs was calculated from the uptake studies and time-activity curves obtained for control and athymic mice. Relative organ-mass scaling method was used to obtain the corresponding values of residence times in humans [2]. This was used as input in the software to obtain the absorbed dose estimates.

3. Results and Discussion

The residence time of ^{99m}Tc -DTPA-bis-choline in control and athymic mice for ten source organs are shown in Table 1. The radiation dose estimates for a human weighing 70 kg are shown in Table 2. The highest absorbed dose was to osteogenic cells (0.012 mSv/MBq). The effective dose per unit administered activity was estimated to be 0.00467 mSv/MBq (4.67 mSv/GBq). This yielded an

estimated effective dose of 1.73 mSv to adult humans from 370 MBq intravenous administration of ^{99m}Tc -DTPA-bis-choline.

Table 1. Residence time (in hours) of ^{99m}Tc -DTPA-bis-choline for measured organs and rest of the body

Source Organs	Residence Time (h)	
	Control	Athymic
Heart	0.0017	0.0009
Lungs	0.0149	0.0062
Liver	0.0166	0.0808
Spleen	0.0080	0.0008
Kidney	0.0200	0.0088
Stomach	0.0019	0.0006
Brain	0.0010	0.0125
Muscle	0.1702	0.0240
Intestine	0.0076	0.0015
Bone	0.0175	0.0090
Rest of the Body	8.3990	8.5130

Table 2. Absorbed dose estimates of ^{99m}Tc -DTPA-bis-choline in humans determined from mice data

Target Organs	Absorbed Dose (mGy/MBq)
Adrenals	0.0052
Lower Large Intestine Wall	0.0061
Stomach Wall	0.0048
Upper Large Intestine Wall	0.0061
Heart Wall	0.0048
Kidneys	0.0040
Pancreas	0.0056
Osteogenic Cells	0.0124
Testes	0.0045

4. Conclusion

Radiation Dosimetry for ^{99m}Tc -DTPA-bis-choline was estimated for humans based on the distribution data in normal balb-c mice. These dose estimates can be used for planning human studies.

References

- /1/ M.G. Stabin, R.B. Sparks, E. J. Crowe. Nucl. Med. 46 (2005) 1023-1027
- /2/ R.B. Sparks, B. Aydogan. In International Radiopharmaceutical Dosimetry Symp., sixth edn. (1996), 705-716

The Radiation Dose and Distribution Coefficient of ^{210}Po and ^{210}Pb Concentrations in Aquatic Environs of Major Rivers of Coastal Karnataka

Rajashekara K M¹, Prakash V², Narayana Y³*

¹Department of Physics, S J C Institute of Technology, Chickballapur-562 101, India

²Department of Physics, Payyanur College, Edat, Kannur - 670327, India

³Department of Physics, Mangalore University, Mangalagangothri, D.K - 574199, India

*E-mail: km_rajashekar@yahoo.co.in

1. Introduction

Radioactivity present in surface waters is mainly due to the presence of radioactive elements in the earth's crust. Radioactive material released to the aquatic environment is transported and dispersed by advective and turbulent process occurring in the water body. Interactions between radionuclides and suspended matter and sediments may remove radionuclides from the solution [1]. In view of these to understand the distribution and accumulation of ^{210}Po and ^{210}Pb radionuclides in different matrices of the aquatic environments, radiation dose and distribution coefficient K_d are presented and discussed in this paper.

2. Materials and Methods

Standard techniques were followed in the collection of surface water, suspended particulate matter and sediment samples and the samples were collected from selected stations located at Kali, Sharavathi and Netravathi rivers of coastal Karnataka. Chemical deposition method was employed for the determination of ^{210}Po activity [2] and ^{210}Po and ^{210}Pb and counting the activity using a ZnS (Ag) Alpha counter.

3. Results and Discussion

3.1. ^{210}Po and ^{210}Pb activity in water, suspended particulate matter and sediments: The activity of ^{210}Po and ^{210}Pb were measured in different matrices of aquatic ecosystem of the major rivers of coastal

Karnataka. It is found that the activity of ^{210}Pb was higher than that of ^{210}Po in the riverine environs except the Kali and Netravathi River.

3.2. Dose due to Ingestion: The internal Committed Effective Dose (CED) to the population of the region due to ingestion of potable water is calculated from the measured activities of ^{210}Po and ^{210}Pb . The dose contribution was calculated using dose conversion factors from the International Commission on Radiological Protection and International Atomic Energy Agency for 1 L/day water consumption. The mean value of dose rate due to ingestion of ^{210}Po in river water was varied from 0.2-0.4 mSv y^{-1} and in ^{210}Pb it varies from 0.2-0.3 mSv y^{-1} . A dose rate between 0.2 to 0.8 mSv y^{-1} is the typical worldwide range of ingestion radiation dose resulting from water as well as food [3].

3.3. Distribution coefficients, K_d : The distribution coefficient K_d between water, suspended particulate matter and sediment have been calculated for the understanding of distribution and accumulation of these radionuclides in different matrices of the aquatic environment. High K_d values for ^{210}Po and ^{210}Pb indicated that there is a strong adsorption of these nuclides onto suspended particles in aquatic systems comprising of freshwater, estuaries and marine environments.

4. Conclusion

The biogeochemical processes and characteristics of particles in surface waters may play a significant role on the distribution of ^{210}Pb and ^{210}Po . The presence of ^{210}Pb and ^{210}Po in surface water is due to the deposition from atmosphere and leaching from sediment, soil and rock. The effective dose due to intake of river water exceeds the limit recommended by International Commission on Radiological Protection and International Atomic Energy Agency (0.1 mSv y^{-1}). Consequently, K_d values for ^{210}Pb and ^{210}Po were decreased with increasing total suspended matter.

5. References

- /1/ UNSCEAR, Sources and effects of ionizing radiation. New York., United Nations(2000).
- /2/ M.A.R. Iyengar, S. Ganapathy, S.V. Kannan, et al., Procedure Manual, Workshop on Environmental Radioactivity, held at Kaiga., India. 1990, 16 -18 April.
- /3/ <http://www.dwaf.gov.za/iwqs>

Rapid, Simultaneous Analysis of Anthropogenic and Naturally Occurring Radionuclides in Seawater

Sugandhi Suresh^{1}, Sonali P.D. Bhade², Vandana A. Pulhani¹, R M Tripathi¹*

¹Health Physics Division, ²Radiation Safety Systems Division, Bhabha Atomic Research Centre, Mumbai-400085, India

*E-mail: sugandhi@barc.gov.in

1. Introduction

Radiation and radioactivity in the environment is due to the natural and anthropogenic origin. The main source of natural radioactivity is ⁴⁰K, radionuclide of uranium and thorium decay series. The anthropogenic sources of radioactivity in the environment, at global level, are due to the atmospheric nuclear weapon testing and nuclear accidents [1]. Nuclear accident does not usually occur, but when it happens it poses worldwide environmental concern. Hence, there is an urgent need of developing fast and reliable analytical methods to meet the emergent scenario since the conventional radiochemical methods are found to be laborious and time-consuming. The present study aims to develop a robust methodology for measurement of anthropogenic (⁹⁰Sr) and naturally occurring uranium radionuclides in seawater. The solvent extraction method using tributylphosphate (TBP) as an extractive reagent along with the Pulse Shape Analysis (PSA) Liquid Scintillation Counting (LSC) system is standardized for the trace detection of these radionuclides.

2. Experiment

2.1 Solvent Extraction Method: Standardisation of the solvent extraction method was done by spiking simulated seawater with ⁹⁰Sr/⁹⁰Y along with uranium standards in quadruplicate samples and only uranium standard in another set of quadruplicate sample. Based on this method, the separation and analysis of Nat.U and ⁹⁰Sr was carried out in field sea water samples. Ten numbers of sea water samples (10L each) were equilibrated with stable carriers of yttrium and iron. Fe(OH)₃/ Y(OH)₃ was precipitated and the supernatant was discarded thus eliminating the interfering alkali and alkaline earth metals. The precipitate was dissolved in 1:1 HNO₃ and dried. The residue was taken in 10 M HNO₃ and extracted with TBP thrice.

The aqueous phase was discarded. The organic phase (TBP extractants) was combined and counted for the activity concentrations of ^{90}Sr (via ^{90}Y) and Nat.U using Quantulus 1220 LSC with PSA technique for discriminating alpha and beta particles.

2.2 Conventional Radiochemical Method: Ten simulated sea water samples (10 L each) were analysed for Nat.U, ^{90}Sr by conventional radiochemical method to compare results obtained by solvent extraction method and counted using Gas Flow Beta Counter (GFBC) and Alpha Spectrometer (AS).

3. Results and Discussion

Table 1 summarizes the measured activity concentrations of Nat.U and ^{90}Sr in simulated seawater samples. The measured activity concentration of Nat.U and ^{90}Sr in the combined TBP extractants (organic phase) and by conventional methodology are in close agreement.

Table 1. Activity concentrations of Nat.U and ^{90}Sr in seawater

Sample code	Nat. U (mBq/L)		^{90}Sr (mBq/L)	
	LSC	AS	LSC	GFBC
SW1	109.0±5.5	110.0±2.5	9.9±0.9	9.5±1.0
SW2	93.5±4.7	100.1±2.3	12.0±1.2	10.3±1.1
SW3	70.1±3.5	65.2±2.0	11.5±1.1	11.9±0.7
SW4	75.4±3.8	83.3±1.5	11.3±1.1	12.0±0.9
SW5	74.6±3.7	70.5±1.2	9.3±0.9	9.8±0.9
SW6	72.3±3.6	70.1±1.2	4.0±0.5	5.5±0.6
SW7	112.8±5.6	123.6±2.5	11.5±1.2	10.5±1.0
SW9	74.5±3.7	75.4±2.0	7.8±0.8	7.5±0.8
SW10	83.2±4.2	88.2±1.5	11.1±1.1	11.2±1.0

4. Conclusion

Conventional method for Nat.U and ^{90}Sr estimation in seawater is time consuming and laborious. The measured activity of Nat.U and ^{90}Sr in the combined TBP extractants is similar to that estimated by conventional method. Hence, TBP extractants alone can be taken up for analysis. The interferences due to natural ^{40}K and anthropogenic ^{137}Cs , ^{226}Ra and ^{228}Ra are eliminated by the step involving $\text{Fe}(\text{OH})_3$ precipitation which simultaneously provides the advantage of pre-concentration of radionuclides of interest. Simultaneous measurement of Nat.U and ^{90}Sr by solvent extraction method followed by counting by LSC with PSA technique is relatively faster and simpler that suffice the emergency scenario. The procedure can be further modified to separate any other transuranic elements if present.

References

/1/ N. Casacuberta, P. Masqu , J. Garcia-Orellana, et al., Biogeosciences 10(6) (2013) 3649-3659

Low Specific Activity ^{64}Cu ions – Bio-marker for Melanoma

A. Gopalakrishna^{1,7}, S. Chakraborty², A. Chakraborty³, Y. Pawar³, B. Mohanty⁴,
M. Tawate³, K. V. Vimalnath², R. Chakravarty², S. Banerjee^{3,7,*}, B. K. Nayak^{5,7},
S. V. Suryanarayana⁵, H. Naik⁶, P. C. Chaudhari⁴, A. Kumar¹, P. Maletha³,
Kamaldeep^{3,7}, A. Dash^{2,7}

¹Medical Cyclotron Facility, Board of Radiation and Isotope Technology, Mumbai 400012, India,

²Radiopharmaceuticals Division, Bhabha Atomic Research Centre, Mumbai-400085, India,

³Radiation Medicine Centre, Bhabha Atomic Research Centre, Mumbai 400 012, India,

⁴Advanced Centre for Treatment and Research in Cancer, Navi Mumbai 400706, India,

⁵Nuclear Physics Division, Bhabha Atomic Research Centre, Mumbai 400085, India

⁶Radiochemistry Division, Bhabha Atomic Research Centre, Mumbai 400085, India

⁷Homi Bhabha National Institute, Mumbai 400094 India

*E mail: sharmila@barc.gov.in

1. Introduction

Melanoma is the most aggressive type of skin cancer and is diagnosed in ~100,000 patients worldwide. $^{64}\text{CuCl}_2$ has been identified as a potential theranostic agent for using the human copper transporter 1 (hCTR1) as a molecular target, overexpressed in many types of cancer cells, including melanoma, prostate cancer. Radionuclidic characteristics of ^{64}Cu (EC 43.8%, β^+ 17.8%, β^- 38.4%) and $T_{1/2}$ of 12.7 h, enable its utilization as a PET diagnostic and as a therapeutic agent. Since CTR1 has been found to mainly and specifically transport Cu(I) instead of Cu(II) [1], this study aims to compare the biological efficacy of ^{64}Cu as $^{64}\text{Cu(I)Cl}$ and $^{64}\text{Cu(II)Cl}_2$, in C57BL/6 mice bearing melanoma tumors in a B16F10 tumor model.

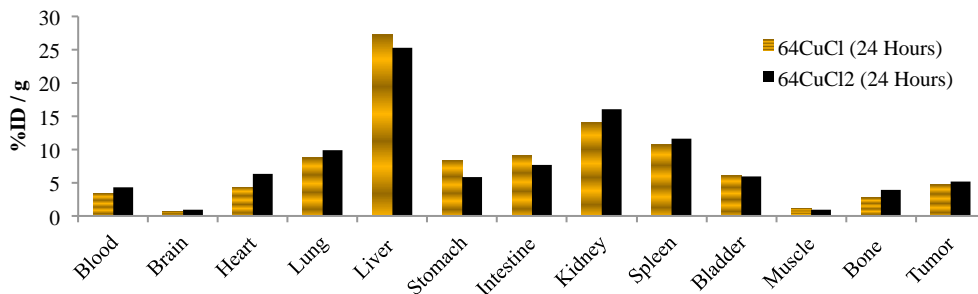
2. Materials and methods

LSA ^{64}Cu was prepared in the Dhruva research reactor, BARC, India via $^{63}\text{Cu}(n, \gamma)^{64}\text{Cu}$ and procured in the form of $^{64}\text{Cu(II)Cl}_2$ solution. $^{64}\text{Cu(I)Cl}$ was prepared by adding $^{64}\text{Cu(II)Cl}_2$ with Vit C [2]. Mouse melanoma cell line B16-F10 (C57-BL6 mice origin) was obtained from the National Centre for Cell Sciences (Pune, India). For developing tumor model, the cells were subcutaneously injected in C57-BL6 mice at 5×10^5 cells/ mice in 200 μl PBS. Tumors were allowed to develop for 15 days until they reached a volume of 100 mm^3 , when bio-distribution experiment was initiated. Anesthetized

B16F10 tumor-bearing mice ($n = 4$) were injected with approximately 3 MBq via the tail vein. The animals were sacrificed by cardiac puncture 24 hours post-anesthesia post-injection (p.i.). Various organs, tissues, and tumors were excised after sacrifice, and the weight of each organ and tumor was also determined by using an analytical balance. The radioactivity associated with each organ and tissue was determined with a NaI(Tl) counter. Figure 1 shows the biodistribution data.

3. Results and Discussion

The tumor uptake of LSA $^{64}\text{Cu}(\text{II})$ and $^{64}\text{Cu}(\text{I})$ was 5.14 ± 0.52 and 4.71 ± 0.56 % injected dose / g (ID/g) at 24 hours post injection. This is comparable to the tumor uptake of high specific activity $^{64}\text{Cu}(\text{II})$ and $^{64}\text{Cu}(\text{I})$ as 6.56 ± 0.61 and 5.95 ± 0.24 % ID/g respectively, in B16F10 tumor-bearing mice at 24 hour post injection [2]. Figure 1 shows no significant difference in biodistribution between $^{64}\text{Cu}(\text{I})$ and $^{64}\text{Cu}(\text{II})$. This could happen because of the dilution of Vit C, and oxidation reaction under physiological conditions resulting in the quick changing from Cu(I) to Cu(II) *in vivo*[2]. Both $^{64}\text{CuCl}_2$ and $^{64}\text{CuCl}$ displayed high tumor-to-muscle ratios and small uptake in brain. The biodistribution data indicated that $^{64}\text{CuCl}_2$ and $^{64}\text{CuCl}$ were excreted through both the liver and kidneys.



4. Conclusion

The comparable tumor uptake of LSA ^{64}Cu ions to no carrier added ^{64}Cu ions would lower the cost of molecular imaging. Targeted radionuclide therapy of melanoma remains an underdeveloped field [3]. The concept of personalized medicine and targeted radionuclide therapy has gained clinical acceptance and the assured supply and availability of theranostic isotope ^{64}Cu will aid in the same.

References

- /1/ Igor *et al.* An all-atom model of the structure of human copper transporter Cell biochemistry and biophysics 63, 223–234, (2012).
- /2/ Jiang *et al.* Pilot Study of $^{64}\text{Cu}(\text{I})$ for PET Imaging of Melanoma Scientific Reports 7: 2574, (2017)
- /3/ A. Norain, E. Dadachova. Semin Nucl Med 46:250-259 (2016)

Comparative Uptake Study of Cesium on Encapsulated Nano Magnetites

Joyeeta Mukherjee^{1*}, Pranesh Sengupta²

¹Health Physics Division, BARC, Mumbai, India

²Material science Division, BARC, Mumbai, India

*E-mail: joyeeta@rrcat.gov.in

1. Introduction

Radioactive cesium is one of the major radiation hazardous nuclide present within high-level and low level wastes. The environmental threat originates due to its easy transportability via the environment, moderate half life ($t_{1/2}$ of ^{137}Cs ~30.4yrs), and high solubility in water as a consequence of high mobility within aqueous media [1]. The reusability, quickness, simple and reliable procedure of synthesis, low consumption of solvent, physically amenable and generation of less or practically no secondary waste make sorption a more favorable option for effective uptake study. In the present work three different nano magnetite viz. bare magnetite, oleic acid coated hematite-magnetite composite material and silica coated magnetite have been used for cesium (I) sorption. Magnetite nanomaterials have been chosen for the present study mainly because of their easy separation and separation of sorbed materials by a strong magnet so that production of secondary waste could be minimized as well as clumsy procedure of filtration and other steps has been minimized as well as encapsulation by long chain fatty acid and silica enhances the magnetites stability and sorption capacity.

2. Materials and method

In the present study, nano magnetite was prepared via co-precipitation route [2].

3. Result and Discussion

Effect of pH and initial concentration on Cs (I) uptake study: Sorption behaviour of cesium on to all these three magnetites at different pH has been shown in Figure 1. The detection of cesium was carried out by Atomic Absorption Spectroscopy (AAS) method. It shows at pH 5, maximum value (99%) of

sorption efficiency for Cs(I) ion takes place by magnetite, after that uptake slightly decreases (90%) in neutral to alkaline medium of pH range 6-10, after that sorption nearly remaining a constant because in all pH range the cesium remains as Cs(I) ion in solution [3]. The effect of Cs(I) concentration on sorption was investigated and the comparative results are shown in figure 2. The sorption capacity of the three magnetite based nanomaterials for cesium ions was determined, by studying the sorption as a function of cesium ion concentration, at 300 K, in a batch mode experiment. The concentration of inactive cesium ions in the aqueous solution was increased from 10 mg/L to 100 mg/L, and the q_e , maximum sorption capacity was determined. It was observed that, q_e increases gradually with increase in cesium ion concentration, and reaches a saturation value. The initial concentration provides an important driving force, to overcome all the mass transfer resistances to the Cs(I) ions between the aqueous and the solid phases. Therefore, a higher initial Cs ion concentration will enhance the sorption process. Magnetite encapsulated with silica, having high gradient magnetic separation [4], and more stable sorption sites from silica surface shows the best sorption capacity among the others.

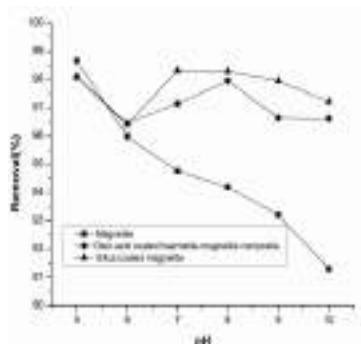


Figure 1. Effect of pH on percentage removal

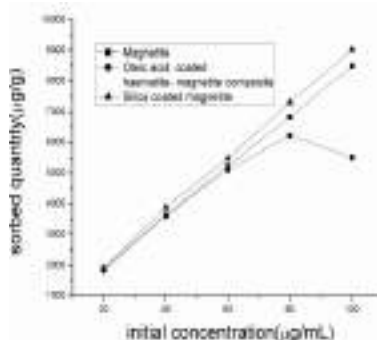


Figure 2. Effect of initial concentration on sorbed Cs (I) quantity

References

- /1/ Md. R. Awwal, T. Yaita, Y. Miyazaki, et al., Scientific Reports 6 (2016) 19937.
- /2/ S. Laurent, D. Forge, M. Port, et al., Chem. Rev. 108 (2008) 2064
- /3/ Y.Park, Young Chae Lee, et al, Chem Eng 162 (2010) 685
- /4/ A. D. Ebner, J. A. Ritter, J. D. Navratil, Ind. Eng. Chem. Res., 40 (2001) 1615

Study of The Dependence of Evaporation Residue Cross Section on Incident Channel Parameters

K Hajara^{1}, M M Musthafa¹*

¹Department of Physics, University of Calicut, Kerala, India, 673635.

*E-mail: khajara3@gmail.com

1. Introduction

The study of nuclear reaction dynamics in heavy-ion-induced collisions is a topic of intense research now-a-days. When two heavy ions scatter off each other many new reaction channels become possible since they impart large amount of energy and angular momentum. The fission fragment angular distribution measurements, the fission fragments mass distribution measurements, precession neutron multiplicity measurement, evaporation residue crosssection measurement, etc., are the important methods for the study of the non compound nuclear processes. The results of each of these methods vary very significantly for many of the reactions with the same compound nucleus (CN), with the same energy and angular momentum formed through same entrance channel.

In the preactinide region, i.e., in the less fissile systems, sensitivity of the fission-fragment angular distributions to the contribution from non compound nuclear (NCN) fission is reduced as angular anisotropy becomes high even for CN fission and the difference in angular anisotropy for CN and NCN fission decreases [1]. This is due to the fact that fission mainly results from higher l waves. In this mass region, evaporation residues would be a better probe to investigate the fusion hindrance. In this work the variation of ER Cross section for different parameters like entrance channel mass asymmetry, Coulomb repulsion, deformation, incident channel kinetic energy, compound nuclear spin, compound nuclear fissility, etc., have been studied for the exact prediction of the dependence of the compound and non compound nuclear reactions on these parameters.

1.1 Evaporation Residue Cross section: Evaporation Residue (ER) Cross section measurements can be used as a very sensitive probe to understand the reaction dynamics of a compound and non compound nuclear reactions. The total expression of the evaporation residue cross-section is generally assumed to be a combination of three factors which can be mathematically represented as:

$\sigma_{ER}(E_{cm}) = \sigma_{capture}(E_{cm})P_{CN}(E_{cm})P_{survival}(E_{cm})$, where $\sigma_{capture}$ is the capture cross-section for the formation of the di-nucleus system and E_{cm} is the entrance channel kinetic energy of the system in the centre of mass, P_{CN} is the probability of complete fusion of the di nuclear system to form the compound nucleus[2]. In systems prone to quasi-fission, the probability of complete fusion (P_{CN}) is reduced considerably and this results in suppression of ER cross-section. This suppression of measured ER cross-section (in comparison with respective statistical model calculation) is treated as an evidence of quasi-fission. The theoretical ER cross section have been measured using the statistical model code PACE4.

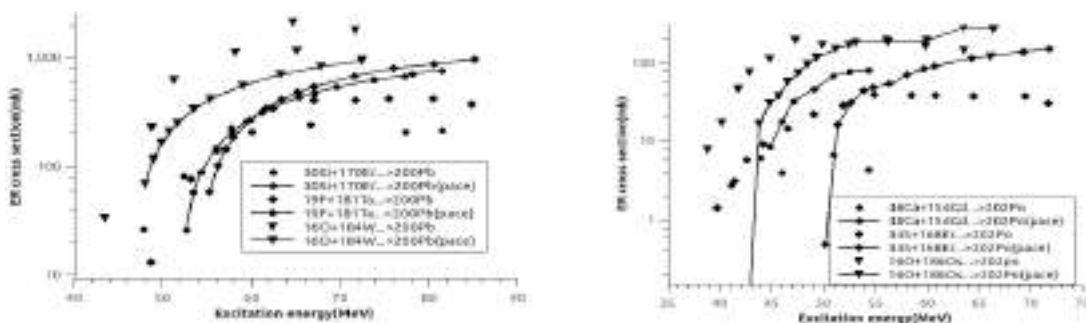


Figure 1. Plot of ER cross section of ^{200}Pb and ^{202}Po compound nucleus formed through different channels.

2. Result and Discussion

Measurement of the ER cross section of these systems shows that it strongly depend on Z_1Z_2 , mass asymmetry of the incident particle, deformation of the incident channel or the compound system formed, spin of the compound nucleus, shell closure of both the incident particle and compound system formed and the compound nuclear fissility etc. A comparable reduction of the ER cross section from the theoretical prediction shows the deviation of the system from the compound nuclear formation. The exact cause for this deviation is not restricted to a single parameter. The variation of two or more parameters together are responsible for this behavior.

References

- /1/ K. Sudarshan, R. Tripathi, S. Sodaye, et al. Phys. Rev. C 95, (2017) 024604
- /2/ T. Banerjee, S. Nath, S. Pal, Phys. Rev. C 91, (2015) 034619

ED-XRF Analysis of Some Herbs Used to Cure Respiratory Diseases in Ayurvedic Treatment

*S. Ibrahim¹**, *M. M. Musthafa¹*, *K. P. Binsiya¹*

Department of Physics, Calicut University

*E-mail: rv.salma@gmail.com

1. Introduction

Energetic X-Ray beams can be used as probes to characterize materials with high resolution. X-ray Fluorescence (XRF) is an important technique for qualitative and quantitative analysis elements in different matrices as it allows rapid multi-elemental characterization of materials in solid or liquid form with high-detection sensitivities. Fingerprints of the probed material can be generated which can be used for standardization and quality evaluation. In the present work, EDXRF method has been used for trace element (TE) analysis of herbs used as drugs to cure respiratory diseases.

2. Experiment

Fresh samples of the herbs were collected from authentic sources. The samples were washed, dried, ground into fine powder and made in to pellets. List of herbs studied are shown in the table 1. XRF measurements were performed using XEPOS ED-XRF spectrometer at Calicut University.

Table 1. Sample details

SI No	Botanical Name	Common Name	Part Selected
H1	<i>Cinnamomum tamala</i>	Elavangam	Leaves
H2	<i>Piper longum</i>	Thippali	Fruit
H3	<i>Piper nigrum</i>	Kurumulaku	Fruit
H4	<i>Elettaria cardamomum</i>	Elam	Fruit
H5	<i>Cinnamomum zeylanicum</i>	Karuvappatta	Stem bark

3. Results and Discussion

Elemental profiles of the five samples are plotted in Figure 1. Concentration of each particular element present in all the five samples is compared. It shows wide variation of trace elemental concentration in

different herbs used. Heavy metal pollutants like Arsenic, Lead and Mercury are less than the allowable limit in the samples. Hooker et al. reported that Cr, Mg, Zn have important role in the metabolism of cholesterol [1]. The presence of Cr and Mn in plants may be correlated with the therapeutic properties against diabetics and cardio vascular diseases [2].

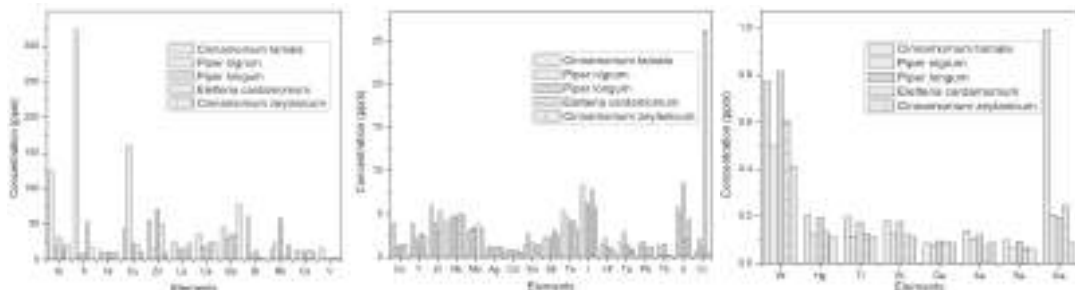


Figure 1. TE profile comparison of the samples

4. Conclusion

The concentrations of trace elements in five medicinal herbs used for treatment of respiratory diseases are determined by EDXRF technique. It was observed that, of all the elements present, concentration of K and Ca is highest in H2. H1 was found to contain significantly high concentration of Ti and Ga when compared to other samples. Cr is found to be present with a significant concentration in H4. Cu concentration is the highest in H2. Ranges of elemental concentrations have been found to vary widely. The TE profiles can be used to produce a fingerprint of a particular plant part which further can be used in standardization of herbal formulations.

Acknowledgement: The authors thankfully acknowledge CSIF, University of Calicut for providing the EDXRF facility.

References

- /1/ J. D. Hooker, The Flora of British India Vol. III (1982) 640.
- /2/ S. Ahmed, A. Rehman, M. Qadiruddin, Y. Badar, J. Fac. Phar., 2 (1994) 83–90

Environmental Impact of Natural Radioactivity in Soil and Groundwater of a Uranium Mineralized Zone of Indian Himalaya

Mukesh Prasad^{1}, G. Anil Kumar¹, R. C. Ramola²*

¹Department of Physics, Indian Institute of Technology Roorkee, Roorkee - 247 667, India

²Department of Physics, H.N.B. Garhwal University, Badshahi Thaul Campus, Tehri Garhwal - 249 199, India

*E-mail: bijalwanmukesh111@gmail.com

1. Introduction

People are always exposed to natural radiation, which is mainly due to the activity of natural radionuclides: ^{238}U series, ^{232}Th series and ^{40}K present in the earth's crust, in building materials, air, water, food and the human body. Therefore, understanding of the distribution of these radionuclides in soil, rocks and water is important from radiation protection point of view. In addition, the distribution of natural radionuclides plays an important role in geo scientific research and in establishing guidelines for the use and management of these materials. In this study, natural radioactivity measurements in soil/rocks and groundwater of a well-populated uranium mineralized zone of Himalayan region located in Uttarakhand state of India were carried out for radiation protection purpose.

2. Materials and methods

The activity concentrations of ^{226}Ra , ^{232}Th and ^{40}K were measured using a low level NaI(Tl) gamma ray spectrometer system. The activity levels of radon in groundwater samples were measured using semiconductor detector based RAD7 and scintillation detectors based RnDuo monitors. The measurements of uranium in groundwater were done using LED Fluorimetry and ICP MS techniques.

3. Results and Discussion

The descriptive statistics of ^{228}Ra , ^{232}Th and ^{40}K levels and associated hazard assessment quantities are given in the Table 1. A considerable number of locations were found to have radiation level higher

than the reference values recommended by United Nations Scientific Committee on Effects of Atomic Radiation (UNSCEAR).

TABLE 1. Activity levels of primordial radionuclides and associated hazard assessment quantities

	Activity levels of ^{228}Ra , ^{232}Th and ^{40}K (Bq kg^{-1})			Hazard assessment quantities				
	^{228}Ra	^{232}Th	^{40}K	Ra_{eq}	H_{ex}	H_{in}	γ Index	α Index
Min	34.2 ± 4.43	28.7 ± 9.3	15.2 ± 3	146	0.40	0.49	0.54	0.17
Max	229 ± 23.4	295 ± 29.5	1360 ± 194	599	1.62	2.06	2.08	1.15
AM	97	129	541	322	0.87	1.13	1.15	0.48
Median	92	115	478	307	0.83	1.10	1.09	0.46
GM	87	119	365	306	0.83	1.07	1.09	0.43
SD	45	51	389	109	0.29	0.39	0.38	0.22

The dose estimated using soil radioactivity was found in good agreement with the ambient dose measured using portable survey meter (Fig 1). The levels of radon and uranium were also found higher than the respective safe limits recommended by USEPA and WHO. An inter comparison exercise made between results of uranium measurements obtained using LED fluorimeter were inter compared with ICPMS for quality control purpose shows a good agreement between the two techniques (Fig 2).

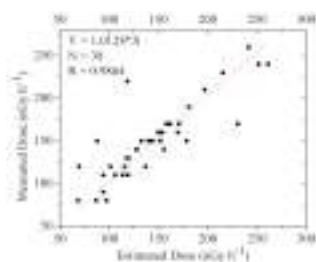


Fig 1: Correlation between γ - absorbed dose rate measured by portable survey meter and estimated from soil radioactivity

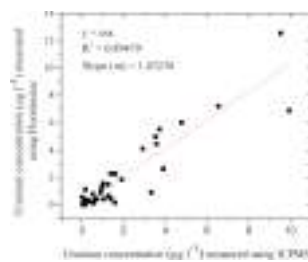


Fig 2: Inter-comparison of results obtained using LED fluorimetry and ICPMS for quality control purpose

4. Conclusion

Natural radioactivity levels in soil, groundwater and associated health risk values exceed safe limits at majority of locations. The results are useful in radiation protection, geo scientific research and in establishing guidelines for the use and management of these materials.

References

/1/ WHO (World Health Organization) (2004) Guidelines for drinking water quality. World Health Organization, Geneva

Identification of Radionuclides Found in Deflector Cleaning Waste of K-130 Cyclotron

K.Srihari¹, Kousiki Ghosh Jana, Mausumi Sengupta Mitra, R.Ravishankar, Tapas Bandyopadhyay*

¹HBNI -VECC, 1/AF, Salt Lake, Kolkata 700064, India

* E-mail: ksrihari@vecc.gov.in

1. Introduction

The accelerated ion beam has to be extracted from its trajectory and diverted into the beam line by deflector. The high potential given to the deflector, at the beam extraction part so that the charged particles trajectory changes from circular path and enter into the deflector. The high energy beam causes activation of deflector material. This enhances the radiation exposure levels to radiation workers during deflector maintenance work. The maintenance of deflector causes generation of radioactive waste. In the present study the swipe samples were collected from the deflector base plate and identification of radionuclides were performed by gamma spectroscopy analysis, with HPGe detector. K-130 cyclotron, VECC, Kolkata is a positive ion accelerator which delivers ^1H , ^4He beam and heavy ion beams to users. The identification of isotopes is important from radioactive waste management point of view.

2. Materials and Methods

The analysis of the swipe samples was done with the HPGe detector. The HPGe is 30% Relative Efficiency and with bias +2500V is used for gamma spectrometry. The resolution of the detector is 2.4 KeV at 1.332 MeV of gamma. The calibration of the detector is done with EU-152, Co-60, Cs-137 standard source and the calibration factor determined. The background spectrum and the sample spectrum are measured with HPGe detector assembly system. The resultant spectrum of swipe sample was given in the Figure 1.

The data after subtracting background gives the contribution of the swipes, which gives the net activity present in the sample. The deflector is made of inconal alloy with the typical composition of Cu, Fe, Cr, Ni, Si, C, and Mn.

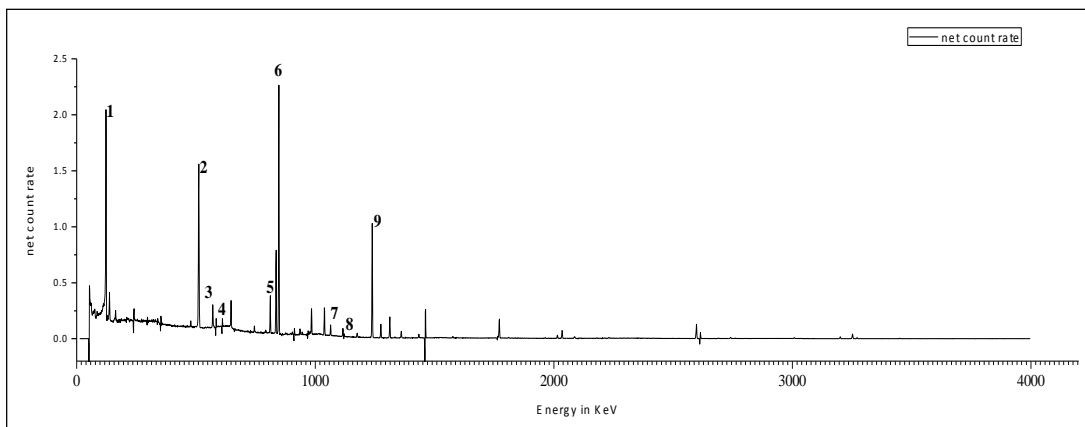


Figure 1. Swipe sample spectrum with identified peaks

3. Results

The Analysis of swipe samples done with HPGe detector and identification of induced isotopes in the deflector assembly system of K-130 cyclotron done.

Peak number	Isotope	Half life	Production mode
1	⁵⁷ Co	271.79 d	${}^4\text{He} + {}^{58}\text{Ni} \rightarrow {}^{57}\text{Co} + {}^4\text{He} + {}^1\text{H}$
2	¹⁸² Os	22.10 h	-
3	¹⁸⁵ Os	93.6 d	${}^4\text{He} + {}^{182}\text{W} \rightarrow {}^{185}\text{Os} + {}^1\text{n}$
4	⁴⁹ V	330 d	${}^1\text{H} + {}^{52}\text{Cr} \rightarrow {}^{49}\text{V} + {}^4\text{He}$
5	⁵⁸ Co	70.86 d	${}^4\text{He} + {}^{58}\text{Ni} \rightarrow 3{}^1\text{H} + {}^1\text{n} + {}^{58}\text{Co}$
6	⁵⁶ Co	77.27 d	${}^4\text{He} + {}^{58}\text{Ni} \rightarrow {}^4\text{He} + {}^1\text{H} + {}^1\text{n} + {}^{56}\text{Co}$
7	⁶⁸ Ga	67.629 m	${}^4\text{He} + {}^{65}\text{Cu} \rightarrow {}^1\text{n} + {}^{68}\text{Ga}$
8	⁶⁵ Zn	244.26d	${}^4\text{He} + {}^{63}\text{Cu} \rightarrow {}^1\text{H} + {}^1\text{n} + {}^{65}\text{Zn}$
9	^{131m} Te	30 h	-

4. Conclusion

The half-lives are varying from minutes to days. The Maximum half-life of the radionuclide present is 330 days. Necessary safety procedures to be followed during maintenance. The waste generated in deflector maintenance has to be stored for minimum 2-3 years period so that the activity levels reduced to background levels.

High Dose Gamma Irradiation Effect on The Properties of Copper Nanowires

R P Chauhan, Pallavi Rana, Suresh Panchal, Chetna Narula*

Department of Physics, National Institute of Technology, Kurukshetra-136119, India
*Email: chauhanrpc@gmail.com

1. Introduction

In the realization of future integrated-circuit interconnects, copper is the best-chosen material, as it is more abundant and less expensive than other metals. The devices based on nanowires are also affected by the irradiation. The present study has been carried out to investigate the influence of high dose of gamma rays on the structural and transport properties of copper nanowires of 80 nm diameter.

2. Experiment

2.1. Materials and method: A two-electrode electrochemical cell was used in electrodeposition that was poured with an aqueous solution of 1M $\text{CuSO}_4 \cdot 5\text{H}_2\text{O}$. Conducting copper tape worked as a cathode and a copper rod acted as anode. At room temperature, the experiment was carried out for 15 min at an applied potential of 0.35V. After the deposition, the electrolyte was drained out and the samples were removed from the cathode and cleaned.

Exposure parameters: Copper nanowires of 80 nm diameter were exposed to gamma rays using Co-60 source at the IUAC, New Delhi, India from doses 250-450 kGy. Pre- and post-irradiated samples were characterized with SEM, XRD, and with two-probe set up assisted by Keithley source meter.

3. Results and Discussion

SEM images of the copper nanowires showed their array of cylindrical shape (Figure 1(a)). The images revealed the uniform and homogenous growth of nanowires of identical diameter equal to the diameter of the pores of the template. The images of post irradiated samples were also recorded which confirmed no damages in the polycrystalline nanowires as shown in figure 1(b). The structural properties of the nanowires were examined by XRD using CuK_α radiation before and after gamma irradiation. The miller

indices of planes observed in the XRD pattern matched with the standard JCPDS cards-04-0836 of copper. When XRD spectra of post-irradiated nanowires were compared with the pristine, no shifting in the '2 θ ' position was observed. There was no significant intensity variation found up to 200 kGy.

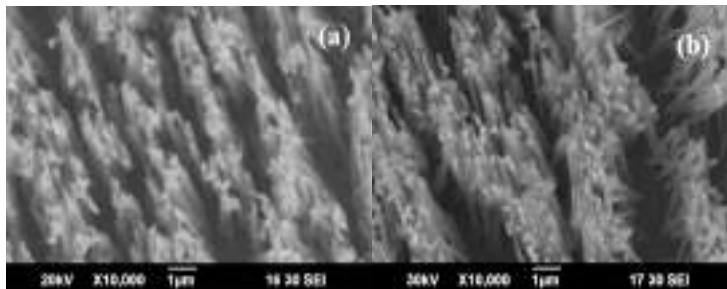


Fig 1: SEM Images of (a) pre- (b) post- irradiated copper nanowires

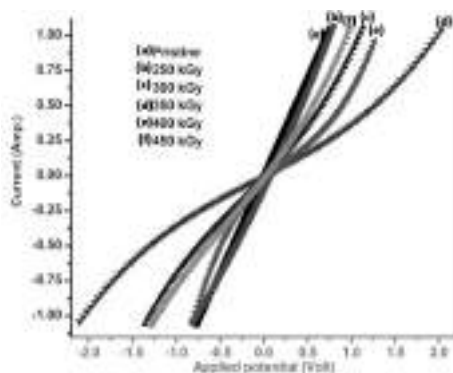


Fig 2: Polynomial fitted I-V graph of pristine and gamma irradiated copper nanowires

I-V characteristics of pre- and post-irradiated nanowires were drawn using a two-probe set-up, shown in figure 2. In case of post-irradiated nanowires from 250 kGy, the I-V characteristics appear to be drastically affected. Herein, the first impression from the I-V graphs comes out to be variations in the electrical conductivity of irradiated nanowires with gamma dose. At low gamma doses the conductivity of the nanowires increased while it decreased for higher doses..

4. Conclusion

The gamma rays induced changes in the granular properties of copper nanowires. The combined facet of gamma irradiation and applied potential difference transformed the structural, granular and electrical properties of the copper nanowires.

Acknowledgement: - The authors wish to thank to the Director, IUAC, New Delhi, India for providing the irradiation facility and the Director, NIT Kurukshetra, India for providing SEM and XRD facilities

Efficient Adsorption of Uranium from Aqueous Solutions and Simulated Seawater by Zeolite Imidazolate Framework

Jagannath Panda^a, Abinash Sahu^b, Rojalin Sahu^{a*}

^aSchool of Applied Sciences, KIIT Deemed to be University, Bhubaneswar-24

^bOSCOM, Chatrapur, Ganjam, Odisha

*E-mail: rsahufch@kiit.ac.in

1. Introduction

Recently, varieties of metal organic frameworks (MOF) have been used to adsorb uranium from water. In this work, Zn based ZIF-8 (Zeolitic Imidazolate Framework) has been used as an adsorbent to adsorb uranium from aqueous medium as well as from simulated seawater. To investigate the adsorption efficiency of the material, we have measured the uranyl concentration before and after treating with the material by using ICP-OES.

2. Experiment

2.1. Materials and preparation of ZIF-8: ZIF-8 has been synthesized by placing a 2:1 mixture of 2-methylimidazole (20 g 243.59 mmol) and 10 g 121.80 mmol of ZnO (2:1) in a stainless-steel jar along with 5 mL of ethanol. The mixture was grinded for 60 min. ZIF-8 has been characterized by Powder XRD, TGA, SEM and TEM.

3. Results and Discussion

The formation of ZIF-8 with SOD topology has been confirmed from the PXRD pattern (Figure 1). The FT-IR spectrum of U@ZIF-8 and ZIF-8 synthesized are shown in Figure 2. Absorption bands at 2929 cm⁻¹ and 3135 cm⁻¹ were attributed to the aromatic and aliphatic C-H stretch of the imidazole respectively. The absorption band at 420 cm⁻¹ was observed for the Zn-N stretching mode, while those in the 1100–1400 cm⁻¹ region were associated with the C-N stretch. The new band at 886cm⁻¹ was attributed to O=U=O in ZIF-8 material.

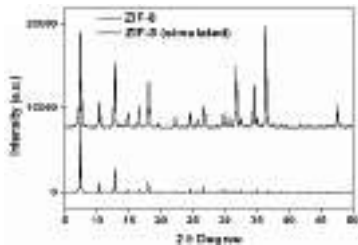


Fig 1: Powder X-ray diffraction of ZIF-8

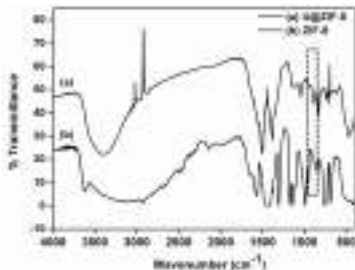


Fig 2: FTIR of ZIF-8 and U@ZIF-8

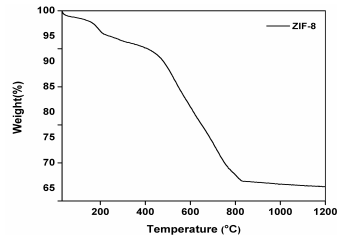


Fig 3: TGA of ZIF-8

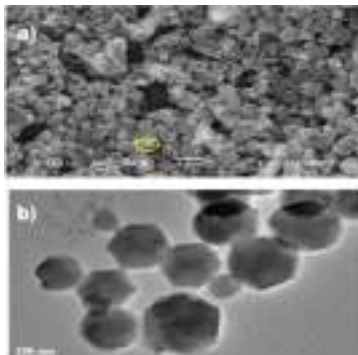


Fig 4: SEM and TEM Image of ZIF-8

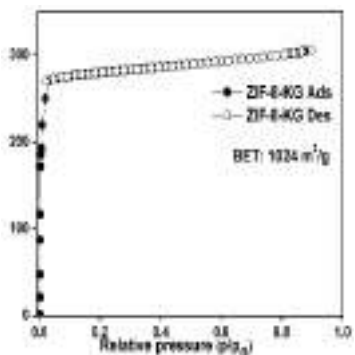


Fig 5: Adsorption Isotherm of ZIF-8

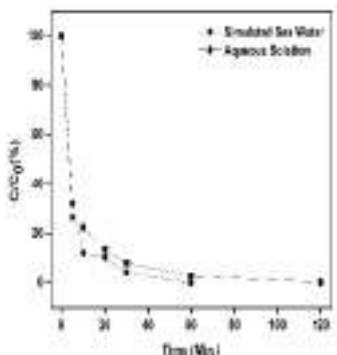


Fig 6: Change in concentration of Uranium after adsorption

Thermal stability of the synthesized material is shown in Figure 3. It exhibited a gradual weight-loss step of 11.8% up to ca. 200 °C, corresponding to the removal of guest molecules (may be H₂O) or unreacted species from the surface of the nano-crystals. SEM images show some of the particles are round in shape and some particles are hexagonal in shape (Figure 4(a)). From the TEM the images, Fig. 4(b) it is clear that the adopted synthesis facilitate crystal formation and well defined rhombic dodecahedron shaped crystals were seen for ZIF-8 sample with an average size of 100-200 nm. BET study of the sample shows that ZIF-8 is a mesoporous material and having surface area of 1024 m²/g as shown in Fig. 5. The adsorption of uranium in the material (ZIF-8) from aqueous solution and simulated seawater has been shown in the plot C/C₀ (%) vs time which is depicted in the figure 6.

4. Conclusion

We have synthesized the rhombic dodecahedral Zn based ZIF-8. It is a mesoporous material and has significant removal efficiency of U (VI) from aqueous medium as well as simulated seawater.

Acknowledgement: KIIT deemed to be university is highly acknowledged

Radiochemical Purification of ^{32}P from Sulphur Target Irradiated in KAMINI Reactor

*J. S. Brahmaji Rao, G. V. S. Ashok Kumar, R. Senthilvadiyu, R. Kumar**

Fuel Chemistry Division, Materials Chemistry & Metal Fuel Cycle Group, IGCAR,
Kalpakkam, Tamil Nadu-603 102
*E-mail: rkumar@igcar.gov.in

1. Introduction

^{32}P is a pure β^- emitter with β^-_{max} of 1.7 MeV and $t_{1/2} = 14.3$ days. ^{32}P is being used in pain palliative care for metastatic bone cancer in the form of either $\text{Na}_3^{32}\text{PO}_4$ or $\text{H}_3^{32}\text{PO}_4$ and for the treatment of arthritis of knee joints using ^{32}P -labeled hydroxyapatite [1]. ^{32}P can be produced either using the nuclear reaction $^{31}\text{P}(n, \gamma) ^{32}\text{P}$ by irradiating phosphorous in a thermal reactor or using $^{32}\text{S}(n,p) ^{32}\text{P}$ by irradiating elemental sulphur or sulphur bearing compounds with fast neutrons [2]. However, the latter method yields ^{32}P of high specific activity. ^{32}P can thus be produced in the Fast Breeder Test Reactor (FBTR) at IGCAR. This paper describes the development of a flow-sheet for the purification of ^{32}P produced using sulphur powder as the target by irradiating it with small fast flux available in the KAMINI research reactor at Kalpakkam. This method could be applied for the production of ^{32}P by irradiating sulphur target in FBTR subsequently.

2. Experimental

About 300 mg of sulphur powder was irradiated in Pneumatic Fast Transfer Facility (PFTS) position of KAMINI reactor for 6 h with its total neutron flux of about $1.6 \times 10^{11} \text{ cm}^{-2} \text{ s}^{-1}$ and its associated small flux of fast neutrons. The irradiated target was subsequently transferred to a distillation chamber which was connected to a series of bubblers and a vacuum pump (Fig. 1). The distillation of the irradiated sulphur was started by heating it to a temperature of 250°C to 300°C and maintaining it at a low pressure of about 10 mbar. The distillation was completed in about 5 h. After the complete distillation, the vacuum was released and the contents were allowed to cool. The residue was leached out as $\text{H}_3^{32}\text{PO}_4$ by boiling it with 10 mL of 0.1M HCl and the ^{32}P source was further purified from other

cationic impurities, if any, by cation-exchange chromatographic technique using DOWEX 50WX8 (100-200) resin. The eluted samples of 15 mL size were assayed for their ^{32}P content by Cerenkov technique using HIDEX 300SL LSC system. A clear base line separation of ^{32}P was achieved with no other cationic impurities present in the sample.

3. Results and Discussions

Pure ^{32}P source was obtained as phosphoric acid ($\text{H}_3^{32}\text{PO}_4$) in HCl medium. Activity of ^{32}P in the purified fraction was quantified by using Cerenkov mode of counting. The yield was found to be $\sim 39 \mu\text{Ci/g}$ of sulphur powder. The purified fraction of ^{32}P obtained was further analysed by gamma spectrometry using HPGe detector. The analysis confirmed the absence of any other gamma emitting impurities. The pure fraction of ^{32}P source obtained above was again assayed at regular intervals for a period of about six weeks in order to obtain the profile of the decay by using Cerenkov counting. The half-life of 14.3 days was obtained from the decay curve and it was found to be in good agreement with the value reported [2] i.e. 14.29 days. Thus, the purity of the sample was ascertained by confirming the absence of any other beta emitting nuclides as well.

Thus, a flow sheet has been established for the purification of ^{32}P source from the irradiated sulphur target. This flow sheet could be used for the production of ^{32}P by using sulphur powder as the target in FBTR which is expected to provide a much higher yield owing to its higher flux of fast neutrons. However, an appropriately safe leak tight irradiation capsule needs to be designed for irradiation, without loss of the target migration due to the vaporisation at the high operational temperature of 550°C in FBTR.

References

- /1/ K. Rajeswari, Vimalnath, H. Sarma, et al., Appl. Radiat. Isotopes 116 (2016) 85
- /2/ M. Ananthakrishnan, Phosphorous-32 ($^{32}\text{P}_{15}$) in Manual for Reactor Produced Radioisotopes; IAEA-TECDOC-1340 (2003) 158.

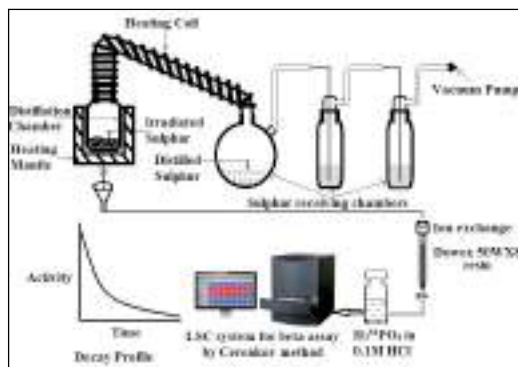


Figure 1. Schematic of distillation & purification of ^{32}P from the irradiated sulfur target

Application of ^{210}Pb Chronology Assessing for Marine Contamination in Mumbai Harbour Bay

Moushumi D. Chaudhury, Vandana Pulhani, Vikram Joshi, Sujata Gothankar, S.K.Jha, R. M. Tripathi*

Health Physics Division, Bhabha Atomic Research Centre, Trombay, Mumbai.
*E-mail: mausamdc@gmail.com

1. Introduction

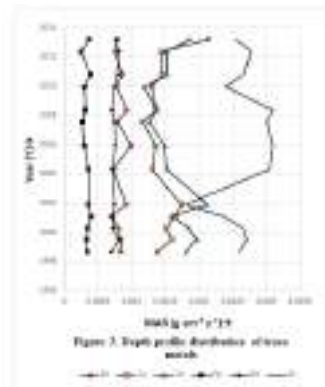
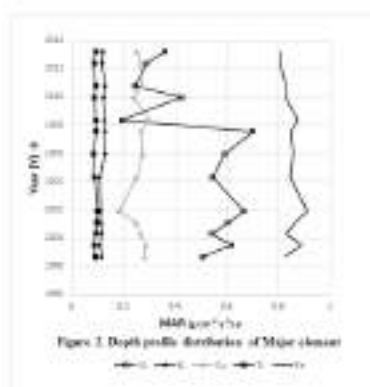
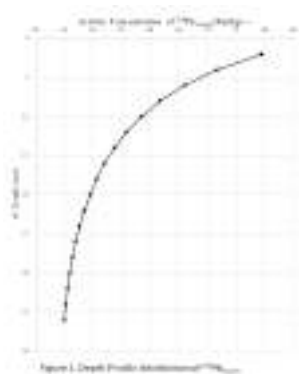
Rapid urbanization, large scale industrialization and uncontrolled increase in population in and around the coastline of Mumbai have resulted into degradation of marine coastal ecosystem. In the present study, an attempt has been made to investigate the year-wise vertical distribution pattern of selected trace elemental contamination of Mumbai Harbour Bay (MHB) coastal marine sediments to have a better understanding of the degree of anthropogenic influences. This has been achieved by estimating the recent sedimentation rate along the coastline region by the application of $^{210}\text{Pb}_{\text{excess}}$ Radiometric dating technique using Constant Initial Concentration model (CIC).

2. Experiment

The sampling area was between Lat:19°07'38.78" and Long :72°58'16.12"E in MHB, stagnant, triangular and brackish landlocked mass of water which widens out and opens to the Arabian Sea in the south and the Ulhas River through the Thane Creek in the north. Sediment core samples were collected using a Kazak corer, with an inner diameter of 7.0cm and length of 90cm. Cores were sliced along the length at intervals of 2cm each. Sample preparation for estimation of $^{210}\text{Pb}_{\text{excess}}$ by gamma spectroscopy were sealed for 3months to achieve secular equilibrium between ^{226}Ra , ^{214}Pb and ^{214}Bi and ^{238}U . Total ^{210}Pb , assuming secular equilibrium with ^{210}Po was measured in core sediment fractions by radiochemical methodology followed by alpha spectroscopy using ^{209}Po tracer. Stable elements were measured by EDXRF technique.

3. Results and Discussions

Mass accumulation rate (MAR) was estimated using CIC model with $^{210}\text{Pb}_{\text{excess}}$ chronometer [1]. The linear sedimentation rate was found to be $2.4\pm 0.5\text{cm/y}$ and MAR was estimated to be $0.18\text{g/cm}^2/\text{y}$. Distribution of $^{210}\text{Pb}_{\text{excess}}$ with depth is shown in Figure 1 and it is used to derive the age of the core fractions. The depth profile distribution of the major and some trace elements in $\text{g/cm}^2/\text{y}$ are shown in Figures 2 & 3 respectively. K, Ca, Ti, Fe Pb, Rb and Ni do not show much variation with depth, whereas same is not true with Al, Cu, Zn and Sr. The deposition rate of Al and Fe are approximately 4 and 8 times more than that of K respectively. There is a huge depression in the concentration of Al during the period of 2007-2008. The sub-surface variations can be influenced by many factors such as biological activity or sudden increase/decrease in the sedimentation rate due to mud slide, shore erosion or random climatic change. Changes in rainfall intensity affects the runoff, detachment of soil particles, erosion, and sediment transport, which further affects the sedimentation yield. As the effect is observed for only Al it might be linked to either its specific physicochemical behaviour or changes in the anthropogenic inputs in that year. As the accumulation of Al post 2007 has remained uniform it can be attributed to reduced anthropogenic inputs. The concentrations of Cu, Zn and Sr are reasonably high and well correlated with MAR data which had been observed to be extremely low during the year 2001 MAR and reported to be affected by increased biological activity and mixing.



References

- 1/ B.S. Shukla. (2002). Sedimentation rate through environmental radioactivity (models and applications). Canada: Environmental Research and Publications Inc.

Validation of Irradiation Parameters f and α for k_0 Based IM-NAA Method in KAMINI Reactor

*Manish Chand, J.S. Brahmaji Rao and R.Kumar**

Fuel Chemistry Division, Indira Gandhi Centre for Atomic Research, Kalpakkam - 603102,
*E-mail: rkumar@igcar.gov.in

1. Introduction

KAMINI reactor has a high flux pneumatic fast transfer system (PFTS) [1], two thimble positions and one west beam port for carrying out neutron activation analysis (NAA). Two new aluminium dry tubes i.e. DT1 and DT2 were introduced in KAMINI reactor for irradiation studies of the samples of large and irregular geometry [2]. DT1 and DT2 are 35 and 90 cm away from the core centre, respectively. Characterization of the newly installed dry tubes were accomplished for profiling the flux variation, thermal to epithermal flux ratio (f) and epithermal flux shape factor alpha (α) [3]. For present study, the characterized irradiation parameters f (143 ± 9) & α (-0.289 ± 0.010) of DT1, which is close to the core centre, were used in k_0 based IM-NAA method for elemental analysis of minerals samples.

2. Experimental

About 5 g (large sample) and its sub samples 100-200 mg (small sample) of minerals samples and 200 mg of Coal fly ash (CFA) standard were prepared and irradiated in DT1 and PFTS position in KAMINI reactor, respectively and the quantification has been carried out by k_0 based IM-NAA utilizing in-situ relative detection efficiency (Figure 1) and relative method after assaying by HPGe detector.

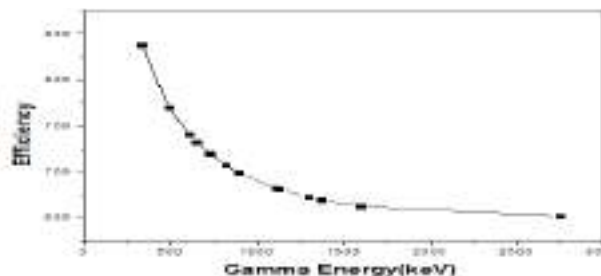


Figure 1. In-situ relative detection efficiency using gamma rays of ^{140}La , ^{24}Na , ^{59}Fe , ^{46}Sc , ^{124}Sb

3. Results and discussion

The elemental concentration ratio of 14 elements present in the mineral samples were obtained with respect to Sc by including characterized parameters f & α and converted into the absolute value by using the concentration of Sc obtained by the relative method. The elemental concentration obtained by k_0 based IM-NAA method is compared with the relative method using the sub samples and standard sample irradiated in PFTS position of KAMINI reactor. The observed elemental concentration obtained from k_0 based IM-NAA (Table-1) was found to be within $\pm 5\%$ of the value obtained from relative method.

Table 1. Measured elemental concentration ($\mu\text{g/g}$) in Minerals samples

Elements	Energy (keV)	Stock piled		current arising	
		Relative conc. wrt Sc	Absolute conc.	Relative conc. wrt Sc	Absolute conc.
La	815.7	1.76	7.74 \pm 0.32	2.58	6.97 \pm 0.24
Na	1368.6	4921.05	21655 \pm 1504	3696	9979 \pm 936
As	559.08	227.7	1002 \pm 49	266.7	720.1 \pm 32
*Sc	589.3	1	4.40 \pm 0.11	1	2.7 \pm 0.6
Fe	1099	58026	255314 \pm 2250	53936	145627 \pm 1050
Ga	834.08	44.8	197 \pm 5.7	-	-
Zn	1115.5	6639	29212 \pm 140	17567	47431 \pm 430
Ag	884	61.8	272 \pm 13	71.9	194.1 \pm 1.2
W	685.7	0.81	3.6 \pm 0.10	5.89	15.9 \pm 0.6
Au	411.8	0.037	0.2 \pm 0.01	0.37	1.00 \pm 0.08
Cd	527.9	16.6	73.0 \pm 5.7	383.5	1055.5 \pm 32
Cu	1345	835	3674 \pm 134	-	-
Co	1173.2	-	-	5.08	13.7 \pm 0.6
Sb	602	2.9	12.8 \pm 0.5	84.74	228.8 \pm 9.6

*Sc value calculated from relative method.

4. Conclusion

The observed elemental concentration obtained from k_0 based IM-NAA was within $\pm 5\%$ in comparison with the relative method. Hence this method has validated the parameters (f and α) evaluated for the newly characterized location and can be utilized for analysing large and irregular geometry samples for future studies.

5. References

- /1/ J.S. Brahmaji Rao, E. Senthilvadivu, N.P. Seshadreesan, et al., J Radioanal Nucl. Chem 294 (2012) 137.
- /2/ A. G. C. Nair, R. Acharya, K. Sudarshan, et al., Anal. Chem. 75 (2003) 4868.
- /3/ C. Manish, J.S. Brahmaji Rao, N.P. Seshadreesan, et al., NUCAR; Mumbai (India) p. 296-297; 20-24 Jan 2014.

Analysis of Muscle Tissue Substitute with Respect to Photon Interaction, Build-up Factor and Relative Kerma

Inderjeet Singh¹, Rohit¹, Bhajan Singh¹, B.S. Sandhu¹, Arvind D. Sabharwal^{2}*

¹Physics Department, Punjabi University, Patiala-147002, India;

²Physics Department, G.S.S.D.G.S Khalsa College, Patiala-147001 India

*E-mail: arvindsabharwal1976@gmail.com

1. Introduction

To study doses received by tissue of any part of human body, when exposed to ionizing radiations, several materials have been used to simulate human tissues and are known as tissue equivalent materials. Tissue substitute should have the same radiological properties as real tissue and should have precise value of photon interaction parameters such as effective atomic number (Z_{eff}), mass attenuation coefficient (μ/ρ), mass energy absorption coefficient (μ_{en}/ρ), electron density (N_{el}), energy absorption build-up factor (EABF), exposure build-up factor (ExBF) and relative kerma.

2. Experiment

2.1 Materials and Methods: The tissue substitute materials such as Rossi liquid [Water (56.90); glycerol (28.40); urea (7.60); sucrose (8.40)], Goodman liquid [water (65.60%), glycerol (26.80%) and urea (7.60%)], Paraffin wax [$\text{C}_{25}\text{H}_{52}$] and Nylon [$(\text{C}_6\text{H}_{11}\text{NO})_n$] are used in this paper [1]. Z_{eff} of tissue substitute are experimentally determined by using back-scattering of 662 keV gamma photons. For EABF and ExBF, G.P fitting parameters are obtained by interpolation from the Z_{eff} . The μ/ρ and μ_{en}/ρ obtained by WinXCom program (0.015-15 MeV) are used to determine the relative kerma. A 3" x 3" NaI(Tl) detector is used for recording the pulse-height distribution.

3. Results and Discussions

When gamma photons are incident on the target material, it is either absorbed or scattered. The recorded spectra with and without target are subtracted to get contribution of back-scattered photons

from target. Measurement of back-scattered photons is carried out as a function of target thickness. Saturation thickness of Rossi liquid, Goodman liquid, Paraffin wax and Nylon tissue substitute are found to be 24.25 mm, 23.9 mm, 25.30 mm and 24.9 mm respectively. In our earlier work, saturation thickness of pure elements when plotted provided a calibration line for known values of Z ($6 \leq Z \leq 50$). This calibration line [2] serves as the basis for finding Z_{eff} of tissue substitutes under investigation as shown in figure 1(a). Calculated value of EABF and ExBF depends on the energy of gamma photon, penetration depth and the chemical composition of tissue substitute. The values of EABF and ExBF are lower for low energy region due to dominance of photoelectric absorption figure 1(b). For intermediate energy range (<3 MeV), EABF and ExBF values increases with photon energy, due to dominance of Compton process and it results in multiple scattering, which further contributes to increase EABF and ExBF values. For higher energy region (>3 MeV) other interaction process (pair production) dominates which decrease their value. In figure 1(b), the value of EABF and ExBF tends to increase with increase in penetration depth from 1 to 40 mfp because in intermediate energy multiple scattered count increases with increase in penetration depth.

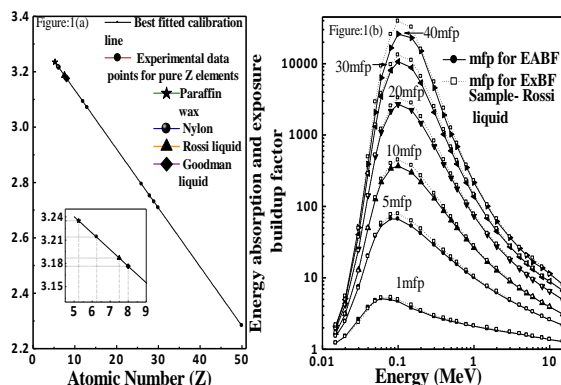


Figure:1(a) Variation of logarithmic saturation thickness with Z ,
 Figure:1(b) Variation of EABF and ExBF with energy for selected penetration depth

4. Conclusion

The multiple back-scattering of gamma photons is used to investigate Z_{eff} for muscle tissue substitutes. The value of EABF and ExBF are lower for photoelectric absorption and pair production while for Compton process their values are higher because of multiple back-scattering. For low Z_{eq} materials, ExBF is larger than EABF whereas for high Z_{eq} materials, EABF is significantly higher than ExBF.

Reference

/1/ ICRU Report 44, Bethesda, MD, USA, 1989.
 /2/ I. Singh, B. Singh, B.S. Sandhu and A. D. Sabharwal., Rad. Effect. Def. solid, 172 (2017) 204-215.

A New Approach to Measure Milk Fat Content by Using Multiple Back-scattering of Gamma Photons

Rohit¹, Inderjeet Singh¹, Bhajan Singh¹, B.S. Sandhu¹, Arvind D. Sabharwal^{2}*

¹Physics Department, Punjabi University, Patiala-147002, India;

²Physics Department, G.S.S.D.G.S Khalsa College, Patiala-147001 India

*E-mail: arvindsabharwal1976@gmail.com

1. Introduction

Determination of milk fat content in dairy products is very important due to its nutrition value. The consumption of milk in India has been increasing after green revolution. Several methods have been developed to measure the fat content of milk, for example Rose-Gottlieb, Gerber, Babcock methods, resonant frequency U-tube oscillation [1] and UV spectroscopic method [2]. In present work, a new technique based on multiple back-scattering of gamma rays is discussed which is used to determine the percentage of fat concentration in milk. A densitometer has been constructed to determine the fat content in milk and results are compared with conventional methods for fat determination.

2. Experimental Set-up and measurements

A 3"×3" NaI(Tl) Scintillator detector is used to detect the gamma photons coming from the 662 keV source of ¹³⁷Cs. To avoid contribution of any unwanted signal, detector is properly shielded with a lead cylinder of thickness 5 mm. For the construction of densitometer, different milk solutions having different known fat content (0.5% to 6.5%) are taken in vial one by one, and are irradiated by 662 keV gamma photon source to obtain their spectra. Recorded spectrums are used to plot a calibration line after correcting them for detector efficiency in order to determining the fat content of any unknown milk sample in the fat range of 0.5% to 6.5%.

3. Results and Discussions

In the multiple back-scattering experiments, back-scattered flux is a linear function of number density of liquid. To find contribution of only back-scattered photons, pulse-height distribution is recorded

with and without target for each sample of milk having different fat content for same time as shown in figure 1(a). The numbers of multiple back-scattered counts increases due to increase in fat content/density of milk. The obtained pulse height distribution is converted into a true photon spectra by applying a response correction to it [3]. These multiple back-scattered counts are then plotted with respect to the percentage fat content in milk in order to obtain a calibration line in figure 1(b). When an unknown sample of milk is taken and after recorded its spectrum when fit into the calibration line During investigation an unknown milk sample of unknown fat content is undertaken and its fat is calculated from the calibration line [fig 1(b)]. Value of fat content is $4.4\% \pm 2.27\%$. This is compared with Gerber's (Centrifugation) method. It is found that value of fat is $4.3\% \pm 0.56\%$, which is close to our experimental results with an error of 2.27%.

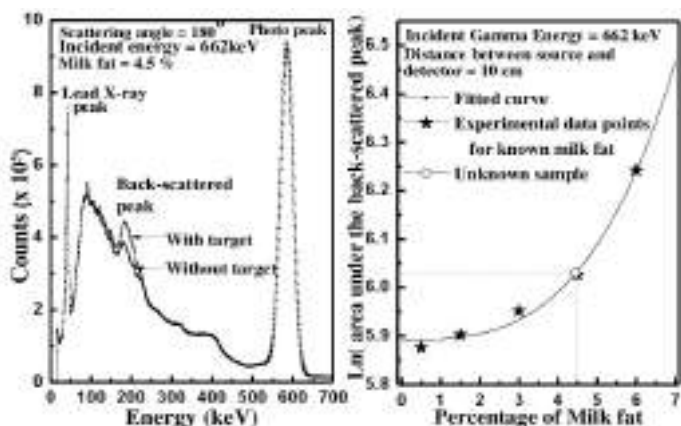


Figure 1: (a) Recorded pulse-height distribution with and without water target for time duration of 15s
Figure 1: (b) Observed variation of natural logarithm with percentage of milk fat

4. Conclusion

Observed results reveals that the intensity of multiple back-scattered photons increases linearly with the number density of milk, which helps to construct the densitometer to measure its fat content. Also the calibration line provides a non-destructive method to calculate fat of any unknown sample of milk in range of 0.5% to 6.5%.

Reference

- /1/ Forcato,D.O., M.P.Carmine, G E.Echeverría, et al., J.Dairy Sci 88 (2005) 478–481
- /2/ Badertscher, R., T. Berger, and R. Kuhn. Int. DairyJ. 17 (2007) 20–23.
- /3/ I. Singh, B. Singh, B. Sandhu, A. Sabharwal, Radiation Effects And Defects In Solids 172 (2017) 204

Distribution of Radionuclides in Beach Sand Samples Along the Coastal Line of Kerala, India

Ramsiya M¹, Vishnu CV¹, Antony Joeph¹, Eappen KP².*

¹Department of Physics, University of Calicut, Kerala 673635, India

²Ex- BARC and Consultant, IEC - New Delhi.

*E-mail: ramsiyaashraf@gmail.com

1. Introduction

The coastal areas of Kerala is enriched with monozite sand-a rich source of radioactive Th and U, thus analysis of radioactive levels in sand samples are necessary from radiological protection stand points.

2. Experiment

Sampling areas are highly populated beaches from the coastal regions of Thiruvananthapuram Shangumugham (Sh), Alappuzha (Al), Kollam (Neendakara (N), Chavara (Ch); Ernakulam Kuzhupilly (Kuzhu), Munampam (Mu), Cherai; Thrissur (Vadanapilly, Chavakkad), Malappuram (Ponnani) and Kozhikode (Kappad beach) districts. Samples collected were then dried in an oven at 110 °C for 24 h. The samples were then counted for gamma activity, for a period of 36000 seconds to get a reasonable area under the photo-peaks, corresponding to various gamma energies. The activities of radium were estimated by measuring the area under the photo peaks of ²¹⁴Pb (351.9 keV) and ²¹⁴Bi (609.3 keV). The thorium activity was determined from the ²²⁸Ac (911.2 keV), ²¹²Pb (238.6 keV) and ²⁰⁸Tl (583.2 keV) photo peaks. The ⁴⁰K was measured directly from the full energy photo peaks of 1460 keV.

3. Results and Discussions

Activity of ²²⁶Ra, ²³²Th and ⁴⁰K in superficial beach sand samples obtained is given in Figure 1. Activity of ²²⁶Ra and ²³²Th in the analysed samples in Kollam district Neenkara, Chavara and Karithura are higher than UNSCEAR 2008 reference limit of 32 Bq/kg for radium and 45 Bq/kg for thorium [1]. The radiological hazard parameters like Absorbed dose rate, Annual effective dose rate, Radium equivalent activity, and External hazard index were estimated and presented in table 1.

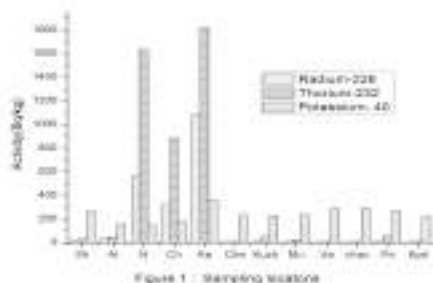


Table 1. Summary of radiological parameters in various beaches of Kerala, India

Location	No.of samples	Absorbed dose rate, (nGyh ⁻¹)	Annual effective dose rate, (mSvy ⁻¹)	Radium equivalent activity, (Bq/kg)	External hazard index
Shangumugham(Sh)	3	37± 3	0.04± 0.00	80± 7	0.22± 0.01
Alapuzha(Al)	3	54± 17	0.06± 0.02	119± 39	0.32± 0.10
Neendakara(N)	10	1094± 533	1.34 ± 0.65	2477± 1209	6.69± 3.26
Chavara (Ch)	10	712± 2 450	0.87 ± 0.55	1609± 1024	4.35± 2.76
Karithura(Ka)	6	1651 ±590	2.02± 0.67	3715± 1259	9.97± 3.51
Cherai(Che)	5	18.29±3.18	0.02±0.00	34.93±5.31	0.09±0.01
Kuzhupilly(Kuzhu)	5	48.54±4.59	0.05±0.00	104.±10	0.28±0.02
Munampam(Mu)	5	31.63±3.81	0.03±0.00	65.16±9.05	0.18±0.02
Vadanapilly(Va)	5	19.49±1.62	0.02±0.01	36.15±3.41	0.10±0.00
Chavakkad(Chav)	5	19.90±2.48	0.02±0.00	36.13±4.37	0.10±0.01
Ponnani(Po)	4	69.73±8.86	0.08±0.01	151.29±21.73	0.41±0.05
Kappad(Kpd)	4	18.01±1.03	0.02±0.00	34.71±1.84	0.09±0.00

4. Conclusion

The results show that the coastal areas of Kollam district comes under the High Back ground Radiation Area (HBRA) whereas the other beaches like Shangumugham, Alapuzha, Kappad, Ponnani, Kuzhupilly, Munampam, Cherai, Vadanapally and Chavakkad are normal background areas. The remarkable difference in radiological parameters is observed between HBRA and NBRA. Among the NBRA, the absorbed dose rate in Ponnani (69.73 nGy/h) exceeds the reference limit of 60 nGy/h (UNSCEAR 2008). Radium equivalent activity, external hazard index, absorbed dose rate of surface samples along the coastal areas of Kollam district are higher than the internationally accepted limit.

References

/1/ UNSCEAR (2008) Sources and effects of ionising radiation, vol 1.

Techneium-99: New Resins Developments For Separation And Isolation From Various Matrices

N. Maudoux¹, L. Phelippeau¹, M. Bas¹, N. Vajda², A. Bombard^{1},
S. Happel¹, C. Dirks³*

¹TrisKem International, 3 rue des Champs Geons, 35170 Bruz, FRANCE

²Radanal, Budapest, HUNGARY

³Munich Technical University, Munich, GERMANY

*E-mail : abombard@triskem.fr

1. Introduction

Techneium-99 is of interest in decommissioning and radioactive waste management as it is part of the so-called difficult-to-measure (DTM) long-lived fission products. As it is a beta emitter potentially interfering radionuclides need to be removed before its radiometric quantification e.g. by LSC. The development of analysis and determination of radionuclides by mass spectrometry urges the need to reduce and/or eliminate isobars prior to analysis. Further for both detection techniques it is beneficial to avoid eluting Tc using highly concentrated acid. Accordingly rapid, easy and highly selective separation of Tc from different matrices, arising from different production processes remains of high interest. Triskem International has developed two resins designed for technetium extraction from acidic and alkaline media with special focus on its separation from Mo. TK201 resin is based on a tertiary amine, which allows for the loading in moderately acidic conditions, and elution of technetium in acidic or alkaline conditions. TK202 resin is based on a polyethylene glycol group grafted onto a polymer support. This resin allows for extraction of Tc-99 e.g. from strongly alkaline media such as 5M NaOH and subsequent and quantitative elution of Tc in water. In different experiments, rhenium was used as stable homologue of Tc. In both resins, separation of rhenium is clean and quantitative.

2. Experiment

2.1. Determination of mass distribution coefficients (D_w) using multi-element solution: performances of the TK201 resin were first tested for different acidic media conditions in HCl and HNO₃ acids from 0.01M up to 8M.

TK202 on the other hand was tested under various alkaline conditions. In both cases 50mg of resin were put in contact with 1mL of multi-elements solution for one hour. After centrifugation an aliquot of the supernatant solution was measured by ICP-MS and LSC for D_w determination. In these first experiments, rhenium was used as chemical homolog of Tc.

2.2. Elution studies: Based on obtained D_w values, various elution studies were performed to evaluate the separation of the Tc, Re, Mo and Ru on dynamic modes per say using columns under gravitational flow as well as cartridges using a vacuum box. Collected fractions were analyzed using ICP-MS or LSC in case of Tc-99 measurement.

3. Results and Discussion

The tertiary amine present in TK201 resin acts as a weak anion exchanger. Figure 1 presents elution curve on TK201 for a pH 2 HNO_3 load solution. Re is retained at pH 1-2 (HNO_3) while Mo, Nb, Zr, Th, U, Sr and Cs are eluted. Re is selectively eluted from the resin in 0.1M NH_4OH or alternatively in $\geq 1M HNO_3$. The TK202 resin is based on a different extraction mechanism (aqueous biphasic system) that requires high salt environment such as strong alkaline conditions to allow for Tc uptake. Figure 2 shows an elution curve on TK202 using strong alkaline medium 5M NaOH as load solution for Mo, Re and Tc. Mo is directly eluted while Re and Tc are cleanly separated and eluted in water.

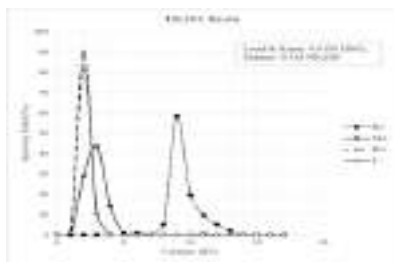


Figure 1. Elution curve of TK201 Resin with acidic medium load.

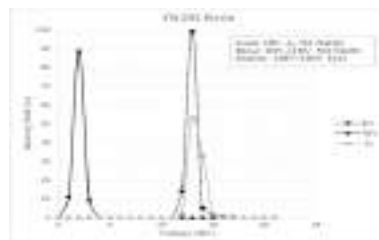


Figure 2. Elution curve of TK202 Resin with alkaline medium load

4. Conclusion

The different results of the D_w and elution curves showed the high efficiency of TK201 and TK202 resins for the uptake and clean separation of Re/Tc respectively from acidic and alkaline load media and subsequent specific elution of Tc/Re respectively in slightly acidic or basic and water respectively.

New TK200 Resin: Uses for Actinides Preconcentration and Separation

A. Bombard^{1*}, S. Happel¹, M. Bas¹, N. Vajda², C. Dirks³

¹TrisKem International, 3 rue des Champs Geons, 35170 Bruz, FRANCE

²Radanal, Budapest, HUNGARY

³Munich Technical University, Munich, GERMANY

*E-mail : abombard@triskem.fr

1. Introduction

Tri-Octyl Phosphine Oxide (TOPO) is widely used in liquid-liquid extraction, especially in the extraction of actinides, and uranium in particular, from acidic media. The TOPO based TK200 Resin has been characterized with respect to the weight distribution ratios (D_w) of U, Th, Pu, Np, Am and a number of other cations in different concentrations of HNO_3 and HCl. Further the influence of elevated amounts of iron on the extraction of selected elements has been evaluated. Based on obtained data methods for the separation of U, Th and Pu have been developed. Initial results showed the ability of the TK200 Resin to preconcentrate U(VI), Pu(IV) and Th(IV) at pH2, a medium commonly used to preserve aqueous samples, and subsequently elute them sequentially.

Additional uses of the TK200 resin are found in the field of radiopharmacy with the separation of Ga-67/8 from solid or liquid Zn targets in conjunction with ZR Resin, and the separation of Zn isotopes from Cu targets. First results are presented for above mentioned applications.

2. Experiment

2.1. Determination of mass distribution coefficients (D_w) using multi-element solution: performances of the TK200 resin were first tested for different acidic media conditions in HCl and HNO_3 acids from 0.01M up to 8M. 50 mg of resin were put in contact with 1mL of multi-elements solution for one hour. After centrifugation an aliquot (100 μ L) of the supernatant solution was diluted and measured by ICP-MS for D_w determination. Further D_w data were obtained for Am, Pu and Np, as well as U and Th employing radioactive tracers and LSC measurement.

2.2. Elution studies: Based on obtained D_w values various elution studies were performed, amongst others on improved U/Th separation and the preconcentration and subsequent separation of the actinides. Studies were performed using columns under gravitational flow as well as cartridges using a vacuum box. Collected fractions were analyzed using ICP-MS or LSC (in case of actinides) to allow calculating respective chemical recoveries.

3. Results and Discussion

Figure 1 exemplarily shows the uptake of selected elements with varying acidic tested conditions. U and Th show high uptakes from 10^2 up to 10^4 from pH 2 to high acid concentrations for both HCl and HNO₃ media. Other metallic elements tested show no or very little uptake with D_w less than 10.

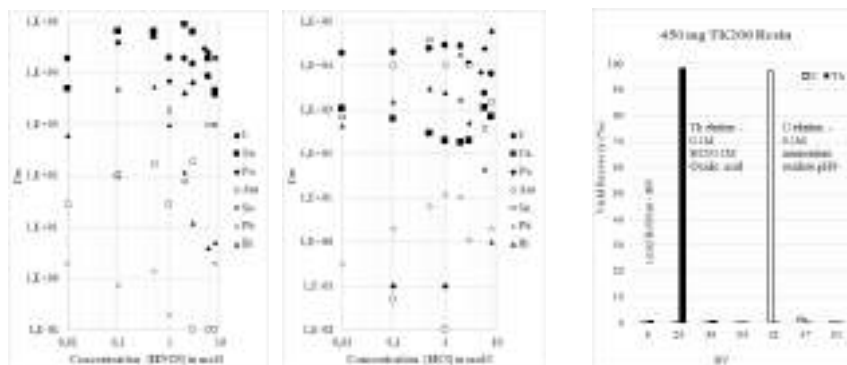


Figure 1. D_w curves for various elements in HNO₃ and HCl media. Figure 2. Elution study for Th/U separation

Figure 2 presents an elution study showing that a very clean U/Th separation might be achieved. It was further shown that U, Th and Pu could be concentrated from 1L of acidified water (0.01M HNO₃) and subsequently sequentially separated on the TK200 resin.

4. Conclusion

The different results of the D_w curves, elution curves and tests on real samples showed the high efficiency of the TK200 resin to retain hexa- and tetravalent actinides from pH 2 to high acid concentrations. The TK200 resin offers the possibility to preconcentrate actinides at pH 1-2 and subsequently elute each of them in separated fractions including Americium in the case of pH 1-2 load. It has also the possibility to do clean and effective uranium-thorium separation.

References

/1/ T. Braun and G. Gherini.(eds.): Extraction chromatography. Elsevier Scientific Pub. Co., 1975

Use of Electron Beam Irradiation for Improving Reactivity of Dissolving Pulp for Viscose Process

Sachin Gondhalekar, Pravin Pawar, Sunil Dhumal*

Aditya Birla Science and Technology Company Private Limited, Talaja 410208, India
*E-mail: sachin.gondhalekar@adityabirla.com

1. Introduction

Viscose fibres are produced by chemical intensive process. Low pulp reactivity is a reason for higher consumption of chemicals, especially CS₂ and NaOH. Electron beam irradiation (EBI) is a potential way to improve the reactivity of pulp. In the EBI process, electron energy from an electron accelerator is transferred to cellulose pulp, which penetrates the crystalline regions of cellulose and increases the accessibility of cellulose to NaOH and CS₂ [1]. In this paper, effect of EB irradiated pulp on viscose dope properties are studied and its possible implications on commercial process are discussed.

2. Materials and Methods

Hardwood type dissolving grade pulp, prepared by pre-hydrolysis kraft process (Sappi, USA) was used to prepare viscose dope at lab facility. Pulp samples were treated at 2 and 5 kGy radiation dosage by electron accelerator and structural changes were captured with the help of different analytical techniques. The ripening index (RI), filterability index (kw) and gamma number of viscose dope were measured by conventional method. Chemical composition of pulp was determined by standard procedure. Reactivity of the pulp was measured by Fock method.

3. Results and Discussions

The pulp properties of electron beam (EB) irradiated samples (Table 1) indicate that Fock reactivity of the pulp increases with increase in the irradiation dosage. Electron energy, weaken the anhydroglucose unit and loosen the crystal lattice, which makes penetration of NaOH and CS₂ easier [2]. However, chain scission also happens during the irradiation, which decreases the average molecular weight of the

cellulose. Degradation also results in conversion of α -cellulose in short chain cellulose fractions and hemicelluloses, due to which the productivity is affected.

Table 1. Effect of EB dosing on pulp properties

Irradiation dose (kGy)	Fock reactivity	Average molecular weight (kmol/kg)	Alpha cellulose, % (dry basis)	Hemi and degraded cellulose, % (dry basis)
0	15.33	257629	94.43	5.57
2	26.52	220748	93.95	6.05
5	33.85	191244	93.40	6.60

The viscose dope prepared from the treated pulp shows improvement in kw and RI as shown in Table 2. Improvement in the kw and RI indicates the improved accessibility of NaOH and CS₂ towards EB irradiated cellulose. However, no significant change in gamma number was observed.

Table 2. Dope properties of viscose prepared by EB treated pulp

Irradiation dose, (kGy)	kw	RI	gamma number
0	77	12.0	50.64
2	51	12.3	48.90
5	29	13.0	52.40

4. Conclusion

EBI treatment showed increase in pulp reactivity, which translates in improvement in the viscose dope properties. On the other hand, EBI treatment showed drop in molecular weight. This can be favorable as it can reduce the ageing time in the process. However, decrease in α -cellulose content of the pulp is a factor of concern, which needs to be further studied.

Acknowledgement: All authors acknowledge Board of Radiation and Isotope Technology, Navi Mumbai, India for treatment of pulp samples with different EB dosing.

References

- /1/ K. Fischer. Macromolecular Symposia. 12 (1) (1987) 303.
- /2/ T.M. Stepanik, S. Rajagopal, D. Ewing, R. Whitehouse. Radiation Physics and Chemistry. 52 (1998) 505

Measurement of Natural Radioactivity and Gamma Self Absorption Correction in Construction Materials

Salma Boukhalfa^{1}, Rachid Khelifi²*

^{1,2}Université Saad Dahlab Blida 1, Laboratoire De Physique Théorique Et Interaction Rayonnement Matière,
Blida 09000, Algérie

*E-mail: boukhalfasalma@gmail.com

1. Introduction

For an aim to measure the radioactive elements of families ^{235}U , ^{238}U , ^{232}Th and ^{40}K (Primordials). This article is devoted to the measurement of natural radioactivity in the different building materials used in Algeria using a low-noise background gamma spectrometry system using a 3"× 3" NaI (TI). The correction of the self-absorption for the analyzed samples is taken into account. In order to evaluate the radioactive risk after the correction of self-absorption, the Radium equivalent activity, the external and internal hazard and the annual dose are calculated. The results of calculations of these are lower than that of the limit given by UNSCEAR.

2. Experimental

2.1. Sample preparation: Samples used for gamma spectrometry analysis are subject to the rules for preparation and storage according to the international standard [1]. The collection of samples is carried out at construction stations. Subsequently they are dried at 100°C for 24 h, grind and sieve at 200 µm, then they are stored in polyethylene containers of 200 cm³ for 28 days so that they reach secular equilibrium.

2.2. Gamma spectrometry analysis: A gamma spectrometry chain is associated with a 3"×3" scintillation detector with a 7% resolution at 661 keV placed vertically in a lead castle to collect gammas emitted by the sample. Finally, a computer equipped with an acquisition card and a data processing software "GAMMA VISION" is used for spectral analyzes.

2.2. Correction of self-absorption: The correction of this phenomenon is carried out using an experimental device, where the method to use is called the transmission method. This method was developed by Cutschall [2]. It depends on the energy of the incident photon, the density of the sample,

its volume and the atomic number Z of the medium (matrix) [3]. In contrast, the self-absorption correction factor C_{auto} is the ratio of the self-absorption factor of the sample to that of the standard.

3. Results and Discussion

After the correction of self-absorption. The estimation of the diametric parameters is taken into account. Table.1 summarizes the results of gamma spectrometry analysis.

Table1. The equivalent Radium, the external and internal hazard, the annual dose received by the building materials used in Algeria

Sample	Cement	Sand	Grave	Concrete	Brick	Tile
Radium equivalent (Bq kg^{-1})	88.25	83.21	86.46	67.84	99.15	80.27
Internal Hazard	0.31	0.30	0.30	0.19	0.34	0.30
External Hazard	0.16	0.15	0.16	0.19	0.18	0.15
Annual dose (mSv y^{-1})	0.21	0.20	0.21	0.16	0.23	0.19

4. Conclusion

We found the presence of the following radioelements in the six samples: the family of ^{238}U , which is calculated from the gamma rays of ^{214}Bi (1764.5 keV and 1120.3 keV), the family of ^{232}Th which is also calculated from the gamma rays of ^{208}Tl (2614.6 keV and 583.1 keV), and the ^{40}K to 1460.8 keV. The specific activities of ^{238}U , ^{232}Th and ^{40}K are varied with an average value between 25.019, 20.135 and 401.757 Bq kg^{-1} respectively. The effective annual dose due to these materials ranges from 0.16 to 0.21 mSv y^{-1} . The results obtained are below the limit given by UNSCEAR.

References

- /1/ UNSCEAR. United Nation Scientific Committee on the Effect of Atomic Radiation. Expose from natural sources of radiation, United Nations, New York (2000).
- /2/ N.H. Cutshall, I.L. Larsen, C.R. Olsen, Nucl. Instrum. Methods in Phys. Res., 206 (1983) 309-312
- /3/ J.P. Bolivar, M. García-Léon, R. Garcia-Tenorio. Appl. Radiat. Isotopes, 48 (1997) 1125-1126

Studies on ^{208}Po -Hesperidin Association

Susanta Lahiri^{1,2}, Dibyasree Choudhury¹, Nabanita Naskar^{1,3}, Kalpita Ghosh^{4**}*

¹Saha Institute of Nuclear Physics, 1/AF Bidhannagar, Kolkata-700064, India

²Homi Bhabha National Institute, 1/AF Bidhannagar, Kolkata-700064, India

³Department of Environmental science, University of Calcutta, Ballygunge Circular Road, Kolkata-700019, India

⁴Charuchandra College, 22, Lake Place Road, Lake market, Kalighat, Kolkata-700029, India

*E-mail: susanta.lahiri@saha.ac.in

**E-mail: kalpita_das@yahoo.co.in

1. Introduction

Lead-bismuth eutectic (LBE) has enormous potential as source of clinically important radioisotopes [1] and is one of the planned targets for production of rare ion beams. However, the production of α -emitting Po radionuclides from proton irradiated LBE targets are of major concern. It is a known fact that long-lived radioisotopes may be used for some therapeutic studies such as brachytherapy, therefore in this paper, we have attempted to utilize the high-energy α - particles emitted by ^{208}Po ($T_{1/2} = 2.898$ a, $\alpha = 5.1$ MeV) in therapy by synthesising its radiopharmaceutical using a natural resource, hesperidin. The use of hesperidin in targeted therapy of cancer is well established [2] and its efficient free radical scavenging property justifies the present study.

2. Experimental

2.1 Production of ^{208}Po : LBE foil (7 mg/cm^2) was irradiated was 18 MeV proton beam and 3000 μC integrated charge at BARC-TIFR Pelletron, India. Before irradiation the foil was coated with a two-component glue to arrest the evaporation of any volatile radioisotopes from the target. The target was kept aside for 10 months to decay all short-lived radioisotopes. Also even ^{210}Po ($T_{1/2} = 138.38$ d) decayed $\sim 80\%$ about this time, if formed at all.

2.2 Isolation of Hesperidin: The flavonoid hesperidin was extracted from orange peel by an established method [3] and confirmed from melting point and IR spectrometry.

2.3 SLX studies of ^{208}Po -Hesperidin association by LSC: The irradiated foil was dissolved in 3 M HNO_3 .

The α -emitting ^{208}Po radionuclides produced in proton irradiated LBE targets were measured by liquid scintillation counting-triple to double coincidence ratio (LSC-TDCR) technique by optimizing α/β separation. Time resolved alpha counts at optimized condition, enabled identification of ^{208}Po in the target matrix. Solid-Liquid extraction (SLX) was carried out with hesperidin at different pHs. 5 mg hesperidin was added to 1.5 mL liquid phase containing ^{208}Po solution of particular pH. The systems were shaken and settled for 30 minutes. 1 mL liquid phase was taken out by syringe filter and to it 10 mL Aqualite cocktail (from HIDEX) was added and counted for 1000 s in LS counter. Since change in acidity of the medium changes α/β optimization, therefore for every pH condition the reference was different. The reference was prepared in similar way without addition of hesperidin. After optimizing the pH, the extractions were also carried out by varying the weights of hesperidin.

3. Results and discussions

Figure 1 shows the extraction of ^{208}Po by hesperidin at different pH conditions. Maximum extraction of 48% was observed at pH 1.66. At this pH, weight of hesperidin was varied (figure 2). Extraction increased linearly with weight and was found to be 75% with 16 mg hesperidin.

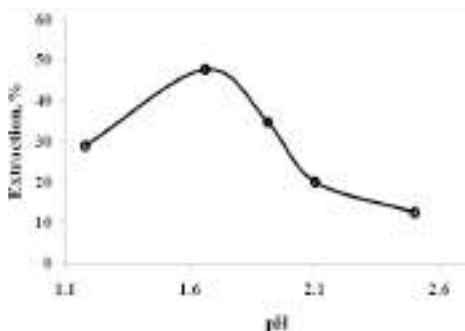


Figure 1. ^{208}Po Extraction at different pH

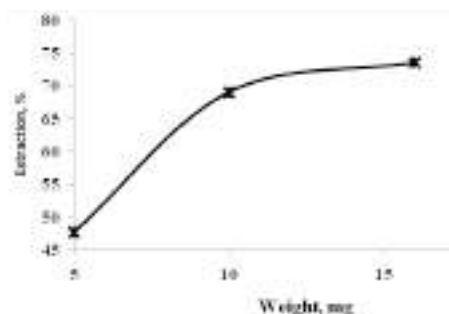


Figure 2. ^{208}Po Extraction with weight of hesperidin

Conclusions

^{208}Po was successfully extracted by hesperidin, which demonstrates the possibility of *in vivo* use of ^{208}Po -hesperidin association as targeted radiopharmaceutical especially where long term exposure is required.

References

- 1/ D. Choudhury, S. Lahiri, Appl. Radiat. Isotopes 137 (2018) 33-40.
- 2/ K.S. Devi, T. Rajavel, S.F. Nabavi, et al., Ind Crops Prod. 76 (2015) 582-589.
- 3/ R. Ikan, Natural Products (A Laboratory Guide) 2nd Edition, Academic Press Inc, USA, 1991, 10

Hot Fusion of Fission Fragments for The Synthesis of Doubly Magic Nucleus $^{310}_{126}\text{X}_{184}$

*Dalip Singh Verm**, *Kushmakshi*

Department of Physics and Astronomical Science,
Central University of Himachal Pradesh, Dharamshala, District Kangra, (H.P)-176215, INDIA
*E-mail: dsverma@cuhimachal.ac.in

1. Introduction

Superheavy elements and their isotopes can be synthesized in a number of reactions like hot and cold fusion, fusion of fission fragments, transfer reaction and reactions with radioactive beams etc. In this paper, we have opted for the fusion of fission fragments and the suitable target-projectile combinations have been predicted on the basis of the quantum mechanical fragmentation theory [1], where the cold valleys in the potential energy surfaces between the fission fragments have been considered in hot optimum orientations giving same compound nucleus. We have predicted suitable target-projectile combinations for production of doubly magic nucleus $^{310}_{126}\text{X}$, beyond $Z=118$ in Sn and Ba valleys.

2. Methodology

The fragmentation potential between the colliding nuclei is,

$$V_T = \sum_{i=1}^2 V_{LDM}(A_i, Z_i) + \sum_{i=1}^2 [\delta U_i] + V_p(R, A_i, \beta_{\lambda i}, \theta_i) + V_c(R, Z_i, \beta_{\lambda i}, \theta_i)$$

where $V_{LDM}(A_i, Z_i)$ is the liquid drop binding energies calculated using the Seeger's formula [2] with its refitted bulk and asymmetry constants to reproduce the ground state binding energies of recent exp. [3] and theoretical data [4]. The shell corrections δU_i are calculated using the Myers and Swiatecki formula [5] with shell closures at 2, 8, 14, 28, 50, 82, 126, 184 (for both N and Z) and 258 (for N only). V_C and V_P are the Coulomb and Proximity potentials, respectively. The Schrödinger wave equation is solved for mass asymmetry (η) coordinate with V_T to give the pre-formation probability P_0 .

3. Calculations & Results

Fig.1(a) shows V_T calculated for the optimum hot fusion configurations [1] for the decay of $^{310}_{126}X$ as a function of fragment mass number (A_2). Figure 1(b) shows that only the region around Sn and Ba has relatively large P_0 (i.e, greater than 10^{-3}). Next, we have calculated the fission barriers, decay rates and half-lives for the fragment combinations shown in Figure 1(b), which are shown in table 1.

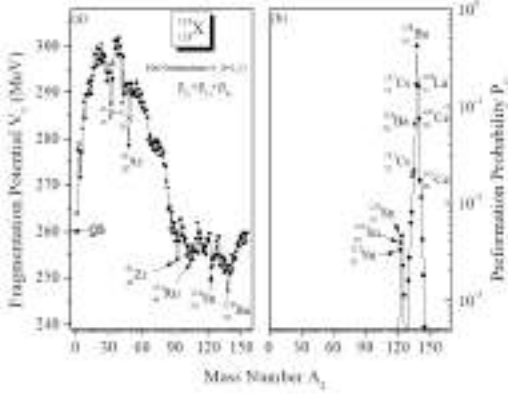


Figure 1. (a) Fragmentation potential (b) preformation probability as a function of fragment mass number A_2 .

From the table, we find that for $^{122}\text{Sn}+^{188}\text{Os}$ the fission barrier is greater than that for $^{124}\text{Sn}+^{186}\text{Os}$, but $^{124}\text{Sn}+^{186}\text{Os}$ has the minimum decay rate and the maximum half-life in the Sn-valley. Similarly, in the Ba-valley the maximum fission barrier, the minimum decay rate and the maximum half-life are obtained for $^{135}\text{Cs}+^{175}\text{Lu}$. So, in the Sn and Ba-valleys the favourable target projectile combinations for the synthesis of $^{310}_{126}X$ should be $^{122}\text{Sn}+^{188}\text{Os}$ and $^{135}\text{Cs}+^{175}\text{Lu}$.

Table 1. Probable beam target combinations for the production of compound nucleus $^{310}_{126}X^{184}$

S.No.	Probable T-P combination	Fission Barrier (MeV)	Decay Rate (s^{-1})	$T_{1/2}$ (s)
1.	$^{122}\text{Sn}+^{188}\text{Os}$	13.03	6.66×10^{17}	1.04×10^{-18}
2.	$^{123}\text{Sn}+^{187}\text{Os}$	11.85	5.73×10^{17}	1.21×10^{-18}
3.	$^{124}\text{Sn}+^{186}\text{Os}$	12.46	4.52×10^{17}	1.53×10^{-18}
4.	$^{135}\text{Cs}+^{175}\text{Lu}$	12.44	4.91×10^{19}	1.41×10^{-20}
5.	$^{136}\text{Ba}+^{174}\text{Yb}$	10.87	2.08×10^{20}	3.33×10^{-21}
6.	$^{137}\text{Cs}+^{173}\text{Lu}$	10.7	5.72×10^{20}	1.21×10^{-21}
7.	$^{138}\text{Ba}+^{172}\text{Yb}$	10.35	1.41×10^{21}	4.92×10^{-22}
8.	$^{139}\text{La}+^{171}\text{Tm}$	7.89	5.46×10^{20}	1.27×10^{-21}
9.	$^{140}\text{Ce}+^{170}\text{Er}$	6.05	2.43×10^{20}	2.96×10^{-21}

4. Conclusions

For synthesis of $^{310}_{126}X^{184}$, $^{122}\text{Sn}+^{188}\text{Os}$ and $^{135}\text{Cs}+^{175}\text{Lu}$ are most suitable combinations.

References

- /1/ R. K. Gupta *et al.*, J. Phys. G: Nucl. Part. Phys. 31 (2005) 631 and refs there in.
- /2/ P. A. Seeger, Nucl. Phys. 25 (1961) 1.
- /3/ M. Wang, G. Audi *et al.*, Chinese Physics C 41 (2017) 030003.
- /4/ P. Möller *et al.*, Atomic and Nuclear Data Tables, 109-110 (2016) 1.
- /5/ W. Myers and W. J. Swiatecki, Nucl. Phys. 81 (1966) 1.

Calculation Method for Detection Efficiency of Voluminous Samples

Salma Boukhalfa^{1}, Kahina Belkessa¹ and Rachid Khelifi¹*

¹LPTHIRM, Faculté des Sciences, Université de Blida 1, BP 270, Route de soumaa, Algérie

*E-mail: boukhalfasalma@gmail.com

1. Introduction

The natural radioactivity evaluation using a gamma ray spectrometry chain with a 3"×3" NaI (TI) detector needs of voluminous samples analysis. This objective requires a good knowledge of the detection efficiency for voluminous sample. In a first step, the spatial efficiency using a multi-gamma ray of a point source has been determined. After then, a method of Gauss-Tchebyshev polynomials was developed for an integral calculation of voluminous sample. In this case, a spatial function that depends on virtual detector center Z_c was determined. Monte Carlo simulation efficiency has been validated by measurement with known sources. The results obtained for efficiency show a very good agreement between Gauss-Tchebyshev calculations method and Monte Carlo simulation.

2. Experiment

2.1. Determination of Spatial Efficiency: Before addressing integral calculations for voluminous efficiency, the point source was measured using a ^{152}Eu source and a 3"×3" NaI (TI) detector. The choice of the positions of the source varies according to the dimensions of the containers used. The latter allow us to determine the virtual detector center Z_c that is a function of solid angle and incident photon energy [1]. In the following, the values of Z_c inside crystal and the Gauss-Chebyshev polynomials are used for the determination of the voluminous efficiency value as a function of energy.

2.2. Monte Carlo simulation: To validate the Monte Carlo code by point sources [2, 3]. A simulation based on the definition of the geometric parameters identical to that of the geometry optimized to experimental measurements as well as the density of material used is also defined.

3. Results and Discussion

Figure 1 shows variation of point efficiency as a function of Z (cm) distance of the detector surface.

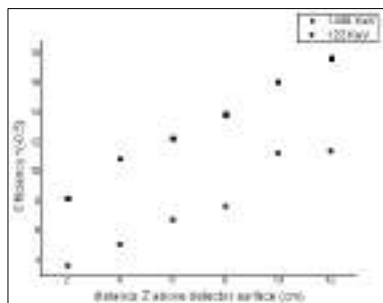


Figure 1. The position Z_c of the virtual center inside the crystal for both 122 keV and 1408 keV.

The distance $Z_c(E)$ can be derived on basis of the calculated efficiencies for points on the Z axis. The extrapolation of the straight line through the points in Z against $\epsilon^{-0.5}$ plot to the intersection with the Z axis give the $Z_c(E)$ value. A functional dependence for the detector efficiency and using of Gauss-Tchebyshev polynomials has been taken. From the results obtained, similar results were obtained by R.M.W Overwater [1].

Table 1. Summarizes the experimental values and simulated by Monte Carlo at 1460 keV.

Efficiency	Exp	MC	$\frac{\text{Exp} - \text{MC}}{\text{Exp}}$
Voluminous	3.54 e-5	3.00 e-4	0.15

4. Conclusion

To make qualitative analysis of samples reliable and feasible for gamma spectrometry for voluminous samples. The simulation of the detector with the use of the Gauss-Tchebyshev polynomials allow us to go back to the desired calibration values. A remarkable agreement between the semi-empirical method and the Monte Carlo simulation. For an application to natural radioactivity in both methods used, the calculated voluminous efficiency of ^{40}K (primordial) where its main line is at 1460 keV is calculated

References

- /1/ R.M.W. Overwater, The Physics of Big Sample Instrumental Neutron Activation Analysis, 5 (1994).
- /2/ William, L. Ademir, X. Silva and César Salgado, (2015) International Nuclear Atlantic Conference.
- /3/ Z. Ahmed, M. Darweesh, J. Applied Phys. 8 (2016) 130-133.

Studies on Extraction of Zirconium by Potato Peel - A Potential Bio-sorbent

Nabanita Naskar^{1,2}, Dibyasree Choudhury², Shalmali Basu¹, Kakoli Banerjee^{3*}

¹Department of Environmental Sciences, University of Calcutta, Kolkata-700019, India

²Saha Institute of Nuclear Physics, 1/AF Bidhannagar, Kolkata-700064, India

³Prabhu Jagatbandhu College, Andul-Mouri, Howrah-711302, India

*E-mail: kakolika@gmail.com

1. Introduction

Search for low cost, easily available greener reagents became an important area of research in all chemical and related areas. In nuclear industry, recycling and recovery of huge amount of Zr (of the order of 1000MT/y) [1] from fuel cladding waste is a challenging problem. To cope up with the hugeness of the problem from environmental point, such a reagent is required which is also available plenty in nature. Earlier potato peel has been utilized as a suitable biosorbent for a few metal ions [2] due to the presence of several bioactive polyphenolic compounds but never explored as an adsorbent of Zr. In this work, attempt has been made to use potato peel as suitable bio-adsorbent for Zr.

2. Experimental

2.1. Preparation of potato peel charcoal (PPC): Potato peels were randomly collected from local domestic waste and washed under running tap water. The peels were then soaked in deionized water for 2 h followed by rinsing in 0.1 M HCl, to make the peel surface protonated to mimic it as an ion exchanger. The peels were dried overnight and burnt to nearly charred form in hot plate. Dried materials were grinded to fine-powder and preserved in desiccator for future use.

2.2. Production of ⁸⁸Zr: Natural yttrium foil (37 mg cm⁻²) was irradiated with 18 MeV proton beam for 8.6 h at Variable Energy Cyclotron Centre, Kolkata with an integrated charge of 27000 μC to produce ⁸⁸Zr(T_{1/2} = 83.4 d) and ⁸⁸Y(T_{1/2} = 106.6 d) by ^{nat}Y(p,2n) and ^{nat}Y(p,pn) reactions respectively. The γ-spectrometric studies were performed using p-type HPGe detector having resolution of 2.1 keV at 1.33 MeV. The photopeaks of 392.9 and 898.06 keV were monitored to measure ⁸⁸Zr and ⁸⁸Y respectively.

2.3. Adsorption of Zr (IV) onto potato peels: The irradiated Y foil was dissolved in minimum volume of 1 M HCl and uptake behavior of Y and Zr by PPC was examined by solid-liquid extraction (SLX) technique. 20 mg of PPC was added separately to 3.5 mL acid solutions at different pH(s) containing 0.5 mL active stock. Each set was shaken for 30 min followed by overnight settling. 1.5 mL supernatant from each set was taken out and counted in HPGe detector. The extent of adsorption was calculated by comparison with the initial activity, prepared in the similar way without adding PPC. At the pH condition showing maximum Zr adsorption, weight variation (10-100 mg) of PPC was done.

3. Results and Discussion

Maximum extraction of Zr (IV) was observed at pH 2 (Figure 1) and with 60 mg PPC (Figure 2). Also a suitable separation condition between Y and Zr was obtained by using PPC at pH 2 and with 20 mg of PPC. The uptake of the radioisotopes by PPC may be due to the replacement of labile H^+ (present on the sorbent surface) by the metal ions in cationic forms. The selectivity of Zr(IV) over Y(III) by potato peel is probably is due to the higher oxidation state of Zr. However, with increasing amount of PPC, Y adsorption was also observed.

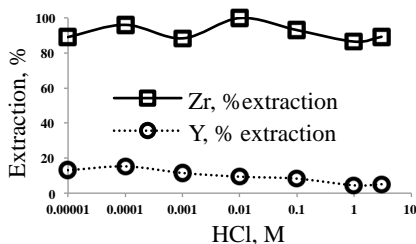


Figure 1. Effect of pH on adsorption study

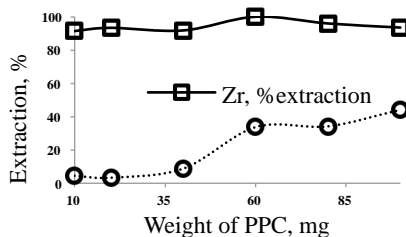


Figure 2. Effect of different weight of PPC on adsorption study

4. Conclusion

Potato peel is a potential bio-adsorbent, which is economically viable, easily available in abundance and a natural reagent. The present study has shown the ability of PPC to adsorb Zr, thus providing a simpler way to recycle and recover Zirconium from nuclear cladding materials.

Acknowledgement: Authors are grateful to Professor Susanta Lahiri for his guidance. SB and NN are thankful to Dr. Punarbasu Chaudhuri, Department of Environmental Sciences, University of Calcutta. DAE-SINP 12 five year plan project TULIP is also acknowledged.

References

- 1/ E. D. Collins, G.D. Del Cul, Waste Management Sym. Conference. (Feb 27–Mar 3, 2011), United States
- 2/ T. Aman, A.A. Kazi, M.U. Sabri, Q. Bano, Colloids and Surfaces B: Biointerfaces. 63 (2008) 116-121.

Evaluation Of The β -delayed Neutron Emission Probability Data And A Study of Their Systematics[#]

G. Mukherjee^{1,2}, K. Bannerjee^{1,3}*

¹Variable Energy Cyclotron Centre, 1/AF, Bidhannagar, Kolkata 700064, INDIA

²HBNI, Training School Complex, Anushaktinagar, Mumbai 400094, INDIA

³Dept. of Nucl. Phys., Research School of Phys. and Eng., ANU, Canberra, ACT 2600, AUSTRALIA

*E-mail: gopal@vecc.gov.in

[#] Work done under the Research Contract No. 17877 of IAEA, Vienna, Austria

1. Introduction

Study of neutron rich nuclei is in the forefront of present day nuclear physics research. Several experimental facilities are being built to study the properties of the neutron rich nuclei. The study of the decay properties and subsequently, the excited states produced by the decay of the neutron rich nuclei are most common and one of the important aspects. It may so happen that after the β -decay of the neutron rich parent nucleus, the populated excited states lie above the neutron separation energy of the daughter. In that case, the daughter nucleus emits a neutron and populates the states of the neighbouring isotope of the daughter. The neutron, thus emitted, is called the β -delayed neutron (bDN). This process may continue to emit one or more neutrons following a β -decay, depending on the Q-value and the neutron separation energy (S_n). The theoretical and experimental investigation to obtain the probability of emission of i number of β -delayed neutrons, P_{in} ($i = 1, 2, 3$) is one of the important topics of present day research [1,2]. Such process has practical implication in several fields, such as r-process nucleosynthesis network calculations, reactor operation, and nuclear fuel post processing, etc. In order to generate a database of the measured quantities of this process, a worldwide collaboration has been developed. As a part of that collaboration, we have evaluated the P_{in} data of the nuclei with $Z = 41 - 48$ and have carried out a systematic study of the data.

2. Evaluation procedure

A common procedure has been followed to compile and evaluate the published data on bDN emitters and potential bDN emitters.

The compilation includes half-life ($T_{1/2}$) in sec (s), P_{1n} ($i = 1, 2$ and 3) values in percent (%), the references, the experimental methods, whether neutron spectra are provided and a comment on $T_{1/2}$ measurement published until 2016. The adopted values are given in the evaluation table with a note on the basis of the adopted value. There were 103 nuclei with 10 isomeric states included in the tables between Nb ($Z = 41$) to Cd ($Z = 48$). Among these, only 32 have measured P_{1n} data and no data on P_{2n} and P_{3n} were found.

3. Systematic investigation of the data on P_{1n} values

The systematic behaviour of the P_{1n} values are very interesting and phenomenological models have been developed to understand the systematics [3], We have investigated the systematics of the adopted P_{1n} values in this work and their correlation with different parameters, such as, the Q-value, the separation energy, the neutron-richness of the parent, etc. Fig. 1 shows the variation of P_{1n} with mass number for different nuclei. Interestingly, certain elements do not follow the general trend of increase of P_{1n} with mass. Other correlations are also studied and will be presented in the symposium.

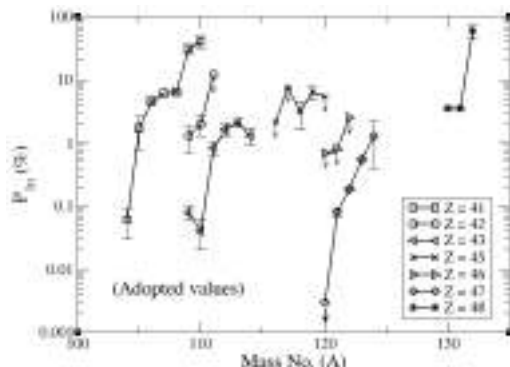


Figure 1: Adopted values of the β -delayed 1-neutron emission probability (P_{1n}) as a function of mass number (A).

Acknowledgement: Financial assistance of IAEA through the Research Contract No. 17877 is gratefully acknowledged. Authors are thankful to Prof. B. Singh (McMaster Univ., Canada) and Dr. Paraskevi Demetriou (IAEA, Austria) for guidance and to NNDC for supplying many of references.

References:

- /1/ R. Caballero-Folch et al., Phys. Rev. Lett. **117**, 012501 (2016).
- /2/ M. R. Mumpower et al., Phys. Rev. C **94**, 064317 (2016).
- /3/ E. A. McCutchan et al., Phys. Rev. C **86**, 041305(R) (2012).

Shell Effect on The Dynamics of The Fusion Fission Process

A. Sen^{1,2,}, T.K. Ghosh^{1,2}, S. Bhattacharya¹, K. Bannerjee^{1,#}, C. Bhattacharya^{1,2}, Samir Kundu^{1,2}, G. Mukherjee^{1,2}, A. Asgar¹, A. Dey¹, A. Dhal¹, Moin Shaikh¹, J.K. Meena¹, S. Manna^{1,2}, R. Pandey^{1,2}, T.K. Rana¹, Pratap Roy^{1,2}, T. Roy¹, V. Shrivatava³*

¹Variable Energy Cyclotron Centre, 1/AF, Bidhan nagar, Kolkata 700064.

²HBNI, Anushaktinagar, Mumbai 400094.

³Saha Institute of Nuclear Physics, 1/AF, Bidhan nagar, Kolkata 700064.

[#]Present address: ANU, Canberra, ACT 2600, Australia.

E mail: a.sen@vecc.gov.in

1. Introduction

The elements beyond $Z=104$ in the periodic table, called super heavy elements (SHE), exists because of shell effects. For the production of SHE, fusion of two heavy nuclei is required. After the two fusing nuclei come into the contact configuration, the di-nuclear system may evolve in shape to form a compact equilibrated heavy nucleus, or it may decay into fission like events before forming a compound nucleus which is known as quasi-fission. The competition between these two processes exhibits complex behaviour. Production of SHE requires understanding of the evolution of shell effects with excitation energy and quasi-fission mechanism for a wide region of nuclei from pre-actinides to super heavies. Keeping in view the same, our group in VECC has embarked on an experimental program to understand the fusion fission dynamics of heavy nuclei with $A\sim 200$ through fission fragment mass distribution as a probe. It is to be mentioned that fission fragment mass distribution is used widely as a sensitive probe to study both the phenomena of shell effects and quasi fission. [3].

2. Experiments

Three experiments at different accelerator facilities in India (VECC, TIFR, and IUAC) have been conducted in order to study two different heavy nuclei (^{210}Po & ^{224}Th) and elucidate the fusion fission dynamics. Two indigenously developed MWPC gas detectors were used to detect the fission fragments and construct the fission fragment mass distributions using the TOF difference technique.

The reaction ${}^4\text{He} + {}^{206}\text{Pb} \rightarrow {}^{210}\text{Po}$ was studied at VECC K-130 cyclotron, with alpha beams of energy 37-55 MeV. The motivation of this experiment was to look for the evolution of shell effects with excitation energy and in particular the weak shell effects at $E^* \sim 30$ MeV as predicted by Möller *et al.* [1]. In the second set of experiments the nucleus ${}^{224}\text{Th}$ was studied via two different reactions ${}^{16}\text{O}$ on ${}^{208}\text{Pb}$ at TIFR, Mumbai and ${}^{19}\text{F}$ on ${}^{205}\text{Tl}$ at IUAC, New Delhi. While one set of projectile target combination is doubly magic, the same nucleus was populated via another channel where neither the projectile nor target is magic. This experiment shall reveal the role of magicity in the entrance channel in the fusion fission dynamics and its role in quasi fission, if any.

3. Results & conclusions

The analysis of the fission fragment mass distribution of the ${}^{210}\text{Po}$ nucleus at an excitation energy of 30.8 MeV clearly shows that the mass distribution is mostly symmetric in nature (red broken line in Fig 1(a)) along with a weak asymmetric distribution (blue line in Fig 1(a)) with the heavier fragment centred around the mass ~ 140 u, which is reminiscent of a weak shell effect. On increasing the excitation energy, this fine structure was no longer seen, indicating washing out of shell effects at higher energies [2]. In the other set of experiments analysis shows mass distributions from the two reactions are symmetric in nature. The results of the experiments will be presented in the conference.

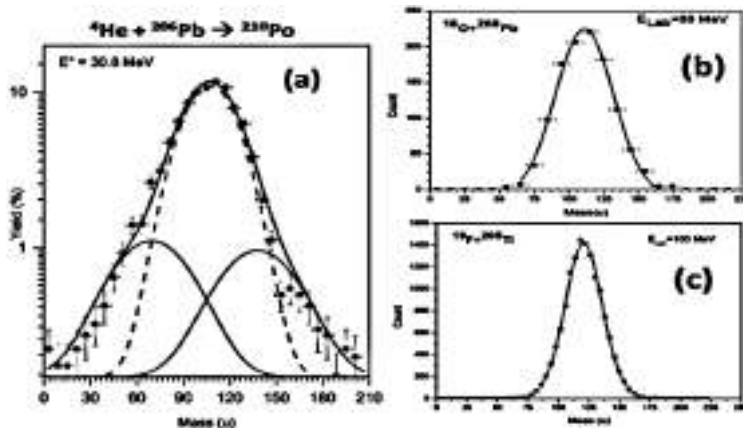


Fig 1: (a) Mass distribution of ${}^{210}\text{Po}$. (b) Mass distribution of ${}^{224}\text{Th}$ via ${}^{16}\text{O} + {}^{208}\text{Pb}$ reaction. (c) Mass distribution of ${}^{224}\text{Th}$ via ${}^{19}\text{F} + {}^{205}\text{Tl}$ reaction.

References:

- /1/ P. Möller, *et al.*, Phys. Rev. C 91, 044316 (2015).
- /2/ A. Sen, T.K. Ghosh, *et al.*, Phys. Rev. C 96, 064609 (2017).
- /3/ A.N. Andreyev, *et al.*, Rep. Prog. Phys. 81, 016301 (2018).

Electron Beam Irradiation Effect on Structure, Morphology and, Optical Properties of PVDF HFP/PEO Blend Polymer Electrolyte Film

*Yesappa L, Ashokkumar SP, Vijeth H, Vandana M, Basappa M, Niranjana M, Ganesh S, Devendrappa H**

Department of Physics, Mangalore University, Mangalagangothri -574199, India
*E-mail: dehu2010@gmail.com

1. Introduction

Uses of polymer blends have increased since last few years due to prominent advantages like easily process ability, lightweight, less cost, mold into desired shape and size, and environmental stability. The polymer blends are prepared to reduce costs by combining high-quality polymers with cheaper materials to explore a polymer for desirable properties for various purposes [1]. Advancement in technology rushed researchers to study effect of radiation on material physical properties performance in the radiation environment may offers to use in the medical applications, optoelectronic, nanotechnology and space applications. The changes in polymer physio-chemical properties can be done by exposing to ionized radiations and it results in degradation of polymer to form the free radicals by chain scission process. The modified polymers has become an important research area, especially in industrial applications like wire, cable, and electronic devices [2]. Variations in structure, morphology and optical response of PVDF-HFP/PEO polymer blend electrolyte films before and after electron beam (EB) irradiation was briefly discussed in this paper.

2. Experiment

2.1 Materials and Methods: The PVDF-HFP: PEO (w/w 90:10, PHP10) polymer blend electrolyte films by the solution cast method using DMF as solvent and peeled off after evaporation at room temperature. The films were characterized by the FTIR, XRD, FESEM and UV-Visible spectroscopy to study the changes in structure, morphology and optical properties before and after irradiation using 8 MeV electron beam (EB) energy at 40, 80 and 120 kGy doses.

3. Results and Discussion

Figure 1(a) shows decrease in optical band gaps from 5.24 eV of unirradiated to 4.7 eV for 120 kGy EB dose. This confirms that optical properties of the polymer blend electrolytes can be changed by irradiation.

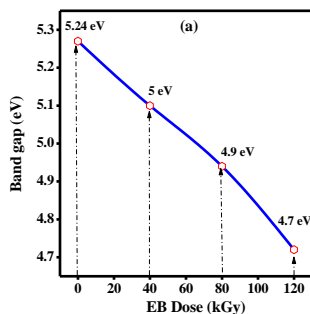


Fig 1: (a) Plot of optical band gap versus EB irradiated polymer blend electrolyte films at various dosage.

3.1. Discussions

The EB energy can bring changes in structure and morphological PHP10 film. Direct optical band gap energy of PHP10 films before and after irradiation was studied and observed for the decrease in E_g with increasing EB dose, resulting in decrease in delocalization of π electrons due to the increased amorphous phase. The irradiation process may damage the polymer chain by chain scission and crosslink is led to the formation of carbon clusters which may enhance the electrical conductivity in the EB irradiated polymer electrolyte films.

4. Conclusions

Changes in structure and morphology was confirmed by FT-IR, XRD, and FESEM analysis of unirradiated and irradiated films. The optical absorption increases and redshift with increase EB dose is attributed to the transition of electrons from one state to another state as a result to decrease the optical band gap and increases the optical absorption properties of polymer blend electrolyte films with increased EB dose.

Acknowledgement: The author thankful to DAE-BRNS for sanctioning major research project (letter No. 34(1)/14/39/2014-BRNS/dated10-12-2014).

References

- /1/ L. Yesappa, M. Niranjana, S.P. Ashokkumar, et al., RSC Adv.8 (2018) 297–309.
- /2/ K. Subramanya, V. Manjunatha, S. Raghu, Phys. D: Appl. Phys. 44 (2011) 105403

Assessment of Natural Radionuclide Enrichment and Radiation Hazard from Building Materials in Kannur District, Kerala

K. Nadira Mahamood, C.S. Kaliprasad, Y. Narayana, V. Prakash*

Department of Studies & Research in Physics, Payyanur College, Kannur, Kerala, India- 670 327

*E-mail: nadirasufaid@gmail.com

1. Introduction

The study of exposure to natural radiation is important because the major contribution of collective dose to the world population is from natural radiation exposure. The degree of radiation exposure depends on the occupation, type of dwellings, location of habitation and lifestyle of the population. All building materials, both of natural origin and containing industrial by-products, contain various amounts of natural radionuclides as they are derived from the rocks and soils, which always contain radionuclides of uranium and thorium series and radioactive isotope of ^{40}K [1]. In the present study, concentration of radionuclides ^{40}K , ^{226}Ra and ^{232}Th are analysed in cement, granite, tiles, sand, rock powder, redoxide, black oxide, fly ash, wall putty, bricks, roof tile and red stone samples which are often used as building materials in Kannur district, Kerala, India. Radium equivalent activity (Ra_{eq}), gamma absorbed dose rate (D), annual effective dose equivalent (AEDE), alpha index (I_{α}), gamma index (I_{γ}), external hazard index (H_{ex}), internal hazard index (H_{in}), excess lifetime cancer risk (ELCR) and annual gonadal dose equivalent (AGDE) associated with the natural radionuclides are calculated to assess the radiation hazard of the natural radioactivity in building materials. Basic statistics are used to describe the statistical characteristics of the radionuclide activities for all the radionuclides.

2. Experiment

2.1. Materials and methods: Different building material samples, used in the study were collected from the identified locations of Kannur district, Kerala. The samples were crushed and oven dried at 110°C till a constant dry weight was obtained.

The samples were then sieved using 250µm British standard mesh and stored in air tight plastic containers for 30 days to bring ^{222}Rn and its short lived daughter products into equilibrium with ^{226}Ra [2, 3]. Each samples were subjected to gamma spectrometric analysis using high efficiency 2" × 2" NaI (TI) detector and the activity concentration of ^{40}K , ^{226}Ra and ^{232}Th in the samples were determined.

3. Results and Discussion

Table 1 shows activities of radionuclides concentration and associated radiological parameters. The higher radium equivalent activity was obtained by sand samples collected from rural areas of Kannur district. The activities of ^{40}K , ^{226}Ra and ^{232}Th for all samples were compared with world average values and the calculated values were well within the admissible limit. The correlation between the activity concentration of ^{40}K , ^{226}Ra and ^{232}Th was plotted and frequency distribution was greatly studied. The study showed that these building materials contributed no significant radiation hazard and hence these materials can be safely utilized by the inhabitants for the construction of dwellings.

Table 1. Activity of ^{40}K , ^{226}Ra and ^{232}Th and associated radiological parameters

Statistical parameters	Activity (Bq/Kg)			R_{eq} (Bq/Kg)	H_{ex}	H_{in}	AGDE (mSv/y)	Absorbed dose (nGy/h)	AEDE (mSv/y)	ELCR $\times 10^{-3}$
	^{40}K	^{226}Ra	^{232}Th							
Min	15.64	6.96	2.98	17.67	0.05	0.07	.06	7.99	0.04	0.14
Max	129.74	35.78	23.12	69.98	0.19	0.29	0.21	31.31	0.15	0.54
Mean	50.51	20.56	11.83	41.29	0.11	0.17	0.13	18.79	0.09	0.32
SD	29.11	8.98	5.41	14.93	0.04	0.06	0.05	6.71	0.03	0.12
Variance	847.64	80.72	29.31	222.94	0.002	0.004	2.10	45.01	1.10	1.33
Skewness	1.021	0.10	0.03	0.077	0.08	0.14	0.029	0.035	0.03	0.04

Acknowledgement: First author wishes to acknowledge the University Grants Commission for providing Maulana Azad National Fellowship as MAN-JRF.

References

- /1/ Dhanya Balakrishnan, Umadevi A G, J. P Abraham et al., Int. J. Fundamental Physical Sci., 2 (2012) 41-43.
- /2/ Herbert LV, de Planque G, editors. EML Procedure Manual, 26th ed. New York, Environmental Measurement Laboratory (1983)
- /3/ Prakash M M, Kaliprasad C S, Narayana Y, J. Radiat. Res. Appl. Sci. 10 (2017) 128-134.

Local Structural investigation of NBS glass for Beta irradiation damage using EXAFS & TDPAC

Ashwani Kumar^{1*}, Nidhi Sharma², S.A. Khader³, R.K. Mishra⁴, D. Bhattacharya²,
Neetika Rawat¹

¹RadioAnalytical Chemistry Division, Bhabha Atomic Research Centre, Mumbai 400085, India

²Atomic & Molecular Physics Division, Bhabha Atomic Research Centre, Mumbai 400085, India,

³Electron Beam Facility, BRIT-VASHI, Bhabha Atomic Research Centre, Mumbai 400085, India,

⁴Waste Immobilization Plant, Bhabha Atomic Research Centre, Mumbai 400085, India,

*E-mail: kashwani@gmail.com

1. Introduction

Borosilicate glasses owing to its chemical durability, thermal stability and ability to accommodate large quantities of the waste has been considered one of the matrices for vitrification of High Level Waste (HLW) generated during reprocessing of spent nuclear fuel. The structural damage to glasses from radioactive decay of immobilized actinides and long-lived fission products is an important facet for understanding its stability towards immobilization of waste. In initial 500 Years, beta radiation from fission products activity of immobilized waste, such as ¹³⁷Cs and ⁹⁰Sr, will dominate the radiation effects [1]. Hence it is important to understand the structural changes due to Beta-irradiation damage. In present work, a Sodium-Boro-Silicate (NBS) glass of composition similar to Trombay Waste glass has been studied for irradiation damage using Extended X-ray Absorption Fine Structure (EXAFS) and Time Differential Perturbed Angular Correlation (TDPAC) spectroscopy.

2. Experiment

2.1. Glass Synthesis: The (Na₂O-BaO-B₂O₃-TiO₂-SiO₂) glass was synthesized using melt quench technique. Glass was synthesized for EXAFS experiment containing natural HfO₂. The Hf content was kept to be 0.5% in order to get the good statistical data from EXAFS at fluorescence mode. For TDPAC Study, the glass was doped with ¹⁸¹Hf radioactive probe during the synthesis along with natural HfO₂ to maintain Hf content to be 0.5 %.

3. Results and Discussion

Figure 1 shows the Forward Fourier Transform of EXAFS spectrum recorded at Hf-L3 edge in Fluorescence mode. Figure 2. shows Electric Field Gradient (EFG), V_{zz} , calculated from the hyperfine interaction parameters obtained from fitting of TDPAC data. Table 1 shows the results from the EXAFS data fit and the hyperfine interaction parameter results from TDPAC. Monoclinic structure of Hafnia taken as the standard model to fit EXAFS data whereas TDPAC data is compared with hyperfine interaction parameters of Hafnia (^{181}Hf doped). EXAFS show decrease in average coordination number of Hafnium as function of irradiation dose.

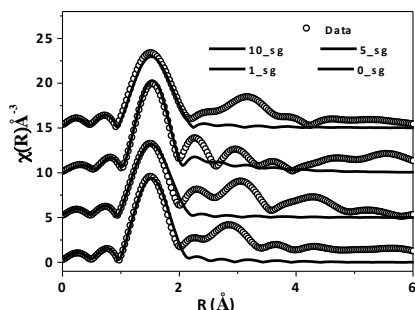


Fig 1: Forw. Four. Trans. of EXAFS spectrum and its fit

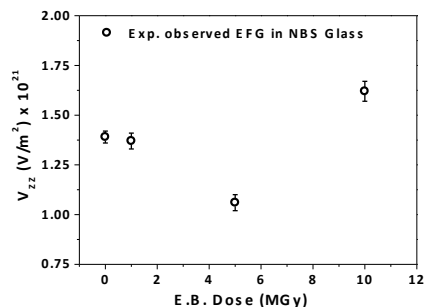


Fig 2: Electric Field Gradient, V_{zz} , at probe site

TABLE.1 EXAFS and TDPAC Results of NBS Glass as function of E.B. Irradiation dose

Glass	EXAFS Results				TDPAC Results			
	Cord. No.	R (2.04, Hf-O)	σ^2 , Debye Waller Factor	R-factor	Wq (Mrad/s)	η	δ	V_{zz} , experimentally determined (V/m^2) $\times 10^{21}$
Hafnia	7	2.04			820 (2)	0.364 (0.005)	0.081 (0.003)	15.01 (0.03)
0 MGy	7.1 (0.8)	2.03 (0.01)	0.008 (0.002)	0.002	78 (2)	0.45 (0.04)	0.38 (0.02)	1.39 (0.03)
1 MGy	6.6 (0.8)	2.03 (0.02)	0.009 (0.003)	0.006	77 (2)	0.51 (0.04)	0.36 (0.02)	1.37 (0.04)
5 MGy	6.5 (0.3)	1.99 (0.1)	0.007 (0.001)	0.004	59 (2)	0.71 (0.09)	0.44 (0.02)	1.06 (0.04)
10MGy	6.3 (0.2)	2.04 (0.01)	0.008 (0.001)	0.002	90 (2)	0.42 (0.05)	0.39 (0.02)	1.62 (0.05)

4. Conclusion

EXAFS, TDPAC study show the minimum in Hf-O bond distance and in EFG observed at 5MGy dose.

References

/1/ W.J. Weber, R.C. Ewing, C.A. Angell, G.W. Cormack. J. Mat. Res. 12 (1997) 1948-1978.

Probing Electronic Environment in Simulated Waste Glass for β -irradiation Damage using TDPAC

Ashwani Kumar^{1*}, S.A. Khader², R.K. Mishra³, Neetika Rawat¹

¹RadioAnalytical Chemistry Division, Bhabha Atomic Research Centre, Mumbai 400085, India

²Electron Beam Facility, BRIT-VASHI, Bhabha Atomic Research Centre, Mumbai 400085, India,

³Waste Immobilization Plant, Bhabha Atomic Research Centre, Mumbai 400085, India,

*E-mail: kashwani@gmail.com

1. Introduction

Borosilicate glasses owing to its chemical durability, thermal stability and ability to accommodate large quantities of the waste has been considered one of the matrices for vitrification of High Level Waste (HLW) generated during reprocessing of spent nuclear fuel. The structural damage to glasses from radioactive decay of immobilized actinides and long lived fission products is an important facet for understanding its stability towards immobilization of High Level Waste. Beta radiation from fission products activity of immobilized waste, such as ¹³⁷Cs and ⁹⁰Sr, will dominate the radiation effects in initial 500 Years [1]. Hence it is important to understand the structural changes due to Beta-irradiation damage. In present work, a Simulated Waste NBS (Sodium-Boro-Silicate) glass of composition similar to Trombay Waste glass has been studied for irradiation damage using Time Differential Perturbed Angular Correlation (TDPAC) spectroscopy.

2. Experiment

2.1. Glass Synthesis: *Na₂O-BaO-B₂O₃-TiO₂-SiO₂-Simulated Waste Oxides* Glass was synthesized using melt quench technique. Glass was doped with ¹⁸¹Hf radioactive probe during the synthesis. Electron Beam (E.B.) Irradiation was performed at Electron Beam facility, BRIT-Vashi.

2.2 Probe Preparation: A 5mg of HfOCl₂ of natural composition was taken in sealed quartz tube and irradiated in neutron flux of 5×10^{13} n/(sec.cm²) at Dhruva Reactor for a week followed by cooling of 2 days. Stock Solution was prepared by dissolving irradiated HfOCl₂ in 6mL of 6 M HCL solution.

3. Results and Discussion

Figure 1 shows the TDPAC spectrum of a Simulated Waste glass irradiated with E.B. dose of 10 MGy and Figure.2. shows the Forward Fourier Transform of TDPAC spectrum along with its fit. Table 1 shows the hyperfine interaction parameters obtained from TDPAC data fit. TDPAC data is compared with hyperfine interaction parameters of Hafnia. EFG (V_{zz}) and the Quadrupole Interaction Frequency around probe atom dropped drastically in glass when compared with Hafnia. Both show increasing trend with irradiation after dropping at 1 MGy dose.

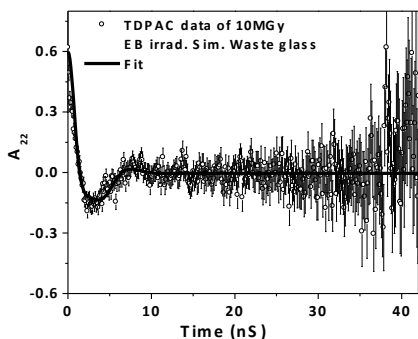


Figure.1. TDPAC Spectrum of Simulated Waste glass irradiated with 10 MGy E.B. dose

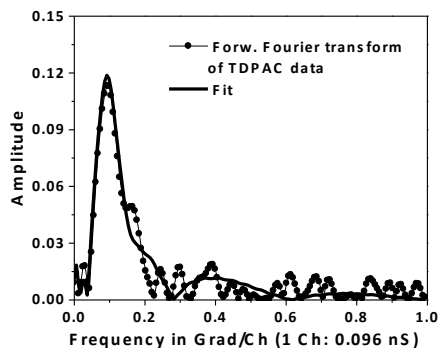


Figure. 2. For. Four. Trans. of TDPAC spectrum and spectrum Fit.

TABLE.1 TDPAC Results of Simulated Waste Glass as function of E.B. Irradiation dose

Simul. Waste Glass	W_Q (Mrad/sec)	η , Assym. Parameter	δ	χ^2 of the fit	V_{zz} experimentally determined (V/m^2)
Hafnia	820 (2)	0.364 (0.005)	0.081 (0.003)	1.3	$15.01 (0.03) \times 10^{21}$
0 MGy	79 (2)	0.46 (0.03)	0.33 (0.02)	1.0	$1.42 (0.03) \times 10^{21}$
1 MGy	69 (2)	0.55 (0.05)	0.39 (0.02)	0.6	$1.24 (0.04) \times 10^{21}$
5 MGy	74 (3)	0.53 (0.07)	0.42 (0.03)	0.8	$1.32 (0.06) \times 10^{21}$
10 MGy	82 (4)	0.47 (0.06)	0.27 (0.03)	0.7	$1.46 (0.06) \times 10^{21}$

4. Conclusion

TDPAC study has been performed to probe the changes in electronic environment as function of E.B. Irradiation Dose. The EFG around probe atom is found to be order of 10 times smaller than in Hafnium oxide indicating drastic reduction in electron density around the probe atom in glass. As irradiation dose increases, Quadrupole Interaction Frequency (W_Q) and EFG (V_{zz}) show increasing trend.

References

/1/ W.J. Weber, R.C. Ewing, C.A. Angell, G.W. Cormack, J. Mat. Res. 12 (08), 1948-1978 (1997).

Radiological Status in Marine Materials Collected from The St. Martin Island of Bangladesh

Al Amin¹, M.H.Miah¹, Shahadat Hossain², Mayeen Uddin Khandaker^{3}
M. N. Mustafa⁴*

¹Department of Physics, University of Malaya, 50603 Kuala Lumpur, Malaysia

² Radioactivity Testing and Monitoring Laboratory, Atomic Energy Center, Bangladesh Atomic Energy Commission, Chittagong, Bangladesh

³Center for Radiation Sciences, School of Healthcare and Medical Sciences, Sunway University, 47500 Bandar Sunway, Selangor, Malaysia

⁴ Southern University, Chittagong 4000, Bangladesh

*E-mail: mu_khandaker@yahoo.com

1. Introduction

All living beings on the earth has been continuously exposed to varying amounts of ionizing radiation originated from both natural and man-made sources. The St. Martin is the only coral island of Bangladesh located at the southern part of Bay of Bengal surrounded by huge black stone, and is famous for tourism due to the crystal clean water with rich biodiversity including the presence of various species of coral reefs, turtles, algae etc. In addition to the various kinds of fishing activities by the local populace, thousands of tourists every year visits this island for leisure and left behind many organic and inorganic materials as food wastes. Wind transformation and processes of hydrodynamics of long-shore and tidal currents from the Bay of Bengal are the influential for sediment transport mechanisms that can alter the radioactive balance in the surrounding materials of this Island. Radionuclides in marine materials like coral reefs, turtles, algae etc. is rarely measured and assessed relative to other human habitats and marine ecosystems. Coral reefs provide habitats for many species of marine biotas. Chemicals in coral skeleton have also been widely investigated to reconstruct past climate change and environmental pollution [1, 2]. However, only very limited information are available on the radioactive status in coral reefs relative to other environmental matrices, such as crust, rocks, sandy beach, building materials, and marine organisms. Therefore, it is important to monitor the level of natural radioactivity in the aforementioned marine materials that are abundantly found surrounding to this island and the estimation of associated radiation hazards to the public health.

2. Materials and Methods

Activity concentrations of primordial radionuclides in coral reefs, including the beach sand and sediment collected from the surrounding coastal waters of the Island were measured by conventional γ -ray spectrometry, and in-situ γ -ray dose by portable radiation survey meter [3]. Prior to sampling, a hand-held halogen quenched Geiger Müller survey meter was used to observe the ambient gamma radiation. At each sampling point, 3 readings were recorded and the mean is reported. The surface sand samples (0-20 cm) were collected per sampling point and mixed together thoroughly to give a composite sample of 1 kg that represent the sampling point. The sand samples were stored in polyethylene bags, sealed and labelled properly for transportation to the laboratory.

3. Results and Discussion

The mean activity concentrations (Bq/kg) for ^{226}Ra , ^{232}Th and ^{40}K in the studied samples are 13.1 ± 2.1 , 16.6 ± 2.7 and 85.0 ± 43.3 respectively which are lower than the world average values 35, 35 and 450 Bq/kg respectively, while the black beach sand show higher activity of 7000 ± 560 Bq/kg and 12400 ± 868 Bq/kg for ^{226}Ra and ^{232}Th respectively. The main contributor of radionuclides enrichment in such sample is the presence of monazite rich black sands. The measured data were compared with the literature data and also the recommended limits set by the relevant international bodies. The radiological parameters including radium equivalent activity (Ra_{eq}), external and internal hazard (H_{ex} and H_{in}), representative gamma level index ($\text{I}_{\gamma\text{r}}$), absorbed gamma dose rate (D_{R}) and annual effective dose equivalent were also calculated.

4. Conclusion

The studied coral reefs collected from the surrounding of St. Martin Island pose no significant radiological threats to the local populace and tourists going to the beaches for leisure. However, the radioactivity in beach sand (particularly black beach sand) show quite higher value that needs perpetual monitoring. The findings of this research work forms the baseline radioactivity in this area, and this might be helpful for radiation monitoring framework and regulatory controls.

References

- /1/ N. Saha, G.E Webb, and J.X. Zhao. Science of the total environment 566 (2016) 652-684.
- /2/ K.F. Yu. Science China Earth Sciences 55(8) (2012) 1217-1229.
- /3/ H.K Shuaibu, M.U. Khandaker, T. Alrefae. Marine Pollution Bulletin 119(1) (2017) 423-428.

Indoor Radon Measurements in Newly Houses of Tashkent City by CR-39 Detectors

Abdisamat Vasidov, Sevara Vasidova

Institute of Nuclear Physics, Tashkent, Uzbekistan
Email: samad@inp.uz

1. Introduction

About 60% of annual radioactive dose may be received by people originates from natural radioactive gas radon-222 and its daughter products (RDP) is due to the geographic locating and building materials of dwellings. Recently mostly private houses of Tashkent have been constructed three-level apartments: first one – basement, cellar story and sauna; second one - hall, drawing room, kitchen and bathroom; third one – bedrooms and bathrooms. The main building materials used in these houses, are burnt bricks (BB), cement, plaster (PL), wood, wallpapers (WP), oil color (OC). The aim was to carry out measurements of the radon volume activity (RVA) and determination of radon exhalation rate (RER) from building materials and assessment annual effective dose (AED) for inhabitants.

2. Experimental

The CR-39 track detector 0.70 mm thickness was cut into square pieces of 25x25 mm² and a serial number engraved on each piece for ease identification. The CR-39 detectors were fixed into two cylindrical plastic chambers with radiuses of 2.6 and 2.6 cm and heights of 7 and 14 cm for measuring RVA and RER, respectively. The entries of chambers were sealed with filter paper, for limits access of radon progeny and ambient air dusts. The chamber with V=148 cm³ was used for measured RVA and installed at a height of 200 cm from the ground level in rooms. Another chamber with V=310 cm³ was used for determination RER and the chambers were fixed in vertical position to surface of investigated materials or walls of room. The CR-39 detectors records α -particles from ²²²Rn only. The CR-39 chambers were exposed within 30-35 days. After end expose the detectors were chemically etched in 6N NaOH solution at 70°C for 12 h.

The etched detectors were washed in tap water 20-25 min and in distilled water 5-7 min and then the detectors were dried with hot air. The α -track images of CR-39 were observed with a track counting system, which consisted of an optical microscope, a color charged couple device camera, and an image processor of computer.

3. Results and discussion

As results of indoor RVA measurements of cellars and rooms of Tashkent the following results have been received: cellars 64-94 and 535-953; halls 72-81 and 181-284; kitchens 82-128 and 288-446; bedrooms 66-92 and 314-455 $Bq \cdot m^{-3}$. In Figure 1, shows the density of α -tracks of the CR-39 detector in sauna and bedroom at the same exposures.

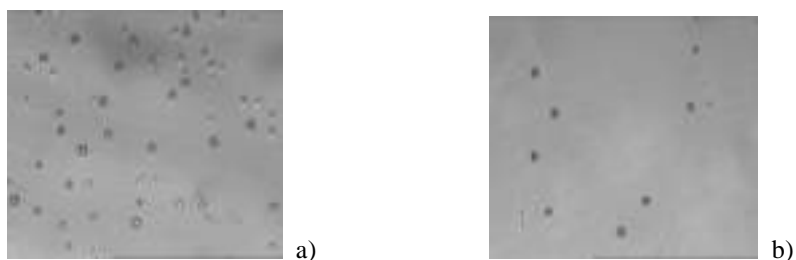


Figure 1: The density of α -tracks of CR-39 in sauna –a) and bedroom –b)

The walls of rooms were constructed from burnt bricks and surface of walls covered plaster, oil color and wallpapers were followed for RER: base soil 2.1-3.6; BB 0.10-0.15; BB+PL 0.13-0.16; BB+PL+OC 0.06-0.09 and BB+PL+WP 0.05- 0.07 $Bq \cdot m^{-2} \cdot h^{-1}$. The values of AED were assessed: 2.1-6.7 for halls; 3.0-9.4 for kitchens and 2.2-9.7 $mSv \cdot y^{-1}$ for bedrooms.

Applications of Dosimetric Measurements to Quality Studies and Optimization of Operating Conditions at A Linear Accelerator

Abdelmajid Choukri^{1}, Ahmed El Mouna Ould Mohammed Yeslem¹,
Oum Keltoum Hakam¹, Slimane Semghouli²*

¹Team of Nuclear Physics and Techniques, University of Ibn Tofail, Faculty of Sciences, Kenitra, Morocco.

²Department of Health Techniques, Higher Institute of Nursing Professions and Health Techniques, Morocco.

*E-mail: choukrimajid@yahoo.com

1. Introduction

Radiation therapy based on the use of an accelerator plays an important role in the treatment of malignant tumour. The quality control for linear accelerator is one of the keys to ensure correct and safe implementation of radiotherapy. This requires proper focusing of the beam in order to destroy the tumor only and avoid irradiation of the healthy cells.

The National Center of Oncology in Nouakchott is equipped with a linear accelerator, which provides photons of two energies: 6 MV and 18 MV. In addition, the Center is equipped with radiotherapy, nuclear medicine and chemotherapy equipment that comply with the international standards and are controlled by the International Atomic Energy Agency (IAEA). All dosimetric measurements were used firstly to check the Quality of the accelerator by comparing them with IAEA standards and in secondly to determine the optimum conditions for different radiotherapy operations.

2. Experiment

Measurements of percentage depth dose and dose profile were carried out using a water phantom. The system is controlled for the acquisition of the dosimetric data by MEPHYSTO mc² software. The dosimetric measurements were carried out using an ionization chamber associated with an electrometer. The material used in this work is:

- 1) Linear accelerator CLINAC 2100DHX with two energies of photons: 6 MV and 18 MV.
- 2) Mini water tank MP3-P (water phantom) with a length of 60 cm.

- 3) Cylindrical ionization chambers: TM31010 Semiflex chamber of 0.125 cm^3 and PTW 0.6 cm^3 .
- 4) PTW electrometer
- 5) Medical Physics Control Center MEPHYSTO mc²: MEPHYSTO is software developed and used for the acquisition of therapeutic beam data and data analysis in radiotherapy.

3. Results and Discussion

Measurement of PDD (percentage depth dose) and BP (beam profile) have been carried out and compared to (TPS) calculation for 6 MV and 18 MV photons beam, using the 0.125 cm^3 ionization chamber for the mostly used treatment field dimensions in treatment by linear accelerator. All the measurements were performed for Skin- Source-Distance (SSD) of 100 cm.

Figure 1 and 2 show the results obtained for 6MV.

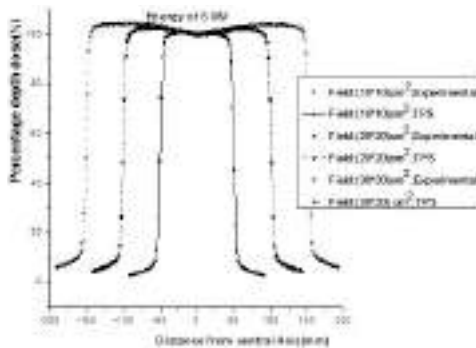
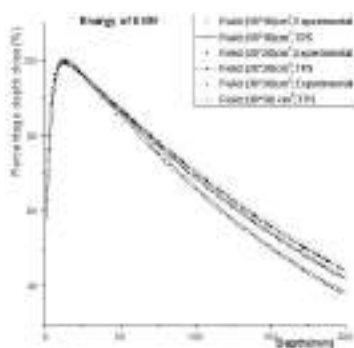


Fig 1: PDD results and comparison with TPS for 6 MV Fig 2: Beam profiles for the 6 MV

4. Conclusion

In this quality control work, we have compared the PDD and BP measurements with results calculated by TPS. Measured results are comparable for all chosen treatment field dimensions to those calculated by TPS. These measurements also allowed determining the optimal conditions for effective irradiation.

Acknowledgement: Assistance from all staff in National Center of radiotherapy in Nouakchott in Mauritania

References

- /1/ M Yeslem, A. El Mouna, M.O. Cheibetta, et al., Innovations in Smart Cities and Applications pp 759-765, Lecture Notes in Networks and Systems book series (LNNS, volume 37), Springer International Publishing AG 2018.
- /2/ A. El Mouna, A. Choukri, O.K. Hakam, S. Semghouli. Int. J. Advanced Res., 6 (2018) 361-369.

Measurements of U Isotopes Activities in Drinking Water Samples by Alpha Spectrometry and Ra Isotopes by Gamma Spectrometry

Abdelmajid Choukri^{1}, Oum Keltoum Hakam¹*

¹Team of Nuclear Physics and Techniques, University of Ibn Tofail, Faculty of Sciences, Kenitra, Morocco

*E-mail: choukrimajid@yahoo.com

1. Introduction

Alpha-particle spectrometry is the most frequently used technique for the activity determination of alpha emitters. It is a highly sensitive and modern measurement technique, which can be used to radiochemical and radiological studies of the natural environment as well as the radio-chronological based on the nuclear phenomena. Considering a small penetration range of alpha particles, the use of alpha spectrometry should precede a labor-intensive radiochemical separation of analyzed radionuclides in addition to the use of appropriate radiotracers to take into account lacks due to different chemical separation steps.

2. Experiment

Water samples are collected in a polyethylene tank and immediately slightly acidified to pH 2-3 with concentrated HNO₃. After filtration, an iron carrier (FeCl₃) and a known amount of ²³²U-²²⁸Th equilibrated spike solution are added. U & Th are coprecipitated with Fe(OH)₃ by addition of NH₄OH. A known quantity of barium in BaCl₂ form is then added. Ra isotopes are co-precipitated with BaSO₄ formed by addition of H₂SO₄. The two precipitates are recovered by centrifugation and/or filtration. The two fractions are then separated.

After complete mixing and oxidation, U and Th are separated and purified on a single resin exchange column using a combination of acids and organic solvents. They are extracted separately with TTA (1-(2-thenoyl)-3,3,3-trifluoroacetone) in toluene. The two organic phases containing U and Th are evaporated onto aluminum foils drop by drop under a mild temperature so as to avoid projections. Any ingress of aqueous solution with the organic part may pierce the aluminum foil.

Production of ^{186g}Re Using 12MeV Protons on Natural WO_3 Target

S.V.Thakare^{1}, K.C.Jagadeesan¹, Rubel Chakraborty¹,
S.V. Suryanarayana², K.P.Muthe³, Ajay Singh³, B.K.Nayak², A.Dash¹, A. Saxena²*

¹Radiopharmaceuticals Division, Bhabha Atomic Research Centre, Mumbai 400085, India,

²Nuclear Physics Division, Bhabha Atomic Research Centre, Mumbai 400085, India,

³Technical Physics Division, Bhabha Atomic Research Centre, Mumbai 400085

*E-mail: svt@barc.gov.in

1. Introduction

^{186g}Re ($T_{1/2}=89.2\text{h}$) has theranostic decay properties that make it attractive for use in targeted radionuclide therapy of cancer [1]. This radionuclide can be produced by irradiation of natural tungsten target in high flux research reactor. ^{186}Re has greater potential for development of theranostic radiopharmaceuticals compare to other radionuclide because of its emission of medium energy beta particle (E_β endpoint 1.07 and 0.93MeV) which can be used to treat a range of tumour sizes and its imaginable photon emission at 137 keV (9.5%). The drawback of ^{186}Re is its the low specific activity obtained from the (n, γ) production method. Despite high thermal and epithermal neutron cross sections of ^{185}Re (106b and 1632b respectively), research reactors are able to produce marginal specific activity of $\sim 111\text{GBq/mg}$ ($\sim 3\text{Ci/mg}$) which activate only 2% of ^{185}Re leaving 98% of the enriched ^{185}Re [2].

An alternative to neutron activation for production of ^{186g}Re is accelerator production through (p,n) reaction using thick natural WO_3 target. This result in much higher specific activity as the ^{186g}Re can be chemically separated from the target [3]. Earlier, cross section of $^{181-184}\text{Re}$ were measured and separation was carried out from proton irradiated tungsten target [4].

2. Experiment

High purity natural WO_3 powder was pelletized with high pressure in a die under high temperature ($\sim 700^\circ\text{C}$) condition. The diameter of the target pellet was 10mm with surface density and surface area as 11.63mg/mm^2 and 78.53 mm^2 respectively. The optimal proton energy range for production of ^{186g}Re via $^{186}\text{W}(p,n)^{186g}\text{Re}$ is the energy range that has a large ^{186g}Re production cross section together with the least production of isotopic and non-isotopic radioactive impurities. This energy range is

obtained by considering the excitation functions of all possible reactions due to other isotopes present in target. TALYS1.8 calculations have been performed to obtain required reaction cross sections. From this calculation it was found that proton energy of 15MeV is optimum for a high thick target yield of ^{186g}Re in order to limit the formation of other radionuclides [5,6]. In this experiment, the WO_3 target of thickness of around 1mm was irradiated by ~200nA proton current at energy of 12MeV for 60 h using the 6m height irradiation facility of Pelletron Accelerator at BARC-TIFR facility.

3. Results and Discussion

Several Re isotopes namely ^{181}Re , $^{182m}\text{Re}/^{182}\text{Re}$, ^{183}Re , ^{184}Re , and ^{186g}Re have been identified in the proton-induced reactions due to the presence of various W isotopes. It is interesting to note that ^{186g}Re was produced exclusively from the (p,n) reaction on ^{186}W which has a considerable cross section and yield for ^{186g}Re around 15MeV for thick target.

Studies were carried out for radionuclide purity of ^{186g}Re by ratio of yield versus proton energy using TALYS1.8. The production of ^{186g}Re per coulomb increases however the ratio of ^{186g}Re to all Re radionuclidic activity decreases as the incident proton energy increases. Using TALYS and SRIM calculations, this study for maximising thick target yields has been extended to enriched targets.

4. Conclusion

Thick target yields have been used successfully for the production of ^{186g}Re medical radionuclide. The calculations show that the 140MBq/C activity can be produced using natural target of WO_3 . The ratio of ^{186g}Re activity to all $^{178-187}\text{Re}$ activity is 0.04 at 12MeV proton energy. Thus the production of ^{186g}Re can be optimized by using enriched WO_3 target and suitable proton energy.

Acknowledgement:- The Authors would like to thank the Pelletron Accelerator facility for providing the support for the irradiation.

References

- /1/ Tara Mastren et. al., Nuclear medicine and Biology 49 (2017) 24-29
- /2/ Ehrhardt, G.Blumer, M.,Su, F.,Vanderheyden,J.,Fritzberg,A., Appl. Radiat. Isot, 48 (1997) 1-4
- /3/ E.R. Balkin, K. Gagnon, E. Dorman, R. Emery, Y. LI et. al. Radiochimica Acta, 105 (2017) 1071-1081
- /4/ D Choudhury, N Naskar, S. Lahiri. <https://doi.org/10.1515/ract-2017-2869>
- /5/ X. Zhang et. al, Radiochim. Acta 86 (1999) 11-16
- /6/ M.L. Bonardi, F. Groppi, S. Manenti, E. Persico, L.Gini. App.Radiat. Isot. 68 (2010) 1595-1601

Photons from Low Power X-Ray Tube for Chemical Shift Studies

*Preeti Rao and Raj Mittal**

Nuclear Science Laboratories, Physics Department, Punjabi University, Patiala, 147002, India.

*E-mail: rmsingla@yahoo.com

1. Introduction

In X-ray fluorescence of isolated atoms, the energies of emitted X-rays are certain because of certainty of excited and ground states. In composite materials, atom experiences potentials of neighbouring nuclei and discreteness of states gets modified [1]. The energies of X-ray lines are shifted. The shift due to chemical environment is called chemical shift [2]. Measured shifts provide information about chemical bonding types, structures of molecules/complexes and activity of composite materials in changing environment. Photon induced X-ray emission is the promising technique to measure the energy shift with higher accuracy. Fluorescent X-ray energy measurements with available low-power X-ray tube in the lab and SOLVER method in EXCEL [3] have been employed for wheat plants grown on soils from different sites and the soils for shift measurements. K and Ca being essential macronutrients of plants are tagged by measuring K $K\alpha$ and Ca $K\beta$ X-ray energy shifts to have a notion of soil environment on nutrients' chemical states.

2. Experiment and data analysis

Pot experiment was performed on soils from 10 different sites of Punjab, India and thick pellets of 2.5 cm diameter of each plant and soil were prepared [4]. In a geometrical set up with 100 watts, Neptune X-ray tube with Rhodium anode and Amptek X123 spectrometer with Si PIN detector of resolution 145eV at 5.959 keV Mn X-rays, emitted X-ray spectra of plants and soil targets were recorded. Tube voltage and current was 8 kV/0.03 mA to excite potassium/calcium K edges with dead time losses <1%. Resolved potassium $K\alpha$ and calcium $K\beta$ peaks were considered for analyzing peak positions using SOLVER program.

Centroid positions were evaluated in channel number and converted into energies using energy calibration of the detector. Punjabi University ground is protected from additional / external organic/inorganic material contaminants so the soil was taken as reference and corresponding energy shifts for K(K_α) and Ca(K_β) peaks were evaluated and listed in table 1.

Table 1. K(K_α) and Ca(K_β) X-ray energy shifts for plant/soil samples.

Sl. No.	Place	Site	Peak Energy Shift (eV)± 0.001 eV			
			Soils		Wheat Plants	
			K(K _α)	Ca(K _β)	K(K _α)	Ca(K _β)
1.	Punjabi University Campus	a) Ground	0	0	0	0
		b) Botanical Garden	2.032	-6.88	-0.562	1.941
		c) Sewage site	1.464	-2.407	5.404	13.622
2.	Ajrawar Village	a) Pond site	-3.386	-7.721	6.474	13.411
		b) Road Side	-6.594	-10.815	5.645	12.453
3.	Patiala City	a) Runnel site	-11.207	-13.311	4.158	13.842
		b) River (Badi Nadi)	-18.338	-20.905	4.381	8.24
4.	Nabha City	a) Farm	-11.373	-16.737	4.377	13.739
		b) Mechanical Factory	-10.194	-13.029	9.011	16.971
		c) Sewage site	-8.319	-14.313	8.654	21.082

3. Results and Discussions

The sign of shifts are opposite for plants and soils supported by the findings of Kaur et al.[5]. Ca(K_β) shifts are more than that for K(K_α) as calcium exists in double positive ionic state Ca²⁺ has capability to get tightly held on negatively charged sites as compared to K⁺. In comparison to university campus soil, village soil looks less polluted than the soils from both the cities Nabha and Patiala. Even river in patiala city shows bad condition than runnel due to its feeding with industrial waste. High shifts in farm soil indicate the change in chemical configuration of soils due to applied fertilizers and pesticides. But, plant soil relationship seems complicate as no definite criteria results to choose the soil conditions for selected seeds.

References

- /1/ B. K. Agarwal X-Ray Spectroscopy, 2nd Edition, Springer-Verlag, Berlin Heidelberg (1991).
- /2/ R. E. Van Grieken and A. A. Markowicz A Handbook of X-ray Spectrometry, 2nd Edition, Marcel Dekker Inc., New York (2002).
- /3/ N. Kallithrakas-Kontos, Spectrochim. Acta B 51(1996), 1655.
- /4/ P. Rao and R. Mittal, Asian J. Phys. and Chem. Sci. 2 (2017), 1.
- /5/ K. Kaur, K. Deep, M. Bansal, M. K. Tiwari and R. Mittal, Arch Appl Sci Res. 4 (2012), 2152.

Projected Application of a Mixer-settler in Transactinide Elements (TAN) Separation Science

*Rupesh H. Gaikwad¹**

¹Department of Chemistry, Maharshi Dayanand College of Arts, Science and Commerce, Mumbai 400012, India
*E-mail: rupeshhgaikwad@gmail.com

1. Introduction

The difficulties involved in the production and rapid chemical isolation of a few single atoms of transactinides (TAN) from numerous other reaction products and the subsequent detection of the nuclear decay require the development of unique separation methods. Due to very low production rates and short half-lives, TAN nuclei must be chemically processed "one-atom-at-a-time" [1] on a very short time scale. Here in I propose liquid phase chemistry for the separation of TAN elements.

2. Proposed liquid phase chemistry process

Liquid - liquid extraction is a well-understood separation technique and is extensively used for studies of trans-actinide elements. Adoption of this technique has overcome the single atom and short $t_{1/2}$ limitations inherent in TAN study. So the method is proposed for separation of elements from TAN.

3. Proposed automated mixer settler column separation

Manually performed chemical separation become impractical due to few atoms per day detections. So automated liquid-phase chemical separation systems become operational due to faster chemical separation. In early 1980s, Hulet et al., carried out the automated extraction chromatographic studies of Rf-chloride [2]. Later, to improve the speed and reduce cross contamination the ARCA II (automated rapid chemistry apparatus) was built by the GSI-Maniz collaboration, featuring two magazines of 20 miniaturized chromatography columns [3]. In separation science, continuous counter-current operation is always preferred to batch and cross-current operations and is achieved through the use of equipments like mixer-settlers.

For laboratory scale counter-current studies, multiple-stage mixer-settler units are found to be suitable from the point of view of operation. In addition, it is easy to carry out a stage-wise sampling of the two phases in mixer-settlers. The analysis of stage samples gives a complete profile of the behaviour of various species during the extraction process. Counter-current studies will be carried out using mixer-settlers. A schematic diagram of a typical four-stage mixer-settler unit is shown in Fig.1. Organic and aqueous phases will enter in each mixing compartment from opposite directions and are thoroughly mixed using a mechanical mixer. The mixed phase will then move to settling compartment, where organic and aqueous phases will be separated from each other because of the difference in their densities. Separated phases will move to the following mixing compartments in different directions, maintaining overall movement of the two phases in opposite directions. The mixing and settling time in each stage will be calculated as follows:

$$\frac{\text{Total volume of the liquid in mixing/settling compartment (ml)}}{\text{Total input of liquids per minute (ml/min)}}$$

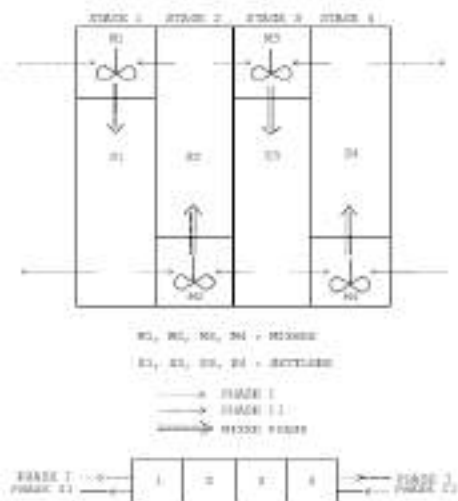


Figure 1. Schematic diagram of a four stage mixer-settler unit

Here, I propose a continuous mixer-settler or liquid-liquid separation of TAN elements. The synthesized nuclides from the GAs-filled Recoil Ion Separator, (**GARIS**) or **TransActinide Separator and Chemistry Apparatus (TASCA)** are subjected to the 4 stage mixer-settler for separation.

4. References

- /1/ D. Turbet, C. LeNaour. In The Chemistry of Superheavy Elements; M. Schädel Ed. Kluwer Academic Publisher; Dordrecht (2003) 318.
- /2/ E.K. Hulet, R.W. Lougheed, J.F. Wild et al. J. Inorg. Nucl. Chem, 42 (1980) 79.
- /3/ M. Schädel, W. Brüchle, E. Jäger et al. Radiochim. Acta 48 (1989) 171.

Determination of Radiation Shielding Parameters for Organic Compounds at Different Gamma Photon Energies using Compton Scattering Geometry

Mohinder Singh^{a,}, Akash Tondon^b, Bhajan Singh^b, B. S. Sandhu^b*

^aDepartment of basic and applied sciences, Punjabi university, Patiala, 147002, India.

^bDepartment of Physics, Punjabi university, Patiala-147002, India.

*E-mail: mohindersingh@pbi.ac.in

1. Introduction

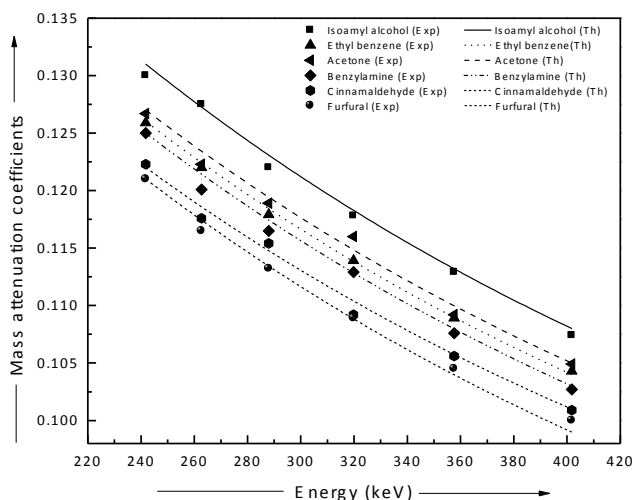
The study of interaction of gamma radiation with matter finds a wide range of applications in the field of medical, biological, industrial, geological and agricultural sciences. The present work emphasizes on the transmission of gamma photon energies in the range (241.8-401.8 keV) obtained by Compton scattering technique [1] for some organic liquids (Isoamyl alcohol (C₅H₁₂O), Ethyl Benzene (C₈H₁₀), Acetone (C₃H₆O), Propylene glycol (C₃H₈O₂), Benzylamine (C₇H₉N), Cinnamaldehyde (C₉H₈O), Furfural (C₅H₄O₂)). The mass attenuation (μ_m) and molar extinction coefficients (ϵ) and effective atomic number (Z_{eff}) are determined for these liquids and results are compared with theoretical data.

2. Experiment

The purpose of the present work is to have the radiological data for low-Z organic compounds using narrow-beam transmission geometry using scattering technique. The primary gamma rays from the radioactive source (¹³⁷Cs of 4Ci) are scattered from thick Al scatterer at a particular angle. The scattered photons (form secondary gamma ray source) corresponds to selected angle, are allowed to impinge on thin walled plastic container, which can be filled with desired solutions of organic compounds. The NaI (Tl) scintillation detector of 6.7% energy resolution is used to records the transmitted events. The unattenuated (I_0) and attenuated intensity (I) are the recorded counting rate under the Compton scattered peak. From this data, mass attenuation coefficient (μ_m) is determined using Beer-Lambert law.

3. Results and Discussion

Parameters μ_m , ϵ and Z_{eff} are measured for organic liquids at energies from 241.8, 262.7, 288.4, 319.8, 357.6, 401.8 keV using Compton scattering technique. From experimentally determined values of μ_m , all other parameters are deduced using simple relations [2]. The homogeneity of the solution was maintained throughout the experiment. The values of μ_m , ϵ and Z_{eff} are found to decrease slowly with increase of incident energy of compounds



under investigations. The experimental variation of mass attenuation coefficients of various compounds as a function of incident photon energy is shown in Figure 1. These values are compared with theoretical results calculated using WinXCom [3] and are found to be in good agreement within experimental estimated errors of the order of $\approx 3.5\%$.

4. Conclusion

Advantage of the present technique using Compton scattering process is that one can get the required photon energy in a range depending on the catering angle. The values of interaction parameters μ_m , ϵ and Z_{eff} are found to be higher for low energy than that at high energy leading to the result that low energy photons are attenuated more owing to higher probability of interaction processes, especially Compton scattering process. The uncertainties in the determined parameters range from 0.10 to 2.56% throughout the photon energy range. There is a need to measure number of such parameters for high atomic number at these energies to account for photoelectric and Rayleigh scattering process.

References

- /1/ P. Limkitjaroenporn, J. Kaewkhao, S. Asavavisithchai. Ann. Nucl. Energy 53 (2013) 64
- /2/ M. Singh, A. Tondon, B. Singh, B.S. Sandhu, Radiat. Phys. Chem. 145 (2018) 80
- /3/ L. Gerward, N. Guilbert, K.B. Jensen, H. Levring. Radiat. Phys. Chem 71 (2004) 653.

Effect of Aluminium Ion Implantation on Structural, Morphological, Electrical and Mechanical Properties of a Template Electrosynthesized Cu Nanowires

*Rashi Gupta, Rajesh Kumar**

University School of Basic and Applied Sciences,
Guru Gobind Singh Indraprastha University, New Delhi-110078, India
*E-mail: rajeshkumaripu@gmail.com

1. Introduction

High aspect ratio metal nanostructures such as nanorods, nanotubes and nanowires have attracted considerable attention [1, 2] due to their novel properties and potential applications in electronics, magnetics, photonics, optoelectronics and biological sensors. Copper has a special interest due to important role in the electronic industry based on its excellent electrical and thermal conductivity. The physical as well as chemical properties of nanowires depend not only on their materials properties but also on their morphologies and structures. The low energy ion implantation is an important technique to generate new and metastable states of the material by introducing atoms and defects athermally. The penetration depth of ions depends on the rate and nature of the energy transfer events in the solid as the ion slows to rest. When ions are implanted into nanomaterials, they collide with the target atoms and interact through three different phenomena; electron collision, nuclear collision and charge exchange. Here, copper nanowires of diameter 200 nm were synthesized by template assisted electrochemical deposition using polycarbonate ion track etch membrane and were implanted with low energy ions.

2. Experiment

The electrolyte consisted of 1M $\text{CuSO}_4 \cdot 5\text{H}_2\text{O}$ solution and pH was adjusted using sulphuric acid. A polycarbonate membrane having cylindrical channels of diameter 200 nm manufactured by Whatman was used as a scaffold to direct the growth of nanowires. Cu microwires were potentiostatically deposited in the channels of the template at 25 °C by applying a constant potential of 0.35V in a two-electrode electrochemical cell for 16 minutes. A variation of 8-12 mA was observed during the

deposition process. The growth mechanism of the microwires starts on the application of an external electric field, which builds a potential difference across the length of the template [3]. The wires were implanted with the low energy aluminium ion at Inter University Accelerator Centre, New Delhi, India and fluences were varied from 5×10^{10} ions/cm² to 5×10^{13} ions/cm².

3. Results and Discussion

Figure 1 shows SEM image of pristine Cu nanowires. wires are uniform in diameter, vertically aligned and smooth. Implantation effects on the wires were studied using different characterizations like X-ray diffraction, energy dispersive spectroscopy, current-voltage characteristics curve and Hall-Petch relation.

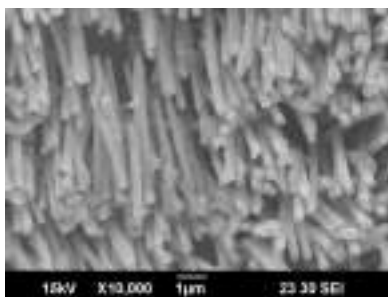


Fig. 1 SEM image of pristine Cu nanowire of 200 nm diameter

4. Conclusion

X-ray diffraction was used to calculate change in the crystallite size and preferred orientation of the nanowires after implantation. FESEM images confirmed the cylindrical morphology of nanowires. It also revealed no changes in morphology of nanowires on implantation. EDS analysis confirmed the presence of implanted ions in the samples. The conductivity of the nanowires was found to change linearly with the ion fluence.

5. References

- /1/ C.R. Martin, Science 266 (1994) 1961–1966.
- /2/ Y. Xia, P. Yang, Y. Sun, Y. Wu, B. Mayers, B. Gates, et al., Adv. Mater. 15 (2003) 353–389.
- /3/ R. Gupta, R. Kumar, R. P. Chauhan, S. K. Chakarvarti, Vacuum, 148 (2018) 239–247.

A Comparison of Expanded Uncertainties by Pseudo-Cyclic Epithermal INAA in Conjunction with Anticoincidence Counting using Comparator and k_0 Procedures for measuring Iodine Levels in Ghanaian Foods

B.J.B. Nyarko^{1,2}, E.H.K. Akaho², J.J. Fletcher³, A. Chatt^{1}*

¹*Trace Analysis Research Centre, Department of Chemistry, Dalhousie University, 6274 Coburg Road, Room 212, PO BOX 15000, Halifax, NS, B3H 4R2, Canada*

²*Ghana Atomic Energy Commission, P.O. Box LG80, Legon-Accra, Ghana*

³*Physics Department, University of Cape Coast, Cape Coast, Ghana*

* E-mail: chatt@dal.ca

1. Introduction

A combination of different types of instrumental neutron activation analysis (INAA) technique was developed for the determination of iodine in various food items from Ghana. The methods involved conventional INAA, epithermal INAA (EINAA), pseudo-cyclic INAA (PC-INAA) and pseudo-cyclic EINAA (PC-EINAA) in conjunction with conventional and anti-coincidence (AC) gamma-ray spectrometry using both single comparator and k_0 standardization procedures [1]. The lowest detection limit of $0.5 \mu\text{g kg}^{-1}$ was obtained by the PC-EINAA with anticoincidence counting (PC-EINAA-AC) method for 5 cycles of irradiation-delay-counting using a comparator. The expanded uncertainties associated with the measurement of iodine by the PC-EINAA-AC method using the comparator and k_0 standardization procedures were evaluated following ISO GUM procedures. The NIST RM 8415 Whole Egg Powder was selected for the validation of the PC-EINAA-AC method as well as for calculating expanded uncertainties. The iodine levels in Ghanaian foods are also reported here.

2. Experimental

Several food samples were obtained from local markets and farms in both northern and southern regions of Ghana. Some samples were freeze-dried and others were oven dried [1].

About 350-850 mg of samples were placed in pre-cleaned polyethylene irradiation vials. The comparator standard solutions of iodine were made from Fisher Scientific Company Certified ACS grade potassium iodide solids. About 0.5 g of BDH “Analar” grade potassium hydroxide per liter was added to the above standard solutions to make them slightly basic and thus stabilize the iodide in solution. The elemental gold standard used in the k_0 calculations was made from plasma emission spectroscopy standard solution supplied by Seignior Chemical Products Canada Ltd. Five Standard Reference Materials (SRMs) obtained from the U.S. National Institute of Standards and Technology (NIST) were used to validate the PC-EINAA-AC methods. The SRMs were: Bovine liver NIST 1577b, Oyster tissue NIST 1566b, Peach leaves NJST 1547, non-fat milk powder NIST 1549, and Apple leaves NIST 1515. Most of the irradiations were carried out in the Cd-lined outer pneumatic site #9 in a neutron flux of $2.5 \times 10^{11} \text{ cm}^{-2} \text{ s}^{-1}$ of the Dalhousie University SLOWPOKE-2 Reactor facility. A 30-min irradiation, 5-min decay, 20-min counting, and 5 cycles were used for the determination of iodine through the 442.9 keV photopeak of ^{128}I (half-life 24.99 min) in SRMs and about 79 food items. The anti-coincidence gamma-ray spectrometry system consisted of a high purity germanium (HPGe) p-type coaxial detector with a relative efficiency of 25% surrounded by a $10'' \times 10''$ Na(Tl) guard detector and gave a peak-to-Compton plateau ratio of 582:1 at the 662-keV photopeak of ^{137}Cs .

3. Results and Discussion

The k_0 standardization procedure required a large variety of measurements and calculations [1]. Our results obtained using both k_0 and comparator procedures were in good agreement with the certified values for the SRMs indicating reliability of the PC-EINAA-AC method. The expanded uncertainty ($k=2$, ~95% CL) of 1.81 ± 0.48 was obtained for the k_0 procedure compared to that of 1.85 ± 0.22 for the single comparator procedure. The value for the k_0 procedure appears to be slightly influenced by the uncertainties in the nuclear constants and detector full photopeak efficiency determination. Details of various parameters in the pre-irradiation, irradiation and post-irradiation steps will be presented. The PC-EINAA-AC method using single comparator was used for the analysis of foods for iodine. The mass fraction ($\mu\text{g kg}^{-1}$) ranges of different food groups were as follows: (1) cereals and grain products: <1.0-670; (2) legumes and nuts: <1.0-450; (3) vegetables: 10-2450; (4) meat, egg and game: <1.0-2100; (5) marine and river fish: 650-4780; (6) fresh river and lake fish: 32-2890; (7) milk and milk products: 123-3870; (8) staple foodstuff: <1.0-200; (9) beverages: 35-1850; and (10) fruits: <1.0-340.

Reference

/1/ B.J.B. Nyarko, PhD Thesis, University of Cape Coast, Cape Coast, Ghana (2007).

Fusion - fission Dynamics for The Pre-actinides and Actinides Near The Coulomb Barrier Energies

Abhirup Chaudhuri

Homi Bhabha National Institute, Training School Complex, Anushakti Nagar, Mumbai - 400094, India

1. Introduction

The dynamics of the fusion process plays critical role to decide whether the system will fuse or not. A systematic study of the fusion-fission dynamics for wide region of nuclei (pre-actinides, actinides, super heavies) is important for understanding the basic fusion-fission reaction mechanism. The stability of the SHE is determined by nuclear shell effects. However, the production of SHE is hindered by the dynamical process of quasi fission in which the composite system breaks before complete equilibration in all degrees of freedom. An experimental program was undertaken to understand the evolution of nuclear shell effects with excitation energy and role of entrance channel on fusion fission and quasi-fission process for pre-actinides and actinides nuclei.

2. Experiment

The experiments were carried out using the major accelerator facilities available in India. Fission fragment mass distributions were measured using two large area position sensitive mutli-wire proportional counters that were developed at VECC. The flight times of the complementary fragments, the position of the impact points of the fragments on the detectors (X and Y), and the energy losses in the gas detectors were measured in an event by event basis. From these measurements, masses of the correlated fission events could be extracted assuming full momentum transfer from target to projectile.

3. Results and Discussion

The fission dynamics of actinides and pre-actinides nuclei at beam energies close to the Coulomb barrier were systematically studied.

It is well known that the asymmetry in fission fragment mass distribution arises due to shell effects in nuclei [1]. In the experiment carried out VECC cyclotron, the evolution of fission fragment mass distribution with excitation energy (in the range 21 - 64 MeV) was studied for the nucleus ^{236}U populated in $^4\text{He}+^{232}\text{Th}$ reaction. Measured mass distributions for excitation energies between 43.6 - 64.2 MeV were found to be symmetric in shape. However, the shape of the fission fragment mass distribution was found to change from symmetric to asymmetric at excitation energies ~ 40 MeV which is an indication of washing out of shell effects. This experiment clearly demonstrated for the first time that shell effect is washed at an excitation energy of 40 MeV in ^{236}U [2].

The experiment carried out at the BARC-TIFR pelletron facility in Mumbai, addressed the role of shell correction at the saddle point. The fission of the N=126 shell closed nuclei ^{210}Po , populated by reaction $^{12}\text{C}+^{198}\text{Pt}$ was studied for this purpose, as recent experimental data and theoretical calculations indicated dramatic ambiguity regarding the presence or absence of shell correction at saddle point for this nucleus. We clearly showed that there is no shell correction at fission saddle point [3].

To study the dynamics of fusion fission and quasi-fission reactions, an experiment was carried out at the IUAC pelletron facility, New Delhi. The fission of ^{200}Pb nuclei was studied by populating it through two different entrance channels $^{16}\text{O} + ^{184}\text{W}$ and $^{19}\text{F} + ^{181}\text{Ta}$. The measured mass distributions at an excitation energy range of 50 MeV to 80 MeV were symmetric and the width of the mass distributions were found to increase monotonically suggesting absence of any quasi-fission and fast fission. The new data [4] calls for the development of advanced theoretical models and new measurements for similar nuclei.

Acknowledgement: The work is part of the PhD thesis carried out at VECC, Kolkata. The author would like to thank accelerator staffs and all his collaborators: T.K. Ghosh, K. Banerjee, S. Bhattacharya, C. Bhattacharya, A. Sen, J. Sadhukhan, P. Bhattacharya, S. Kundu, T.K. Rana, P. Roy, G. Mukherjee, S. Manna, R. Pandey, P. Sugathan, K.S. Golda, D.C. Biswas, K. Mahata, A. Srivastava, A. Asgar, A. Dubey, T. Roy, V. Shrivastava, S.Pal, N. Saneesh, G. Kaur, B. N. Joshi.

References

- /1/ T.K. Ghosh, A. Chaudhuri et al. *Pramana J. Phys.* 85, 291 (2015).
- /2/ A. Chaudhuri, T.K. Ghosh et al. *Phys. Rev. C* 91, 044620 (2015).
- /3/ A. Chaudhuri, T.K. Ghosh et al. *Phys. Rev. C* 92, 041601 (2015) (R).
- /4/ A. Chaudhuri, A.Sen, T.K. Ghosh et al. *Phys. Rev. C* 94, 024617 (2016).

Measurement of Natural Radionuclides For Samples Very Rich In Thorium By Gamma Spectrometry - Mandena Deposit, South Madagascar

*Duong Van Hao**

University of Mining and Geology (UMG), Hanoi, Vietnam

* E-mail: haodnth@gmail.com

1. Introduction

Beach sand placers are high radiation background area. This paper deals with samples from Mandena deposit. The deposit as black sand placer located in the East-South of Madagascar, which was estimated about 20 million tones in total of ilmenite (66.7%), rutile (2.3%) and zircon (2.8%) minerals. The placer have very high concentration of ^{232}Th as well as ^{238}U activity while low ^{40}K activity concentration. During the measurement of studied samples, the problems of interference gamma line of ^{232}Th progenies were contributed in the area of calculated gamma line for ^{40}K , ^{238}U and ^{226}Ra . The problems need to subtract from interference gamma lines between those radionuclides and their progenies for determination of each radionuclides are the questions. The ^{238}U and ^{226}Ra activity concentration were enough high and separated from interference while ^{40}K was undeterminable. Meanwhile what is the activity relation can accept us to clarify in question also. In this case the proposal methodology is used to determine natural radionuclides for ^{232}Th -rich samples.

2. Experimental

The activity of ^{40}K , ^{238}U , ^{226}Ra and ^{232}Th were determined using HPGe detector of relative efficiency of 42% and resolution of 1.9 keV at 1332 keV line. The detector was calibrated using the IAEA reference materials RGU, RGTH, RGK as standard samples. The gamma lines of 1001 keV from ^{234}Pa and 609.3, 1120.3 and 1764.5 keV from ^{214}Bi were used to determine the activity of ^{238}U and ^{226}Ra , while that of ^{232}Th were determined from 911.2 and 968.9 keV lines of ^{228}Ac and 583.0 and 2614.5 keV from ^{208}Tl . The maximum counting time was 50 h and the obtained uncertainty was less than 3%. The self-gamma absorption resulted from the difference in density of the samples and standard ones

were introduced to follow the method described by Jodłowski (2006). To avoid the photo absorption in the sample, all of the gamma lines were used higher than 500 keV.

As the activity of ^{232}Th as well as ^{238}U were very high in the study samples, the number of counts from the gamma lines 1459.1, 1000.7, 610.6 and 583.4 keV emitted from ^{228}Ac , which is the progeny of ^{232}Th and interference with the analytic gamma lines were also very high. In addition the gamma lines such as 1120.6, 1458.5 keV and 1765.4 keV of ^{234}Pa , 584.1, 1121.7 and 1458.9 keV of $^{234\text{m}}\text{Pa}$, 581.7 keV of ^{234}U , 609.3 keV of ^{218}Rn and 910 keV of ^{210}Tl , all progeny of ^{238}U , contributed significant amount also. Therefore the ^{40}K concentration in the samples of this study after subtraction the amount contribute from ^{28}Ac and $^{234\text{m}}\text{Pa}$ is very low, it is not possible to determine ^{40}K . In this section the sample of the determination of the ^{40}K activity concentration was corrected to eliminate the interference of the ^{232}Th progeny and calculated as follow (2), (3):

$$A_{K-40} = A_{total} (I_{total} - I_{Ac-228}) / I_{total} \quad (1)$$

$$I_{Ac-228} = \varepsilon_{\gamma-Ac-228} A_{Th-232} M_{sp} P_e T \quad (2)$$

Where: A_{K-40} , A_{total} , A_{Ac-228} – is the activity of ^{40}K subtracted from the interference of ^{232}Th progeny, active total calculated from gamma line 1460.8 keV, activity of ^{228}Ac from gamma line 1459.1 keV contributed in gamma line 1460.8 keV. I_{total} , I_{Ac-228} – is the measured number of counts in the gamma line 1460.8 keV, number of counts in the gamma line 1459.1 keV from ^{228}Ac contributed in the gamma line 1460.8 keV. Due to short half time period of ^{228}Ac (6.13h), the radioactive equilibrium between ^{232}Th and ^{228}Ac always regarded as established in the solid materials. $A_{Ac-228} = A_{Th-232}$ – is the activity of ^{232}Th . $\varepsilon_{\gamma-Ac-228}$ – is the emission efficiency of the gamma ray of 1459.1 keV from ^{228}Ac . M_{sp} – mass of sample. P_e decay rate of gamma line 1459.88 keV of ^{228}Ac . T – time of measurement.

3. Results

The measured activity concentrations of ^{238}U , ^{226}Ra and ^{232}Th range from 2063 to 4224, 1501-2878 and 11013-24379 Bq/kg respectively. The activity concentration of ^{232}Th is higher than ^{238}U by five times, equivalent to fifteen times in mass. Due to the very high ^{232}Th and very low ^{40}K concentration in analyzed material, the contribution of 1459.7 keV ^{228}Ac line in (1460.8 keV + 1459.1 keV) peak is close to 100%. As a result, after subtraction of the ^{228}Ac contribution, the determined ^{40}K activity is with very high uncertainty, larger than the measured value.

Acknowledgment: The authors are thankful to Prof Nguyen Dinh Chau, Drs Jodłowski Paweł, Beata Ostachowicz, Jakub Nowak and Akinniyi Akinsunmade for their useful discussions.

Measurement of Excitation Functions of The $^{206/207/208}\text{Pb}(^{11}\text{B},\text{x})^{212}\text{Fr}$ Reactions and Complex Formation Studies of Fr with Crown Ethers

Y. Komori^{1}, H. Haba¹, T. Yokokita¹, S. Yano¹, N. Sato¹, K. Ghosh¹,
Y. Sakemi², H. Kawamura³*

¹RIKEN Nishina Center for Accelerator-Based Science, Wako, Saitama 351-0198, Japan

²Center for Nuclear Study, the University of Tokyo, Bunkyo, Tokyo 113-0033, Japan

³Frontier Research Institute for Interdisciplinary Sciences, Tohoku University, Sendai, Miyagi 980-8578, Japan

*E-mail: yukiko.komori@riken.jp

1. Introduction

Francium (Fr) is the heaviest alkali metal with the atomic number 87. It is one of the least-studied elements among the naturally occurring elements because all its isotopes are short-lived. Owing to experimental difficulties, the chemical properties of Fr have not been studied in detail so far. The chemical properties of Fr cannot be simply deduced from the extrapolation from the lighter homologs in the periodic table because relativistic effects come into play in such a heavy atom as Fr [1]. Therefore, it is of great interest and importance to clarify the chemical properties of Fr and to elucidate the influence of relativistic effects on the chemical properties of Fr. In this study, we plan to study complex formation properties of Fr by solvent extraction with crown ethers. We will use the second longest-lived isotope of Fr, ^{212}Fr ($T_{1/2} = 20$ min), which can be produced in the $^{206/207/208}\text{Pb}(^{11}\text{B},\text{x})^{212}\text{Fr}$ reactions. Because no experimental excitation functions are available for these reactions, we measured them using the stacked-foil technique to optimize the production conditions of ^{212}Fr .

2. Experiment

The metallic $^{206/207/208}\text{Pb}$ targets were prepared by vapor deposition on 3.1- μm Al foils (>99% chemical purity). The target stacks consist of 20 sets of ^{206}Pb (99.51%-enrichment, 791- $\mu\text{g}/\text{cm}^2$ thickness), ^{207}Pb (99.40%-enrichment, 851- $\mu\text{g}/\text{cm}^2$ thickness), or ^{208}Pb (99.59%-enrichment, 642 $\mu\text{g}/\text{cm}^2$ thickness). The 3.1- μm Al foils were inserted between the $^{206/207/208}\text{Pb}$ targets to catch ^{212}Fr atoms that recoiled out of the targets.

Each stack was irradiated for 10 min with a 100.9-MeV ^{11}B beam supplied from the RIKEN AVF cyclotron. The average beam current was 48.6, 48.8, and 50.0 pA for the ^{206}Pb , ^{207}Pb , and ^{208}Pb stacks, respectively. After the irradiation, each foil was subjected to γ -ray spectrometry with Ge detectors.

3. Results and Discussion

The radioactivity of ^{212}Fr was determined from its 227.72-keV (γ -ray intensity $I_\gamma = 42.6\%$) γ line. Figure 1 shows the excitation functions for the $^{206}\text{Pb}(^{11}\text{B},5n)^{212}\text{Fr}$, $^{207}\text{Pb}(^{11}\text{B},6n)^{212}\text{Fr}$, and $^{208}\text{Pb}(^{11}\text{B},7n)^{212}\text{Fr}$ reactions. The excitation functions predicted by the PACE4 code [2] are also shown by solid, dashed, and dashed-and-dotted lines in the figure. The maximum cross section for the production of ^{212}Fr is available in the $^{206}\text{Pb}(^{11}\text{B},5n)^{212}\text{Fr}$ reaction at around 73.6 MeV. The PACE4 code reproduces well the shapes of the excitation functions, however, it overestimates the cross sections for the $^{207}\text{Pb}(^{11}\text{B},6n)^{212}\text{Fr}$ and $^{208}\text{Pb}(^{11}\text{B},7n)^{212}\text{Fr}$ reactions. Based on the measured excitation functions, we decided to produce ^{212}Fr in the $^{206}\text{Pb}(^{11}\text{B},5n)^{212}\text{Fr}$ reaction for the chemistry studies of Fr. In the conference, we will also present the results of the solvent extraction experiments of ^{212}Fr with several crown ethers.

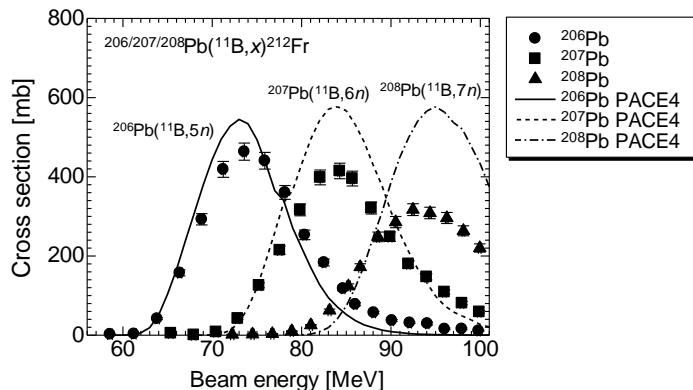


Fig 1: The excitation functions for the $^{206/207/208}\text{Pb}(^{11}\text{B},x)^{212}\text{Fr}$ reactions.

References

- /1/ V. Pershina *et al.*, Chem. Phys. 395 (2012) 87.
- /2/ O.B. Tarasov, D. Bazin, Nucl. Instrum. Meth. B 204 (2003) 174.

Quantification of Short-Lived Radioisotopes from 1.4 GeV Proton Irradiated LBE Target

Dibyasree Choudhury¹, Susanta Lahiri^{1,2,}, Nabanita Naskar^{3,1}, Melanie Delonca⁴, Thierry Stora⁴, Joao Pedro Ramos⁴, Elodie Aubert⁴, Alexandre Dorsival⁴, Joachim Voltaire⁴, Ricardo Augusto^{4,5}, Alfredo Ferrari⁴*

¹Saha Institute of Nuclear Physics, 1/AF Bidhannagar, Kolkata 700064, India

²Homi Bhabha National Institute, India

³University of Calcutta, 35 Ballygunge Circular Road, Kolkata 700019, India

⁴CERN-ISOLDE, 1211 Geneve 23, Switzerland,

⁵Ludwig-Maximilians-Universität München, Munich, Germany

*E-mail: susanta.lahiri@saha.ac.in

1. Introduction

Lead-bismuth eutectic (LBE) targets upon irradiation with high intensity and high energy proton beam produce intense flux of neutrons. Alongside, these targets have also been proposed as robust source of beneficial radioisotopes. Earlier, a radionuclidic inventory of 1.4 GeV proton irradiated six cylindrical LBE targets of lengths 1-8 mm and diameter 6 mm was published [1]. However, there is always need for independent verification of such high end experiments. Moreover, in earlier experiment no quantitative information for the short-lived radionuclides ($T_{1/2} < 5$ d) was available. Therefore another experiment was performed in which the length of the LBE target was enhanced to 50 mm. The short-lived radioisotopes were identified and quantified from time resolved offline γ -spectrometric data.

2. Experimental

A cylindrical LBE target of 6 mm diameter and 50 mm length, coated with about 0.5 mm glue, was irradiated with 1000 pulses of 1.4 GeV proton beam and 0.33 μ A current. A total of 5×10^{15} protons were delivered on the target in 2455 s. The target was kept aside for 27 h followed by series of time resolved γ -spectra were collected for a stretch of 11 days. A p-type HPGe detector Falcon 5000 (Canberra) was used for offline γ -spectroscopic measurements. The energy and the efficiency calibration of the detector were performed using standard sources like ^{152}Eu , ^{133}Ba and ^{60}Co .

3. Results and discussions

Total 50 short-lived radionuclides were identified and quantified (Table 1). The products were compared with that of earlier data [1] for 8 mm long target, which was irradiated with 10^{13} protons. It has been found that most of the radionuclides are common in both the experiments. However, few radionuclides were identified in the current 50 mm target only, some of these radionuclides are in neutron rich side (^{69m}Zn , $^{72,73}\text{Ga}$). Few radioisotopes (^{42}K , ^{48}Sc , $^{69,77}\text{Ge}$, ^{77}Br , ^{79}Kr , ^{97}Zr , ^{96}Tc , ^{97}Ru , ^{111}In , ^{119m}Te , ^{129}Cs , ^{132}La , ^{153}Tb , ^{171}Er , ^{170}Lu , ^{187}W , $^{185,188,190m2,195m}\text{Ir}$, ^{207}Po) were identified in earlier experiment but not in current experiment. Some of the isotopes were produced as daughter products (^{86}Y , ^{146}Eu , $^{200,201}\text{Tl}$).

Table 1. Production yield (kBq) of the short-lived radioisotopes at EOB in 50 mm LBE target

S.No.	Radioisotope	Yield (kBq) at EOB	S.No.	Radioisotope	Yield (kBq) at EOB
1.	Zn-69m (13.7 h)	147±39	26.	Ta-175 (10.5 h)	1141±16
2.	As-72 (26 h)	32±3	27.	Ta-176 (8.09 h)	4331±445
3.	Ga-72 (14.1 h)	3289±1300	28.	Re-181 (19.9 h)	546±41
4.	Ga-73 (4.86 h)	15293±2916	29.	Os-182 (22.1 h)	1660±27
5.	Br-76 (16.2 h)	70±40	30.	Re-182 (64 h)	931±50
6.	Br-82 (35.3 h)	24±5	31.	Re-182m (12.7 h)	3174±170
7.	Y-86 (14.7 h)	daughter product	32.	Os-183m(13 h)	621±56
8.	Zr-86 (16.5 h)	109±9	33.	Ir-186 (16.6 h)	932±23
9.	Y-87 (79.8 h)	13.2±3	34.	Ir-187 (10.5 h)	1748±652
10.	Y-87m (13.37 h)	838±27	35.	Pt-189 (10.87 h)	1571±197
11.	Nb-96 (23 h)	171±10	36.	Pt-191 (2.8 d)	707±34
12.	Rh-100 (20.8 h)	279±15	37.	Au-192 (4.94 h)	12359±359
13.	Rh-101m (4.3 d)	10±2.5	38.	Au-193 (17.65 h)	1327±2
14.	Xe-125 (17 h)	347±34	39.	Hg-193m (11.8 h)	1380±143
15.	Ba-135m (28 h)	200±34	40.	Hg-195m (41.6 h)	298±60
16.	Eu-146 (4.61 d)	daughter product	41.	Tl-198 (5.3 h)	5595±415
17.	Gd-147 (38.06 h)	13.4±2	42.	Tl-199 (7.42 h)	4197±772
18.	Tb-151 (17.6 h)	549±60	43.	Pb-200 (21.5 h)	114±13
19.	Dy-153 (6.4 h)	932±549	44.	Tl-200 (26.1 h)	daughter product
20.	Tb-154 (21 h)	1721±±309	45.	Tl-201 (3.04 d)	daughter product
21.	Dy-157 (8.14 h)	268±42	46.	Pb-201 (9.33 h)	1962±425
22.	Tm-165 (30.06 h)	167±16	47.	Pb-203 (51.8 h)	363±7
23.	Lu-169 (34 h)	412±32	48.	Bi-203 (11.76 h)	775±64
24.	Hf-170 (16.0 h)	61±19	49.	Bi-204 (11.22 h)	1356±43
25.	Hf-173 (23.6 h)	1159±28	50.	At-209 (5.41 h)	625±5

Bold indicates not reported in reference 1 (8 mm LBE target length)

Acknowledgement: This work is a part of SINP-DAE 12 Five year plan project TULIP. One of the authors, NN, acknowledges UGC for providing the necessary fellowship.

References

/1/ M. Maiti, K. Ghosh, T. Mendonca, T. Stora, S. Lahiri, J. Radioanal. Nucl. Chem. 302 (2014) 1003.

Measurement of Gross α , β in Water Samples Collected from Indian Sundarbans

Nabanita Naskar^{1,2}, Sayantani Mitra¹, Susanta Lahiri^{2,3}, Punarbasu Chaudhuri¹*

¹Department of Environmental Science, University of Calcutta, Kolkata-700019, India

²Saha Institute of Nuclear Physics, 1/AF, Bidhannagar, Kolkata-700064, India

³Homi Bhabha National Institute, India

*E mail: susanta.lahiri@saha.ac.in

1. Introduction

Sundarbans is the world's largest mangrove ecosystem shared by India and Bangladesh, crisscrossed by a complex network of tidal waterways, mudflats and many Islands. Earlier natural radioactivity of ^{238}U , ^{232}Th , ^{137}Cs in soil and ^3H in water samples had been reported from this region that may provide baseline data for future studies [1, 2]. Besides, gross α/β measurement is another parameter in the field of radio-ecological monitoring. This study makes an attempt to study gross α/β in water samples collected from different parts of Indian Sundarbans, using Liquid Scintillation Counter (LSC)- TDCR (Triple to Double Coincidence Ratio) technique, which would provide an insight towards natural radioactivity in water samples and also serve as reference for further radiological investigations.

2. Experiment

Thirty five water samples were collected from different parts of Indian Sundarbans and were preserved with nitric acid till further experiments. 200 mL of sample was taken in beaker and evaporated to ~20 mL. 8 mL of the residue was taken in 20 mL polyethylene vial and mixed with 12 mL aqualight cocktail (make HIDEX) followed by gentle shaking. All samples were kept for dark adaptation for 1 h to avoid luminescence. Vials were counted with Ultra Low Level Liquid Scintillation Counter HIDEX 300 SL for 3600 s in optimized window settings and PLI (Pulse Length Index) of 4. 8 mL distilled water in 12 mL cocktail was considered as blank and afterwards subtracted from the sample counts. The data for blank corroborated well with the background sample supplied by Hidex. The experiment was validated with IAEA 443 Irish seawater Certified Reference Material.

3. Result and discussion

It was observed that value of gross α was BDL (Below Detectable Activity) for all samples (not shown here). For gross β , mean and median activities were 0.24 and 0.22 Bq/L for 35 water samples. Table 1 provides some representative tubewell and riverine samples out of thirty-five samples.

Table 1 shows the sampling sites, their coordinates and gross β [Bq/L] obtained in few samples.

Tubewell samples	Coordinates	Gross β, Bq/L
Shibrampurgram	21°34'40.29"N, 88°16'21.71" E	0.66±0.64
Patibunia	22°31'36.59"N, 88°21'46.93" E	0.15±0.56
Purandar	22°12.384' N, 88°41.234' E	0.34±0.59
Kakdwip	21°50'44.55"N, 88°12'19.57"E	1.33±0.74
Kultali Forest Office	21°59.291' N, 88°35.169' E	0.25±0.58
Henry Island	21°34'48.12"N, 88°16'03.08"E	0.12±0.55
Atharo Banki Road	22°20.716' N, 88°45.023' E	0.22±0.57
Bhagankhali	22°16.865' N, 88°41.092' E	0.12±0.55
Kaikhali	21°01'20.52" N, 88°37'01.29" E	0.11±0.55
Riverine samples	Coordinates	Gross β, Bq/L
Kultali Confluence	21°59.334' N, 88°35.144' E	0.20±0.57
Piyali River	22°08'15.28"N, 88°36'03.52" E	0.22±0.57
Henry Island river	21°34'40.29"N, 88°16'21.71" E	0.10±0.55
Godkhali jetty	22°10.062' N, 88°47.271' E	0.27±0.58
Hogol river	22°12.119' N, 88°42.726' E	0.04±0.54
Kaikhali	22°01.324' N, 88°37.021' E	0.26±0.58
Bidya gomor confluence	22°03'19" N, 86°54'86" E	0.15±0.56
Sudhanyakhali	22°06'19.3" N, 88°47'59" E	0.28±0.58
Dobanki	21°59'35.6" N, 88°45'26.9" E	0.21±0.57

As recommended by World Health Organization (WHO) [3], the limit of gross α and β below which no further analysis is required are 0.5 Bq/L and 1 Bq/L respectively. It is clearly evident from the average value that the present result did not cross the permissible limit recommended by WHO. Thus, it may be said that the environment of Indian Sundarbans is devoid of any nuclear contamination/ interventions.

References

- /1/ Chaudhuri et al., *J Radioanal Nucl Chem* 310, 1381-1396 (2016)
- /2/ Lahiri et al., 9th International Conference on Radioisotopes and Expo (9 ICI), 12-16 Nov, 2017, Doha, Qatar.
- /3/ WHO, 2011. Guidelines for drinking-water quality, fourth ed., WHO Library Cataloguing-in-Publication Data NLM classifications: WA 675, Geneva

Study of Natural Radioactivity and Radon Exhalation Rate in Rocks and Water samples in Garhwal Himalaya Region

Manjulata Yadav^{1}, Mukesh Prasad², R.C Ramola¹*

¹Department of Physics, H.N.B.Garhwal University Campus, Badshahithaul, Tehri Garhwal-249199 C

²Department of Physics, Indian Institute of technology Roorkee-247667, India

*E-mail: Manjuyadav187@gmail.com

1. Introduction

Dissolved uranium in ground water is second most important factor to outdoor environment. Due to varying concentrations of uranium, thorium, and their daughter products in ground water, the estimation of natural radionuclides in drinking water becomes relevant in assessing their contribution to internal dose by ingestion.

2. Experiment Techniques

2.1 Sample collection and preparation: Rock and soil samples were crushed and dried. The dried samples of 500 g were packed in Marinelli beakers and stored for a period of one month before gamma spectrometric analysis. The estimation of natural radionuclides in soil samples were carried out using NaI(Tl) detector of size 63 mm x 63 mm. The samples were counted for three hour.

2.2 Radon Mass Exhalation rate: The radon exhalation rate was measured by the “Seal can technique. The radon exhalation rate was measured by the relation

$$E_x = \frac{CV\lambda}{M[T + \frac{1}{\lambda}(e^{-\lambda t} - 1)]}$$

Where, E_x is radon exhalation rate ($\text{Bq}\cdot\text{m}^{-2}\text{h}^{-1}$), C is measured radon concentration ($\text{Bq}\cdot\text{m}^{-3}\text{h}$), V is the effective volume of Can (m^3), λ is the decay constant for radon (h^{-1}), T is the exposure time (h) and M is the mass of the soil samples.

3.Result and discussion

3.1 Radioactivity determination: Figures 1 and 2 illustrate the concentration of ^{226}Ra , ^{232}Th for soil and rocks samples collected by different locations in study area. The results show that the activity concentrations in the rock samples are high compared to soil samples. The rocks samples from two locations (UK1 and UK15) have recorded the higher values for thorium and potassium (not shown in figure). High values of radium and thorium were measured at some locations (UK1,UK15,UK4) showing the presence of significant amount of uranium and thorium bearing minerals. Radium equivalent activity is an index that has been introduced to represent the specific activities of ^{226}Ra , ^{232}Th , and ^{40}K by a single quantity, which takes in to account the radiation hazards associated with them. Radium equivalent activity (Ra_{eq}) in rock samples vary from 46 Bq.kg $^{-1}$ to 763 Bq.kg $^{-1}$, with an average of 213 Bq.kg $^{-1}$, and soil samples 26 Bq.kg $^{-1}$ to 242

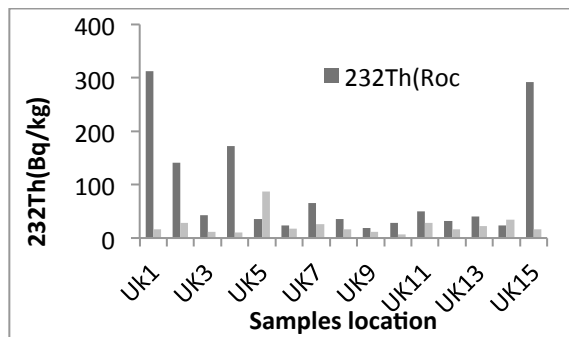
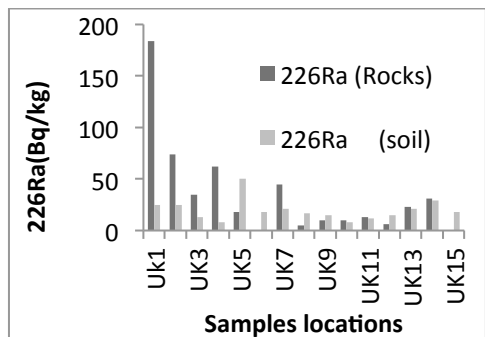


Figure 1. Radium activity in soil and rock samples Figure 2. Thorium activity in soil and rock samples

3.2 Radon mass exhalation rate: The value of radon mass exhalation in the location of UK1, UK2, UK3 are much greater than the evaluated value of radon in other samples. Here we can found that the positive correlation between the radium and radon mass exhalation rates.

3.3 Uranium in water: Fig 3 shows uranium contents in water with the location of study area. It is very low in UK1,UK2, UK13 areas but radium in soil of this area are in excess. This may be due to the reason that soil-water interface plays an important role in dissolving the uranium in water.

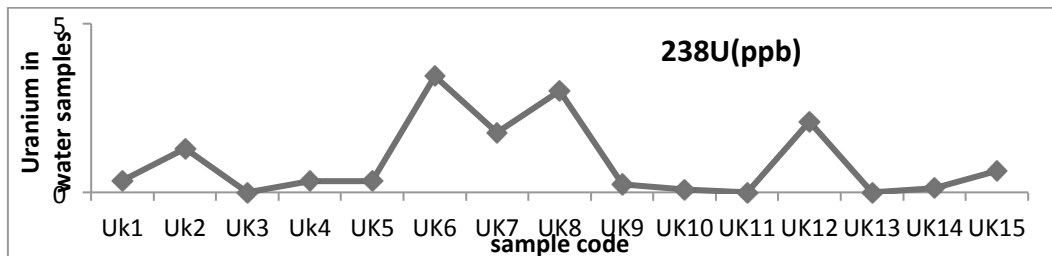


Figure 3. Uranium in ground water

Determination of ^{129}I in Aerosols Using Pyrolysis and AgI-AgCl Coprecipitation Separation and Accelerator Mass Spectrometry Measurement

Luyuan Zhang^{1,2,4*}, Xiaolin Hou¹⁻⁴, Yunchong Fu^{1,2}, Miao Fang^{1,2}, Ning Chen^{1,2}

¹ State Key Laboratory of Loess and Quaternary Geology, Institute of Earth Environment, Chinese Academy of Sciences, Xi'an 710061, China

² Shaanxi Key Laboratory of Accelerator Mass Spectrometry and Application, Xi'an AMS Center, Institute of Earth Environment, Chinese Academy of Sciences, Xi'an 710061, China

³ Center for Nuclear Technologies, Technical University of Denmark, Risø Campus, Roskilde 4000, Denmark

⁴ Open Studio for Oceanic-Continental Climate and Environment Changes, Pilot National Laboratory for Marine Science and Technology (Qingdao), Qingdao 266061, China

* E-mail: zhangly@ieecas.cn

1. Introduction

Long-lived ^{129}I in aerosols is vital for reconstruction of level and distribution of short-lived and highly radiotoxic ^{131}I , as well as understanding the knowledge of atmospheric dispersion of iodine. However, aerosol ^{129}I concentration is difficult to measure due to its low concentration in the areas remote from nuclear pollution sources.

2. Experiment

The aerosol samples were collected on glass fiber filter in Xi'an, China. Iodine is separated from the aerosol samples by pyrolysis method, and prepared as AgI-AgCl coprecipitate for AMS measurement (Fig.1). Stable iodine (^{127}I) was measured using ICP-MS (Agilent 8800, USA). ^{129}I was measured by a 3MV Tandem AMS system (High Voltage Engineering Europa) at the Xi'an AMS center.

3. Results and discussion

Even though the pyrolysis behaviors of various iodine species were different, all iodine can be quantitatively recovered. Iodate can be released from the aerosols by decomposition to iodine at a temperature over 500°C. The chemical yield of iodine in the pyrolysis is $81.5 \pm 5.8\%$. The detection limit for ^{129}I in aerosol is 1.3×10^4 atoms m^{-3} , at least reducing the required aerosol sample size by a

factor of three, in contrast to the method using alkaline-ashing separation coupled to solvent extraction. For aerosol samples collected in Asia with $^{129}\text{I}/^{127}\text{I}$ ratio of $(0.1-10) \times 10^{-9}$, a volume of 1000 m^3 air is sufficient for determination of ^{129}I . The method was applied to analyze the aerosol samples collected in Xi'an, an inland Chinese city. It was observed that ^{129}I concentrations in the range of $(0.38-5.19) \times 10^5$ atoms m^{-3} , and $^{129}\text{I}/^{127}\text{I}$ ratios of $(21.7-252) \times 10^{-10}$. This is comparable to those collected in Japan before the Fukushima nuclear accident and Spain, but much lower than those in Northern Europe.

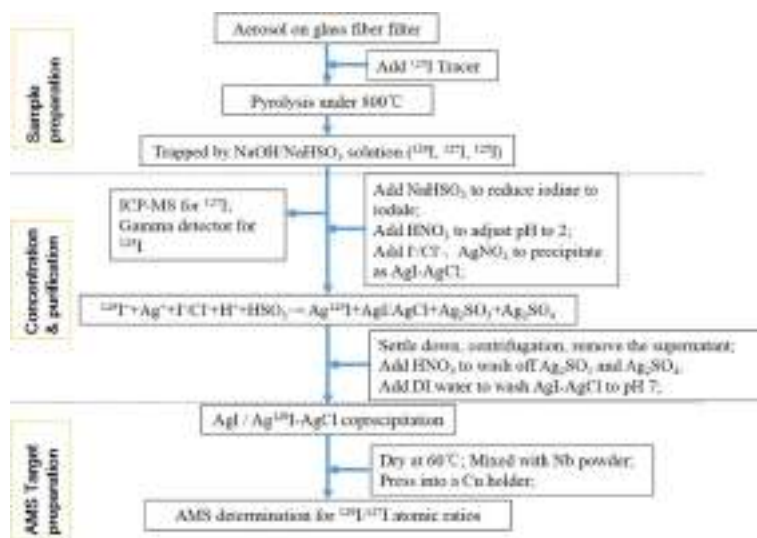


Figure 1. Flowchart of aerosol preparation for determination of ^{129}I using AMS

4. Conclusion

An accurate analytical method for determination of ^{129}I in aerosol samples was developed by separation of iodine isotopes using pyrolysis and AgI-AgCl coprecipitation in combination with AMS measurement. This developed method is efficient with less labor force and only smaller sample size is required (a maximum of 1000 m^3 for ^{129}I level in Asia). It makes atmospheric ^{129}I study with highly temporal resolution and a better understanding of atmospheric processes of stable and radioactive iodine, possible.

Acknowledgment: This work is supported by National Natural Science Foundation of China (No. 11605207 and 91643206), Ministry of Science and Technology of China (No. 2015FY110800).

References

- /1/ Xu S, Zhang LY, Freeman SPH, Hou XL, Shibata Y. Environ Sci Technol 49 (2015) 1017.
- /2/ Zhang LY, Hou XL, Xu S. Atmos Chem Phys 16 (2016) 1971.

Clinical Dose Formulation and Evaluation of ^{177}Lu -DOTA-bisphosphonate: A Next Generation Radiopharmaceutical for Palliative Care of Painful Bone Metastases

Sudipta Chakraborty^{1}, K. V. Vimalnath¹, Rubel Chakravarty¹, H. D. Sarma²,
K. Kamaleswaran³, Ajit Shinto³, Ashutosh Dash¹*

¹Radiopharmaceuticals Division, Bhabha Atomic Research Centre, Mumbai 400085, India

²Radiation Biology and Health Sciences Division, Bhabha Atomic Research Centre, Mumbai 400085, India,

³Nuclear Medicine and PET Services, Kovai Medical Centre and Hospital, Coimbatore 641014, India

*E-mail: sudiptac1273@gmail.com

1. Introduction

In recent years, a new macrocyclic bisphosphonate ligand, namely, (4-{{(bis(phosphonomethyl)carbamoyl)methyl}}-7,10-bis(carboxymethyl)-1,4,7,10-tetraazacyclododec-1-yl)acetic acid (BPAMD) showed improved uptake osteoblastic lesion sites when labeled with ^{68}Ga for PET imaging and ^{177}Lu for palliative care [1, 2]. We report herein an easily adaptable strategy for the expedient formulation of clinical dose of ^{177}Lu -BPAMD using moderate specific activity ^{177}Lu produced via (n, γ) route and its preliminary clinical investigation. We believe that adaptation of this strategy would enable a large number of nuclear medicine centres to use this promising radiopharmaceutical routinely.

2. Experimental

2.1. Clinical dose formulation of ^{177}Lu -BPAMD: For the preparation of clinically relevant dose of ^{177}Lu -BPAMD (~3.7 GBq), 0.2 mL aqueous solution of BPAMD (0.2 mg, 350 nmol) in MilliQ water was added to 0.2 mL of 0.1 M sodium acetate buffer containing 5 mg of gentisic acid (pH ~4.5). To this, 0.1 mL of $^{177}\text{LuCl}_3$ solution in 0.01 M HCl (~3.7 GBq, specific activity ~370 MBq/mg) was added and the resultant mixture was heated under shaking at 90° C for 30 min. Subsequently, the reaction mixture was cooled, diluted to 5 mL using sterile 0.9% saline and filtered through 0.22 μm syringe filter. Radiochemical yield was determined by radio-TLC in 0.1 M sodium citrate (pH 4).

2.2. *In vitro* stability studies: The *in vitro* stability of ^{177}Lu -BPAMD formulation was studied in normal saline as well as in human serum at 37° C upto a period of 14 d and 2 d, respectively.

2.3. Biodistribution studies: Preclinical biological evaluation of the ^{177}Lu -BPAMD formulation was carried out in healthy Wistar rats following the protocol reported by authors previously [3, 4].

2.3. Preliminary investigation in human patient: Human biodistribution and pharmacokinetics of ^{177}Lu -BPAMD was ascertained in a male patient (70 years) suffering from bone pain due to skeletal metastases originated from primary carcinoma in the prostate. Around 444 MBq dose of the formulation was administered to the patient through intravenous route. The clinical investigation was approved by the local institutional ethics committee of Kovai Medical Centre and Hospital, Coimbatore, India, and written consent was obtained from the patient.

3. Results and Discussion

The radiochemical yield of ^{177}Lu -BPAMD formulated in a clinically relevant dose of ~370 MBq was found to be $98.2\pm 0.4\%$ (n=5). *In vitro* stability studies showed that the radiochemical purity of ^{177}Lu -BPAMD was $94.6\pm 0.5\%$ (n=5) even 14 d after formulation when stored in normal saline at 37 °C. Similarly, when incubated with human serum at 37°C, ^{177}Lu -BPAMD formulation was found to retain $96.2\pm 0.3\%$ (n=5) radiochemical purity up to the period of 2 d. Biodistribution studies in healthy Wistar rats revealed fast skeletal accumulation of the preparation within 1 h post-administration [$2.62\pm 0.38\%$ injected dose/g (%ID/g) in femur] that increased at 24 h post-administration [$2.88\pm 0.29\%$ ID/g] and nearly retained even at 14 d post-administration [$2.53\pm 0.39\%$ ID/g], upto which studies were carried out. The administered activity not accumulated in skeleton was rapidly cleared through renal route within 3 h. Investigation of pharmacokinetics of ^{177}Lu -BPAMD in human patient with proven skeletal metastases showed its specific skeletal accumulation with preferential localization in osteblastic lesion sites.

4. Conclusion

The objective of the present study, viz. development of a protocol for formulation of clinical doses of ^{177}Lu -BPAMD using moderate specific activity ^{177}Lu for its routine use has been accomplished.

References

- /1/ Fellner,M., Baum,R.P., Witte,E.G., Kubi'cek,V., et al. Eur. J. Nucl. Med. Mol. Imagigng 37 (2010) 834.
- /2/ Meckel,M., Nauth,A., Timpe,J., et al. Caner Biohther. Radiopharm. 30 (2015) 1.
- /3/ Chakraborty,S., Vimalnath,K.V., Rajeswari,A., et al. J. Label. Compd. Radiopharm. 60 (2017) 410.

Potential Use of Iron-oxide Immobilized Natural Sand in The Removal of Cs(I) and Sr(II) from Aqueous Solutions

Diwakar Tiwari, Lalhmunsiana*

Department of Chemistry, School of Physical Sciences, Mizoram University, Aizawl-796004, India

*E-mail: diw_tiwari@yahoo.com

1. Introduction

Caesium and strontium are important radionuclides often present in radioactive liquid effluents and they are considered as the hazardous elements. Cs has high tendency to incorporate to terrestrial and aquatic habitats as it is similar to Na and K. ^{90}Sr mainly present as the Sr(II) ion which could replace calcium ions and increases the possibility of leukemia and other diseases in the human body [2, 3]. Therefore, the removal of radiotoxic Cs(I) and Sr(II) from the human environment is highly necessary. Literature survey showed that iron-oxide modified sands were successfully utilized for the removal of various hazardous pollutants such as arsenic, antimony, heavy metals and some organic dyes. However, the application of this material in the removal of radiotoxic ions is limited. Therefore, it is an interesting to assess the efficiency of iron-oxide modified sand for the removal of Cs(I) and Sr(II) from aquatic environment.

2. Experiment

The bare sand was collected from the river bank. The iron-oxide particles were immobilized on the sand surface by simple impregnation method. The materials were characterized using SEM-EDX, XRD and FT-IR analyses. Moreover, the stability of immobilized iron particles and the amount of iron incorporated on the sand were evaluated. Batch experiments were performed to study the effect of solution pH, initial Cs(I)/Sr(II) concentrations, contact time, and presence of heavy metal ions and ionic strength in the removal of Cs(I) and Sr(II) using iron-oxide immobilized sand (IIS).

2. Results and discussion

The SEM images were obtained for bare sand and modified sand showed that the iron oxides were incorporated onto the sand surface as small sized particles and increases the surface heterogeneity on the sand surface. The amount of iron loaded on the sand surface was determined to be 4.52 mg/g. The stability test showed that iron-oxide particles were strongly aggregated on the sand surface. The IIS showed an enhanced uptake of Cs(I) and Sr(II) compared to the bare sand at various pH (i.e. pH 4.0 to 10.0). The Langmuir adsorption capacity of IIS were found to be 5.102 and 1.324 mg/g for Cs(I) and Sr(II), respectively. The time dependent adsorption data follows pseudo second order kinetic better than pseudo first order kinetic model. The presence of other heavy metals caused a slight decreased in the removal of Cs(I)/Sr(II) by IIS. The effect of ionic strength studies indicate that Cs(I) and Sr(II) were weakly bound through electrostatic attraction and form outer sphere complexes on the surfaces of IIS. Further, the loading capacity of Cs(I) and Sr(II) in the column packed with IIS were found to be 1.642 and 0.616 mg/g, respectively.

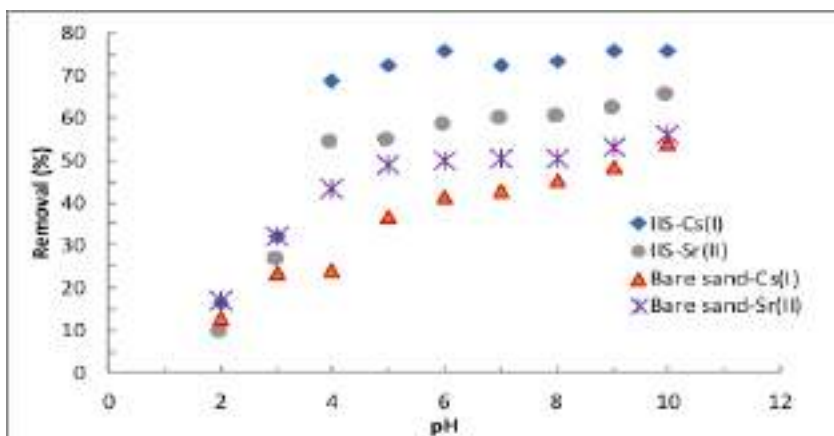


Figure 1: Effect of solution pH on the removal of Cs(I) and Sr(II) using bare sand and iron-oxide modified sand

References

- /1/ M.R. Awual, S. Suzuki, T. Taguchi, et al., Chem. Eng. J. 242 (2014) 127–135.
- /2/ J. Pan, X. Zou, Y. Yan, et al., Appl. Clay Sci. 50 (2010) 260–265.
- /3/ Y. Wang, H. Huang, S. Duan, et al., ACS Sustainable Chem. Eng. 6(2018) 2462–2473.

Heavy Ion Activation: Treasure of Non-Conventional Neutron Deficient Radionuclides

Susanta Lahiri^{1,2*}

¹Saha Institute of Nuclear Physics, 1/AF Bidhannagar, Kolkata 700064, India

²Homi Bhabha National Institute, India

*E-mail: susanta.lahiri@saha.ac.in

1. Introduction

The non-conventional radionuclides are getting more importance in the field of nuclear medicine, mainly due to the possibility to make personalized diagnosis and therapy on case-to-case basis. For last twenty years, we are engaged in production and separation of non-conventional neutron deficient radionuclides by heavy ion (HI) activation [1]. The varieties of projectiles like ${}^7\text{Li}$, ${}^{11}\text{B}$, ${}^{12}\text{C}$, and ${}^{16}\text{O}$ have been used for production of such radionuclides. One has liberty to go far away from the stability line by HI activation by choosing appropriate target projectile combination. Also due to larger difference in atomic number between product and target radionuclide, the separation of no-carrier-added (NCA) radionuclides become easier. This is especially true for rare earth radionuclides. We have also developed excellent separation methods of the HI induced NCA radionuclides from the target matrix. Some of the HI activation products are also excellent PET radionuclides. The disadvantage of heavy ion activation is the production cross section of HI induced reactions are much less compared to proton or α -particle activation. The lower cross section currently prohibits the use of HI activation products for their use in human application. However, there is continuous technological development in accelerator technology. In future it may be possible to produce required amount of NCA radionuclides in combination of high current ion source (e.g., ECR ion source), CW accelerators and advanced target technology. It is noteworthy to mention that though the yield of the radionuclides by HI activation is not sufficient for human application, but sufficient for pilot studies in laboratory scale such as small animal PET imaging, or bio-distribution studies.

2. Results

Some of the representative non-conventional radionuclides produced through HI activation have been listed in Table -1.

Table 1: Some non-conventional radionuclides produced by HI activation

	Radionuclide	Half-life	Decay mode	Principal energies, keV	γ -	HI Production route
Conventional	^{144}Ce	284.9 d	β^-	133.5		
	^{141}Ce	32.5 d	β^-	145.4		
Non-Conventional	^{135}Ce	17.7 h	EC	265.2, 300.0		$^{nat}\text{Sb}(^{16}\text{O}, xn)$ [2]
Conventional	^{152}Eu	13.5 a	EC	121.8, 344.2, ...		
	^{154}Eu	8.6 a	EC	123.1		
Non-Conventional	^{145}Eu	5.9 d	EC	654.3, 893.7		$^{nat}\text{Cs}(^{16}\text{O}, xn)^{145,146}\text{Eu}$ [3]
	^{146}Eu	4.6 d	EC	633.1		
	^{147}Eu	24.1 d	EC	121.2		$^{nat}\text{La}(^{12}\text{C}, xn)^{147,149}\text{Eu}$ [4]
	^{149}Eu	93.1 d	EC	271.7		
Conventional	^{153}Gd	240.4 d	EC	97.4, 103.2		
Non-Conventional	^{147}Gd	38.1 h	EC	229.3, 396.0		$^{nat}\text{Ce}(^{12}\text{C}, xn)^{147,149}\text{Gd}$ [5]
	^{149}Gd	9.3 d	EC	149.7, 298.7		
Conventional	^{167}Tm	9.2 d	EC	207.8		
Non-Conventional	^{163}Tm	1.8 h	EC	104.3, 241.5		$^{nat}\text{Eu}(^{16}\text{O}, xn)^{163,165}\text{Lu}(\beta)$
	^{165}Tm	30.1 h	EC	242.8, 296.0		$^{163,165}\text{Yb}(\beta)^{163,165}\text{Tm}$ [6]
Conventional	^{169}Yb	32 d	EC	109.8, 130.5		
Non-Conventional	^{164}Yb	1.3 h	EC	390.6, 445.4		
	^{165}Yb	9.9 min	EC	80.1		$^{159}\text{Tb}(^{12}\text{C}, 6n)^{165}\text{Lu}(\beta)^{165}\text{Yb}$ [7]
Non-Conventional	^{167}Lu	51.5 min	EC			$^{159}\text{Tb}(^{12}\text{C}, 4n)^{167}\text{Lu}$ [7]
Conventional	^{99}Mo	65.9 h	β^-	140.5		
Non-Conventional	^{93m}Mo	6.85 h	β^+	263.0, 684.4		$^{nat}\text{Y}(^7\text{Li}, 3n)^{93m}\text{Mo}$ [8]

* The radionuclides in bold can also act as non-conventional PET radionuclides

References

- /1/ S. Lahiri, J. Radioanal. Nucl. Chem 307 (2016) 1571-1586.
- /2/ D. Nayak, S. Lahiri, Radiochim. Acta 88 (2000) 115-119.
- /3/ S. Lahiri, D. Nayak, N. R. Das, Appl. Radiat. Isotopes 52 (2000) 1393-1397.
- /4/ D. Nayak, S. Lahiri, A. Ramaswami, et al., Appl. Radiat. Isotopes 51 (1999) 261-268.
- /5/ D. Nayak, S. Lahiri, S. K. Das, et al., Appl. Radiat. Isotopes 51 (1999) 1-7.
- /6/ D. Nayak, S. Lahiri, A. Ramaswami, et al., Radiochim. Acta 87 (1999) 75-78.
- /7/ S. Lahiri, D. Nayak, A. Ramaswami, et al., J. Radioanal. Nucl. Chem. 243 (2000) 701-705.
- /8/ D. Nayak, S. Lahiri, Appl. Radiat. Isotopes 66 (2008) 1793-1798.

Author Index

A

Acharya R	71
Ahmad Idris	187
Ahmad Shakeb	223
Ahuja Sumedha	87
A.K. Vishnu Prasad	225
Akaho E.H.K	309
Alam Md. N.	179, 181
Aliev Ramiz	57
Alwani Abdul	215
Amin Al	291
Amirdhanayagam Jeyachitra	127
Andrighetto A.	53
Ansari Zarina	227
Araújo J. P.	11
Arun B.	143
Asgar A	281
Aubert Elodie	317
Augusto Richardo	317
Avila R.	93

B

B C Anand	177
Babu K. S	183
Bagla Hemlata K	101,103,105,125
Bahroun N.	73
Ballan M	53
Bandyopadhyay Tapas	245
Belkessa Kahina	275
Banerjee D	183
Banerjee Kakoli	277
Banerjee S	95,175,179, 181,235
Bannerjee K	279,281
Barua Bijoy Sonker	185
Barua L.	175, 179
Bas M.	263,265
Basu Shalmali	277
Belyshev Sergei	57
Bernardes A.P.	45
Bhade Sonali P.D	233

Bhattacharya C.	281
Bhattacharya D.	287
Bhattacharya S	281
Bhoite R.	175
Bhuyan M	223
Binsiya K. P.	241
Block M.	37
Bombard A.	263, 265
Borgna F.	53
Boukhalfa Salma	269, 275
Brahmaji Rao J.S	251, 255
Brown Jeremy	29
Buehler L.	45
Busser C.	63

C

C V Vishnu	225, 261
Catherall R.	45
Chakraborty A.	175, 235
Chakraborty Rajesh	147
Chakraborty S.	235
Chakraborty Sudipta	325
Chakravarty Rubel	235, 299, 325
Chand Manish	255
Chatt A.	73, 309
Chattopadhyay Pabitra	147
Chattopadhyay S	175, 179, 181
Chattopadhyay Swapan	5
Chaudhari P.C	235
Chaudhuri Abhirup	311
Chaudhuri Punarbasu	107,115,193,319
Chaudhury Moushumi D.	137, 253
Chaudhury Sanhita	145
Chauhan Amit	167
Chauhan R.P.	247
Chavan Sushma S	125
Chen Ning	323
Chevrier D.M.	73
Chhetri P.	37
Chijioke Nwokoma Oliver	97
Chopra Sundeep	61,115

Choukri Abdelmajid	295,297
Choudhury Dibyasree	81,117,123,271,277, 317
Chowdhury Faruque-Uz-Zaman	185
Cocolios T.E	45,49
Corradetti S.	53
Correia J. G.	11
Culp Randy	69

D

Dai Xiong-Xin	159
Das S. S.	175, 179, 181
Das Soumen	129, 133
Das Tapas	127,213
Dasgupta S	165
Dash A	127,213,235,299,325
Datta J	165
Delonca, Melanie	317
Deneva B.	63
Dewangan Pradeep Kumar	141
Dey A	281
Dhal A	281
Dhumal Sunil	267
Dirks C.	263,265
Dockx Kristof	49
Dorsival Alexandre	317
Dubla Rupali	189
Düllmann Christoph E	31,37

E

El-Absy M.A	89
El-Amir M.A	89
El-Garhy M.A	89
El-Shahat M.F.	89
Emelianov A.M	211
Ene D.	93

F

Faestermann T	63
Fang Miao	323
Fasih T.W	89
Fedorov N. A.	113
Ferrari Alfredo	317
Fletcher J.J.	309
Fu Yunchong	323
Furkina Ekaterina	57

G

Gaikwad Rupesh H.	303
Gandhi A.	113
Ganesan S.	113
Gangopadhyay Kaushik	115
Gautam Y.P.	203
Ghosh Ahana	115
Ghosh K.	315
Ghosh Kalpita	271
Ghosh Subhajit	213
Ghosh T.K.	281
Ghosh Tilak Kumar	33
Ghumman S. S.	191,221
Giacoppo F.	37
Giesen K.	23
Gondhalekar Sachin	267
Gopalakrishna A.	235
Gopalkrishnan R. K.	183
Goryachenkova T.A.	211
Gothankar Sujata	253
Götz M.	37
Götz S.	37
Groppi Flavia	55
Grozdanov D. N.	113
Guleria Mohini	127
Gupta Merry	191,221
Gupta Rashi	307

H

H Devendrappa	283
H Vijeth	283
Haba Hiromitsu	51,315
Haddad F.	47
Hain K.	63
Hajara K.	239
Hakam Oum Keltoum	295,297
Hao Duong Van	313
Happel S	263,265
Hazari Puja Panwar	229
He Xiao	157
Hirayama Y.	85
Hjerpe T.	93
Ho Manh-Dung	217,219
Hoang Sy Minh Tuan	217,219
Hossain Shahadat	291
Hou Xiaolin	59,323
Hudait A. K	179

I

Ibrahim S. 241

J

Jaeschke B 93
 Jagadeesan K.C. 299
 Jäger E. 37
 Jain A. 161
 Jain Bharti 95
 Jain S.K. 197,253
 Jaison T.J. 161
 Jaiswal Ambika Parmar 229
 Jana Ghosh Kousiki 123,245
 Jayackwreme C.K. 73
 Jayashri T A 139
 Jha S.K. 253
 Joeph Antony 225,261
 John Jaison T 155
 Johnston Karl 9
 Joshi V.M. 203
 Joshi Vikram 253

K

Kailas S. 113
 Kale Pooja 133
 Kaleja O. 37
 Kaliprasad C.S. 285
 Kamaldeep 235
 Kamaleshwaran K.K. 127
 Kamaleswaran K. 325
 Karmakar Rajib 151
 Karpe Rupali 203
 Katti Kattesh V 19,25
 Katti Kavita K 19
 Kaur Gurjit 149
 Kaur Rajveer 221
 Kaushik Aruna 229
 Kawamura H. 315
 Kazakov Andrey 57
 Keesari Tirumalesh 197
 Kershaw K 45
 Kerur B. R 177
 Khader S.A 287,289
 Khan Asma 105
 Khan Fahmida 141
 Khandaker Mayeen Uddin 97,99, 185,291
 Khelifi Rachid 269,275

Kindler B. 37
 Koll D 63
 Komori Y. 315
 Königs U. 23
 Kopatch Yu. N 113
 Korschinek G 63
 Kortmann F. 63
 KP Eappen 225,261
 Krier J. 37
 Krishna N.S 109
 Krishnan G 139
 Kulkarni Savita 95
 Kulriya P. K 1 91,221
 Kumar A 113,235
 Kumar A. Vinod 109
 Kumar Ajay 203
 Kumar Ashwani 287,289
 Kumar Deepak 163,169
 Kumar Dheeraj 133
 Kumar G. Anil 243
 Kumar G. V. S. Ashok 251
 Kumar Pankaj 115
 Kumar R. 191,251,255
 Kumar Rajesh 307
 Kumar Ranjeet 189
 Kumar U. 179
 Kundu Samir 281
 Kushmakshi 273

L

L Yesappa 283
 Laatiaoui Mustapha 43
 Lad S. 175
 Lahiri Susanta 81,107,115, 117,123,
 193,271,317,319, 329
 Lalhmunsiamma 327
 Lavrinovich E.A. 211
 Le Ngoc-Thiem 217,219
 Leal T. 11
 Lefsay A. 73
 Lens L. 77
 Levenets Volodymyr 201
 Liu H. W. 85
 Lommel B. 37
 Lonin Oleksiy 201
 Lopes A. M. L 11
 Ludwig P. 63
 Lugao Ademar B 19,25

Luo Min 159

M

M Basappa 283
M Niranjana 283
M Ramsiya 225,261
M Sheela 129,133
M Vandana 283
Ma Ling-Ling 159
Ma Yuhui 157
Madhusmita 179, 181
Mahamood K. Nadira 131,285
Mahantesha B. K 205
Mahanty Bholanath 171
Maiti Moumita 153,163,167,169
Maletha P 235
Manenti Simone 55
Manna S. 281
Marco V Di 53
Martinez-Palenzuela Yisel 49
Marzari S. 45
Marzaro G. 53
Mastrotto F 53
Mathur Anupam 129,133
Maudoux N 263
Meena J.K 281
Mhatre, Amol M 125
Miah M.H. 291
Mirapurkar Shubhangi 129,133
Mishima T. D 85
Mishra Anil K 229
Mishra M.K. 203
Mishra R.K 287,289
Mishra V. G. 145
Mistry A.K. 37
Mistry J. S. 155
Mitra A. 175
Mitra Sayantani 319
Mittal Raj 301
Mohamed Nader M. A 111
Mohanty B 235
Mohapatra Prasanta K 75,171
Moreira R 11
Mukherjee G 279,281
Mukherjeen Joyeeta 237
Mustafa M. N. 291
Musthafa M M 239,241
Muthe K.P 299

N

Nagame Yuichiro 39
Nagase K. 85
Naidu B. Gowri 91
Naik H. 235
Nanal Vandana 17
Nankar D. P. 161
Narayana Y. 207,209,231,285
Narula Chetna 247
Naskar Nabanita 79,107,115,193,271,
277,317,319
Nasser Saleh Mansoor 99
Nayak B. K 113,235,299
Neumaier B 23
Novikov A.P 211
Nyarko B.J.B 309

O

Ojha S. 115
Oliveira G. N. P. 11
Omelnik Oleksandr 201
Ouyang Jie 159

P

P V Divya 119,121
Padmakumari R. 205
Pal A. K 179
Pan Hai 69
Panchal Suresh 247
Panda Jagannath 249
Pandey Ashok K 125
Pandey R 281
Pandian Arun 127
Pant Amar D. 199
Pant Diksha 197
Patra A. K. 155,161
Patra S.K. 223
Pawar Pravin 267
Pawar Y. 235
Perko Zoltan 29
Petwal V. C. 205
Phelippeau L. 263
Pillai M.R.A 27
Prajapat Rinku Kumar 153,163
Prasad Mukesh 243,321
Prasad Ravi G. V. 69
Prior J 45

Pulhani Vandana 137,203,233,253

Q

Qaim S.M 23
Quddus A 223
Quinto F 63

R

Raeder S. 37
Rajan M.G.R 95
Rajashekara K. M 207,209,231
Raju G. J. Naga 91
Ramadan H.E 89
Ramani Y 143
Ramola R.C 243,321
Ramos Joao Pedro 49,317
Rana Pallavi 247
Rana T.K 281
Rao J. C. 91
Rao Preeti 301
Rashid Md. Abdur 185
Ravi P P.M. 161
Ravi P.M 155
Ravindrachary, V 205
Ravishankar R 245
Rawat Neetika 287,289
Realdon N 53
Reddy Priyanka J. 137,173
Révay Zsolt 67
Rocha-Rodrigues P. 11
Rohit 257,259
Roy A 197
Roy Amitava 13
Roy B. J. 113
Roy Pratap 281
Roy Subinit 15
Roy T. 281
Rozaila Z.Siti 185
Ruhela R. 199
Ruskov I. N. 113

S

S Anilkumar 199
S. Ganesh 283
S P. Ashokkumar 283
Sabharwal Arvind D 257,259
Sachdev S.S. 129,133

Sahanakumari R. 205
Sahu Rojalin 249
Sahu, Abinash 249
Sakemi Y. 315
Sakhare Navin 129,133
Samanta Chhanda 41
Sambamurty T. 109
Sandhu Kirandeep 149
Sandhu B. S. 195,257,259,305
Sanjeev Ganesh 205
Santos M. B 85
Sarita P. 91
Sarkar Gayatri 169
Sarma Haladhar D 127,213,325
Satamkar S. 175
Sato N. 315
Sato Tetsuya K. 35
Savitri P. Padma 109
Sawant P.D 189
Sawant Pramilla D 173
Sawant Y 113
Saxena A 113,299
Sayed Sajida 103
Semghouli Slimane 295
Sen A 281
Sen Kamalika 135,151,227
Sengupta Mitra Mausumi 245
Sengupta Pranesh 237
Senthilvadivu R 251
Shah D. J. 145
Shaikh Moin 281
Shaikh Sabrina A 101
Sharanabasappa 177
Sharma Manoj K 149
Sharma, Nidhi 287
Sharma, Rajveer 115
Shchur Andrey 201
Shinto Ajit S. 325,127
Shrivastava Kamlesh 141
Shrivastava V. 281
Singh Ajay 299
Singh Bhajan 195,257,259,305
Singh Bhupinder 87
Singh Inderjeet 257,259
Singh Manveer 197
Singh Mohinder 195,305
Singh Pritam 135
Singh Sanjay 183

Sinha U.K.	197	Vimalnath K. V.	235,325
Sivakumar Susheela	183	Vinayak	141
Sokolenko Volodymyr	201	Vineethkumar V.	209
Song Li-Juan	159	Viswanathan S.	143
Spahn I	23	Vollaire Joachim	317
Srihari K	245		
Srikanth S.	91	W	
Stegemann Simon T.	49	Wagh S.S	155
Stenberg K.	93	Wallner Anton	65
Stieghorst Christian	67	Wankhede Sonal M	173
Stora, Thierry	45,49,317	Wolterbeek Bert	29
Sudhakar, J.	109		
Sun Gwang Min	217,219	X	
Suresh Sugandhi	233	Xu Dian-Dou	159
Suryanarayan S.V	235,299		
Swain K. K	165	Y	
T		Yadav J.R	189
Tawate M.	175,235	Yadav Manjulata	321
Tegginamata Pratheeka	205	Yadav Poonam	87
Teixeira R. C.	11	Yakushev A.	37
Thakare S.V.	299	Yakusheva V.	37
Tiwari Diwakar	327	Yang, K. F.	85
Tomar B. S.	199	Yano S.	315
Tondon Akash	195,305	Yasmin Sabina	185
Tran Hoai-Nam	217,219	Yeslem A. E. M. O. Mohammed	295
Tran Tuan-Anh	217,219	Yokokita T.	315
Tripathi R M	137,155,161,197,203, 233,253	YolaYahaya Ibrahim	187
U		Z	
Uddin M. M	85	Zhang Luyuan	323
Upadhye T	175	Zhang P	73
		Zhang Zhiyong	157
V			
V Prakash	119,121,131,207,209, 231,285		
Vajda N.	263,265		
Vasidov Abdisamat	293		
Vasidova Sevara	293		
Vasudeva Rao P.R.	3		
Verboom Willem	171		
Verma Dalip Singh	273		
Verma V. P	205		
Vermunt Tuur	29		
Vettorato E.	53		
Vijayalakshmi I.	143		
Viji K	139		



Cover: Oldest and Newest accelerators of India

Front cover: The first cyclotron of India, built indigenously under the leadership of Professor Meghnad Saha in 1942 at University of Calcutta.

Back cover: The upcoming 3 MV Tandatron Accelerator, Facility for Research in Experimental Nuclear Astrophysics (FRENA) at Saha Institute of Nuclear Physics (SINP).